Glazing system with Transparent Insulation Material for Building Energy Saving and Daylight Comfort

Yanyi Sun, **BArch MSc**

Thesis submitted to the University of Nottingham for degree of

Doctor of Philosophy

January 2017

Abstract

Concerns over sustainability in the built environment have resulted in continuous efforts to improve the performance of window system or glazed façade and hence indoor comfort and building energy conservation. An innovative façade system where parallel transparent/translucent plastic slats are sandwiched between glass panes to form a Parallel Slat Transparent Insulation Material (PS-TIM) is proposed as a strategy to effectively reduce heat transfer between the panes of a double glazed window, while maintaining access to daylight. A holistic investigation of the window system with PS-TIMs is conducted in terms of thermal and optical properties, as well as detailed daylight and energy performance predictions of applying PS-TIMs in buildings. Firstly, an experimental investigation is undertaken in a large climate chamber, and the measurement results were used to validate a two-dimensional Computational Fluid Dynamics (CFD) model. Secondly, the validated 2D CFD model is used to solve the dynamic thermal properties of different configurations of PS-TIMs under various environmental conditions. The optical properties (i.e. *Bidirectional Scattering Distribution Function* (*BSDF*)) of PS-TIMs are obtained via a ray-tracing technique based on the structures' geometries and the material optical characteristics of the interstitial structure. The detailed annual daylight performance in different climates and building orientations are predicted using RADIANCE. Finally, the optical and thermal properties obtained from the previous fundamental models are applied in EnergyPlus to predict the energy performance (i.e. heating, cooling and lighting energy consumption) of applying PS-TIMs in buildings in different climates. The investigation results provide a better understanding of the benefits of PS-TIM in terms of energy saving and daylight comfort improvement, as well as offer some tentative suggestions as to how architects and engineers might apply PS-TIM to window system or glazed façade.

Acknowledgement

This thesis is an outcome of four years of hard work with significant help and support from many people in various ways.

First and foremost, I am deeply indebted to my supervisors Dr Yupeng Wu and Dr Robin Wilson, without whom this thesis would not have been possible. Dr Yupeng Wu devoted so much time and effort in helping me, encouraging me and supporting me. I will never forget the days when I struggled with difficult problems, he was always there to give me valuable suggestions and inspired me. I also own a lot of gratitude to Dr Robin Wilson, for his tremendous academic support, critical insight, encouragement and immense kindness during the past four years. I have no words to express my sincere gratitude to them, my supervisors, for their invaluable support and guidance.

It is a great pleasure for me to undertake my PhD work at the Department of Architecture and Built Environment at the University of Nottingham, and I am extremely grateful to insightful suggestions and help from Dr Sergio Altomente, Dr Parham Mirzaei Ahranjani, Dr Peter Rutherford and other staff.

My thanks also go out to the PhD studentship that I awarded from Faculty of Engineering, the University of Nottingham and the State Scholarship Fund that I received from the China Scholarship Council.

Finally, but by no means least, I would like to thank my family and friends. I cannot say enough about my father Deming and my mother Lihua for making me who I am today. And no words can express my gratitude to my husband, Zishang, for being supportive all the time in all that I have done and I ever wanted to do. My most heartfelt thanks to my son, Bailin, who was born during my PhD study and has a nick name with a same pronunciation of the campus where I studied. My very special thanks to my best friends, Runqi and Zhuo, there is no way that I could finish my PhD study without their help and support.

Table of Contents

Chapter 1. Introduction 1

1.1 Background 2

1.2 Research gap 5

1.3 Research aims and objectives 8

1.4 Thesis structure 9

Chapter 2. Transparent Insulation material: A Literature review 12

2.1 Introduction 13

2.2 Classification 13

2.3 Properties of TIM 15

2.4 Applications of TIM in building 23

2.5 Relative research gaps and industrial development of TIMs 30

2.6 Summary of TIMs' current research status and selecting Parallel Slat Transparent Insulation Material (PS-TIM) in this research 32

Chapter 3. Evaluation methods for complex glazing systems and the daylight and energy performance prediction for their building application: A Literature review 34

3.1 Introduction 35

3.2 Thermal investigations of glazing system 35

3.2.1 Experimental investigation method 36

3.2.2 Numerical investigation method 41

3.3 Optical investigations of complex glazing systems 44

3.3.1 Methods to obtain total amount of transmittance or reflectance 45

3.3.2 Bidirectional Scattering Distribution Function (BSDF) 49

3.4 Building daylighting performance predictions with complex fenestration system applied55

3.4.1 Daylight assessment metrics 56

3.4.2 Daylight simulation method 65

3.5 Energy performance prediction for building with complex fenestration systems 68

3.6 Summary 72

Chapter 4. Thermal evaluation of a double glazing unit with integrated Parallel Slat Transparent Insulation Material (PS-TIM) 74

4.1 Introduction 75

4.2 Using experimental investigation to validate numerical model 76

4.2.1 Test samples 76

4.2.2 The climatic chamber and apparatus setup 77

4.2.3 Measurement procedure and data acquisition 80

4.2.4 Analysis of the data 81

4.2.5 CFD modelling of the test samples 82

4.2.6 Comparison between experimental test, standard calculation and CFD 83

4.3 Numerical investigation methodology: CFD simulation 85

4.3.1 Governing equations and assumptions 86

4.3.2 Boundary conditions and material properties 88

4.3.3 Mesh independency 89

4.3.4 Derivation of thermal transmittance 90

4.4 Results and discussion 92

4.4.1 Effects of aspect ratio on convective suppression 92

4.4.2 Thermal visualisation within the PS-TIM structures 94

4.4.3 Thermal conductance of an air cavity with PS-TIM structures..... 97

4.4.4 The effects of slat conductivity, thickness and emissivity on the thermal performance of PS-TIM..... 99

4.4.5 Total thermal resistance and U-value..... 103

4.5 Conclusion..... 105

Chapter 5. Daylight performance prediction of applying glazing systems with Parallel Slat Transparent Insulation Material (PS-TIM)..... 107

5.1 Introduction..... 108

5.2 Ray-tracing method to obtain the BSDF of glazing systems with PS-TIMs..... 109

5.3 Simulation methodology..... 112

5.3.1 Dynamic daylight simulation method..... 113

5.3.2 RADIANCE simulation modelling..... 115

5.3.3 Model validation..... 118

5.4 Results and discussion of the effect of different PS-TIM on indoor daylight performance..... 121

5.4.1 The analysis of the effect of slat pitch..... 121

5.4.2 Analysis of slat tilt angle..... 127

5.4.3 Analysis of slat material properties..... 129

5.5 Conclusion..... 133

Chapter 6. Thermal and energy performance prediction of applying glazing systems with Parallel Slats Transparent Insulation Material (PS-TIM)..... 135

6.1 Introduction..... 136

6.2 Research methodology..... 137

6.2.1 Overview of the research framework..... 137

6.2.2 Theories of thermal model 139
6.2.3 Theories of optical model 144
6.3 Building performance simulations 145
6.3.1 Weather data 146
6.3.2 Prototype office geometry and modelling 146
6.3.3 Modelling of building daylight simulation 149
6.3.4 Modelling assumptions for building energy simulation 149
6.3.5 Importing of thermal and optical characteristics of PS-TIM into EnergyPlus 150
6.3.6 Model verification 151
6.4 Building performance simulation results and discussion 153
6.4.1 Requirement for interior shading to prevent strong daylight 153
6.4.2 Window heat loss and heat gain through windows with PS-TIM 155
6.4.3 Total energy consumption after applying PS-TIM 157
6.5 Conclusion 161
Chapter 7. Applying PS-TIM under different climates 163
7.1 Introduction 164
7.2 Applying PS-TIM under different climates: weather data 164
7.3 Results and discussion 167
7.3.1 Daylight performance 167
7.3.2 Requirement for interior shading to prevent strong daylight 174
7.3.3 Window heat loss and heat gain through windows with PS-TIM 175
7.3.4 Total energy consumption after applying PS-TIM 177
7.4 Conclusion 180

Chapter 8. Conclusion and recommendation for further work..... 182

8.1 Conclusion 183

8.2 Recommendations for further work 187

Appendix A:..... 189

Reference: 190

List of Figures

Figure 1-1: Buildings with large area of glass dominate all around the world 2

Figure 1-2: Disciplined structure of this thesis 11

Figure 2-1: Schematic diagrams of typical types of TIMs: a. glazing-perpendicular structure: (a1) capillary structure, (a2) honeycomb structure, (a3) parallel slats array structure; and (b) glazing-parallel structure; (c) mixed structure and (d) homogeneous structure 15

Figure 2-2: Appearances of five typical TIMs : (a) honeycomb TIM from Wacotech, (b) honeycomb TIM from PANELITE, (c) monolistic aerogel from Technical University of Denmark [43], (d) capillary TIM from Okalux and (c) granular silica aerogel from Lumira. 16

Figure 2-3: Comparison of experimental results of angular dependent transmittance: $\tau(\theta)$ for FEPT square honeycomb, FEPT parallel slat, FEPT V-slat and tubular glass [56], FEPT parallel wall [57], 100 mm honeycomb [59] and 100 mm PC capillary and 100 mm PC honeycomb [60] (adopted from [46]) 19

Figure 2-4: Experimentally measuring the optical properties of TIMs: (a) Measured total or direct transmission coefficient vs. wavelength of float glass, MSA on its own, MSA and GSA with double glazed units, (b) the spectrophotometer and (c) the integrating sphere (adopted from [53]) 20

Figure 2-5: Schematics of (a) square homeycomb (b) section of a square homeycomb cell (adopted from [20]) 21

Figure 2-6: Sound reduction index (R) values for the conventional window and the window integrated with aerogel vs. frequency (adopted from [53]) 23

Figure 2-7: Configurations of applying TIM: (a) in flat-plate solar collectors, (b) in solar wall and (c) in window system or glazing fa çade (adopt from [62]). 23

Figure 2-8: Comparison of the ($\tau\alpha_e$) at various incidence angle (θ) for flat-plate solar collectors with 5 cm PC honeycombs a, 10 cm PC honeycombs, 10 cm glass capillaries [69], 5 cm PC honeycombs b [70], 2 cm MSA [71] and 6 cm FEPT [73] (adopted from [46]) 24

Figure 2-9: (a)-(d) Sunlight distribution through clear glass at equinox in Trondheim, at 63° N; (e)-(h) Sunlight distribution through 35 mm capillary TIM at equinox in Trondheim, at 63 ° N [84] 29

Figure 3-1: Steady-state thermal properties laboratory measurement method (a) hot-plate method, (b) flow meter method and (c) hot-box method 39

Figure 3-2: Illustration of two types of daylighting analysis method: (a) total amount of direct and diffuse transmittance or reflectance; (b) directional distribution of transmittance and reflectance 44

Figure 3-3: The experiment set up of using spectrophotometer and integrating sphere to test transmittance and reflectance (adopted from [124]) 45

Figure 3-4: (a) discretization used in the model, (b) illustration of the direct-direct transmittance of the shading device, (c) illustration of the direct-diffuse transmittance and reflectance of the shading device and (d) illustration of the diffuse-diffuse transmittance and reflectance of the shading device [109] 48

Figure 3-5: (a) Klems 145-patch hemispherical basis with numbered subdivisions; (b) coordinate system for bidirectional measurements [41] 50

Figure 3-6: Virtual goniophotometers generated by using (a)TracePro [32] and (b)OptiCad [156] 54

Figure 3-7: False colour contour in a room with three different window design on solstice and equinox days under clear sky conditions (adopted from [179]) 58

Figure 3-8: Comparison between $DA_{150\ lux}$ 50%, $DA_{300\ lux}$ 50%, $DA_{500\ lux}$ 50% and occupants' subjective daylight evaluation (adopted from[184])..... 60

Figure 3-9: Comparison between *UDI* maps for façade with and without light shelf at different window-to-wall ratio (WWR) (adopted from[192]) 61

Figure 3-10: Overall consideration of *uniformity*, *DA*, *DGI* and energy saving (adopted from [195])..... 65

Figure 4-1: (a) External view of the climatic chamber (b) Internal view of the chamber and air conditioning unit 77

Figure 4-2: View of the system, the test specimen and sensors..... 79

Figure 4-3: Detailed view illustrating the locations of the thermocouples and heat flux meters on the surfaces of the glazed unit 80

Figure 4-4: (a) 2D schematic diagram illustrating the geometry of the glazing system without blind (b) glazing system with horizontally placed slats (c) glazing system with vertically placed slats..... 82

Figure 4-5: Measured, calculated and simulated heat flux through glazing system (a) scenarios 1, 2 and 3 in DG V0 and V90; (b) scenarios 3, 4 and 5 in DG V0 and V90. 85

Figure 4-6: (a) PS-TIM structure in a double glazed unit; (b) 2D schematic illustrating the geometry of the air gap with PS-TIM structure; (c) 2D schematic illustrating geometry of air gap without PS-TIM. 86

Figure 4-7： Relationship of the *Nusselt number* vs *aspect ratio* for different *Grashof number* for (a) small cells and (b) double glazed units. 94

Figure 4-8: Temperature profile of a double glazed unit with and without PS-TIM structures at different *Grashof number*: (a) no-slats; (b) 10 mm-cell structure; (c) 7.5 mm-cell structure; (d) 5 mm-cell structure; (e) 3 mm-cell structure 96

Figure 4-9: Relationship between the average *Nusselt number* and *Grashof numbers* for different cell heights 97

Figure 4-10: Thermal conductance caused by conduction, radiation and convection for an air cavity with and without PS-TIMs with different cell dimension at various glazing pane temperature differences 99

Figure 4-11: Ratio of thermal conductance of an air cavity with PS-TIMs with different cell dimension to an air cavity without PS-TIM at various glazing pane temperature differences 99

Figure 4-12: Thermal conductance ratio ($h_{PS\text{-}TIM}/h_{no\text{-}slat}$) for different slat conductivities (W/mK) at various glazing pane temperature differences of (a) 3 mm PS-TIM and (b) 10 mm PS-TIM 101

Figure 4-13: Thermal conductance ratio ($h_{PS\text{-}TIM}/h_{no\text{-}slat}$) for different slat thickness (mm) at various glazing pane temperature differences of (a) 3 mm PS-TIM and (b) 10 mm PS-TIM 102

Figure 4-14: Thermal conductance ratio ($h_{PS\text{-}TIM}/h_{no\text{-}slat}$) at different slat emissivity at various glazing pane temperature differences of (a) 3 mm PS-TIM and (b) 10 mm PS-TIM 103

Figure 4-15: The thermal resistance ($\boldsymbol{1U}$) of a double glazed window containing PS-TIM structure 104

Figure 5-1: (a) schematic diagram of *BSDF* and (b) Klems 145-patch hemispherical basis with numbered subdivisions 110

Figure 5-2: Schematic diagram of variables: (a) slat pitch (d mm); (b) tilt angle (Φ °) and (c) slat material 111

Figure 5-3: Example of defining the material and geometry of the PS-TIM itself in RADIANCE 112

Figure 5-4: Example of generating the geometry of the glazing system with PS-TIM in RADIANCE 112
Figure 5-5: Example of using genBSDF to obtain the BSDF data of the glazing system with PS-TIM in RADIANCE 112
Figure 5-6: The illustration of the three-phase method 114
Figure 5-7: The diurnal average direct and diffuse solar radiation of London 115
Figure 5-8: Selected points for evaluating illuminance distribution in the office space (a) Plan view and (b) sectional view 117
Figure 5-9: Comparison between measured illuminance and illuminance calculated using Radiance at the 8 selected points in the room 119
Figure 5-10: Comparison between (a) photo of test room and (b) rendered image using RADIANCE 120
Figure 5-11: *UDI* bins for points located along the central line of an office from window to the end wall for the window system with and without PS-TIM: (a) DG; (b) 15 mm PS-TIM; (c) 10 mm PS-TIM; (d) 7.5 mm PS-TIM and (e) 5mm PS-TIM. Simulations are based on a London IWEC weather file. 124
Figure 5-12: (a) Illuminance *uniformity ratios* (b) *daylight glare probability* (*DGP*) of window without and with diffuse translucent PS-TIM with 4 different slat pitches. Simulations are based on a London IWEC weather file. 126
Figure 5-13: (a) Illuminance *uniformity ratios* (b) *daylight glare probability* (*DGP*) for a window with diffuse translucent PS-TIM with slat pitch of 15mm at 7 different tilt angles, and (c) definition of tilt angles, ϕ. Simulations are based on a London IWEC weather file. 128

Figure 5-14: $UDI_{100\text{-}2000\ lux}$ and $UDI_{500\text{-}2000\ lux}$ for diffuse translucent PS-TIM with 7.5 mm slat pitch at 0 ° and -30 ° tilt angles. Simulations are based on a London IWEC weather file. 129

Figure 5-15: Summary of metrics evaluating the performance of applying various PS-TIMs with translucent slats in (a) desirable ranges and (b) undesired ranges. Simulations are based on a London IWEC weather file. 131

Figure 5-16: (a) Illuminance *uniformity ratios* (b) *daylight glare probability* (*DGP*) of window without and with transparent PS-TIM for 4 different slat pitches at 7 different tilt angles. Simulations are based on a London IWEC weather file. 133

Figure 6-1: Flow chart of the comprehensive method for complex fenestration *..... 138

Figure 6-2: Demonstration of heat transfer and the variables used in heat balance equations for (a) double-glazed window (b) window system with PS-TIM between two panes (adopted from [134])..... 139

Figure 6-3: The equivalent thermal conductivity of the air cavity between two panes with and without PS-TIM, pre-calculated by Computation Fluid Dynamics 143

Figure 6-4: The diurnal average temperature and direct and diffuse solar radiation of London 146

Figure 6-5: (a) Plan view and (b) section view of the simulated office room 148

Figure 6-6: (a) window heat loss under cold weather conditions—3 coldest days under London climate; (b) window heat gain under hot weather conditions—3 hottest days under London climate 152

Figure 6-7: (a) Lighting power and illuminance level at points 1 and 2 without interior shade; (b) Lighting power and illuminance level on point 1 and 2 with interior shade on a typical sunny day..... 154

Figure 6-8: Average number of hours per week when discomfort daylight condition exist 155
Figure 6-9: Breakdown of annual heat loss and heat gain for the office with a normal double glazing under five different climates..... 156
Figure 6-10: (a) heat gain and (b) heat loss through windows (kWh/m^2·yr) after applying different configurations of PS-TIM under five climates..... 157
Figure 6-11: Annual heating, cooling and lighting energy consumption when HVAC works between 9:00-17:00 on workdays 158
Figure 6-12: Hourly window (a) heat gain, heat loss and (b) space heating loads of applying window system with and without PS-TIM when HVAC works on working hours..... 159
Figure 6-13: Annual heating, cooling and lighting energy consumption when HVAC is always on. 160
Figure 6-14: Hourly window (a) heat gain, heat loss and (b) space heating loads of applying window system with and without PS-TIM when HVAC when HVAC always on..... 161
Figure 7-1: The diurnal average direct and diffuse solar radiation of (a) Stockholm, (b) London, (c) Beijing, (d) Hong Kong and (e) Singapore 166
Figure 7-2: (a-e) *UDI* bins and (f-j) $UDI_{500\text{-}2000\ lux}$ at points along central line from south-facing window to end wall with and without PS-TIM with 4 different interval distances under 5 different climates: (a) and (f) Stockholm, (b) and (g) London, (c) and (h) Beijing, (d) and (i) Hong Kong and (e) and (j) Singapore..... 170
Figure 7-3: *UDI* bins for points along central line from window to end wall for (a) south, (b) north, (c) west and (d) east orientations with and without PS-TIM with 3 different slat pitches under London climate 172

Figure 7-4: *UDI* bins at points along central line from window to end wall at (a) south, (b) north, (c) west and (d) east orientations with and without PS-TIM with 3 different interval distances under Singapore climate 173
Figure 7-5: Average number of hours per week when discomfort daylight condition exist 175
Figure 7-6: Breakdown of annual heat loss and heat gain for the office with a normal double glazing under five different climates 176
Figure 7-7: (a) heat gain and (b) heat loss through windows (kWh/m^2·yr) after applying different configurations of PS-TIM under five climates 177
Figure 7-8: Annual heating, cooling and lighting energy consumption when HVAC works between 9:00-17:00 on workdays. 178
Figure 7-9: Annual heating, cooling and lighting energy consumption when HVAC is always on. 180

List of Tables

Table 2-1: Physics properties of glazing-perpendicular TIMs [46] 17

Table 3-1: Standards of experimental methods 37

Table 3-2: Goniophtotometers to measure the *BSDF* data 52

Table 3-3: Daylight performance predictions by using different simulation tools with various metrics 67

Table 4-1: Arrangement of mean temperature and surface temperature difference of 5 scenarios for glazing systems 81

Table 4-2: Properties and boundary conditions for different models. 89

Table 4-3: The *U-values* of a double glazed window containing PS-TIM structure .. 104

Table 5-1: RADIANCE simulation parameters 118

Table 5-2: $UDI_{100\text{-}2000lux}$ of window without and with transparent PS-TIM of 4 different interval distances at 7 different tilted angles. 133

Table 6-1: Coefficients for the polynomial regression predicting equivalent thermal conductivities of different PS-TIM configurations for Equation (6-5) 142

Table 6-2: Thresholds used to control lowing of interior shades 150

Table 6-3: Comparison of the annual prediction (kWh/m^2 a) of heating and cooling load obtained using two methods under different climate 152

Table 7-1: Latitude, longitude, summer and winter average temperatures and solar irradiance of 5 cities 165

Nomenclature

Symbols

A	aspect ratio $A = L/s$	-
$a - e$	coefficients for polynomial regression	-
c_p	specific heat capacity	J/kg ·K
$Const.$	constant	-
d	thickness of glass pane	m
D	distance	m
D_λ	Spectral distribution	-
E	fraction of cell wall material	-
E_v	Vertical eye illumiance	lux
E_o	Exterior IR incident on window plane	W/m^2
E_i	interior IR incident on window plane	W/m^2
F	view factor	-
g	gravitational acceleration	m/s^2
h	heat transfer coefficient	W/m^2 ·K
	- also thermal conductance	W/m^2 ·K
J	radiosity	W/m^2
k	thermal conductivity	W/m ·K
L	height of the window air cavity	m
L_s	Luminance of source	cd/m^2
n/N	refraction index	-
n	number	-
P	Position index	-
q	heat flux	W/m^2
q_b	average absorbed heat flux	W/m^2
R	thermal resistance	m ·K/W
s	Width	M
Si	Radiation (short-wave, and long-wave from zone internal sources) absorbed by face i	W/m^2
T	temperature	K/°C
u, v	velocity components	-
U	thermal transmittance	W/ m^2 ·K
$V(\lambda)$	Spectral luminous efficiency for photopic vision	-
x, y	Cartesian coordinates	-
$\Delta T/\Delta t$	temperature difference	K/ °C

α	absorbance	-
β	thermal expansion coefficient	1/K
ε	emissivity	-
ρ	reflectance	-
	-also density of air	kg/m^3
σ	Stefan-Boltzmann constant	$W/m^2 \cdot K^4$
θ	incidence angle	°
φ	azimuth angle	°
λ	wavelength	nm
τ	transmittance	-
μ	dynamic viscosity of air	kg/m s
ω_s	Solid angle	sr

Subscripts

a	air
c	control
C	cold
e	external
g	gas
p	glass pane
H	hot
i	internal
i, j, k	counter
m	mean
n	number
t	total
r	radiation
s	slat
w	wall

Dimensionless numbers

Gr	Grashof number
Nu	Nusselt number
Pr	Prandtl number
Ra	Rayleigh number

Chapter 1. Introduction

1.1 Background

Following Ludwig Mies van der Rohe's conception of the first full glass curtain façade, glass has increasingly become the material of choice for façade construction throughout the 1950s and 60s. Buildings with large glass elements have spread worldwide in recent decades: from London to Beijing; from Stockholm to Singapore (see Figure 1-1); irrespective of the local climate.



Figure 1-1: Buildings with large area of glass dominate all around the world

As well as conveying a sense of architectural innovativeness, the use of large glass elements has the potential to provide the following advantages:

1) For structural purposes: They are lightweight, easy to modularise, and can be quickly installed in a construction site. They are also easy to bend and form, allowing creative and unique building shapes.

2) For daylight purposes: Allowing a greater quantity of natural daylight to enter the building, using large glazing area on building façade can reduce electric lighting demands if accompanied by a good daylight control strategy.

3) For energy purposes: Using large glazing area allows more solar energy transmitted into indoor spaces providing passive heating. This can potentially reduce building heating demands for particular climates.

4) For visual connection purposes: Occupants are afforded a view of the external environment, therefore directly connecting inside and outside. This provides the potential to positively enhance occupant satisfaction, productivity, health and wellbeing.

5) For aesthetic purposes: Glazed façades are associated with particular architectural styles and are therefore synonymous with particular types of buildings.

Conversely, the transparent nature of glass as a building material arouses concerns in response to the recent sustainability agenda. The most common issues are:

1) Potential overheating resulting in high cooling loads due to the potential for significant direct solar gain through glazed façades [1-3];

2) Significant heat loss during cold periods due to relative higher *U-values* compared with other building elements [4-9];

3) Visual discomfort such as glare in the inhabited space [10-12];

4) Possibility of undesirable reflections which might give rise to glare in the immediate surroundings or city [13];

5) A certain degree of infiltration through unintentional air leakage between glazing and frame due to inadequate detailing and / or workmanship [14, 15];

6) Degradation and fading of building components or furniture due to the presence of high levels of transmitted sunlight to the internal environment [16, 17].

Consequently, the design and manufacture of efficient glazing systems to offer improvements requires significant consideration given the number of physical and non-physical variables at play. Especially, with a growing concern in response to the non-renewable energy crisis and global warming, better glazing systems are required to reduce the energy consumptions during the process of building operation. Various strategies have been used to overcome these drawbacks corresponding to energy efficiency, the key two being: 1) increasing the thermal resistance of glazing units, such as using inert gases as cavity fill, multiple glass panes, low emissivity coatings, vacuum glazing and other techniques to reduce the overall heat transfer coefficient of the glazing unit; and 2) controlling solar radiation and daylight entering the room by introducing tinted coatings, reflective coatings, shading devices and smart windows techniques (e.g. electrochromic thermochromics, photochromic etc.).

A further strategy however can potentially be employed that provides a balanced improvement in terms of both increased thermal resistance and controlled solar and daylight admittance namely glazing units with a Transparent Insulation Material (TIM) structure. When compared with strategies solely focused on thermal resistance improvements (e.g. low emissivity coatings, multiple panes, inert gases filling and vacuum glazing etc.), the employment of interstitial TIM structures has the potential to affect the amount and distribution pattern of daylight penetration and thus a more welcome luminous environment may be made. When compared with strategies solely focused on solar and daylight penetration control (e.g. shading devices, tinted coating and reflective coatings etc.), the employment of interstitial TIM structures can reduce the convective and radiative heat transfer between two glazing panes and thus the overall heating energy demand for the building may be reduced. When compared with novel smart window techniques (e.g. electrochromic thermochromics, photochromic etc.),

TIM requires relative low investment and provides long-time stability. In summary, integrating TIM with glazing systems affords the potential towards improved design of building window systems or glazing façade systems. Thus, comprehensive studies on this glazing system are required to provide a better understanding of their benefits in terms of energy saving and daylight perfection.

1.2 Research gap

The thermal behaviour of TIMs has been investigated numerically and experimentally over the past two decades, much of this work focused on their application in solar collectors. Although, applying TIMs has been proven to effectively reduce heat losses and improve the efficiency of solar collectors [18-22], relatively few studies exist regarding the thermal and optical performance of TIMs contained within the cavities of double glazed windows. This lead to an uncomprehensive prediction for TIM's window application, as the fundamental thermal and optical characteristics of TIMs integrated within building windows or glazed façades are entirely different from their application in solar thermal collectors. Firstly, the mean working temperature and temperature difference between two surfaces of a window are much smaller than in a solar collector. Secondly, the natural convection pattern(s) and their intensity(ies) in the vertical cavity between two glazing panes differ from the convection that occurs within the horizontal space between a hot solar absorber and its cold glass cover. The difference can be explained by the fact that buoyancy driven natural convection is more significant in the vertical cavity of a window as compared with that in horizontally oriented cavities in collectors. Furthermore the application of TIMs to window design has to account for the additional functions these components commonly provide, namely the provision of view and effective daylight distribution.

Although the thermal and optical performance of TIMs applied to windows have seen relatively little research, the concept of using interstitial structures, such as horizontal Venetian blinds, pleated blinds, etc. within the air cavity of a double glazing unit has been widely researched [4, 23-38]. These structures share many of the same characteristics as TIMs; and hence such research provides methods used for reference to resolve similar problems in window systems incorporating TIMs [24, 26].

With respect to thermal behaviour, a considerable volume of research of windows with interstitial structures has been undertaken by using Computational Fluid Dynamic modelling to evaluate the possibility of reducing free convection and long-wave radiation between two glazing panes. When compared with pure air cavity between two glazing panes, the heat transfer through the air cavity with interstitial structures has a certain degree of reduction. Research results show that a maximum heat transfer coefficient reduction of 50% [4] or a maximum U-value reduction of 21% [39] can be achieved. However, most of the currently models are imperfect [59]. Detailed investigations of the interstitial structures on the reduction of heat transfer in terms of both convection, which is driven predominately by temperature difference across the two glass panes, and radiation, which is driven predominately by glazing system mean temperature, under different environmental conditions that are commonly encountered in buildings are less well studied.

With respect to optical behaviour, the radiosity method is commonly used to solve the optical performance of window system with interstitial structures [31, 34, 40]. However, this method lacks accuracy when dealing with highly specular reflective surfaces, as it assumed that all the fluxes are spatially averagely diffused by every surface. Meanwhile, this method only results in a total transmittance or reflectance without considering the directional distribution of each flux, which is insufficient for

accurately predicting illuminance distribution in a space. An alternative method, which uses a full-scale optical description of the interstitial structure by a matrix of Bi-directional Scatter Distribution Function (BSDF) is proposed and validated [36, 41-43]]. The BSDF data can be obtained by employing a three-dimensional ray-tracing method [32, 33, 44, 45], which traces the rays from all incoming directions to all possible outgoing directions. In so doing, the angularly resolved transmittance or reflectance of window systems with interstitial structures is able to be considered in the process of predicting daylight performance of applying complex window systems in buildings.

In order to predict the total energy consumption of window systems with interstitial structures in buildings, building energy simulation tools have been widely used. Accurate predictions of their energy consumption require precise definitions of the heat gain, heat loss and visible light transmitting through these window systems. However, current building simulation programs are not accurate enough for modelling these window systems with complex interstitial structures, often because of the simplified thermal and optical models used to solve heat transfer and light transmittance. The two- or three dimensional heat transfer or solar and light transmission that is interfered with by the interstitial structure of complex window system is not considered. Recently, efforts have been made on combining bi-directional distribution function in building performance simulation [17, 19] to achieve a more accurate solar and daylight distribution analysis. However, the free convection and long-wave radiation heat transfer through integrating interstitial structures, which greatly affect the thermal and energy prediction, have not been considered.

1.3 Research aims and objectives

Concerns over sustainability in the built environment have resulted in continuous efforts to improve the performance of glazing systems and hence indoor comfort and building energy efficiency. Glazing systems integrated with Transparent Insulation Material can potentially result in improved design of building window systems or glazing façades in terms of energy saving and daylight distribution. However, such systems are less well studied. ***The research presented here aims to provide a comprehensive understanding of glazing systems integrated with TIMs and investigate their performance in the context of their application to buildings.***

To achieve the research aim, the following objectives are mapped out:

1) To understand the thermal and optical behaviours of TIMs as well as the benefits of applying them to buildings, a literature review of key types of TIMs were completed. With respect to developing a clear picture of how to accurate describe the thermal and optical characteristics of the with systems integrated with TIM, experimental and numerical methods to characterise their thermal and optical features were also reviewed.

2) To obtain the thermal characterisations of the glazing system with TIM, a validated Computational Fluid Dynamics models was used. The CFD model was validated by an experimental test in a climate chamber.

3) To predict the optical characterisations of the glazing system with TIM and formatted these into *BSDF* data, a ray-tracing technique was used. A comprehensive picture of daylight performance when applying window systems with TIMs was also conducted accompanied with dynamic building daylight metrics

4) In addition to the originality of evaluating the thermal and optical performance of a glazing system with specific types of Transparent Insulation Material, this research also developed a comprehensive model, in which all the characteristics obtained from original thermal and optical evaluations are input into building performance simulation tools to improve the accuracy of building energy and daylight performance estimates, when TIMs are applied within the window of a typical office under various environmental conditions.

1.4 Thesis structure

The thesis structure is outlined in Figure 1-2.

Following by a brief introduction, Chapter 2 reviews various TIMs and their application in buildings. The literature review reveals that integrating TIMs within building windows or glazing systems has seen significantly little. Parallel Slat Transparent Insulation Material (PS-TIM) was proposed as a further strategy that could potentially provide a balanced improvement in terms of both increased thermal resistance and adjusted solar and daylight admittance.

In Chapter 3, the thermal and optical investigation methods to evaluate glazing systems with complex interstitial structures as well as the numerical prediction methods to explore the performance of applying these complex glazing systems are reviewed. Such research provides methods applicable for reference to resolve similar problems in the window system with TIMs

In Chapter 4, a 2-D CFD model was used to solve the dynamic thermal conductance of different configurations of PS-TIMs induced by variations in environmental conditions. This CFD model was validated by an experimental

investigation of window systems with interstitial Venetian blind undertaken in a large climate chamber. Detailed investigations of the PS-TIM on the reduction of convective and radiative heat transfer were studied in detail.

In Chapter 5, the optical properties (i.e. *BSDF*) of various PS-TIMs were obtained via a ray-tracing technique based on the structures' geometries and the material optical properties of the interstitial structure. This method defines the directional distribution of each flux, which is essential for accurately predicting of illuminous environment in a space when applying PS-TIM in the building windows.

In Chapter 6, the detailed dynamic annual daylight performance (i.e. *useful daylight illuminance, daylight glare probability* and etc.) of applying various PS-TIMs were predicted using RADIANCE. The influence of slat pitch (the distance between neighbouring slats), slat tilt angle, as well as the optical performance of the slat material itself for the PS-TIMs were also investigated.

In Chapter 7, a comprehensive model was developed, in which the thermal characterisations obtained from original Computational Fluid Dynamics simulation and BSDF data obtained from a ray-tracing calculation were input into the building performance simulation tool EnergyPlus to obtain building energy and daylight performance estimates. RADIANCE simulation results for daylight performance was also used as a supplementary analysis for the prediction. The energy performance of a building (i.e. heating, cooling and lighting energy consumption) when applying glazing system with PS-TIM was predicted.

Finally, the chosen PS-TIMs have also been investigated under different climate conditions and different building orientations to provide an indication of how site-specific variables influence their daylight and energy performance in Chapter 8.

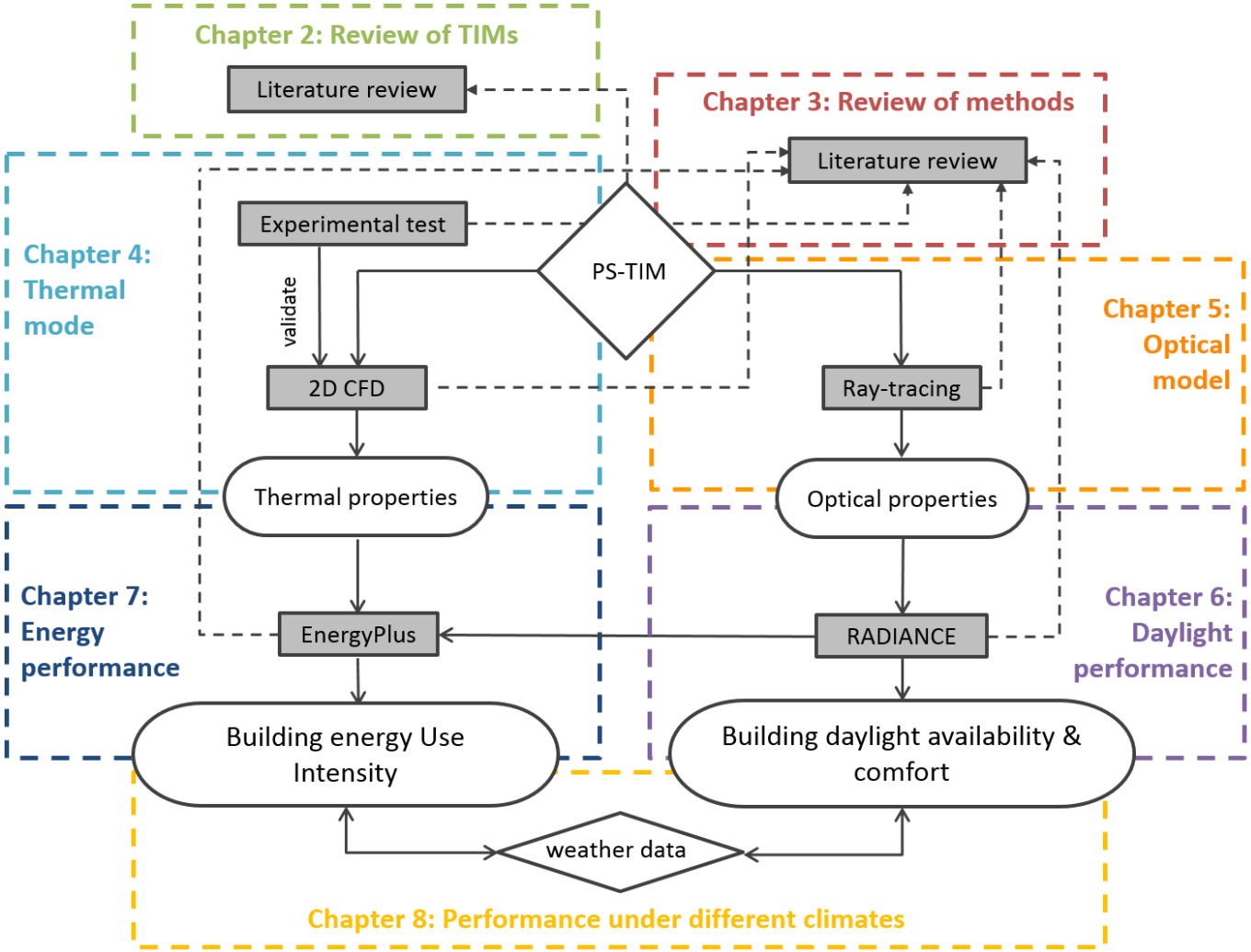


Figure 1-2: Disciplined structure of this thesis

Chapter 2. Transparent Insulation material: A Literature review

2.1 Introduction

Buildings currently account for over 40% of total energy consumption in developed countries. The design and specification of the building envelope is a major determining factor for energy use in any building. Along with an increased expectation for indoor comfort, the performance of building envelopes has seen gradual improvement over a period of several decades. Transparent Insulation Materials (TIM) are helping to sustain these improvements as when integrated into glazing systems these can reduce heat loss by providing high thermal resistance while effectively transmitting solar energy [46].

This chapter introduces key types of TIMs and describes their characterisation in terms of both thermal and optical behaviours as well as the benefits that may be realised through their application to buildings.

2.2 Classification

Transparent Insulation Materials are always assembled with at least one transparent cover (e.g. glazing pane). TIMs are generally classified into four categories, according to the structure of the TIM layer and its relation with the glazing cover, as shown in Figure 2-1: (a) glazing-perpendicular structure, (b) glazing-parallel structure, (c) mixed structure and (d) homogeneous structure. There are three typical types of glazing-perpendicular structure: 1) capillary, 2) honeycomb, and 3) parallel slats array [46]. Glazing-perpendicular TIMs (Figure 2-1 (a1)-(a3)) divide the air cavities into small horizontal, linear cells. The cell walls provide additional viscous resistance to the onset of free convection and interfere with the thermal radiation transferred from one pane of the double glazed unit to the other, hence increasing the thermal resistance of the glazing system [47]. Glazing-parallel structures (Figure 2-1 (b)) consist of a number of glass or

plastic layers lying parallel to the glazing panes. Increasing the number of layers reduces heat loss but results in a reduction in solar and visible transmittance due to the increased reflectance and absorbance provided by the additional layers [46]. Mixed TIMs (Figure 2-1 (c)) are combinations of glazing-perpendicular and glazing-parallel structures. This structure can achieve more effective convection suppression than the glazing-perpendicular or glazing-parallel structure with a sacrifice of reduction in light or solar radiation transmittance. Homogenous TIMs (Figure 2-1 (d)) are receiving increasing attention, with recent research into silica aerogel offering a translucent material that can fill in the air cavity of a double glazed unit (Figure 2-1 (d)). The high porosity of aerogels results in a very low thermal conductivity (e.g. 0.005 ~ 0.02 W/mK) [48]. There are two types of silica based aerogels: monolithic silica aerogel (MSA) and granular silica aerogel (GSA). MSA can be clear enough to see through but its high cost and fragility currently limits commercial uptake [49]. GSA has a low solar transmittance (less than 0.5) due to bulk scattering effects and is commonly used in skylights [50, 51]. Currently, the glazing-perpendicular TIMs and aerogels are the most common TIM types receiving attention in the fields of both research and industry.

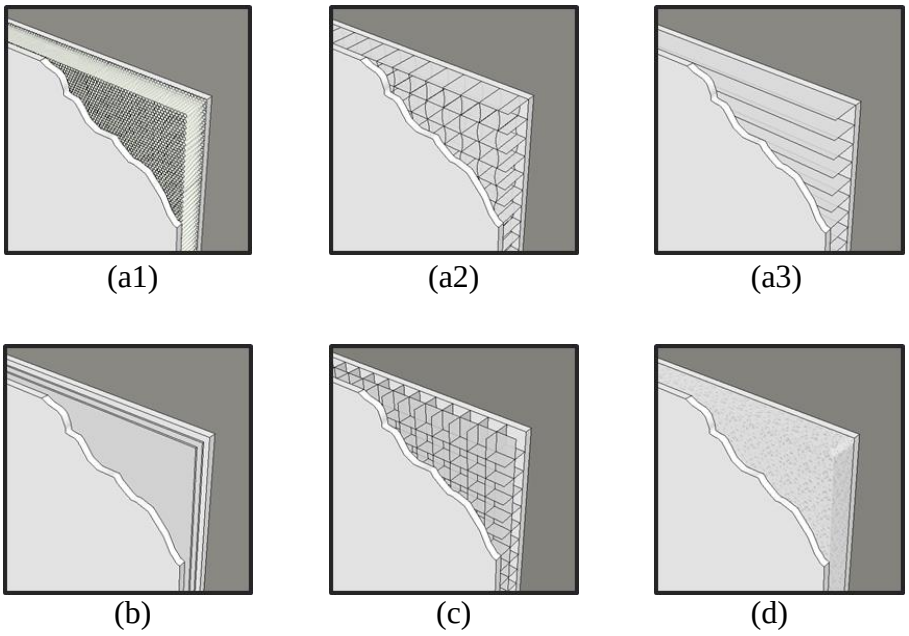


Figure 2-1: Schematic diagrams of typical types of TIMs: a. glazing-perpendicular structure: (a1) capillary structure, (a2) honeycomb structure, (a3) parallel slats array structure; and (b) glazing-parallel structure; (c) mixed structure and (d) homogeneous structure

2.3 Properties of TIM

- **Appearance**

The appearance of a Transparent Insulation Material varies with the structural geometry and the material from which the TIM is constructed. Figure 2-2 shows several typical designs of TIMs with glazing-perpendicular structures and aerogels. Most of the honeycomb TIMs and monolithic silica aerogel are in the main visually transparent, although at certain viewing angles disruption of the scene beyond can occur (see Figure 2-2 (a), (b) and (c)). Other TIMs, such as capillary TIMs and granular silica aerogel, are more opaque in design and in addition only transmit a small proportion of incident solar energy and daylight (see Figure 2-2 (d) and (e)).



(a) (b) (c)



(d) (e)

Figure 2-2: Appearances of five typical TIMs : (a) honeycomb TIM from Wacotech, (b) honeycomb TIM from PANELITE, (c) monolistic aerogel from Technical University of Denmark [43], (d) capillary TIM from Okalux and (c) granular silica aerogel from Lumira.

- **Density and temperature stability**

The density and temperature stability (i.e. the maximum temperature below which the material is stable) of TIMs are also determined by the material from which they are composed, along with their structural geometry. Normally, glazing-perpendicular TIMs with capillary and honeycomb have a density of around 20 ~ 50 kg/m^3 [52]. Table 2-1 illustrates the density, cell size, and maximum resistance temperature of several common TIMs

Silicon dioxide (SiO_2, amorphous quartz) forms the basis of most aerogels and comprise approximately 96% air and 4% open-pored structure of silica [53]. The densities of monolithic silica aerogel lie between 3 ~ 500 kg/m^3 [52]. Those aerogels

used in TIM designed also for effective transmission of solar energy are produced with supercritical drying and have density of between 100 ~150 kg/m^3 [52].

Table 2-1: Physics properties of glazing-perpendicular TIMs [46]

Type	Material	Density (kg/m^3)	Cell width (mm)	Maximum temperature (^{o}C)
Capillary	Polymethylmethacrylate	31	3	90-105
Capillary	polycarbonate	30	3	120
Capillary	polyethylene	18	3	160
Capillary	polytetrafluorethylene	48	3	150
Capillary	polyestercarbonate	30	3	175
Capillary	polyethersulfone	36	3	215
honeycomb	polycarbonate	36	4.2	120
honeycomb	polycarbonate	33	3.4	120

- **Optical properties of TIM**

The optical properties of TIM are determined by the base materials' characteristics (e.g. transmittance, reflectance and absorbance) as well as their geometric configuration (e.g. parallel slat arrays, honeycomb, capillary etc.). The optical properties of various TIMs have been investigated both numerically and experimentally. Numerical models for the optical properties of glazing-perpendicular TIMs have been developed based on radiosity methods, and experimental investigations are typically performed using a spectrophotometer and integrating sphere.

Feland and Edwards [54], Hollands et al. [55], Symons [56], Plazer [57], Kaushika and Padmapriya [58], Plazer [59, 60] and Arulanatham and Kaushika [61] analysed the optical properties of glazing-perpendicular TIMs using numerical simulation. Kaushika and Sumathy [62] summarised the research carried out by Hollands et al. [55], Kaushika and Padmapriya [58] and Arulanatham and Kaushika [61],

stating that the total beam radiation transmittance, $\tau(\theta)$, for TIM arrayed with honeycomb or parallel slats can be expressed as:

$$\tau(\theta) = \frac{\tau_C(\theta) + \tau_E(\theta) \cdot E}{1 + E} \qquad (2-1)$$

where θ is the incidence angle, E is a fraction of the cross-section area occupied by cell wall material; $\tau_E(\theta)$ is transmittance through the wall material; $\tau_c(\theta)$ is the transmittance through the cells, which is calculated by considering the reflection, absorption and the transmission occurred at cell surfaces when solar rays were passing through the cellular TIM. Wong [46] summarised numerical investigation conducted by Symons [56], Plazer [57] and Plazer [59, 60] and concluded that, derived from the summation of all individual rays transmitted or reflected at the cell walls, the $\tau(\theta)$ can be calculated in a simplified form as:

$$\tau(\theta) = [\,\tau(\varphi) + \rho(\varphi)]^n = [1 - \alpha(\varphi)]^n \qquad (2-2)$$

where φ is the azimuth angle; ρ and α are the reflectance and absorbance at the cell wall, respectively; n is the average number of cell wall interactions for the incoming light beam. It is possible to express n using $n = A \cdot tan\,\theta$ for square honeycomb cells and $n = 2A \cdot tan\,\theta$ for circular honeycomb cells, where A represents the width and the diameter, respectively.

In order to validate the theoretical predictions of $\tau(\theta)$, Symons [56], Plazer [57], and Plazer [59, 60] studied by using a spectrometer and an integrating sphere. A detailed analysis of this experimental method can be found in section 3.3.1. Wong et al. [46] concluded that the experimental results support the results from numerical calculation. The $\tau(\theta)$ of honeycomb, parallel slat and V-slat TIM for incidence angle (θ) in the range of 0 ~ 60° is higher than 0.9 as shown in Figure 2-3.

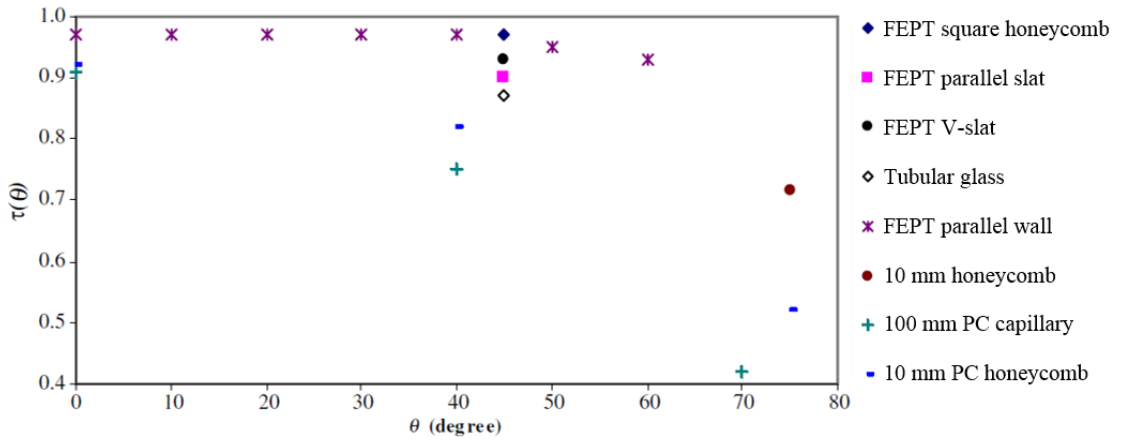


Figure 2-3: Comparison of experimental results of angular dependent transmittance: *τ(θ)* for FEPT square honeycomb, FEPT parallel slat, FEPT V-slat and tubular glass [56], FEPT parallel wall [57], 100 mm honeycomb [59] and 100 mm PC capillary and 100 mm PC honeycomb [60] (adopted from [46])

Buratti and Moretti [51, 53, 63] have also conducted a series of experimental measurements for both light and solar transmittance of various aerogels (i.e. MSA and GSA) by employing a spectrophotometer (shown in Figure 2-4 (b)) along with an integrating sphere (shown in Figure 2-4 (c)) which is used to detect the diffused light transmitted through the TIM sample. The measured wavelength dependent transmission coefficient of MSA on its own and aerogels sandwiched within double glazed units is illustrated in Figure 2-4 (a) [53]. Monolithic aerogel has competitively high transmittance in the near-infrared wavelength range when compared with float glass. The results also show that there is a difference between the measured total transmittance determined using an integrating sphere and the measured direct transmittance without the use of an integrating sphere, thereby confirming the diffuse nature of aerogel.

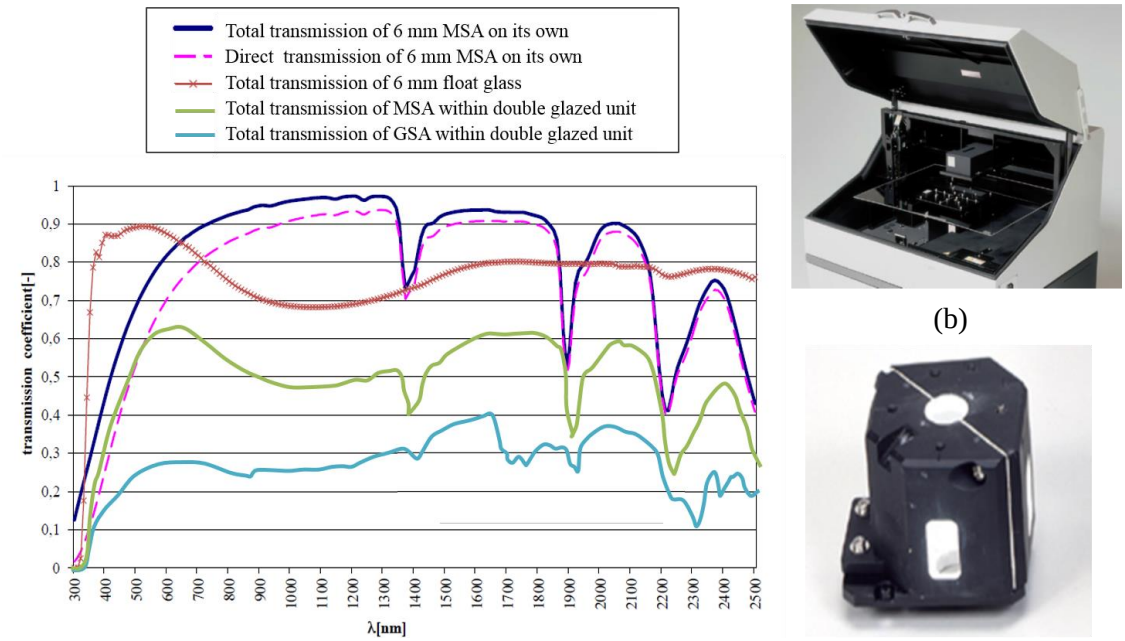


Figure 2-4: Experimentally measuring the optical properties of TIMs: (a) Measured total or direct transmission coefficient vs. wavelength of float glass, MSA on its own, MSA and GSA with double glazed units, (b) the spectrophotometer and (c) the integrating sphere (adopted from [53])

- **Thermal properties of TIM**

The thermal behaviour of glazing-perpendicular TIMs has been investigated both numerically and experimentally. Numerical methods based on finite difference models as well as hot-plate and hot-box experimental methods are the most commonly used methods to explore heat transfer within a TIM.

Numerical studies were primarily used to provide a detailed understanding of the convective, conductive and radiative heat transfer within TIMs [18-21]. Arulanantham et al. [18] used a finite difference method to explore the convective stability of horizontal and inclined air cavities enclosed by square honeycomb and concluded that convection suppression was affected by aspect ratio (A=L/d), thickness of cell wall material (δ) and the inclination of cells (β) as shown in Figure 2-5. Kaushika et al. [19] reported that a honeycomb structure offered better thermal performance for glazing units installed in a horizontal orientation but when units are inclined to more than 30 °to horizontal, parallel slat structures showed better thermal performance. Kumar and Kaushika [20] found that

honeycomb structures with aspect ratios in the range between 10 ~ 15 were suitable for convection suppression in air cavities of depth 5 ~ 20 cm for temperature differences between 20 ~ 120 °C. Arulanantham and Kaushika [21] numerically studied the combined conductive and radiative heat transfer through a honeycomb structure in a solar collector and stated that the heat loss coefficient was determined by the interaction between emissivity of honeycomb cell material and plate type of the collector in which the honeycomb was employed.

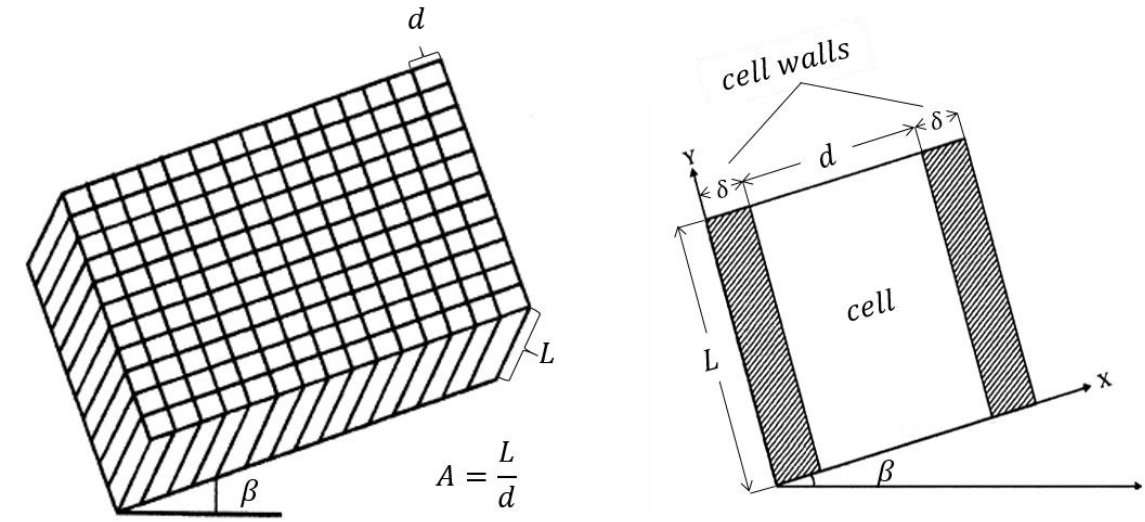


Figure 2-5: Schematics of (a) square homeycomb (b) section of a square homeycomb cell (adopted from [20])

Experiments have also been conducted to measure the thermal conductance of TIMs [22, 59, 64, 65]. In order to evaluate the thermal conductance of capillaries TIMs with various thickness under different tilt angles, a hot-plate apparatus that consisting of a hot (i.e. 230 °C) and a cold (i.e. 5 ~ 60 °C) copper plate, heat flux meters and temperature sensors were utilised by Goetzberger [65] and Platzer [59, 64]. The thickness of TIMs varied from 10mm up to 120 mm and the tilt angle within the range from 0 ~ 180°. They also used the experimental result to validate their numerical calculation and an approximate 3.6% deviation between them were found, when the TIM is tilted within the range of 0 ~ 55°. Suehrcke et al. [22] also used a guarded hot-plate

apparatus to measure the heat transfer coefficient (h_t)across TIMs with both corrugated sheet and honeycomb structure, which are made from cellulose acetate (CA) film with an emissivity of 0.65. They concluded that 30 mm thick CA honeycomb, which had h_t of 3.51 ±0.20 W/m^{2}K, is more effective than 30 mm thick corrugated sheet, which had h_t of 4.02 ±0.20 W/m^{2}K, in reducing heat loss. They also compared their heat transfer coefficients gained from hot-plate measurement with that of numerical simulation, and the results agreed well with a difference less than 3%.

Buratti and Moretti [51] used a hot-box apparatus to investigate the thermal transmittance of window systems integrating monolithic aerogel and granular aerogel and revealed that the windows tested with monolithic silica aerogel offered a lower U-value (0.63 W/m^{2}K) than granular aerogel (1W/m^{2}K).

- **Acoustic properties**

There is a small amount of research exploring the acoustic performance of aerogel based TIMs. It has been determined that window systems with granular aerogel have more efficient acoustic insulation compared with a conventional window system [53]. The measured reduction index, R, of windows integrated with aerogel is higher than that of a conventional window in the range of 100 ~ 2000 Hz as shown in Figure 2-6.

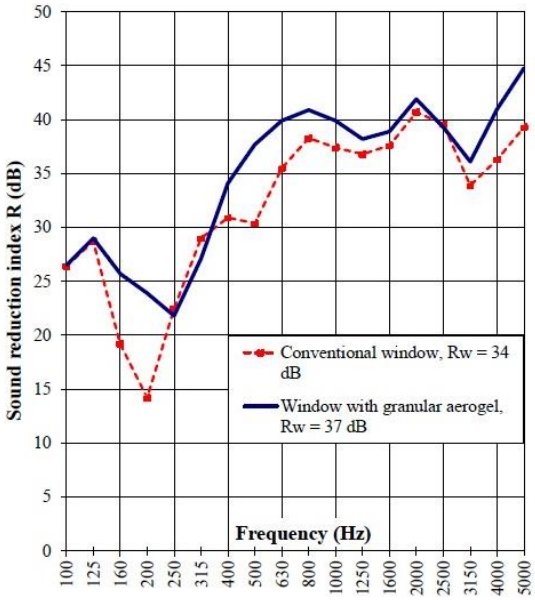


Figure 2-6: Sound reduction index (R) values for the conventional window and the window integrated with aerogel vs. frequency (adopted from [53])

2.4 Applications of TIM in building

There are three main ways to apply TIM in buildings: the first, as well as being the earliest application, is utilising TIM under the front glass cover of a flat-plate solar collector; the second method, which is most often referred to as a solar wall, is using TIM in front of a thermal mass wall or a thermal mass roof; and the third method is utilising TIM in the air cavity of a window system or glazed fa çade. The configurations of these applications are presented in Figure 2-7.

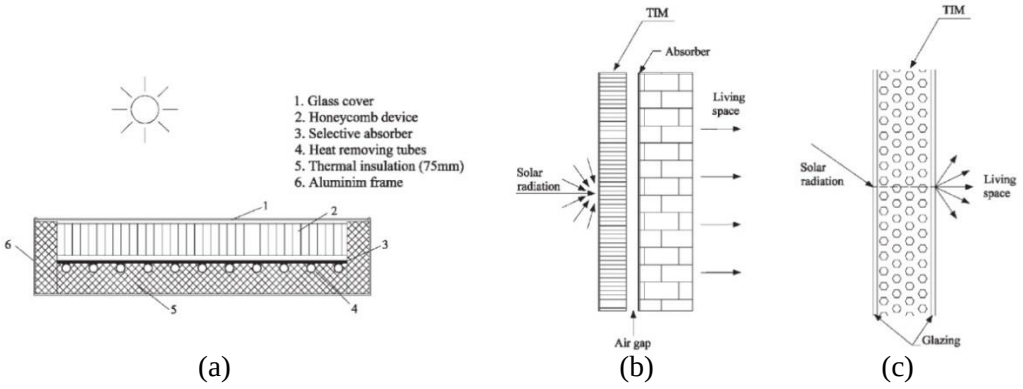


Figure 2-7: Configurations of applying TIM: (a) in flat-plate solar collectors, (b) in solar wall and (c) in window system or glazing fa çade (adopt from [62]).

- **Application of TIM in flat-plate solar collector**

Since the 1960s, researchers have primarily focused on the application of honeycomb structures in solar absorbers as a convection suppression device [66-68]. This has involved theoretical and experimental research on the application of plastic/glass honeycombs and has been expanded to capillaries as well as silica aerogel to flat-plate collectors [56, 65, 69-72]. A coefficient, named the effective transmittance-absorbance product ($\tau\alpha_e$), taking into account both transmission τ of the glass cover and absorption α of the absorber, was used to characterise performance. Wong [46] concluded that the value of ($\tau\alpha_e$) decreases with increase of incidence angle; as a result, there is a negative influence on the optical performance of the solar collectors [46]. A comparison of ($\tau\alpha_e$) at various incidence angles θ for flat-plate solar collectors is shown in Figure 2-8.

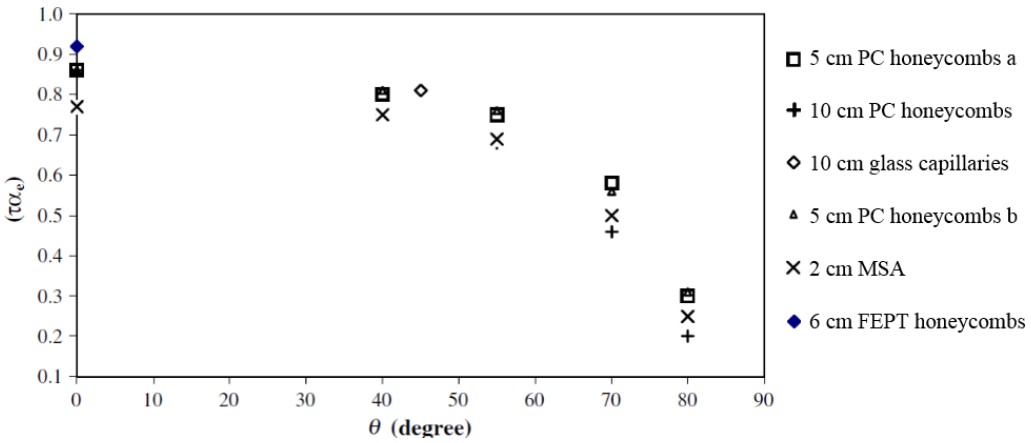


Figure 2-8: Comparison of the ($\tau\alpha_e$) at various incidence angle (θ) for flat-plate solar collectors with 5 cm PC honeycombs a, 10 cm PC honeycombs, 10 cm glass capillaries [69], 5 cm PC honeycombs b [70], 2 cm MSA [71] and 6 cm FEPT [73] (adopted from [46])

For the honeycomb and capillary TIMs made of plastic or glass, Symons [56] stated that the working temperatures of the solar collectors using TIMs could be increased from 90 °C to 150 °C. Rommel and Wagner's research [69] revealed that honeycomb TIM could offer a thermal conductivity of 0.9 W/mK for the cover system at a temperature of over 80 °C. For TIM with silica aerogel, Nordgaard and Beckman's

research [71] showed that the flat-plate solar collector with the integration of MSA could achieve an efficiency of more than 60% at a temperature below 80 °C, the annual energy gains were increased by 41%.

As mentioned above, when a flat-plate collector is integrated with TIM, its thermal efficiency is significantly improved, thus the system is comparable to a vacuum tube collector [62]; however, some issues also occurred, such as fragile and bulky nature of TIMs with glass as the structural material, lower stagnation temperature of TIMs with plastic structural material etc. [62].

- **Application of TIM in solar wall**

Applying Transparent Insulation Material in front of a concrete or masonry wall (Figure 2-7 (b)) allows solar energy to be transmitted and stored in the thermal mass while simultaneously reducing the heat loss back out through the front surface. The combination of TIM and thermal mass was originally reported by Kaushika et al. in 1987 [74]. The system they investigated was integrated into a roof and made use of a square cell, air filled honeycomb slab laid on the top of a blackened absorber and concrete slab for thermal storage. The honeycomb slabs were made of 0.076 mm thick lexan films or 1 mm thick acrylic sheets. In their study, $\tau(\theta)$ was calculated and found to be greater than 0.9 for TIM made from lexan film and 0.6 for TIM made from acrylic sheet. Their results showed that with the presence of honeycomb slabs, the heat collection efficiency of the roof had been significantly improved and the heat loss during night time had been considerable reduced [74]. In their later research of applying the same systems under Boulder, USA's climate, a positive solar gains can be achieved for more than 10 hours during a typical winter day when the thickness of honeycomb was 15 cm [75].

The IEA Solar Heating and Cooling Programme, Task 20 [76, 77] stated that the TIMs have been used as part of solar wall heating systems integrated has been used as part of building renovations throughout Europe. The programme also put forward the suggestion that shading devices and forced ventilation should be applied to these systems in order to avoid overheating problems during summer. Braun [78] tested the performance of demonstration projects through the use of both experimental and numerical methods to explore the space heating potential of south-facing transparently insulated massive walls. In these projects, the transparent insulation applied on these projects were capillaries and honeycombs. The investigation results showed that this passive solar façade system can potentially save 200 kWh/m^2 per year. The difference between the measured and calculated temperatures of the absorber and inside wall was found to be less than 5 °C. Athienitis and Ramadan [79] developed an explicit finite difference model to simulate the thermal performance expected when applying 48 mm plastic transparent honeycomb (square cell) on a south-facing concrete wall, combined with a shading device and forced ventilation. The application of TIM to a building with a high resistance envelope reduced the heating demand to zero on a clear day with minimum outside ambient temperatures of -20 ℃ under a Canada climate. The results also showed that the air circulation enhanced the heat transfer and succeeded in maintaining room temperature to an acceptable value. Wallner et al. [80] developed a TIM based on a novel polymer film that can be easily installed on a façade. Their practical experience of applying 30 m^2 of this system to the south facing wall of well insulated test house showed that solar energy efficiency of 44%, U-value of 0.76 W/(m^2K) and heat fluxes of up to 50 W/m^2 could be achieved on cold sunny days.

Solar walls using Phase Change Materials in place of traditional concrete or masonry walls have been investigated by a number of researchers. Manz et al. [81]

conducted both experimental and simulation studies on a prototype TIM-PCM wall in Zurich, Swiss climate. A layer of 12 mm PMMA capillaries was applied in a double-glazed window in front of PCM in a glass container. The spectral direct-hemispherical transmittances of two PCM samples were measured. The predicted performance of the TIM-PCM system in the month with lowest irradiation (December) showed that only 1% of the time has energy losses through the façade. Heim [82] also conducted simulation studies using ESP-r software to investigate a TIM-PCM wall on a south façade concluding that this design could reduce the temperature fluctuation of inside surfaces. Wong et al. [43] investigated the application of 22 mm PMMA capillary TIM in solar walls on a south facing façade of high-rise and low-rise office buildings. Their simulation results for a full calendar year showed that the room temperature swing during the daytime was reduced. The TIM solar wall was shown to offer a good potential to reduce heating energy load during heating period; but overheating problems might exist in cooling period.

- **Application of TIMs for glazing systems**

Transparent Insulation Materials when used in windows have the potential to significantly reduce heat loss while also maintaining light and solar transmittance. Moreover, the use of TIMs can result in a more homogeneous internal daylight distribution thereby improving visual comfort levels. Thus, applying TIM in window or glazed façade systems can result in a reduction in both lighting and space heating energy consumption. However, TIM window and glazed façade systems have not been as extensively researched as TIM for solar collector and solar wall applications.

Twidell et al. [83] monitored a building for a period of three years in order to investigate performance following the application of a TIM glazing system on the south façades of two blocks of five-storey university residential buildings in Glasgow, UK.

The system consisted of a 100 mm thick layer of honeycomb with 3 mm square cells, encapsulated by an external glass layer. The results showed that during the wintertime there was 40% less energy consumed as compared with the "good" category rating in UK's official indicators over. The financial savings in heating energy cost was 30% less than current and the systems offered a 20 year payback period.

Lien et al. [84] researched the performance of glazing with capillary TIM in terms of daylight distribution, appearance and visual contact as well as energy consumption when applying capillary TIM to terraced houses. In their research, the daylight distribution performance was tested through scale models using artificial light. The profiles of daylight distribution at different incidence angles (representing four different times of day for equinox at a latitude of 63 °N) for window with and without TIM are presented in Figure 2-9. Compared with clear glass, the light transmitted through the capillary TIM is more evenly distributed through the room showing an absence of any obvious sun patches observed in the room with conventional glazing. The comparison also shows that incoming light from a lower altitude spreads the light over larger areas, and also deeper into the room. The researchers also conducted a computer simulation using SUNCODE, applying a capillary based TIM of various thicknesses (35 mm, 100 mm and 200 mm) to the south façades of dwelling houses. The results revealed that replacing part of a traditional south wall with a TIM integrated façade (i.e. 5 m^2 TIM glazing plus 0, 15 or 25 m^2 TIM solar wall) saves between 16 ~ 20% of heating and lighting energy. Overheating risks were also predicted but could be mitigated if the ventilation rate was increased. Lien et al. [84] also described the visual features of their capillary TIM, and highlighted that the visual contact is both limited and disrupted, the extent being related to the thickness of the TIM, as well as the distance and angle from the viewpoint. Increasing the distance from the viewpoint to the TIM

provides a larger range of vision, whereas increasing the thickness of capillary TIM decreases the range of vision. Larger diameter capillaries also result in a larger transparent area. It was found that if the capillaries have a diameter of less than 1mm, nothing can be seen through the material, which instead appears to be fairly white in colour.

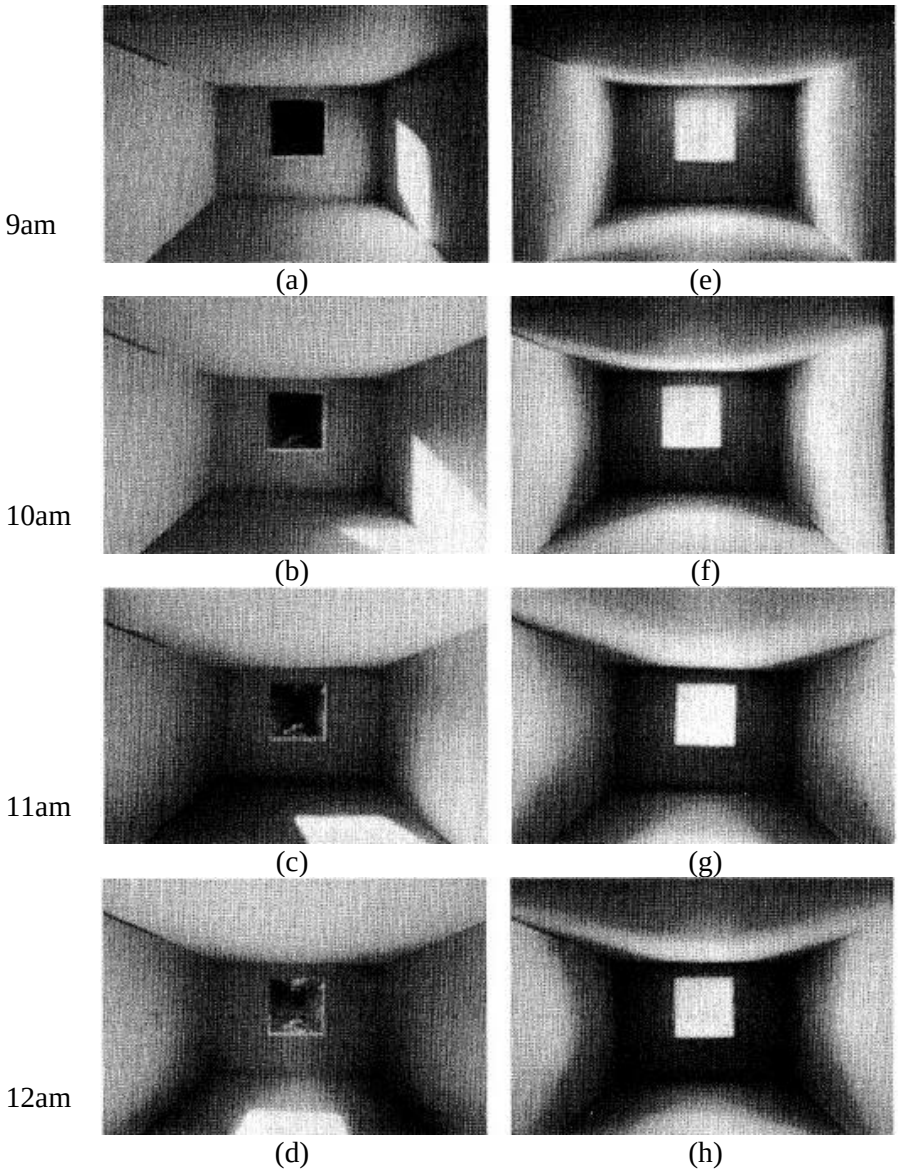


Figure 2-9: (a)-(d) Sunlight distribution through clear glass at equinox in Trondheim, at 63° N; (e)-(h) Sunlight distribution through 35 mm capillary TIM at equinox in Trondheim, at 63 ° N [84]

Bahaj et al. [85] investigated the energy performance of a high-rise commercial building in Dubai where an aerogel glazed façade was used to replace conventional

glazed fa çade. It was found that the aerogel glazed fa çade could reduce air conditioning demands by approximately 17%. When the aerogel glazing was combined with a reflecting component- holographic optical elements HOE) incorporated in the glass laminate- air conditioning savings of approximately 26% were achieved.

Wong et al. [86] conducted a building energy performance prediction using ESP-r software to explore the use of a TIM wall and/or TIM glazing on south facing fa çades of retrofitted high-rise and low-rise office buildings in London, UK. The simulation results for a full calendar year revealed that applying TIM reduces the temperature swings during the daytime. Furthermore, the TIM also has the potential to reduce heating energy load during winter and reduce overheating problems during summer when applied in conjunction with brick wall mass, overhangs and natural ventilation.

2.5 Relative research gaps and industrial development of TIMs

The light and solar transmittance and thermal properties of TIMs have been studied both experimentally and theoretically. However, most of the fundamental studies of thermal and optical characteristics of TIMs focus on their application in solar thermal collectors. Integrating TIMs within building windows or glazing systems has seen much less research. The conditions experienced by a window that incorporates TIMs are distinct from those in solar collector applications, as the working temperature, the pattern and intensity of natural convection within the structure as well as the requirements of light transmittance and vision are completely changed.

In order to apply TIM on buildings, their thermal performance and efficiency, as well as the heating and cooling energy conservation potential have been monitored in physical buildings while also predicted using building simulation tools. A particularly important issue that complicates the application of TIM is the problem of overheating

during summer. Various strategies have been proposed in order to solve the issue of overheating, including mechanical shading devices, forced ventilation and the addition of spectral selective or thermotropic layers. However, a holistic analysis of the energy efficiency of TIMs subjected to varying climate conditions has not yet been conducted.

Furthermore, the daylight performances of TIM applied in buildings has still not been thoroughly researched, analysed and discussed. Daylight studies of this sort of analysis (i.e. temporal variation of luminance level at working plane, glare etc.) for other emerging glazing fa ̧ade systems such as semi-transparent PV and electrochromics glazing can be found within the literature.However, only Lien et al. [84] has undertaken a scale model experiment in order to predict the daylight distribution properties for capillary TIM. Their experimental investigation revealed that the capillary TIM could contribute greatly to the uniform of daylight distribution and reduce the obvious contrast of the direct light patch and its adjacent areas; however, this research is far from rigorous and insufficient for predicting the daylight performance of applying window with TIMs under realistic time varying climate conditions.

In recent years, Transparent Insulation Material has become a commercially interesting product. Various companies that have connections to the glass industry or related fields, for example OKALUX, Panelite, Lumira and Wacotech, have manufactured and launched a range of TIMs. The most common TIMs used in the commercial market are honeycomb, capillary and granular aerogel. However, the TIM market is still very limited. The obstacles of large-scale marketisation of TIM include restricted access to information [87], imperfections associated with the manufacturing process, and the relatively high costs involved.

2.6 Summary of TIMs' current research status and selecting Parallel Slat Transparent Insulation Material (PS-TIM) in this research

It is clear that TIMs have a role to play in improving the thermal resistance of building envelopes, adjusting solar gains and affecting daylight performance. These areas of behaviour influence the environment and energy performance of any space separated from the external environment by elevate working TIMs. Developing the current understanding of these individual performance criteria beyond its current state would assist significantly in developing holistic models that permit a more realistic picture of the nature of the environment and energy demand of buildings integrating TIM.

Although, applying TIMs has been proven to effectively reduce heat losses and improve the efficiency of solar collectors [18-22], relatively few studies exist regarding the thermal and optical performance of TIMs contained within the cavities of double glazed windows. This leads to an uncomprehensive prediction for TIM's window application, as the fundamental thermal and optical characteristics of TIMs integrated within building windows or glazed façades are entirely different from their application in solar thermal collectors. Among all these 4 categories of TIMs (i.e. glazing-perpendicular structure, glazing-parallel structure, mixed structure and homogeneous structure), the homogeneous TIMs, i.e. aerogels, and glazing-perpendicular TIMs are the most common TIM types receiving attention for their applications in building windows in the fields of both research and industry [46]. Either the high cost and fragility of monolithic aerogel [49] or the low solar transmittance of granular aerogel [50, 51] restricts aerogels application in building windows. The glazing-perpendicular structure can be generally classified into three typical types of: 1) capillary, 2) honeycomb, and 3) parallel slats array [46]. Among these, Parallel slat TIM (PS-TIM) is regarded as a

simple but effective structure that offers noteworthy reductions in heat transfer coefficient with least significant sacrifice of solar transmittance [88]. This structure divides the air cavity between two glazing panes into small horizontal, linear cells. The slats themselves are potentially to provide additional viscous resistance to the onset of free convection and interfere with the thermal radiation transferred from one pane of the double glazed unit to the other [47]. The employment of PS-TIM also potentially affects the amount of daylight that transmitted through the window system as well as modifying the daylight distribution within the space it serves. Thus, in this research glazing systems with PS-TIMs were comprehensively investigated in order to provide an indication of how the interstitial TIM structures affect the overall building daylight and energy performance.

Chapter 3. Evaluation methods for complex glazing systems and the daylight and energy performance prediction for their building application: A Literature review

3.1 Introduction

Chapter 2 introduced Transparent Insulation Material in terms of their properties and the relevant characterisation methods, their application in buildings, as well as the current research status along with deficiencies in this field. The application of TIMs has been proven to effectively reduce heat loss of the system that TIMs embodied in. The thermal behaviours of TIMs have been investigated numerically and experimentally: however much of this work focused solely on their application in solar collectors. Relatively few studies exist regarding the thermal and optical performance of TIMs contained within the cavities of double glazing units. Even so, previous researchers have widely studied the performance of using interstitial structures, such as horizontal Venetian blinds, pleated blinds, etc. within the air cavity of a double glazing unit. These structures share many of the same characteristics as TIMs; and hence this body of research provides potential methods for reference tracking similar questions posed in relation to the performance of window systems with TIMs.

In this chapter, the experimental and numerical methods used to evaluate the thermal and optical characteristics of glazing systems with complex interstitial structures are reviewed and summarised. Furthermore, with the determined thermal and optical properties of these window systems, dynamic daylight and energy simulation methods to provide precise building performance predictions are discussed.

3.2 Thermal investigations of glazing system

In this section, the experimental and numerical methods that can be used to evaluate the thermal properties of a building component, with a focus on window systems with complex structures, is introduced and discussed.

3.2.1 Experimental investigation method

There are established international and national standards for measuring the thermal properties (i.e. thermal transmittance, thermal conductance, thermal resistance and U-value) of a window system. The guarded hot-plate, heat flow meter method and guarded or calibrated hot-box methods are three key approaches for measuring steady-state thermal properties under laboratory conditions. For measuring dynamic thermal properties of building components under more realistic environmental conditions, heat flux meters are adopted in the in-situ measurement. The international and national standards for these four methods are listed in Table 3-1.

Table 3-1: Standards of experimental methods

Region	Name	Title	Method
International	ISO 12567 [89]	Thermal performance of **windows and doors** – Determination of thermal transmittance by the hot-box method—Part 1: Complete windows and doors	Hot-box
	ISO 9869 [90]	Thermal insulation – **Building elements**—In-situ measurement of thermal resistance and thermal transmittance Part1: Heat flow meter method	In-situ
	ISO 8990 [91]	Thermal insulation – Determination of steady-state thermal transmission properties—Calibrated and guarded hot box	Hot-box
	ISO 8301 [92]	Thermal insulation - Determination of steady-state thermal resistance and related properties – Heat flow meter apparatus	Heat flow meter
	ISO 8302 [93]	Thermal insulation - Determination of steady-state thermal resistance and related properties - Guarded hot plate apparatus	Hot-plate
USA	ASTM C1363 [94]	Standard Test Method for Thermal Performance of **Building Materials and Envelope** Assemblies by Means of a Hot Box Apparatus	Hot-box
	ASTM C1199 [95]	Standard Test Method for. Measuring the Steady-State Thermal Transmittance of **Fenestration Systems** Using Hot Box Methods	Hot-box
	ASTM C1046 [96]	Standard Practice for In-Situ Measurement of Heat Flux and Temperature on **Building Envelope** Components	In-Situ
Europe	EN 674 [97]	**Glass** in building—Determination of thermal transmittance (U value)—Guarded hot plate method	Hot-plate
	EN 675 [98]	**Glass** in building—Determination of thermal transmittance (U value)—Heat flow mete method	Heat flow meter
	EN 1946-2 [99]	Thermal performance of **building products and components**. Specific criteria for the assessment of laboratories measuring heat transfer properties. Measurements by guarded hot plate method	Hot-plate
	EN 1946-3 [100]	Thermal performance of **building products and components** – Specific criteria for the assessment of laboratories measuring heat transfer properties—Part 3: Measurements by heat flow meter method	Heat flow meter
Russian	GOST 26602.1 [101]	**Windows and doors**. Methods of determination of resistance of thermal transmission	Hot-box

These three steady-state laboratory measurement approaches share the same concept: a fixed temperature gradient is established between two sides of the test sample and the heat flow across the sample is determined. Schematic diagrams for these three approaches are shown in Figure 3-1. The guarded hot-plate apparatus [93, 97, 99] as shown in Figure 3-1 (a) consists of two nearly identical test specimens, a heating unit, located between the specimens and thermally isolated by a guard area, and two cooling units, located on the outer sides of the specimens. A number of temperature sensors equally spaced and thermally coupled to all surfaces are used to determine the average surface temperature at the interfaces between the samples and the heating/cooling units. The DC-power supplied to the heating unit is varied until the desired mean temperature of each specimen (i.e. 10 ± 0.5 °C) and the desired temperature difference between the hot and cold surfaces of the specimens (i.e. 15 ± 0.5 K) are achieved. The measured DC-power is then used to determine the thermal transmittance through the specimen. As shown in Figure 3-1 (b), the heat flow meter measurement method [92, 98, 100] is similar to that of the hot-plate method, as the specimen is sandwiched between heating and cooling units. Instead of measuring the supplied DC-power, the heat flow densities (in W/m^2) are measured using calibrated heat flux meters coupled to the surfaces of the specimen, once the desired mean temperature of each specimen (i.e. 10 ± 0.5 °C) and the desired temperature difference between the hot and cold surfaces of the specimens (i.e. 15 ± 0.5 K) are achieved. The measured heat flow density is then used to determine the thermal transmittance through the specimen. By selecting a sample with sufficient lateral extent and focusing the measurement in the central region it may reasonably be assumed that a one dimensional pattern of heat flow is present and effects due to the presence of non-uniform conditions at the sample edges may be neglected.

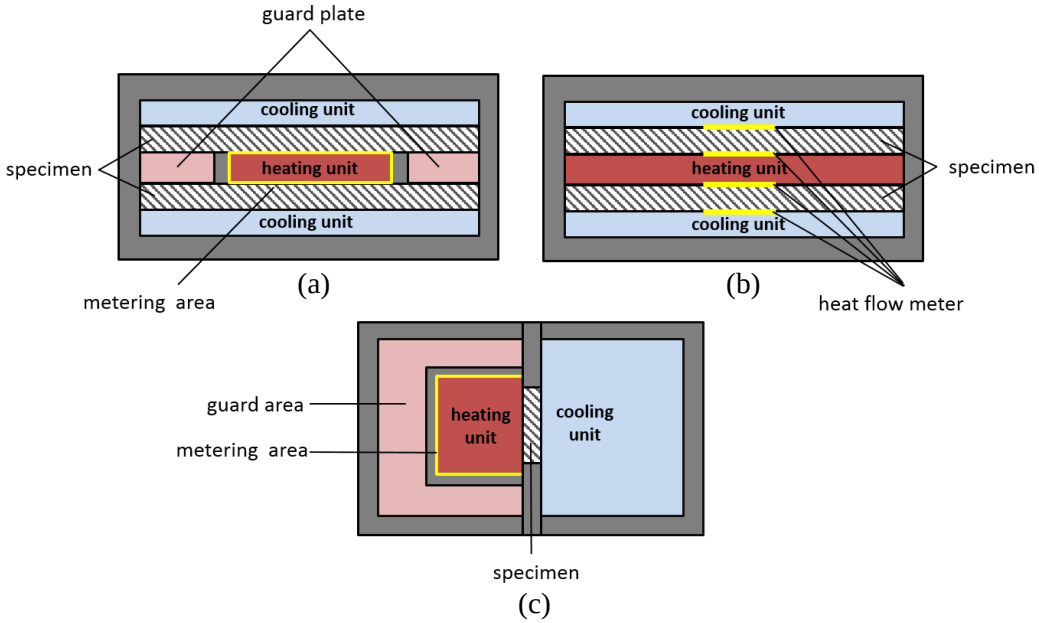


Figure 3-1: Steady-state thermal properties laboratory measurement method (a) hot-plate method, (b) flow meter method and (c) hot-box method

The hot-plate and flow meter methods are suited to characterising homogeneous material, such as single glazing, insulation materials etc. Goetzberger [65] and Platzer [59, 64] Suehrcke et al. [22] used hot-plate method to measure the thermal characteristics of various Transparent Insulation Materials. When facing the issue of measuring the overall heat transfer through large, inhomogeneous structures, such as glazing with frames or shading devices, the hot-box method [89, 91, 94, 95, 101] is better suited and more widely used [102]. In this apparatus (Figure 3-1 (c)), the specimen is mounted between two chambers that are kept at stable hot and cold conditions. The hot chamber serves as a guard to a metering box, which is mounted over the test sample. By maintaining equal temperatures in these two spaces, all the heat supplied to the metering box is assumed to be transmitted through the sample. Measurement of the energy supplied to the metering box is then used to determine the thermal transmittance of the sample[103]. Fang [104] studied the centre-of-glass U-value of a window with high-reflectivity Venetian blinds by using this guarded hot-box configuration. The influence of the blind's slat slope-angles on U-values was evaluated and an empirical correction factor for the window U-value and correction coefficients for window frames and

outdoor wind velocity were proposed. Baidinelli and Bianchi [103] used a hot-box apparatus to measure the thermal conductance of windows with wood and aluminium frames. Fang et al. [105] made comparative tests of flat vacuum glazing systems between guarded hot-box measurements and finite element model simulations, The resulting flanking loss, overall heat transfer coefficients and mean surface temperatures showed good agreement. Chen et al. [106] conducted hot-box measurement under summer conditions for double glazed units with and without embedded semi-transparent thin-film photovoltaics. The experimental results for a double glazed unit revealed a difference of less than 5% when compared with simulation results obtained by using WINDOW and THERM software. Asdrubali and Baldinelli [107] compared three hot-box methods according to ISO 8990 [91], ASTM C1363 [94] and GOST 26602.1 [101] respectively. The results revealed that ISO 8990 and ASTM C1363 are very similar since they only measured the total heat transfer through the specimen; while GOST 26602.1 measured individual thermal characteristics of each component of the specimen, giving more information on the weaknesses and strengths of these components.

The method to obtain the dynamic thermal properties of building components uses thermocouples and heat flux meters to measure both the temperate gradient between any two surfaces of building components, as well as the heat transfer rate through them, on site where they are situated [90, 96]. There are however, various factors that can significantly affect the accuracy of the measurements taken. These include the type and quantity of sensors used, component location, and extreme ambient conditions. There are also some challenges that are out of direct control during measurement, such as seasonal weather, wind speed and radiant energy from the sun, which can make measurements impractical.

3.2.2 Numerical investigation method

The numerical investigation of the thermal properties of window systems can be classified into two major groups: 1) one-dimensional calculation based on standard calculation methods and 2) two- or three-dimensional simulation using finite element or finite volume models.

3.2.2.1 Standard calculation method

Standards describing the centre-of-glazing thermal behaviour of window system includes International Standards ISO 10292 [108] and ISO 15099 [109] and European standard EN 673 [110].

Under these standards, the centre-of-glazing U-value, which is the reciprocal of total thermal resistance consisting of internal and external surface thermal resistance and the thermal resistance of the glazing unit, can be described by the following equation:

$$U = \frac{1}{R_t} = \frac{1}{R_{se} + R + R_{si}} = \frac{1}{\frac{1}{h_e} + R + \frac{1}{h_i}} \qquad (3-1)$$

where, h_e and h_i are the external and internal heat transfer coefficients, respectively. R, which is the total thermal resistance of the glazing unit can be described for double glazing using the following equation:

$$R = \frac{1}{h_r + h_g} + 2\frac{d}{k_p} \qquad (3-2)$$

where d is the thickness of each glass pane, k_p is the thermal conductivity of each glass pane (W/m K); and h_r and h_g are the radiation conductance between two glass panes and the thermal conductance of air cavity, respectively.

According to the empirical equation mentioned in EN673 [109], the radiation conductance h_r is given by:

$$h_r = 4\sigma \left(\frac{1}{\varepsilon_1} + \frac{1}{\varepsilon_2} - 1\right)^{-1} T_m^3 \qquad (3-3)$$

where σ is the Stenfan-Boltzmann's constant, T_m is the mean absolute temperature of the gas space, ε_1 and ε_2 are the corrected emissivities of the surfaces bounding the enclosed space between the panes at temperature T_m.

The thermal conductance of the gas in the cavity is given by:

$$h_g = Nu \frac{k_g}{s} \qquad (3-4)$$

where *s* is the thickness of the air cavity, k_g is the thermal conductivity of the air space, and the Nuseelt number *Nu* is given by:

$$Nu = Const.(Gr \cdot Pr)^n \qquad (3-5)$$

where *Const.* is a constant and n is an exponent that make it possible to account for the orientation for he glazing. For vertical glazing these are 0.035 and 0.38 respectively [109]. The *Grashof number Gr* and the *Pradndtl number* are given by:

$$Gr = \frac{g\beta\Delta T s^3}{v^2} \qquad (3-6)$$

and

$$Pr = \frac{c_p \mu}{k_g} \qquad (3-7)$$

When calculating the *U-value* for the whole window component, including window frames and/or shading devices, international standards ISO 15099 [109], European standards EN 10077-1 [111], EN 10077-2 [112], American standards NFRC 100-2010 [113] and ASHRAE standard [114] provide detailed guidance. Blanusa et al. [115] compared the differences between the ASHRAE calculation method and ISO

15099 method, emphasising that small differences exist between the calculated thermal transmittance values produced by these two methods.

3.2.2.2 Numerical models

Apart from experimental measurement and standard equation calculation methods, finite element or finite volume simulations are the most common approach used in order to obtain the thermal properties of window systems, especially when the air flow pattern in the cavity is of particular interest.

Computational Fluid Dynamics (CFD) tools have been used by researchers to solve the heat transfer problem and explore the air flow pattern in the vertical air cavity of conventional double glazed unit [116-120]. Zhao et al.[116] Wright et al. [118] and Ganguli et al. [119, 120] used a finite volume method to study natural convection in the cavity of double glazed units. They concluded that with an increase of temperature difference across a double glazed unit, multi-cellular flow developed, which tends to increase the convective heat transfer coefficient. There has been some work undertaken to investigate the possibility of reducing free convection by integrating shading devices, such as horizontal Venetian blinds, pleated blinds and different configurations of fins [4, 25, 26, 29, 30] into the cavity of double glazed units. Some of these models have been validated by temperature field visualization obtained by interferometry [23, 27, 28]. However, in most of these studies, long-wave radiation heat transfer, which accounts for two thirds of the total heat transfer across the air cavity [117], is neglected in the numerical modelling. Although improved simulation methods have been implemented by Avedissian and Naylor [29], who used a surface-to-surface model to include radiation, they only used the model to calculate the *U-value* of the whole system instead of evaluating the specific effects on the internal structure have on long-radiative heat transfer.

3.3 Optical investigations of complex glazing systems

There are two primary ways of expressing the optical properties of window system with complex structure (i.e. interstitial shading devices, TIM etc.) as illustrated in Figure 3-2. The first type merely describes the total amount of direct and diffuse hemisphere transmitted or reflected solar energy or daylight flux. The second is termed a Bidirectional Scattering Distribution Functions (BSDF), which represents the directional qualities of reflected or transmitted solar energy or daylight flux.

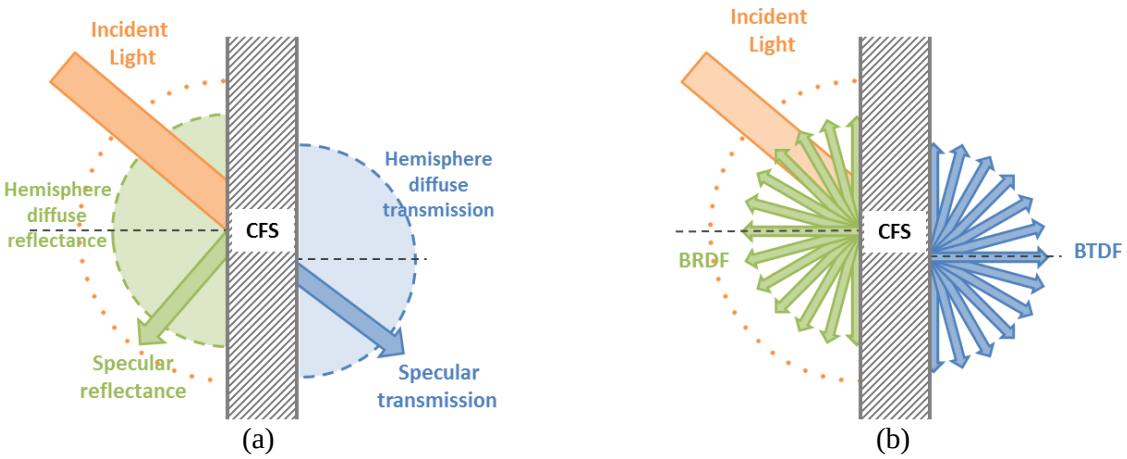


Figure 3-2: Illustration of two types of daylighting analysis method: (a) total amount of direct and diffuse transmittance or reflectance; (b) directional distribution of transmittance and reflectance

Knowing the total amount of transmitted or reflected solar energy through a fenestration system is sufficient for the prediction of solar heat gain. If there is a requirement to retain information relating to the direction of entry of the light to its direction(s) of exit, as the case of daylight distribution calculations, a more sophisticated measure is required.

The following two sections introduce the experimental methods (i.e. spectrophotometer along with integrating sphere or goniophotometer) and numerical methods (i.e. radiosity or ray-tracing) to obtain these two types of measures.

3.3.1 Methods to obtain total amount of transmittance or reflectance

The measurement of transmittance and reflectance of a building component can be obtained using a spectrophotometer along with an integrating sphere. International standard ISO 9050 [121] and European standard EN410 [122] describe the methods used to calculate the light and solar transmittance and reflectance based on the measured spectral transmittance or reflectance data; while the requirements of the measurement apparatus and details of performing optical measurement are described in International Commission on Illumination (CIE) standard [123]. An example of the experimental setup is shown in Figure 3-3 [124].

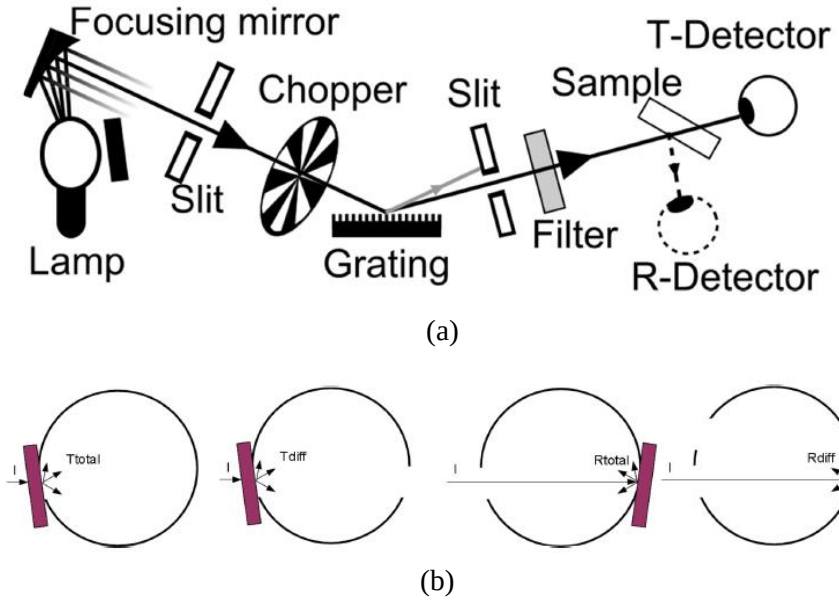


Figure 3-3: The experiment set up of using spectrophotometer and integrating sphere to test transmittance and reflectance (adopted from [124])

As shown in Figure 3-3 (b), an integrating sphere is used to detect the diffuse and the total magnitude of transmittance or reflectance [124]. T_{diff} and R_{diff} are obtained by opening a port and letting the specular component out. T_{spec} is calculated as T_{total}-T_{diff} [124].

Based on the measurement data of light transmittance over a number of wavelength intervals, the overall light transmittance, τ_v, of a glazing component can be calculated using the following equation [122]:

$$\tau_v = \frac{\sum_{380}^{780} D_\lambda \tau(\lambda) V(\lambda) \Delta\lambda}{\sum_{380}^{780} D_\lambda V(\lambda) \Delta\lambda} \qquad (3-8)$$

where D_λ is the relative spectral distribution of light source (e.g. illuminant D65); $\tau(\lambda)$ is the spectral transmittance of the glazing over wavelength interval $\Delta\lambda$ and $V(\lambda)$ is the spectral luminous efficiency for photonic vision defining the standard observer for photometry.

A significant volume of research refers to this methodology in relation to the exploration of innovative glazing materials and window systems in terms of their respective optical performance. Jonsson et al. [125] used a spectrophotometer along with an integrating sphere to measure the transparency and light scattering of antireflection glass coatings and an electrochromic foil. Long et al. [126] and Ye et al. [127] used a UV–visible–NIR spectrophotometer (240 ~ 2600 nm) to measure the spectral transmittance of a thermochromics film (i.e. VO_2). Goia et al. [128], Gowreesunker et al. [129], and Liu et al. [130] investigated the spectral behaviour of glazing systems with different PCM samples using spectrophotometers and integrating spheres. Gao et al. [131] investigated the optical properties (transmittance and reflectance) of glazing units incorporating aerogel granules in the air cavity using a UV/VIS/NIR spectrophotometer (290 ~ 2500 nm) with a 150 mm integrating sphere. Berardi [132] and Buratti and Moretti [51, 53, 63] measured the optical behaviour of a monolithic aerogel panel on its own and sandwiched between two glazing panes with and without the use of an integrating sphere.

This method of combining a spectrophotometer with an integrating sphere is mainly suited to characterising homogenous glazing systems or materials. In the case of a window system that include a complex interstitial structure, such as Venetian blinds, honeycomb etc., the standard integrating sphere measurement method can prove inappropriate as it does not easily accommodate the effects of anisotropy and spatial variation that are observed. The presence of these structures can result in significant deviation in the directional characteristics of transmitted and reflected flux as well as variation in the total amount of flux transmitted/ reflected.

Radiosity methods are commonly used to calculate transmittance or reflectance for these complex fenestration systems, based on knowledge of the measured optical characteristics of each of the individual system component. This method is described in International Standard ISO 15099 [109]. Using a Venetian blind as an example, in the radiosity method, each slat is assumed to be divided into small patches, as shown in Figure 3-4 (a). Each patch is considered as a Lambertian reflector [133] and the view factors between all patches are paired in an iterative calculation [134]. When the beam radiation passes through the structure without intercepting any of the slats (Figure 3-4 (b)), it is regarded as contributing to the direct transmittance, τ_{dir}- τ_{dir}. When either the beam radiation or incident diffuse radiation intercepts the slats, it is regarded as contributing to the spatially averaged diffuse transmittance or reflectance which may be broken down into sub components is direct-to-diffuse (τ_{dir}- τ_{dif}, ρ_{dir}- ρ_{dif}) and diffuse-to-diffuse (τ_{dif}- τ_{dif}, ρ_{dif}- ρ_{dif}) as shown in Figure 3-4 (c, d) [109].

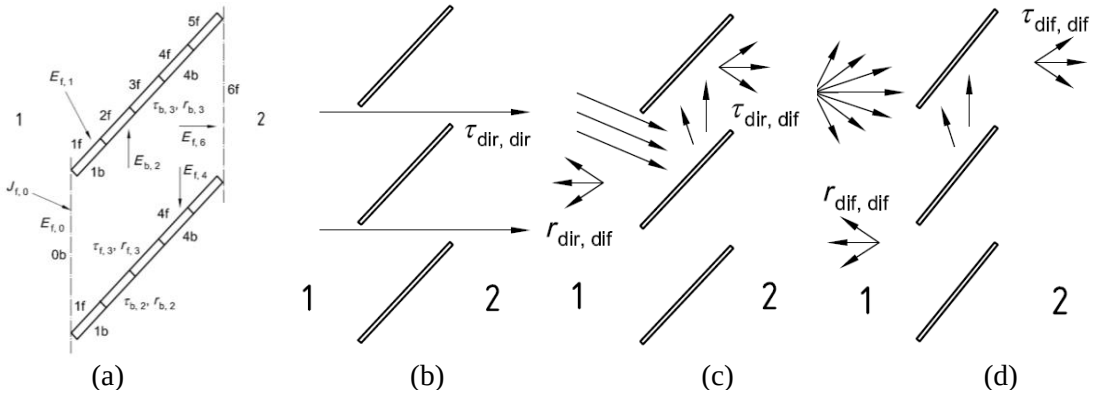


Figure 3-4: (a) discretization used in the model, (b) illustration of the direct-direct transmittance of the shading device, (c) illustration of the direct-diffuse transmittance and reflectance of the shading device and (d) illustration of the diffuse-diffuse transmittance and reflectance of the shading device [109]

The radiosity method as described in ISO15099 has been utilised in building simulation software, such as EnergyPlus, to calculate the transmittance and reflectance of a window system with complex interstitial structures [134]. This method has also been widely used in predicting the optical properties of window systems with integrated Venetian blind [31, 37, 135-141] as a quick and effective numerical method. But this method is not suitable for models with highly specular surfaces as it assumes that all the surfaces are Lambertian reflector. In order to overcome the limitation, previous researchers [34, 35, 142] proposed a mixed method that combines radiosity with a ray-tracing method to yield both the specular and scattering optical characteristics of these complex window systems.

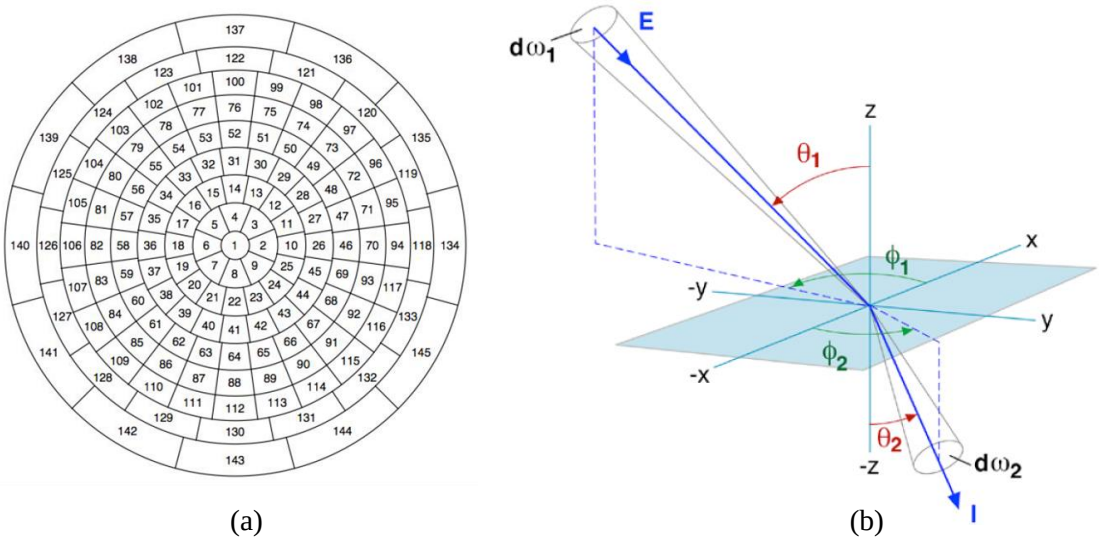
This approach can yield simple averaged optical properties, however, when the application requires the outgoing directions of light to predict its distribution in a space, only knowing the ratio between the amounts of transmitted or reflected light to the amount of incident light is no longer sufficient. A detailed knowledge of directional optical properties is necessary.

3.3.2 Bidirectional Scattering Distribution Function (BSDF)

The *Bidirectional Scattering Distribution Function (BSDF)* comprises a matrix of coefficients that for light from each incident direction quantifies the proportion transmitted in each outgoing direction. It is currently regarded as the most important method for characterising a complex glazing systems allowing them to be represented with precision in daylight analysis simulations. The *BSDF* can be further divided into *Bidirectional Transmittance Distribution Function (BTDF)* and *Bidirectional Reflectance Distribution Function (BRDF)*. The *BSDF* based on Klems' angle basis (Figure 3-5 (a)) [143, 144] is the most commonly used format. It is formed by 145 x 145 matrices including both solar and optical spectra. Each matrix describes reflectance or transmittance distribution in the outgoing hemisphere for a single incidence angle from the incoming hemisphere. Equation (2-11) [41] illustrates how the value of total transmitted radiation is obtained with regard to any particular angle of incidence (θ_1 and φ_1). This value is derived using a matrix calculation based on the result of the sum of the individual products of the luminous coefficients and incident irradiance, for each segment of the hemispherical basis.

$$\tau(\theta_1, \varphi_1) = \sum_{k=1}^{145} BTDF(patch_k) \int_0^{2\pi} d\varphi_2 \int_0^{\pi/2} \cos\theta_2 \sin\theta_2 d\theta_2 \qquad (3-9)$$

where, θ and φ define the boundaries of each patch of the basis as shown in Figure 3-5 (b).



(a) (b)

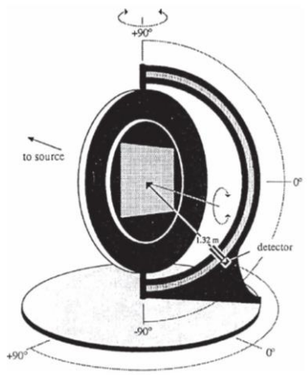
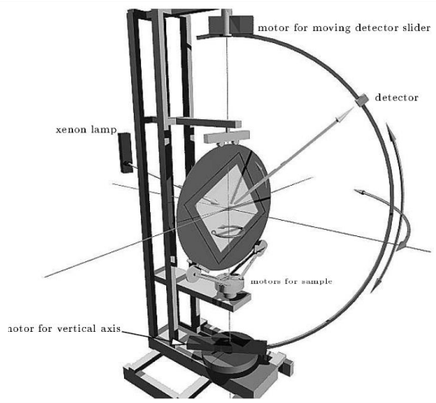
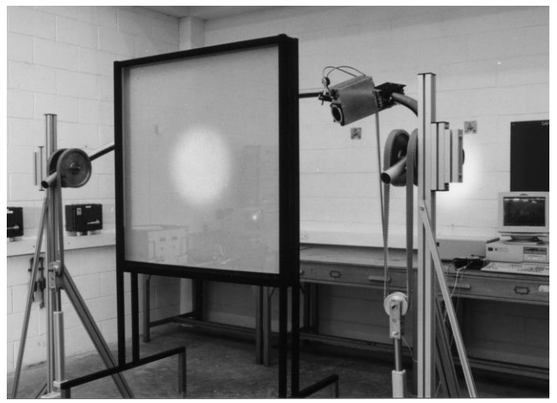
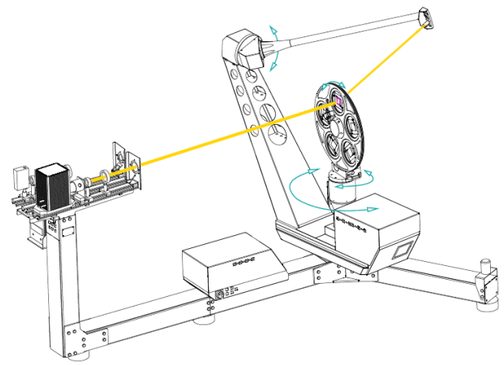
Figure 3-5: (a) Klems 145-patch hemispherical basis with numbered subdivisions; (b) coordinate system for bidirectional measurements [41]

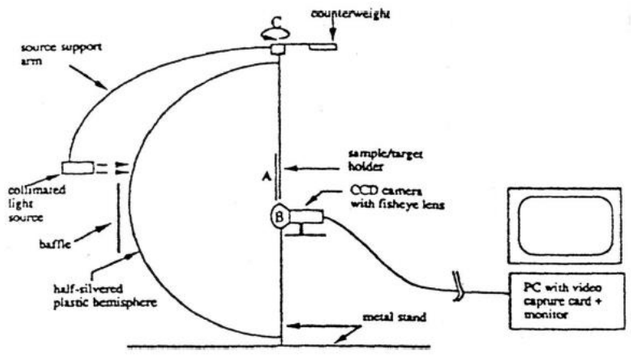
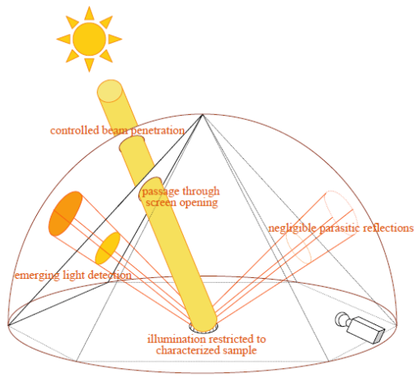
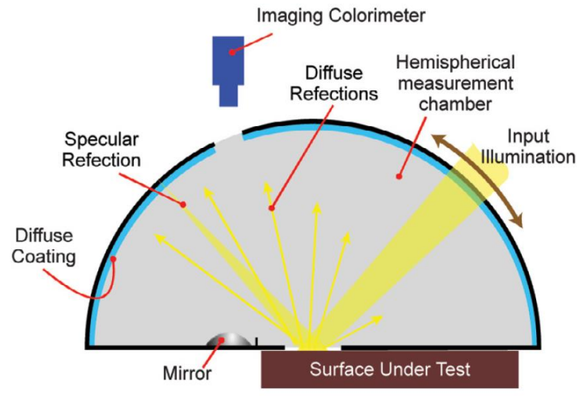
Various investigations, in recent years, have focused on the development of measurement techniques for complex window systems in an attempt to capture the respective BRDF and BTDF data. The instrument is named as goniophotometer and it can be divided into two types: 1) scanning-based method, where each outgoing direction of light is detected by each individual movement of the detector, and 2) video-based method, where digital imaging techniques are used to collect the outgoing direction of light from a single image. The schematic diagrams and features of goniophotometers are illustrated in Table 3-2.

As suggested by the name, the scanning-based method measures all required incoming and outgoing light flux directions by individually moving the sample, detector or light source. Each value in the BSDF matrix is measured discretely. Although, this method can provide an intuitive measurement with high and variable angle resolution [124], it is an onerous time–consuming task (i.e. 4 to 30 days according to [44]). Moreover, according to [44, 124], the scanning of discrete BSDF-related data has the potential risk of omission of significant features between the points being measured.

The principle of a video-based method is to use a CCD camera equipped with a fish-eye lens to collect the light emerging after being reflected or transmitted from the test sample under investigation. By using the camera, only one image is needed to investigate the whole light distribution for any given angle of incidence. Thus, the period of time required for the measurement can be dramatically reduced [145]. For hundreds of incident angles, this method normally requires a period of time somewhere between a few hours to only several minutes [44]. This method was developed by Ward [146] at LBNL in 1992 for the purpose of modelling and photo-realistic rendering of lighting in interior spaces, andnd it was carried forward by Andersen [32, 33, 44, 145, 147] at EPFL. The EPFL device differs from others as the hemispherical receiving screen has been replaced by an approximation to a sphere comprising six triangular diffusing projection screens. The luminance on each pixel recorded over these triangular screens are measured and used to covert to the BSDF data from the images taken by the CCD camera, as shown in Table 3-2.

Table 3-2: Goniophtotometers to measure the *BSDF* data

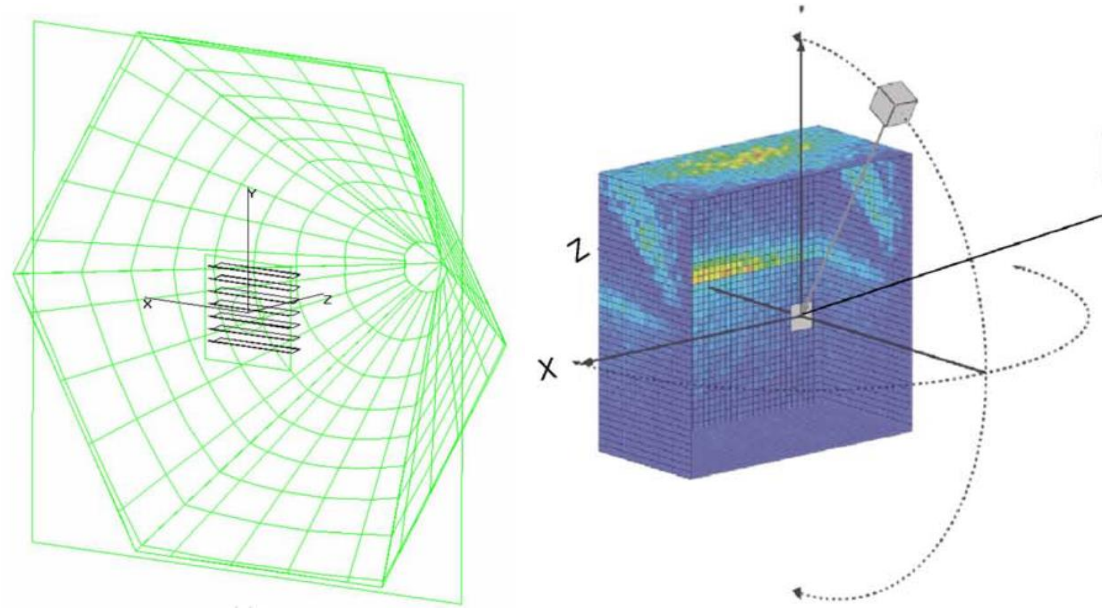
Institute	LBNL, USA	ISE, Germany	Cardiff University, UK	pab Ltd, Germany
Schematic				
Method	Scanning-based	Scanning-based	Scanning-based	Scanning-based
Year	1988	1994	2001	2006
BTDF	√	√	√	√
BRDF	-	√	-	√
Spectral capability	-	-	√	-
Validated by	measured g-value	transmittance measured with integrating sphere	measured g-value, transmittance measured with integrating sphere	-
Ref.	[148-151]	[152]	[153]	[154]

Institute	LBNL, USA	EPFL, Switzerland	Radiant Zemax, USA
Schematic			
Method	Video-based	Video-based	Video-based
Year	1992	2001	-
BTDF	-	√	√
BRDF	√	√	√
Spectral capability	-	-	-
Validated by	-	transmittance measured with integrating sphere	-
Ref.	[146]	[32, 33, 44, 145, 147]	[155]

A range of goniophotometers have been developed, however, their complexity and the levels of skills required to operate them means that they have received relatively low levels of uptake in both academic and commercial sectors.

As an alternative, researchers have been developing and validating virtual goniophotometers based on commercial forward ray-tracing simulation tools and using these in conjunction with virtual representations of complex fenestration systems (based on description of their geometry and optical characteristics) to obtain BSDF data. This approach is easier to implement, less expensive, less time-intense and more flexible for conducting parametric studies. Researchers in LESO-PB/EPFL [32, 33] used commercial ray-tracing software TracePro to model a virtual goniphotometer, which has a same configuration (i.e. receiving surfaces that consist of six triangles) as the experimental goniophotometer in EPFL, as shown in Figure 3-6 (a). The results were validated by comparison with experimental data and showed a difference of between 2 ~14%. Another numerical goniophotometer was developed by de Boer [156] using the ray-tracing tool OptiCad as shown in Figure 3-6 (b). This method used virtual sensors to receive flux on individual geometric positions and then calculated the BSDF values. The singular resolution of this numerical goniophotmeter can be defined by the user [44].

Recently, a free, open-source ray-tracing method- genBSDF implemented in RADIANCE-[157] was proposed and validated by comparing the predicted BSDFs with results obtained using other methods (i.e. TracePro simulation and real goniophotometer measurements) [45]. The results obtained from genBSDF are stored in an XML file, which can be used directly in lighting simulating tools such as RADIANCE, to determine the daylighting performance or input into Window 6 (software generated by LBNL, USA) and then further used in energy simulation tools such as EnergyPlus to predict the energy performance of applying this system in a building.



(a) (b)

Figure 3-6: Virtual goniophotometers generated by using (a)TracePro [32] and (b)OptiCad [156]

3.4 Building daylighting performance predictions with complex fenestration system applied

The quantity, quality and distribution of natural daylight passing through window systems and emerging in a space, play an important role in determining building energy efficiency and indoor environmental quality [158]. For example, excess sunlight in summer results in unwanted glare and presents an overheating risk, insufficient daylight results higher electricity consumption due to the use of artificial lighting, etc. Additionally, appropriate provision of daylight is also proven to have beneficial effects on human health, mood, activity and working efficiency [159].

To address the concern of evaluating the quantity, quality and distribution of daylight accurately, traditional approaches, which are in the main based on the use of rules of thumb or simplified calculation methods are increasingly becoming perceived as inadequate [159]. A number of new and refined metrics, such as Useful Daylight Illuminance and Daylight Glare Probability, have been proposed [160-162] as a means of improving the objectivity and accuracy of studies evaluating the effectiveness of a daylighting strategies and designs. These more sophisticated metrics are made possible through the use of dynamic simulation tools (e.g. RADIANCE [43, 147, 163, 164], Daysim [165-171] etc.). In this section, the daylight assessment metrics, from basic metrics and their limitations to more advanced metrics and their advantages, are introduced and analysed. The daylight evaluation tools, used in building services engineering and related research fields, are discussed and summarised.

3.4.1 Daylight assessment metrics

3.4.1.1 Daylight availability

Daylight availability describes the available daylight transmitted through a window system to an indoor space. It can be defined by static metrics, such as *Daylight factor (DF)* or the *illuminance* or *luminance* in a space on specific days, or through dynamic/ climate-based metrics, such as *daylight autonomy (DA)*, *useful daylight illuminance (UDI)* or *annual light/sunlight exposure*.

- **Daylight factor (DF)**

Daylight factor (*DF*) is the ratio of interior illuminance at a point within a building to the exterior horizontal illuminance under an unobstructed CIE overcast sky [172]. *DF* gains its favour in building daylight assessment because it is the simplest way to calculate daylight availability at a given location in buildings. It considers the worst possible scenario, i.e. an "overcast sky" for daylight assessment and may be paired with representative values of illuminance for a given site to provide estimates of daylight autonomy. Various sources of design guidance and standards recommend *DF* values for different building types, e.g. British Standards for Lighting in Buildings [173], American IESNA standards [174], Chinese Standard for daylight design of buildings [175] etc. Typically these recommend a minimum *DF* of 2% for office spaces. The thresholds of 2% and 5% can also be used to divide a space into three regions [176]: a perimeter region with *DF* of more than 5% where no artificial lighting is required; intermediate regions with *DF* between 2% and 5% where artificial lighting partially supplements daylight and an inner region with *DF* less than 2% that relies on permanent artificial lighting .

However, because *DF* is a static metric it does not take account of a building's site, associated climate, or time of day [177]. Similarly, the assumption that underlies

the concept of *DF* mean that variable sky conditions and in particular direct solar radiation, which has significant influence on the daylight performance, is not considered. Any one of these has the potential to result in a considerable loss of accuracy when there is a need to predict realistic levels or patterns of daylight distribution[178]. While there are some standards that advise against over illumination from daylight (by suggesting maximum *DFs*) there is a general risk that the *DF* approach can be interpreted by designers as a metric that should be "maximised'. This may be achieved by enlarging opening sizes, increasing transmittance of glazing and improving reflectivity of ceiling and wall finishes. These approaches can lead to extreme luminous environments with oversupply of daylight and high glare risk as well as a propensity for thermal discomfort with overheating in summer and under-heating and/or high heating demand in winter [177].

- **Clear sky studies on solstice and equinox days**

Rendering of daylight in a space with a specific window system under clear sky conditions at 9 am, noon and 3 pm on solstice and equinox days is able to provide an easily accessible impression of how daylight distribution change for these key times of day/year. Figure 3-7 shows false colour contours in a room with three different window designs on solstice and equinox days under clear sky conditions [179]. It can be seen that the amended fa çade designs lead to more light being transferred into the depth of the room improving both the daylight levels and distribution uniformity. LEED Version 3.0 requires a minimum light level of 25 footcandles (269 lux) on the equinox at 9 am and 3 pm under CIE clear sky conditions for an office building [180]. The clear sky studies combined with DF leads to a more balanced daylighting design as the high levels of illumination predicted by the former counter the temptation to over illuminate implicit in the latter. Both of these approaches represent climatic extremes and fail to exploit the

opportunities to develop a picture of the luminous environment that reflects its time varying nature of the daylight resource. Alternative approaches that make use of climatic data specific to the site offer a means of achieving this. [177].

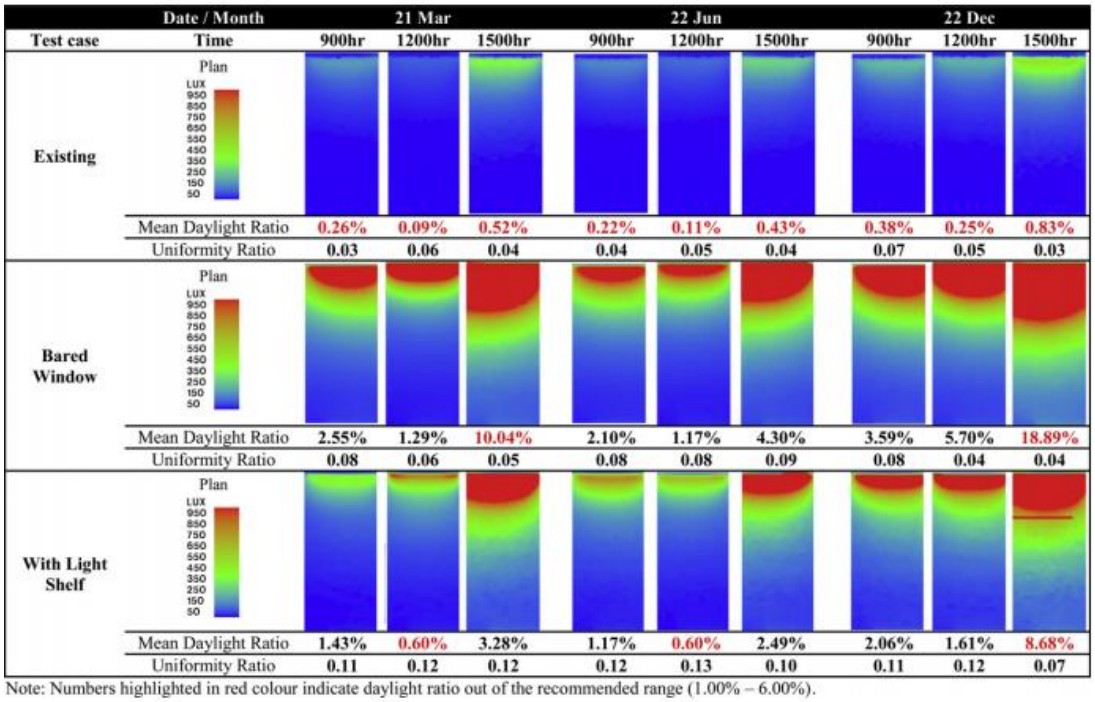


Figure 3-7: False colour contour in a room with three different window design on solstice and equinox days under clear sky conditions (adopted from [179])

The development of daylight simulation software provides the possibility of annual and dynamic simulation of indoor daylight performance and has seen the *DF* approach and the clear sky approaches being gradually replaced by more powerful and sophisticated metrics. Despite this, both the *DF* approach and clear sky studies remain useful and meaningful as a preliminary design metric [181] or as metrics complementary to an accurate dynamic daylighting assessment systems [162, 170, 182].

What these newer dynamic approaches offer is rather than simulating under a standard fixed condition or under a small number of scenarios is to instead make use of a weather file with hourly measurements of solar irradiance. From these, they are able to return a comprehensive set of hourly simulation result for daylight performance

providing a clearer picture of the luminous environment within the building over the course of a typical year.

- **Daylight autonomy (DA)**

Daylight autonomy ($DA_{x\ lux}$) is a climate-based metric defined as the percentage of occupied times in the year when a minimum illuminance threshold (x lux) can be met by daylight alone [183]. Illuminances of 300 lux ($DA_{300\ lux}$) and 500 lux ($DA_{500\ lux}$) are the most common target thresholds for offices, classrooms and libraries [177, 184]. A point in a building is considered as daylight sufficient if the daylight autonomy exceeds 50% of the occupied times of the year (ie $DA_{300\ lux\ or\ 500lux} > 50\%$) [184-186]. This concept is also used in defining spatial daylight autonomy (*sDA*) as described in IESNA LM [187] which is the percentage of floor area achieving a given $DA_{x\ lux}$ [171]. According to the investigations by Reinhart et al. [184, 186], who compared occupants' subjective evaluations of daylight with simulated results for various daylight metrics (Figure 3-8), it was found that the *sDA* was the most reliable metric for predict the perceived daylight condition in interior spaces.

A further modification of the daylight autonomy metric, named continuous daylight autonomy (*cDA* or DA_{con}) defines these time steps in daylight period when the daylight illuminance lies below an illuminance threshold (x lux), these time steps award partial credits (illuminance provided by daylight/ illuminance required)[188]. In seeking to quantify over-illumination, maximum daylight autonomy (*maxDA*) is an extended metric based on *DA* which attempts to assess the possibility of glare [189]. In use max *DA*, sets a threshold of ten times of the required illuminance as the maximum [189]. However, this factor of ten times the design illuminance is based on intuition rather than being grounded in studies of glare[188].

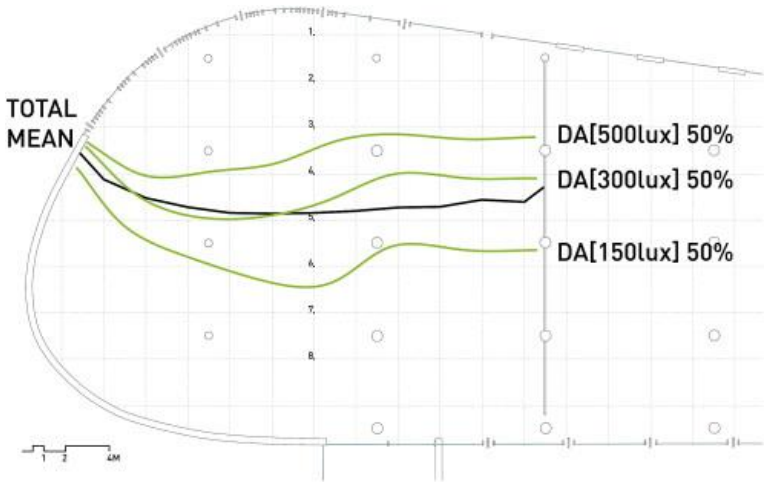


Figure 3-8: Comparison between $DA_{150\,lux}$ 50%, $DA_{300\,lux}$ 50%, $DA_{500\,lux}$ 50% and occupants' subjective daylight evaluation (adopted from[184])

- **Useful Daylight Illuminance (UDI)**

The DA metrics provide an indication of the percentage of daytime hours during which sufficient illuminance can be supplied by daylight alone. However, this value can be misleading because when there is an oversupply of daylight (e.g. illuminance value > 3000 lux), the occupants tend to deploy blinds, shades or curtains to control the visual and thermal discomfort [190]. Based on investigations of occupant response to varying daylight illumination, the *useful daylight illuminance (UDI)* metric was proposed [162]. This places the result from hourly simulation during occupied hours into one of three bins defined by lower and upper illuminance thresholds.

Results landing in the lower bin ($UDI_{<100lux}$) suggest periods when daylight alone is insufficient either as sole source of illumination or to contribute significantly to offsetting use of artificial lighting. Results landing in the upper bin ($UDI_{>2000lux}$) indicate periods when daylight is likely to lead to visual or/and thermal discomfort. Results falling into the intermediate bin ($UDI_{100\text{-}2000lux}$) are considered to be useful, and can be further subdivided assumed a threshold of 500 lux. Values of *UDI* in the range of 100-500 lux land in what has been termed a "supplementary" bin, in which daylight is

deemed sufficient as a sole source of illumination or making a significant contribution to illumination when used in conjunction with artificial lighting. Values of *UDI* in the range of 500-2000 lux land in what has been termed as "autonomous" bin, in which daylight is perceived either as desirable or at least tolerable [162, 191]. Other values for the threshold between the intermediate and upper bin have been proposed e.g. 2500 lux [191] or 3000 lux [190], as have values for the threshold to subdivide the useful bin, e.g. 300 lux [190].

Overlaying plots of *UDI* on the floor plan of the building under investigation can provide an intuitive description of the available daylight distribution in a space [177] or allow quick comparisons between different designs of window system or glazed façade [162, 192]. As an example, Figure 3-9 illustrates results from a study on a façade designed with and without a light shelf at different *window-to-wall ratios* (*WWR*), from which it can be found that there is little benefit in terms daylighting quality in using *WWR* greater than 35% [192].

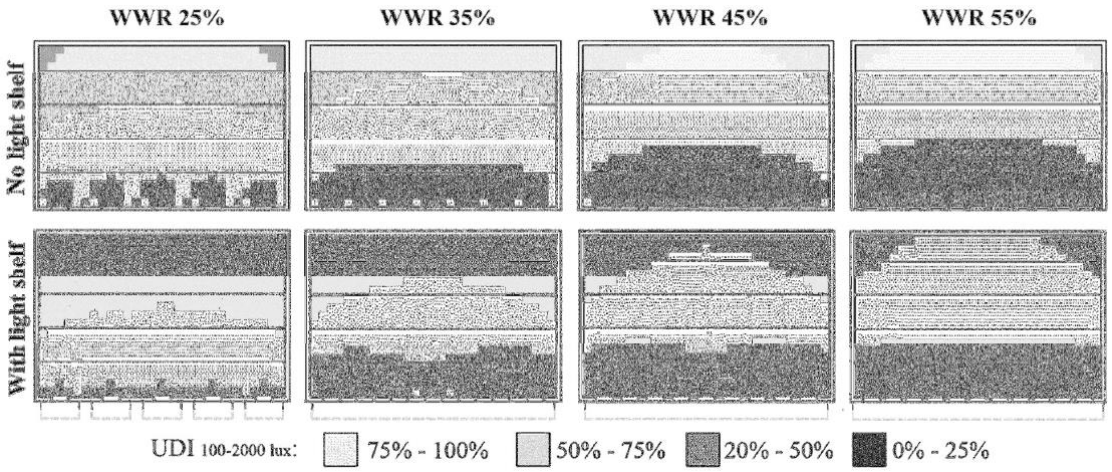


Figure 3-9: Comparison between *UDI* maps for façade with and without light shelf at different window-to-wall ratio (WWR) (adopted from[192])

- **Annual Sunlight/Light Exposure (ASE or ALE)**

Annual sunlight exposure (*ASE*) or *annual light exposure* (*ALE*) is a metric that cumulates the amount of light incident on a given point over the course of a year [177]. It is a well-established metric for assessing whether daylight levels are appropriate in spaces for artwork where the sunlight has a propensity to cause damage [193] or in spaces designed for plants to ensure suffient sunlight for them to grow. In IES LM-83 [187], *ASE* is defined as the percentage of square footage that has direct sunlight for more than 250 hours in a year.

3.4.1.2 Visual Comfort and daylight

Once the requirement for achieving sufficient light for efficient visual performance through daylight design has been met, a second and equally important requirement is to ensure a comfortable and pleasing visual environment [194]. The metrics for quantifying these visual qualities include illuminance uniformity ratio and glare related metrics.

- **Illuminance uniformity ratio (UR)**

Uniformity ratio (UR) is the ratio between maximum and minimum illuminance on a defined plane inside a space [195]. As the natural light variations inside a room can result in sharp illuminance contrasts and as human vision is more sensitive to this contrast than to the absolute amount light within a space, the *uniformity ratio (UR)* becomes a very important metric. CIBSE [196] recommend uniformity should not exceed 1:5 for a naturally lit space and the BREEAM [197] assessment method specifies the daylight ratio between average illuminance of a given task area and its immediate surrounds of 1:2.5.

- **Glare**

Glare describes the condition where the luminance level within the field of vision exceeds the brightness to which eyes are adapted. It is a relatively subjective metric as it is dependent on the observer's personal preference, age, gender etc. According to Reinhart [177], glare can be subdivided into disability glare and discomfort glare; the first describes the inability of a person to see a certain objects in a scene due to glare; while the latter describes the premature tiring of the eyes caused by glare. Disability glare is relatively easy to identify, however, discomfort glare is subtler and harder to quantify. The glare index has been used as a metric for many years; however, early variants such as *unified glare rating (UGR)* is based on a relatively small glare source typical of artificial lighting. In 2006, a discomfort daylight glare index named *daylight glare probability (DGP)* was introduced and validated by Wienold and Christofferen [194]. The *DGP* has become the preferred metric for assessing glare within a daylit space.

DGP is expressed as follows [194]:

$$DGP = 5.87 \times 10^{-5} E_v + 9.18 \times 10^{-5} \, log\left(1 + \sum_i \frac{L_{s,i}^2 \omega_{s,i}}{E_v^{1.87} P_i^2}\right) + 0.16 \quad (3-10)$$

where E_v (lux) is the vertical eye illuminance produced by the light source, L_s (cd/m^2) is the luminance of source; ω_s (sr) is the solid angle of source seen by the observer; and P is the position index, which expresses the change in experienced discomfort glare relative to the angular displacement of the source from the observer's line of sight. The method can be generated by rendering a HDR image for a position in a daylit space for every daylight hour of the year, and then comparing the luminance ratios and adjacencies to determine an average probability that an observer at that point would find it objectionable.

Performing this calculation for even a simple space with one observer position over a period of a year imposes a significant computational overhead and can be highly time consuming, so in practice, a simpler method is necessary. Wienold [160, 161] proposed a simplified version of DGP, DGPs, where the logarithmic term quantifying the luminance and solid angle of the source seen from the observation point is neglected:

$$DGPs = 6.22 \times 10^{-5} E_v + 0.184 \qquad (3-11)$$

In use, the *DGP* thresholds of 0.35, 0.40 and 0.45 can be used to divide the DGP results calculated for occupied hours of a year into four bins: lower than 0.35 is '*imperceptible*' glare sensation, between 0.35 and 0.40 is '*perceptible*' between 0.40 and 0.45 is '*disturbing*', while higher than 0.45 is deemed '*intolerable*'. The visual quality of the space may then be rated according to the following scale: the '*Best*' class corresponds to over 95% of office hours having *imperceptible* glare sensation, '*Good*' class requires over 95% of office hours having glare weaker than *perceptible*, while '*Reasonable*' class will have over 95% of office hours with glare weaker than disturbing [160, 161, 194]. Implicit in these calculation is the assumption that the sun is not contained within the field of view, i.e. *DGPs* cannot be used to evaluate glare probability when the sunlight directly hits the observer [10].

3.4.1.3 Lighting energy consumption

Standard and advanced windows typically form part of an integrated system where artificial lighting is used to complement the daylighting strategy and help ensure illuminance levels do not drop below design targets [172]. This more detailed approach provides not only a more accurate assessment of lighting energy demand but also the ability to quantify how this impacts on the building's wider heating and cooling energy demands. As the examples shown in Figure 3-10 demonstrate, an overall consideration

of *DA, UDI, DGP* etc. and predicted energy consumption could provide a comprehensive understanding of the holistic performance in terms of indoor comfort level and energy efficiency for a particular building design [167, 170, 182, 195].

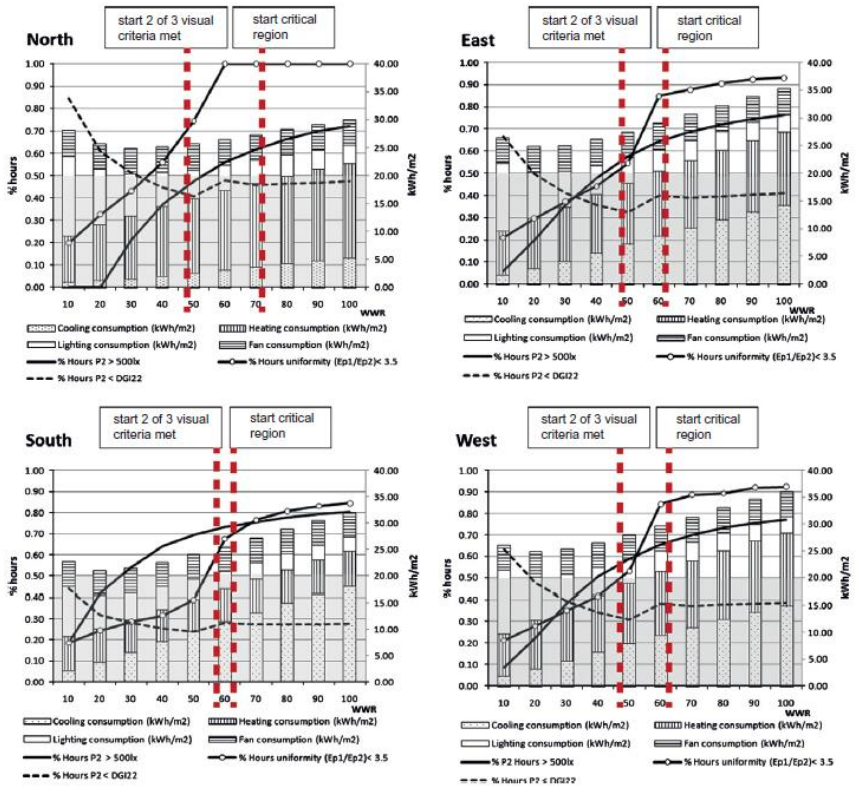


Figure 3-10: Overall consideration of *uniformity*, *DA*, *DGI* and energy saving (adopted from [195])

3.4.2 Daylight simulation method

These sophisticated daylight metrics, introduced in section 3.4.1, are realised by the support of effective simulation tools. Currently, ray-tracing algorithms, radiosity algorithms and split flux algorithms are the most implementable approaches for realising daylight simulation.

RADIANCE, which has been developed by Greg Ward at Lawrence Berkeley National Laboratories, is an open-source, research grade tool for visualizing lighting in virtual environments [157]. It is based on a backward ray-tracing algorithm (Monte Carlo ray-tracer), which means that the rays are emitted from the point of interest and

traced backwards until they either hit a light source or another object [198]. The result from RADIANCE have been validated by several studies [43, 147, 163, 164] and it is regarded by many as the most accurate daylight simulation tool [147, 199]. In spite of its high level of accuracy, RADIANCE provides no graphical user interface [200]. This and its relative complexity mean that the tool takes time to master and this has led to it not being widely adopted. In order to take advantage of the algorithm provided by RADIANCE, and make it much easier for users to operate, a number of commercial software modules have been developed based on RADIANCE, such as DAYSIM, DIVA, and Ecotect.

Radiosity and split-flux methods have been adopted in order to predict spatial daylight performance in the energy simulation software EnergyPlus. The radiosity technique, subdivides reflecting surfaces into nodal patches, and makes use of view factors applied to pairs of nodal patches to create a greater accuracy than split-flux technique in determining the overall contributing factor of reflected light within a space[134]. A number of studies have shown that the radiosity technique is unable to provide results as accurate as the ray-tracing method in relation to particular daylighting problems or scenarios [142, 147, 163, 164, 199, 201].

Daylighting performance predictions by using different simulation tools in recent three years are summarised in Table 3-3.

Table 3-3: Daylight performance predictions by using different simulation tools with various metrics

Simulation software	Research objective(s)	Location	Period	Metrics used	Sensor points	Results	Ref.	Year
Daysim	Optimising window size, orientation and wall reflectance with various metrics, and the inter-relationship between metrics.	Bandung, Indonesia	Annual	DF, DA UDI, DGP lighting energy	2 study points	Optimum solution is WWR 30%, wall reflectance of 0.8 and south orientation.	[170]	2016
EnergyPlus Daysim	Investigating the performance of building integrated solar thermal shading (BISTS) system on building energy consumption and daylight levels.	Los Angeles, USA	Annual	UDI, energy	Grid of 400 points	BISTS can increase the useful daylight level at a single perimeter room and achieve 5.3% primary energy saving.	[167]	2016
Daylight Visualizer 2.6	Investigating the effect of window shape, size and position and inner surface reflectance on daylight factor and lighting energy saving	N/A	Standard overcast sky	DF, lighting energy	Grid: 0.5 ×1 m	Square window provide best DF and upper position allows higher luminance at the back of the room	[181]	2015
Daysim	Investigating the impact of semi-transparent photovoltaic windows on the daylight performance on commercial building fa çade	Toronto, Canada	Annual	cDA, sDA, DGP	Grid: 0.5 ×0.5m	Integration of semi-transparent photovoltaic module with visual effective transmittance of 30% provides sufficient daylight within perimeter zone	[171]	2015
Daysim 3ds Max Design	Investigating the impact of software's choice and weather file's choice on dynamic daylight simulation results	Copenhagen, Denmark; Milan, Italy; Nancy, France; Rome, Italy	Annual	ALE, DA, UDI	3 study points	Both Daysim and 3ds Max provide roughly accurate predictions of dynamic daylight metrics; TRY is not a preferred weather data type for daylight simulation.	[165, 168, 169]	2015
RADIANCE	Investigating the impact of light shelves on UDI for different window-to-wall ratio (WWR)	Toronto, Canada	Annual	UDI	Grid: 0.5 ×0.5m	Light shelves increase illuminance in front of window and provide more homogeneous distribution. WWR above 35% is not advantageous for daylighting.	[192]	2015
DIVA for Rhino	Assessing the daylight in office buildings with different atrium types, proportions and roof aperture designs.	U.S climate zone 3	Annual	DA, sDA, UDI, ASE	Grid: 3.5 ×3.5ft	The well index of atrium design is confirmed as a reliable indicator to characterize atrium proportion by using climate-based daylight modelling	[202]	2015
Fener (RADIANCE-based)	Developing a new modelling approach to analyses complex fenestration systems from a coupled daylight and thermal and energy simulations	Frankfurt, Germany; Rome, Italy	Annual	Illuminance distribution, DA, lighting energy	--	Fener has been validated by EnnergyPlus and classic RADIANCE and proven as a feasible approach to assess thermal and daylighting performance of complex fenestration system	[203]	2015
Daysim, EnergyPlus	Proposing a procedure for creating a response surface in a feasible manner, which takes both energy saving and daylight availability into account	Tokyo, Japan	Annual	DF, cDA, lighting energy	Sensors in line with 0.4m interval distance	The proposed method has been validated and the differences in terms of cDA and energy consumption can be regarded as negligible.	[166]	2015
RADIANCE	Evaluating the indoor daylight quality in patient room in King Abdullah University Hospital	Irbid, Jordan	Selected days	DF, clear sky conditions	8 study points	The daylight quality in the patient room need to be improved by changing optical properties of surfaces and glazing as well as adding shading devices.	[204]	2014
DIVA for Rhino, EnergyPlus	Evaluating visual comfort and building energy demand and proposing lighting and shading control strategies for visual comfort and building energy saving	Incheon, Korea	Annual	DGP, DGPs, DGI, Illuminance level	1 occupant position	Optimised control strategies of shading system is proposed to prevent glare, secure maximum daylight and achieve energy saving	[205]	2014
Ecotect, RADIANCE (Desktop), EnergyPlus	Evaluating the daylight performance, visual comfort and energy consumption in a large space of industrial building	Tianjing, China	Annual	Illuminance level, DA, lighting energy	10 study points	Daylighting design integrated with electricity saving strategies of the On/Off control and the dimming control can achieve 36.1% and 41.5% energy saving, respectively.	[206]	2014

3.5 Energy performance prediction for building with complex fenestration systems

Various building simulation tools, such as EnergyPlus, ESP-r, IES, IDA ICE, TRNSYS, and TAS can be used to explore the energy, thermal and daylight performance of buildings with complex fenestration systems [183]. The challenges related to modelling complex fenestration systems include: 1) precise characterisation of the thermal and optical properties of fenestration systems, in which two- or three-dimensional heat transfer and/or light transmittance might exist due to the presence of complex structural geometries; 2) the potential need to model adaptive features associated with the operation of complex fenestration systems (e.g. switchable glazing, moveable shading, etc.), that may affect a number of properties (e.g. thermal, visual) simultaneously. This section of the review focuses on one of the widely available simulation tools, EnergyPlus, and uses it as an example to explore how complex glazing systems may be accommodated within an energy simulation.

In much of the literature dealing with the application of EnergyPlus to the simulation of glazing systems, the glazing has been modelled using a simplified method: 1) when there is no shading device or there is a plain shade or window screen applied, the optical properties are defined by solar and visible transmittance/ reflectance; 2) when the windows are integrated with internal, external or between-panes Venetian blinds, the optical properties of the window system are obtained using a radiosity-based pre-computation through definitions of the blind's geometry and slats surfaces' properties. For example, Yun et al. [205] investigated the building energy performance and the daylight performance of an office under the climate of Seoul, Korea using EnergyPlus and DIVA-for-Rhino, where Venetian blinds at different slat orientation angles were

applied to a window. In their research, the optical properties of glazing systems were gained through definitions of the slat width, separation between slats and slat reflectance, as well as the slat orientation angles, which varied from 0 °, 15 ° and 30 °. Their results revealed that when the slats were tilted at 30° to the horizontal or when dynamic shading was used (i.e. automatic control of the slat tilt angle) effective energy saving can be achieved. Yoon et al. [207] investigated the influence of external and internal blinds' reflectance on the heat balance and overall energy performance of a room located in Daejeon City in South Korea. The blinds' reflectance and geometries were used to obtain the optical properties of these relative glazing systems. They concluded that a reduction in reflectance of the interior blinds resulted in decrease in heating load and increase in cooling load. The opposite pattern of behaviour was observed for the external blind. These previous studies represented the assessment of glazing systems with complex configurations (e.g. Venetian blind) using pre-computed solar heat gain coefficients and visible transmittances based on radiosity method. The limitations of the radiosity method were explained in section 3.4.1. When applying it in EnergyPlus, the pre-calculated solar and visible transmittances leave them lacking accuracy in terms of representing the highly complex, angle-dependent interaction between incident radiation and the more advanced fenestration systems. Meanwhile, the standard method also restricted the geometric forms of these involved complex configurations to blind, shade or window screen. Standard method is unable to model less common structures (e.g. tubular shading structure, nonlinear shading systems, ect.). The launch of EnergyPlus V7.2 allowed the inclusion of Bidirectional Scattering Distribution Functions (BSDF) in the modelling process, and this has significantly enhanced the software's capability to predict building energy and daylighting performance with complex fenestration systems. However, published articles related to the use of BSDF in EnergyPlus are not common. This is, in

large part, due to the challenge of obtaining the specific BSDF data for window systems under prediction. For the purpose of precisely modelling optical properties (i.e. BSDF) of complex fenestration systems in EnergyPlus, RADIANCE provides a ray-tracing tool to numerically calculate BSDFs and WINDOW establishes a bridge for its implement in EnergyPlus. Femandes et al. [208] have undertaken an accurate modelling of complex fenestration systems by using BSDFs to quantify the potential of energy saving and peak demand by applying an angular selective window system (i.e. expanded metal mesh, tubular shading structure, and micro-perforated screen) in a whole-building simulation. The results revealed that energy saving of between 28 ~ 47% may be achieved in the perimeter zone by applying angular selective window system under the climates of Chicago, Illinois and Houston, Texas. Hoffmann et al. [209] investigated the impact of twelve different shading devices on whole building energy performance under two climates. They used their study to develop optimised strategies to balance solar gain with glare and daylight levels. The optical properties of the shading systems were accurately defined using the BSDF method and hourly scheduled surface gains. The results showed that shading geometry and slat material characteristics significantly affected the amount of heat gain from solar radiation and distribution of transmitted daylight.

When dealing with the adaptive fenestration system, the ability of modifying window thermo-optical properties to counter temporary changes in energy fluxes incident on the building need to be achieved. Firlag, et al. [210] investigated the use of dynamic control algorithms (implemented using the Energy Management System (EMS feature in EnergyPlus) to control an external roller blind mounted to a double-glazed window and an inter-pane cellular shading device with a triple-glazed window that were applied to a typical residential building under four different climates. They also used BSDF data as a precise description of these complex window systems with dynamic

controls. It was concluded that using automated shading devices with proposed control algorithms can reduce solar heat gain, resulting 11.6 ~ 13.0% reduction in building energy consumption. Loonen et al. [211] reviewed available building performance simulation tools that can be used to model adaptive fenestration systems or fa çades. They discussed the requirement for successfully realising modelling and simulation of adaptive systems, compared five commonly used simulation software tools and proposed further development opportunities in this field.

3.6 Summary

The experimental and numerical methods used to predict the thermal characteristics of window systems have been reviewed and summarised. The prediction of thermal properties of complex glazing system with interstitial structures, such as horizontal Venetian blinds, pleated blinds and different configurations of fins, within the air cavity of a double glazed unit has been widely researched both experimentally and numerically [4, 23-38]. These structures offer the potential to improve the thermal efficiency of any window system within which they are employed [24, 26]. A considerable volume of this research into windows with interstitial structures has been conducted using Computational Fluid Dynamics (CFD) modelling to evaluate the possibility of reducing free convection and long-wave radiation exchange between the two glazing panes. Results indicate that heat transfer through air cavities with interstitial structures can be reduced with heat transfer coefficient reductions in the order of 50% [4] or U-value reductions of 21% [39] being achievable. However, in most of these studies, long-wave radiation heat transfer, which can account for up to two thirds of the total heat transfer across the air cavity [117], is neglected in the numerical modelling. Detailed investigations of interstitial structures that consider the reduction of heat transfer in terms of both convection, which is driven predominately by temperature difference across the two glass panes, and radiation, which is driven predominately by glazing system mean temperature are less common.

Methods for determining the optical properties of window systems, especially those incorporating complex structures have also been reviewed. The radiosity method is a commonly utilised, effective approach to determine the optical performance of simple window systems in order to obtain transmittance or reflectance [31, 34, 109]. However, when considering the strong directional effects that TIMs or other complex

interstitial structure can have on the distribution of solar or daylight flux, radiosity approaches prove inappropriate and alternative approaches are required to accurately predict the daylight performance of a space. An alternative method, which uses a matrix of Bidirectional Scatter Distribution Functions (BSDFs) to characterise the optical properties of window system, is proposed and validated in the literature [36, 41-43]. This is a type of angularly resolved transmittance or reflectance capable of describing the behaviours of window systems with complex interstitial structures; and the BSDF data can be obtained via a three-dimensional ray-tracing method [32, 33, 44, 45].

Having determined the BSDFs, ray-tracing techniques may then be used to quantify the visual environment of a space illuminated by daylight via advanced glazing systems. A range of daylighting metrics exists to quantify both the quality and quantity of light with a space. The more recent climate specific metrics are able to offer a more comprehensive picture of the luminance environment and form an effective complement to the BSDF approach to designing spaces lit via advanced glazing systems.

Comprehensive studies of building energy demand require accurate characterisation of the thermal behaviour of advanced glazing systems as well as a comprehensive picture of their luminous behaviour that may be coupled to artificial lighting control model. The ability to import thermal characterization into tools such as EnergyPlus as well as the ability to couple the tool to lighting tools such as RADIANCE creates a framework where such studies may be undertaken.

Chapter 4. Thermal evaluation of a double glazing unit with integrated Parallel Slat Transparent Insulation Material (PS-TIM)

4.1 Introduction

For the purpose of improving the performance of glazing systems and hence improving indoor comfort and achieving building energy conservation, a considerable volume of research reported in the literature has focused on the application of glazing system with advanced interstitial structures. The fundamental investigations of the thermal characteristics of these complex glazing systems are quite important for providing a better understanding of the benefits and defects of these systems. Asdrubali et al. [107] and Chen et al. [106] used a hot box method to investigate thermal transmittance of different complex fenestration systems. Laser interferometry has been used to obtain temperature field visualization and hence to analyse the convection in complicated glazing units with different internal blinds [23, 27, 28]. These experimental techniques are realistic but not convenient ortime efficient for detailed parametric study, especially for those systems in the design stage. Thus, experimental investigations have always been accompanied by numerical studies that have proven indispensable in exploring these complicated building elements. Computational Fluid Dynamics (CFD) tools have been used by a great number of researchers to solve the heat transfer problem and explore the air flow pattern in the vertical air cavity of glazing unit [116-120].

In this chapter, the thermal performance of Parallel Slat Transparent Insulation Material (PS-TIM) were evaluated numerically through CFD simulation. Before that, the accuracy and reliability of this CFD simulation method had been verified through exploring the thermal properties of a double glazed unit with and without a Venetian blind installed in the air cavity between two glazing panes using climate chamber. This structure was selected as this structure shares many of the same characteristics as PS-TIMs. This validated two-dimensional CFD model was then used to investigate the thermal performance of the glazing system with PS-TIM at different slat pitches under

different temperature conditions. It was carried out to explore the convective, conductive and radiative heat transfer that occurs in the air cavity with and without PS-TIM. A variety of cell *aspect ratios,* slat thicknesses and slat thermal properties (conductivity and emissivity) were examined to investigate their effects on overall thermal performance. Instead of studying the *U-value* of glazing systems under a standard condition, simulations were undertaken over a range of different mean temperatures of the glazed unit and a range of temperature differences across its surfaces to allow a comprehensive picture of convective and radiative heat transfer to be established, and their effects on window thermal resistance/ *U-value* determined. The results from these studies were used to generate empirical correlations for the thermal resistance of double glazed unit with interstitial Venetian blind.

4.2 Using experimental investigation to validate numerical model

Experimental studies of the glazing systems with and without a Venetian blind installed in the air cavity between two glazing panes were carried out at the Laboratory at the Energy Technologies Building, University of Nottingham under a series of controlled temperature conditions. The results form experimental investigation were then used to validate the CFD numerical model.

4.2.1 Test samples

Two glazed units of size 1200 mm × 1200 mm × 28 mm were tested. One was a normal double glazed unit composed of two 4 mm-thick low iron panes and a 20 mm-wide cavity filled with air (labelled as 'DG' in preceding discussions). The other was a double glazed unit with a Venetian blind installed in the air cavity between the two glazing panes. The slats were made of aluminium with a thickness of 0.25 mm and width

of 11 mm. During the tests, two configurations were tested: one with the slats horizontal (tilt angle of 0° to the horizontal, labelled as 'V0' in preceding discussions) and the other with the slats vertical (tilt angle of 90° to the horizontal, labelled as 'V90').

4.2.2 The climatic chamber and apparatus setup

The thermal performance of the glazed units was measured in a TAS series 2 LTCL600 climatic chamber as shown in Figure 4-1. The climate chamber comprises two insulated walk-in rooms (both are 4 m × 3.5 m × 2.6 m) providing a steady and cyclic simulation of climatic environment. Each enclosure can be individually controlled and thus it is possible to simulate external climate conditions in one, whilst the other mimics internal conditions. One of the rooms is physically fixed while the other may be wheeled to one side to allow the construction of a 'Test Wall'. Once constructed, the two rooms can be brought together to sandwich the 'Test Wall'. During the test, integral air conditioning units can be used to control the temperature of the two rooms within the range from -25 ℃ to +60 ℃ and the relative humidity between 10 ~ 95%. Various parameters, such as surface temperature, air temperature and heat flux of the 'Test Wall', can be obtained during operation.



(a) (b)

Figure 4-1: (a) External view of the climatic chamber (b) Internal view of the chamber and air conditioning unit

The measurement method followed International Standard ISO 9869-1:2014 for in-situ thermal resistance measurements using heat flow meters [90]. The apparatus setup was informed by International Standard ISO 12567-1:2012 for the determination of window and door thermal transmittance using the hot-box method [89]. Figure 4-2 shows a schematic cross-section of the test apparatus. A 300 mm-thick insulated wall (with a measured *U-value* less than 0.3 W/m^2K) was sandwiched between the two rooms to form the initial 'test wall'. The glazed units were then mounted in an aperture cut in the centre of the wall positioned at least 860 mm away from the inside ceiling, floor and walls of the two rooms. The internal surface of the glazed unit was mounted flush with the surface of insulated wall according to ISO 12567-1:2012 [89]. Silicone sealant covered by tape was used around the joints between the window and the insulated wall in order to seal all air gaps and hold the window firmly in position. In order to diminish the effect of forced convection caused by the fans on the air conditioning units, two baffles made from plywood were set in both the interior and exterior chambers. The distance between the baffles and surfaces of the insulated wall, in which the testing glazed units were installed, was 500 mm.

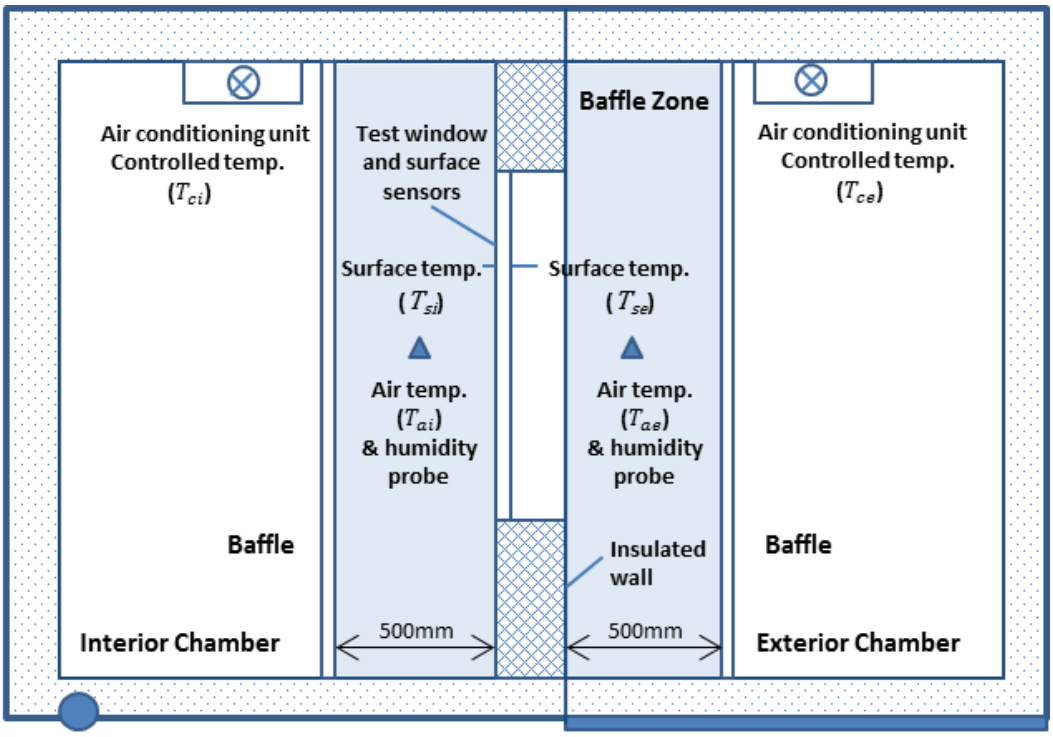


Figure 4-2: View of the system, the test specimen and sensors

Eighteen T type thermocouples (Figure 4-3) with detector diameter less than 0.3 mm were attached on each side of the window unit [89] to measure external and internal surface temperature (labelled as T_{se} and T_{si} shown in Figure 4-2, respectively). Heat flux meters (Hukesflux Type HFP01, with thermal resistance < 6.25 × 10^{-3} $m^{-2}K/W$, measurement accuracy +/-5%) were affixed to the glass by a thin layer of thermal contact paste (Servisol, with thermal conductivity 0.77 W/mK) [90] for heat flux (q) measurements. The thermal resistance of the heat flux meters is low enough for the effects of perturbation of the surface heat flow by their presence to be assumed negligible. Two temperature and humidity probes CS215 (accuracy +/-0.4℃ for temperature and +/-2% for humidity) were used to measure the air temperature (labelled as T_{ae} and T_{ai} shown in Figure 4-2) and humidity in the two baffles space beside the window. Two hot wire air velocity sensors (Testo 425, with measurement accuracy +/- 0.03m/s) were used to monitor the air velocities within the baffle zone. The thermocouples, heat flux

meters and temperature and humidity probes were connected to a 24-channel data logger DT85, which logged data at 1 minute intervals.

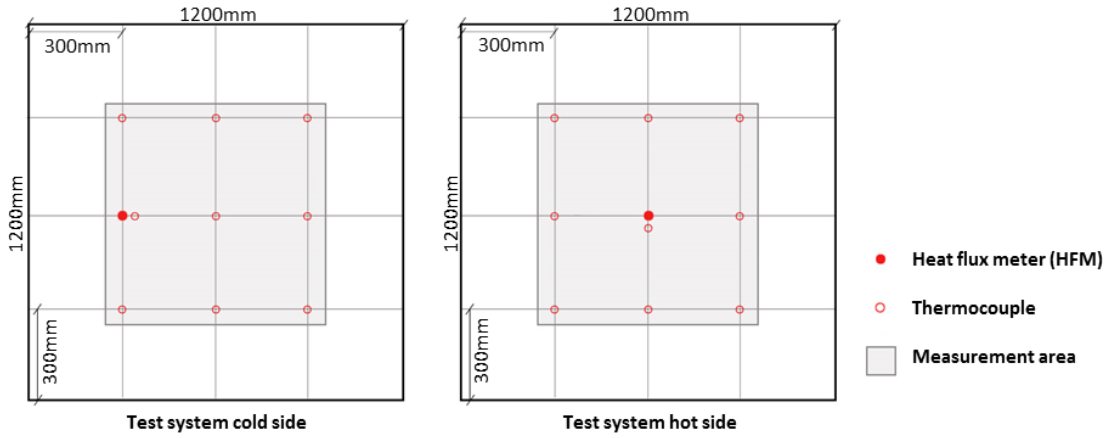


Figure 4-3: Detailed view illustrating the locations of the thermocouples and heat flux meters on the surfaces of the glazed unit

4.2.3 Measurement procedure and data acquisition

Before the test, all sinstruments were. calibrated. At the beginning of the test, 6 heat flux meters and over 30 thermocouples were placed inside and around the measurement area (Figure 4-3) of the glazing surface to verify the uniformity of surface temperature and heat flux. The results showed uniform readings in the measurement area and the extra 4 heat flux meters and thermocouples were then removed to reduce their effect on heat flow.

As both the glazed unit mean temperature and the temperature difference between the panes of the unit affect heat transfer, when testing the window samples, five pairs of controlled temperature settings were used. The five scenarios maintained the surface temperature of the two glazing panes (T_{se} and T_{si}) at approximately the value shown in Table 4-1. Scenarios 1-3 aimed to keep the mean temperature of the glazed unit constant at 10 °C, but vary the surface temperature difference between the two glazing panes from 7 °C to 15°C. Scenarios 4 and 5 sought to keep the surface temperature difference between the two glazing panes the same as scenario 3 (15 °C),

and vary the mean temperature between 7 °C and 14 °C. The mean and surface temperatures of the glazing were controlled by manually adjusting the settings on the air condition unit controlling the chamber temperature (T_{ce} and T_{ci}) until the desired scenario was achieved. To avoid condensation, the relative humidity in the interior room was set at 30%. The measured air speed was less than 0.3 m/s and indicates that natural convection prevails [89].

Table 4-1: Arrangement of mean temperature and surface temperature difference of 5 scenarios for glazing systems

Scenario No.	1	2	3	4	5
Mean temperature of glazed unit (T_m) (°C)	10	10	10	7	14
Surface temperature difference between two glazing panes (T_{se} - T_{si}) (°C)	7	11	15	15	15

Generally, tests were run for a sufficient duration (over 72 hours) to allow the environmental conditions in the test rooms and the heat flow through the window to stabilise for each scenario, and then data measured over a further period of 48 hours were used for analysis.

4.2.4 Analysis of the data

The glazing surface temperature (T_{se} and T_{si}) and heat flux (q) were measured during the experimental test and average method was used to analyse the data [90] and obtain the thermal resistance of the glazing system by using Equation (4-1):

$$R_T = \frac{\sum_{j=1}^{n}(T_{sij} - T_{sej})}{\sum_{j=1}^{n} q_j} \qquad (4-1)$$

where the index j enumerates the individual measurement.

The thermal transmittance, U, can be obtained from Equation (4-2):

$$U = \frac{\sum_{j=1}^{n} q_j}{\sum_{j=1}^{n}(T_{aij} - T_{aej})} \qquad (4-2)$$

The thermal resistance of the double glazed unit without a Venetian blind obtained through experiment was compared with the calculated values determined according to EN673 [110] (details can be found in section 3.2.2.1), as well as simulation results using CFD. The measurement results for the glazed unit with Venetian blind were also compared with CFD simulation results.

4.2.5 CFD modelling of the test samples

This section presents the main features of the numerical model employed to reproduce the experimental test. Two-dimensional finite volume models were developed in the commercial CFD package FLUENT. The thermal performance of a double glazed unit with a Venetian blind at two different configurations (slats horizontally placed (V0), slats vertically placed (V90) were investigated. The air cavity of the glazing system has a width of 20 mm and height of 1200 mm. Schematic diagrams of the normal double glazed window and glazing system with horizontal and vertical slats are given in Figure 4-4.

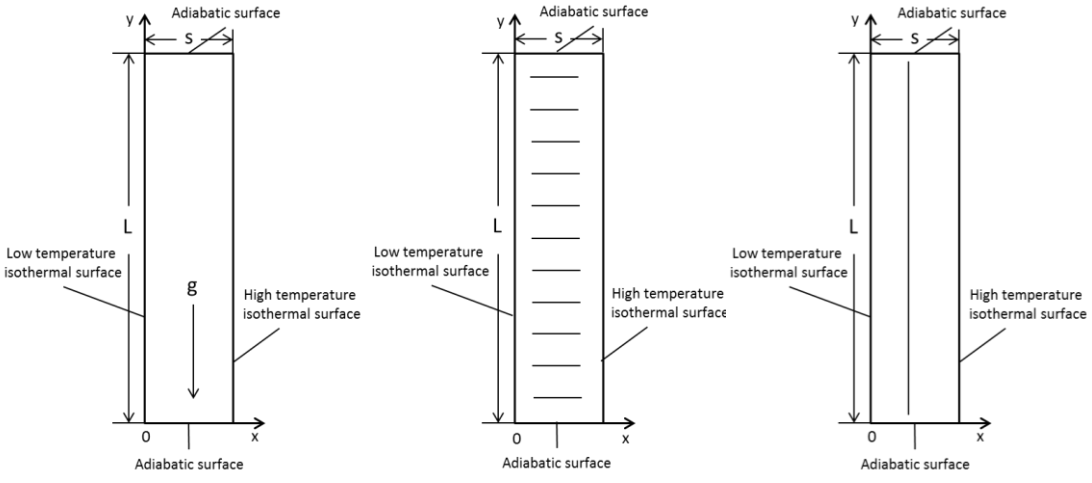


Figure 4-4: (a) 2D schematic diagram illustrating the geometry of the glazing system without blind (b) glazing system with horizontally placed slats (c) glazing system with vertically placed slats

To simplify the CFD simulation process, the following assumptions were made: 1) the internal surfaces of the left and right glazing panes were set as two isothermal walls with different temperatures to represent the temperature difference between indoor and outdoor environments, while the top and bottom ends were assumed to be adiabatic; 2) the enclosure was filled with air with Pr = 0.71, all thermophysical properties (e.g. c_p, λ) of the fluid were assumed to be constant [4, 29, 30], except for the fluid density and viscosity, which vary with temperature. The flows in the air cavity and cells formed between neighbouring slats on Venetian blind remain laminar, because the *Grashof Numbers* never reach the related critical value [25]. The *Surface to Surface* (S2S) radiation model was used to solve the radiative transfer equation. The boundary conditions of the two isothermal surfaces were set to match the mean temperature and surface temperature difference, used in the experimental study.

The thermal conductance (R) of a double glazed unit with and without Venetian blind structures can be expressed in Equation (4-3):

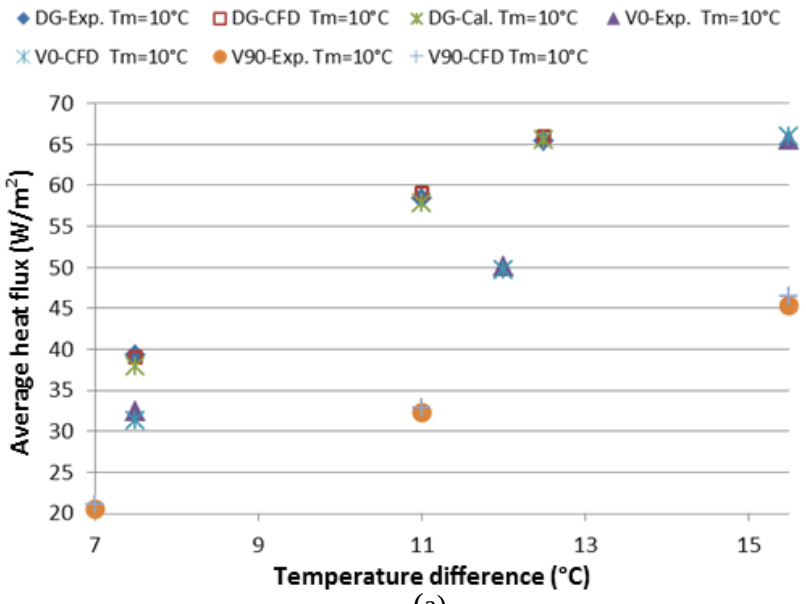
$$R = \frac{\Delta T}{(\frac{\partial T}{\partial x})_w \lambda_a} = \frac{\Delta T}{q} \qquad (4-3)$$

where $(\frac{\partial T}{\partial x})_w$ is the air temperature gradient on the wall and q is the average heat flux of combined convective and radiative heat transfer across the two surfaces. ΔT (°C) is the temperature difference between the hot and cold surfaces of the glazing system.

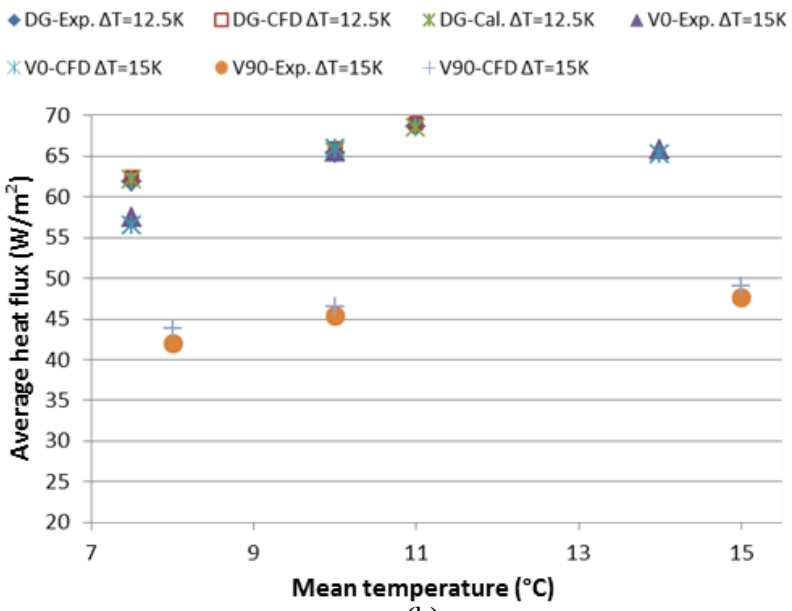
4.2.6 Comparison between experimental test, standard calculation and CFD

For the double glazed unit (DG), the results based on the calculation method set out in EN 673 [110] were compared with measured results. In addition, the measured results of the glazing system with and without Venetian blinds were also compared with the results obtained by CFD simulation to validate the accuracy of CFD modelling.

Figure 4-5 (a) shows the results for each glazing configurations tested under the first 3, in which, the mean temperature of the glazed units was kept at 10 °C. It may be seen that with an increase of temperature difference from 7 °C to 15 °C, the average heat flux for all these structures increases. For example, the heat flux of DG increases from approximately 40 W/m^2 to 65 W/m^2. The average heat flux obtained from CFD simulation shows a difference of less than 1.2% for DG and less than 2.7% for V0 and V90 when compared with the experimental results. Similarly, Figure 4-5 (b) shows the relationship between average heat flux and mean temperature for a constant temperature difference across each glazing system. Increasing mean temperature results in an increase of the heat flux (e.g. from approximately 43 W/m^2 to 48 W/m^2 for V90). Both the CFD simulation and the calculated results match well with the experimental results, the differences are less than 1% for the double glazed unit and less than 4% for the glazed unit with blinds (V0 and V90).



(a)



(b)

Figure 4-5: Measured, calculated and simulated heat flux through glazing system (a) scenarios 1, 2 and 3 in DG V0 and V90; (b) scenarios 3, 4 and 5 in DG V0 and V90

The comparison between these three methods provides a high degree of confidence in the CFD modelling, which means further model developed using this method may be used to extend the thermal analysis of the glazing system with Venetian blinds.

4.3 Numerical investigation methodology: CFD simulation

Schematic diagrams illustrating the geometry of a double glazed unit with and without a PS-TIM structure are shown in Figure 4-6. A double glazed unit was assumed to have an air gap of thickness 15 mm between panes that were 300 mm in height. This was investigated with 4 different geometries of PS-TIM, where the interval distances between the neighbouring slats, D_a, was assumed to be 3 mm, 5 mm, 7.5 mm and 10 mm. These interval distances are selected in order to present a gradual variation of *aspect ratio* from 0.2 to 0.67.

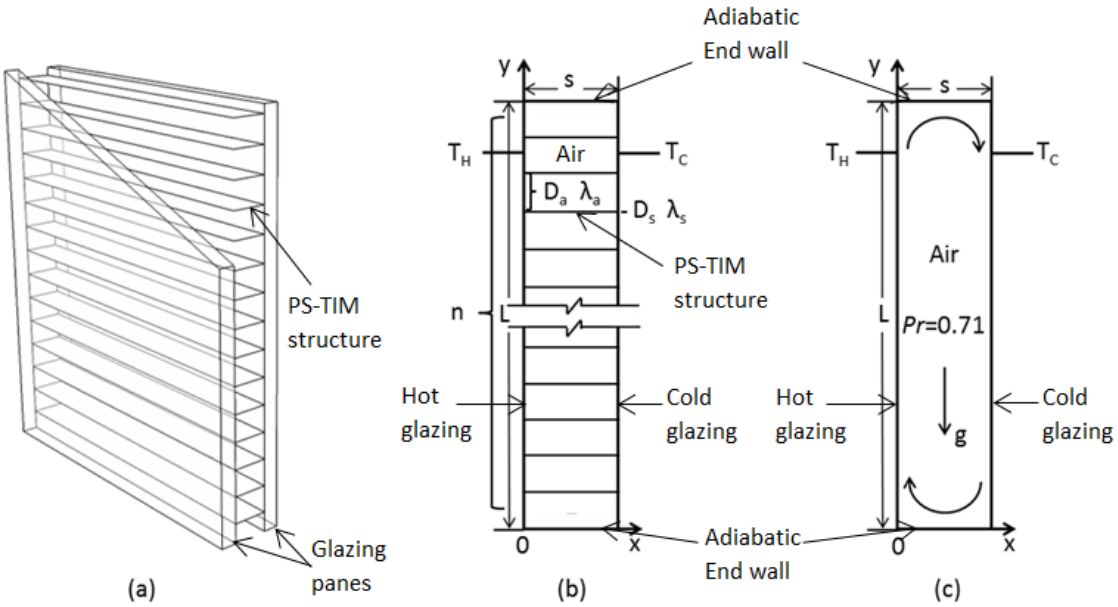


Figure 4-6: (a) PS-TIM structure in a double glazed unit; (b) 2D schematic illustrating the geometry of the air gap with PS-TIM structure; (c) 2D schematic illustrating geometry of air gap without PS-TIM.

4.3.1 Governing equations and assumptions

Two-dimensional finite volume models were developed in the commercial CFD package FLUENT. To simplify the CFD simulation process, the following assumptions were made:

1) the glass surfaces facing into the cavity were set as two isothermal walls with different temperatures to represent the temperature difference between indoor and outdoor environments;

2) the top and bottom surfaces bounding the cavity were assumed to be adiabatic;

3) the enclosure was filled with air whose thermophysical properties (density, viscosity, thermal conductivity) are detailed in Table 4-2;

4) the working fluid, air, has a *Prandtl number* of approximately 0.71.

It is assumed that flows are steady and incompressible in the simulation. Flows in the cavity and cells remains laminar, because the *Grashof Numbers* do not reach the related critical value [25]. The governing Equations are:

Mass balance:

$$\frac{\partial \mathrm{u}}{\partial \mathrm{x}} + \frac{\partial v}{\partial y} = 0 \qquad (4-4)$$

Momentum balance:

$$\rho\left(\mathrm{u}\frac{\partial u}{\partial x} + \mathrm{v}\frac{\partial u}{\partial y}\right) = -\frac{\partial \mathrm{p}}{\partial \mathrm{x}} + \mu\left(\frac{\partial^2 u}{\partial x^2} + \frac{\partial^2 u}{\partial y^2}\right) \qquad (4-5)$$

$$\rho\left(\mathrm{u}\frac{\partial \mathrm{v}}{\partial \mathrm{x}} + \mathrm{v}\frac{\partial v}{\partial y}\right) = -\frac{\partial \mathrm{p}}{\partial \mathrm{x}} + \mu\left(\frac{\partial^2 v}{\partial x^2} + \frac{\partial^2 v}{\partial y^2}\right) + \rho g\beta(T - T_C) \qquad (4-6)$$

Energy balance:

$$\rho c_p\left(u\frac{\partial T}{\partial x} + v\frac{\partial T}{\partial y}\right) = k\left(\frac{\partial^2 T}{\partial x^2} + \frac{\partial^2 T}{\partial y^2}\right)(+S_h) \qquad (4-7)$$

In order to evaluate the effect of the parallel slat structure on convection, the radiative heat transfer between the two glazing panes was initially neglected (this is referred to as the convection-only model). Radiation, conduction and convection were included in the full model, which was used to calculate the overall scale of heat transfer through the air cavity and the resulting *U-value* of the glazing system.

In the full model, radiative heat transfer, S_h in Equation (4-7), was solved using the *Surface to Surface* (S2S) radiation method. All the surfaces were assumed to be grey bodies, diffuse and opaque to thermal radiation. The air in the cavity was assumed to be a non-participating medium. The view factors (F_{kj}), which depend on surfaces' size, separation distance and orientation were computed before the simulating radiation.

The S2S method can be represented by the following equation:

$$J_k = \varepsilon_k \sigma T_k^4 + (1 - \varepsilon_k)\sum_{j=1}^{N} F_{kj} J_j \qquad (4-8)$$

In both models, all thermophysical properties of the fluid were assumed to be constant (e.g. C_p, k) [4, 29, 30] except for the fluid density and viscosity. Variation of density ρ in response to temperature change was treated by means of the Boussinesq approximation. The equation is given as follows:

$$\rho = \rho_0[1 - \beta(T - T_0)] \qquad (4-9)$$

Where ρ_0 is the (constant) density of the air at the mean surface temperature (T_0), and β is the thermal expansion coefficient.

The viscosity was assumed to vary in response to temperature according to piecewise-linear equation as follows:

$$\mu(T) = \mu_n + \frac{\mu_{n+1} - \mu_n}{T_{n+1} - T_n} \qquad (4-10)$$

where $1 \leq n \leq N$ and N is the size of the temperature intervals.

4.3.2 Boundary conditions and material properties

The material characteristics (conductivity, thickness and emissivity) of the PS-TIM structure were varied to explore their influences on the overall performance of the window using the full model. Detailed properties can be found in Table 4-2. From this it may be seen that, four temperature differences between the two glazing panes (10 K, 20 K, 30 K and 40 K) were set as the boundary conditions and their mean temperature was maintained at 10 ℃ (283 K).

Table 4-2: Properties and boundary conditions for different models.

Convection-only model	**Air Properties:**			
	Specific heat capacity (J/kg K)	*Conductivity* (W/mK)	*Thermal expansion coefficient* (1/K)	
	1005	0.025	0.00353	
	PS-TIM properties:			
	Conductivity (W/mK)	*Thickness* (mm)	*Emissivity*	
	0.15	0.1	0.65	
	Boundary conditions (refer to Figure 4-6):			
	Left glazing (K)	Right glazing (K)	Top end	Bottom end
	288/ 293/ 298/ 303	278/ 273/ 268/ 263	Adiabatic	Adiabatic
Convection-conduction-radiation model	**Air Properties:** Same as 'convection-only model'			
	PS-TIM properties			
	Conductivity (W/mK)	*Thickness* (mm)	*Emissivity*	
	0.1/0.2/0.3/0.4/0.5	0.05/0.1/0.15/0.2	0.3/0.65/0.84	
	Boundary conditions: Same as 'convection-only model'			
Convection-conduction-radiation model for *U-value* calculation	**Air Properties:** Same as 'convection-only model'			
	PS-TIM properties: Same as 'convection-only model'			
	Boundary conditions (refer to Figure 4-6):			
	Left glazing (K)	Right glazing (K)	Top end	Bottom end
	290.5	275.5	Adiabatic	Adiabatic
	Glass Properties:			
	Conductivity (W/mK)	*Thickness* (mm)	*Emissivity*	
	0.94	4	0.84	
	Surface *heat transfer coefficient*:			
	External (W/m^2 K)	25	Internal (W/m^2 K)	7.7

4.3.3 Mesh independency

Extensive mesh independence and iterative convergence studies were undertaken. In the final model, smaller size meshes with dimension 0.025 mm × 0.025 mm were arranged near the two glazing surfaces, which then gradually increased in size toward the centre of the cavity.

4.3.4 Derivation of thermal transmittance

The local convective heat flux and combined convective and radiative heat flux can be obtained from the converged temperature field in the CFD simulation. The predicted of convective heat flux at the boundaries of two glazing panes was used to express the local *Nusselt number* (*Nu*) using Equation (4-11):

$$Nu = \frac{(\frac{\partial T}{\partial x})_w s}{\Delta T} = \frac{qs}{k_a \Delta T} \qquad (4-11)$$

where $(\frac{\partial T}{\partial x})_w$ is the air temperature gradient on the glazing surface and q(W/m^2) is the average convective heat flux across the two surfaces. ΔT (K) is the temperature difference between the hot and cold isothermal surfaces.

The *Nusselt number*, which represents the ratio between the pure conduction resistances to a convection resistance [212], is an important dimensionless coefficient that indicates the intensity of convection. It is affected by three dimensionless parameters: the *aspect ratio* of the cavity; the *Prandtl number* and the *Grashof number* of the fluid. The *aspect ratio* ($A = \frac{L}{s}$, for the plane double glazed unit, or $A = \frac{D_a}{s}$, for the PS-TIM unit) describes the geometry of the air cavity. The *Prandtl number* ($Pr = \frac{c_p \mu}{\lambda_a}$) describes the ratio of momentum diffusivity to thermal diffusivity and the *Grashof number* ($Gr = \frac{g\beta \Delta T s^3 \rho^2}{\mu^2}$) describes the relationship between buoyancy and viscosity within a fluid.

The thermal conductance (*h*) of a double glazed window without PS-TIM structure can be expressed in Equation (4-12):

$$h_{no-slat} = \frac{(\frac{\partial T}{\partial x})_w \lambda_a}{\Delta T} = \frac{q\prime}{\Delta T} \qquad (4-12)$$

where *q'* is the average heat flux of combined convective and radiative heat transfer across the two surfaces.

Inclusion of the PS-TIM gives the thermal conductance as:

$$h_{PS-TIM} = \frac{q'}{\Delta T} \cdot \frac{D_a n}{L} + \frac{\lambda_s}{s} \cdot \frac{D_s(n-1)}{L} \qquad (4-13)$$

where D_a is the distance between two neighbouring slats, D_s is the thickness of the slat, n is the number of slats and L is the height of the window.

The thermal conductance (in Equation (4-14), h is abbreviation for either $h_{PS\text{-}TIM}$ or $h_{no\text{-}slat}$) here describes the heat transfer coefficient through the air cavity, which includes the convective and conductive heat transfer through the air, conductive heat transfer through the PS-TIM structure and the radiative heat transfer from internal to external surfaces. Once this was obtained through CFD simulation, the *U-value* of the whole unit can be calculated separately using the following procedure. Firstly, the thermal resistance of the glazed unit (R) is obtained from:

$$R = \frac{1}{h} + \frac{2d}{\lambda_g} \qquad (4-14)$$

where d is the thickness of each glass pane, and λ_g is the thermal conductivity of the glass (W/mK). The two glazing panes were assumed to be ordinary soda-lime silica float glass with thickness of 4 mm, thermal conductivity of 0.94 W/mK and emissivity of 0.84 (see Table 4-2). The thermal conductance, *U-value*, of the unit can be expressed as:

$$\frac{1}{U} = \frac{1}{h_e} + R + \frac{1}{h_i} \qquad (4-15)$$

where, h_e and h_i are the external and internal surface heat transfer coefficients, respectively. For normal exposure of panes, h_e = 25 W/m^{2}K and h_i = 7.7 W/m^{2}K are assumed [196]. For the purpose of normalization of the calculated *U-value*, the

temperature difference between the bounding glass surfaces was kept at 15 K, while the mean temperature was kept at 10 °C (see Table 4-2) [110, 196].

4.4 Results and discussion

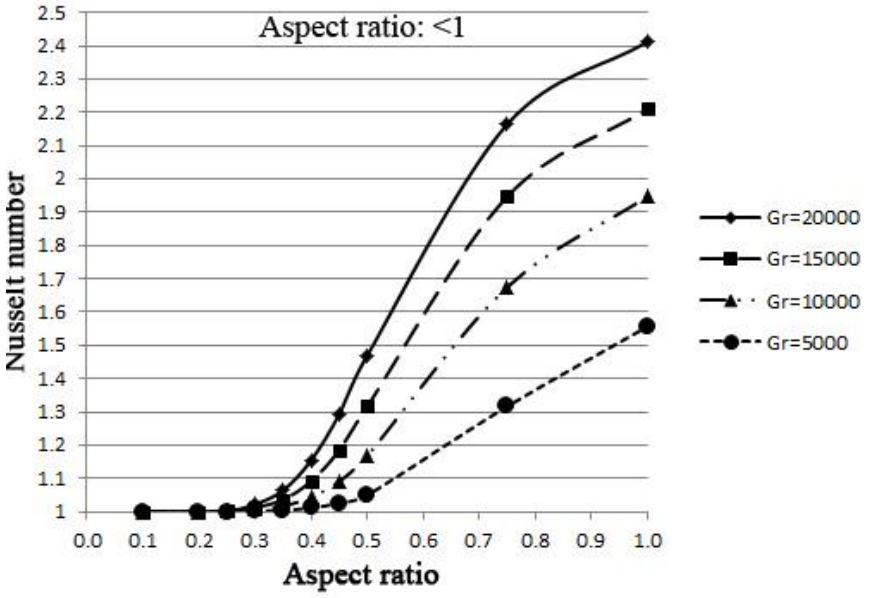
In this section, the simulation results for convective, conductive and radiative heat transfer through the PS-TIM structure located in the cavity of double glazed units are discussed. The overall *U-value* and optical performance of the PS-TIM system are presented.

4.4.1 Effects of aspect ratio on convective suppression

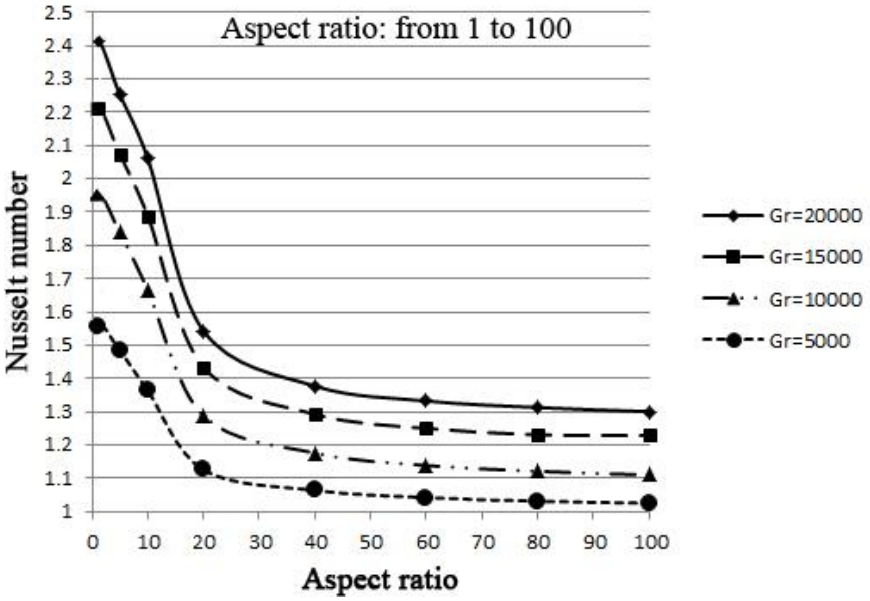
The PS-TIM structure is proposed as a means of suppressing convective heat transfer in the air cavity of a double glazed unit. However, it is useful to understand the free convection that occurs in a single air cavity formed between neighbouring slats and how changing the distance between them, D_a, influences convective suppression. In this section, the influence of *aspect ratio* of a double glazed unit (illustrated in Figure 4-6 (c)) and the *aspect ratio* of a PS-TIM cell (shown in Figure 4-6 (b)) in providing convective suppression are investigated. In order to realise the variation of *aspect ratio*, the width of the air cavity between the two glazing panes was fixed and the spacing between slats was changed. Under these circumstances, variations of the *Grashof number* depends only on the temperature difference between the two vertical glazing surfaces (when ΔT = 10K, 20K, 30K and 40K, Gr = 5000, 10000, 15000 and 20000 respectively).

Figure 4-7 shows the relationship between the *Nusselt number* and *aspect ratio* at different *Grashof numbers* for a single air cavity. Figure 4-7 (b) presents data for air

cavities with *aspect ratios* representative of those observed in conventional double glazed units. Figure 4-7 (a) presents data for *aspect ratios* that are representative of the cells present in a PS-TIM structure. It can be seen that the *Nusselt number* reaches the peak value when the *aspect ratio* is equal to 1. This means that a square cavity provides the smallest viscous resistance to the onset of free convection. In the range of $A = 1 \sim 100$, the *Nusselt number* decreases in response to increasing of *aspect ratio*. This occurs rapidly up to a value of $A = 30$. Thereafter the *Nusselt number* decreases only gradually. This indicates that the shape of the vertical space has significant influence on the free convection until it becomes sufficiently tall. In the range of $A = 1 \sim 100$, a high *Grashof number* leads to a high *Nusselt number*. This means that a higher temperature difference increases the convection in the cavity; therefore the convective heat transfer cannot be fully suppressed over the temperature range examined. When the *aspect ratio* is less than 1, for practical purposes, this would represent a single cell in a double glazed unit where the slat spacing is less than the cavity width. Figure 4-7 (a) shows that the *Nusselt number* declines sharply until it reaches $Nu = 1$ at $A = 0.35$ over the range of the *Grashof number* spanning 5000 to 20,000. This indicates that at the scale of a window, the introduction of the slats and their influence on the geometry of the cell is capable of achieving full convection suppression. This occurs because the resulting resistance is sufficiently high that no matter what the temperature difference between the two panes is convection is not initiated.



(a)



(b)

Figure 4-7：Relationship of the *Nusselt number* vs *aspect ratio* for different *Grashof number* for (a) small cells and (b) double glazed units.

4.4.2 Thermal visualisation within the PS-TIM structures

From section 4.4.1, it can be seen that creating small horizontal rectangular cells leads to full convection suppression within an air cavity of a double glazed unit. Achieving this through the introduction of a PS-TIM structure with small cells was therefore studied further to visualise the effects of slat interval distance on the convective

heat transfer. Four interval distances (D_a = 3 mm, 5 mm, 7.5 mm and 10 mm) were analysed and also compared with a cavity containing no slats.

The predicted temperature profiles are shown in Figure 4-8. For the double glazed unit, when *Gr* = 5000, the fluid travels upwards near the hot surface, and downwards adjacent to the cold surface, describing a primary convection cell. When the Gr number is larger than 1000, secondary cells start to present, which interfere with the isothermal profile. For the 10 mm-cell structure, the curving profile of the isotherms indicates that thermally-induced buoyant flow is present, forming a convective cell. However, for the PS-TIM with 3 mm- and 5 mm-cell structures and the 7.5 mm-cell structure when *Gr* = 5000, the isotherms are uniformly spaced, indicating the heat transfer is conductive in nature. The relationship between the average *Nusselt number* and *Grashof numbers* shown in Figure 4-9, illustrates the effect of convection suppression. The PS-TIM with a 10 mm-cell structure provides less convection suppression as the average *Nusselt number* is similar to, or larger than, that for the cavity without slats at same *Grashof number*. This is because the viscous resistance of a 10 mm-cell is generally less than the tall vertical air cavity of the double glazed unit. For the PS-TIM with a 7.5 mm-cell structure, although its *Nusselt number* increases with *Grashof number*, it only reaches 1.2, which indicates that over the range of *Grashof numbers* studied the convective heat transfer is not significant [213]. Free convection within 3 mm and 5 mm-cell structures is almost fully suppressed over the range of the *Grashof number* from 5000 to 20,000. The visualisations therefore suggest that PS-TIMs with 3 mm, 5 mm and 7.5 mm-cell structures can significantly reduce the average *Nusselt number* and hence reduce convective heat transfer rate, when compared with the air cavity without PS-TIM slats at the same *Grashof number*.

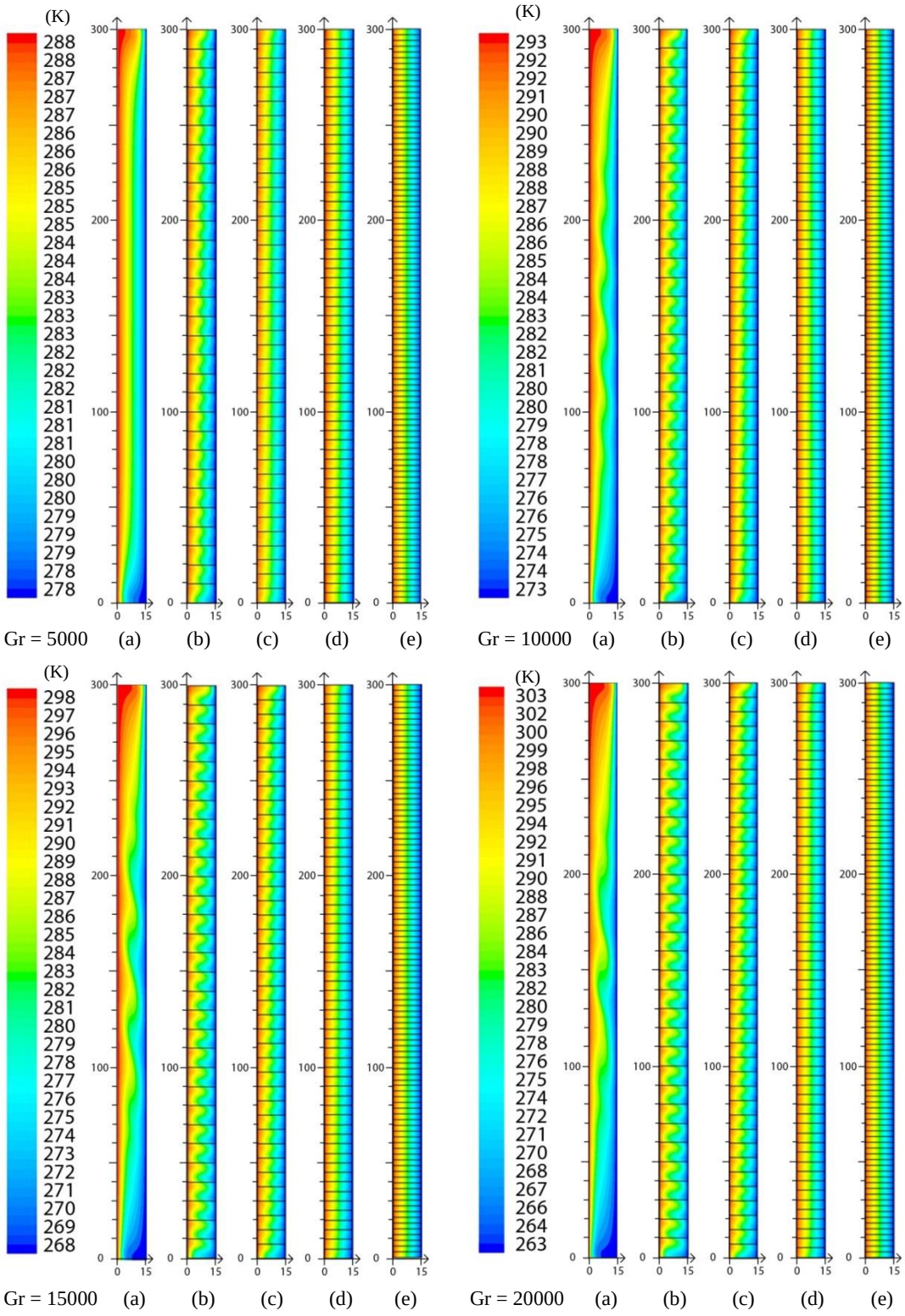


Figure 4-8: Temperature profile of a double glazed unit with and without PS-TIM structures at different *Grashof number*: (a) no-slats; (b) 10 mm-cell structure; (c) 7.5 mm-cell structure; (d) 5 mm-cell structure; (e) 3 mm-cell structure

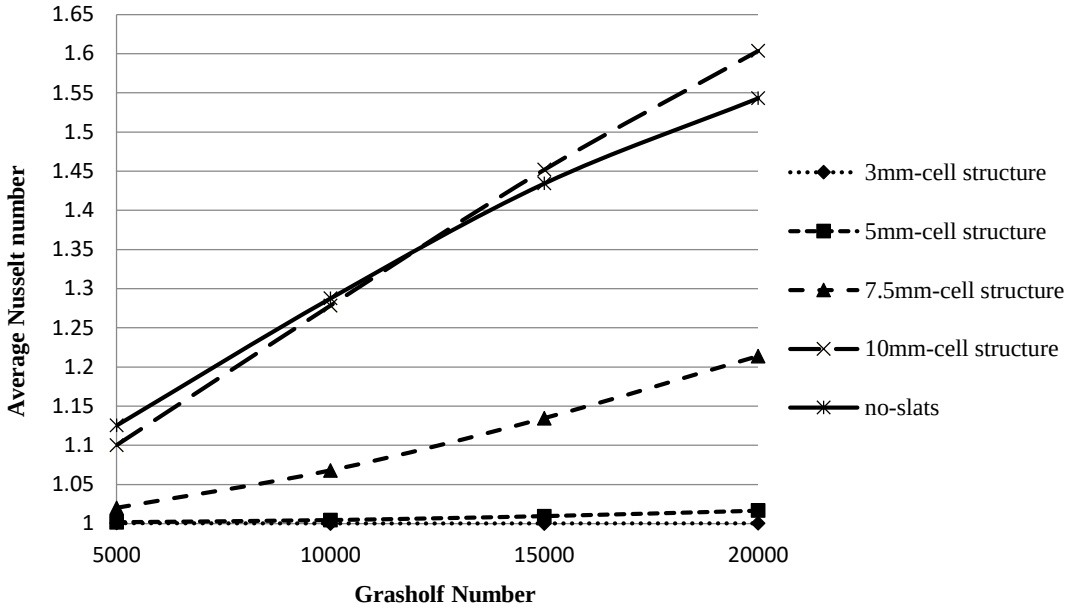


Figure 4-9: Relationship between the average *Nusselt number* and *Grashof numbers* for different cell heights

4.4.3 Thermal conductance of an air cavity with PS-TIM structures

In this section, the full model was used to investigate the thermal conductance of the air cavity with and without PS-TIM structures. The thermal conductance predicted using Equations (4-9) and (4-10) at various temperature differences between the hot and cold glazing surfaces is shown in Figure 4-10. The thermal conductance of the system is the sum of conductive heat transfer through the slat (when PS-TIM structures are present), conductive and convective heat transfer through the air and radiative heat transfer. Radiative heat transfer remains constant in each structure due to the constant mean temperature of 10 K between the two surfaces and for these simulations represents the dominant heat transfer mechanism, accounting for 50 ~ 68% of heat transfer in all the structures examined. Thus, a significant reduction of radiative heat transfer caused by the presence of a PS-TIM structure yields a significant reduction of the total thermal conductance. The scale of this reduction is related to the PS-TIM cell size – for example, 10 mm-cells reduced the radiative heat transfer by over 25% when compared with that of the no-slat structure and 3 mm-cells yielded reductions in the order of 50%. With a

sectional thickness D_s = 0.1 mm and a conductivity λ_s = 0.15 W/mK, conduction accounts for less than 8% of total heat flow in the PS-TIMs with 3 mm and 5 mm-cells and less than 2.7% in the PS-TIMs with 7.5 mm and 10 mm-cells. Conductive heat transfers through the PS-TIM slats is not significant in these simulations.

Figure 4-11 shows the overall effect on heat transfer resulting from the introduction of PS-TIM, into a glazed unit. This is quantified using the thermal conductance ratio $h_{PS\text{-}TIM} / h_{no\text{-}slat}$ (see Equation (4-10) and Equation (4-9)). As can been seen in Figure 4-11, all of the four PS-TIM structures studied are able to provide reduction in thermal conductance as compared with a standard double glazed unit over the assumed range of temperature difference. In general, the smaller the PS-TIM cell height, the smaller the thermal conductance is. For PS-TIMs with 3 mm, 5 mm and 7.5 mm-cell, increasing temperature difference sees improved performance, i.e. the thermal conductance ratio decreases. For example, the 3 mm-cell PS-TIM can achieve a 34.5% decrease of thermal conductance for a 10 K temperature difference and a 45% decrease when the temperature difference is 40 K. This is because, in moving from a temperature difference of 10 K to 40 K, the heat transfer due to air convection decreased from 14% to 37%, while the reduction in heat transfer due to radiation remains constant at around 50%. On the other hand, the 10 mm-cell PS-TIM shows an opposite trend to that apparent in the other three structures. The primary benefit of the slats in this geometry is in their ability to reduce view angles and hence reduce radiative heat transfer. The geometry they create, however, leads to an increase in convective heat transfer as the temperature difference between the glazing panes is increased. The overall reduction of thermal resistance of the 10 mm-cell PS-TIM is 16.4% (at 10 K) to 15% (at 40 K).

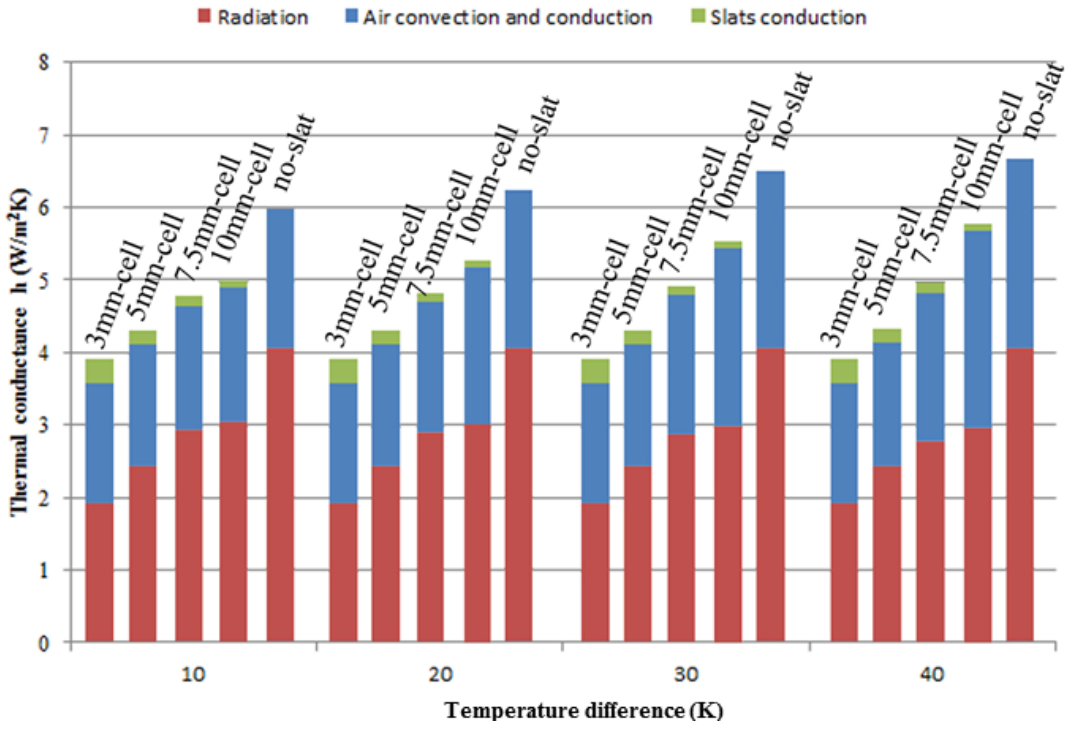


Figure 4-10: Thermal conductance caused by conduction, radiation and convection for an air cavity with and without PS-TIMs with different cell dimension at various glazing pane temperature differences

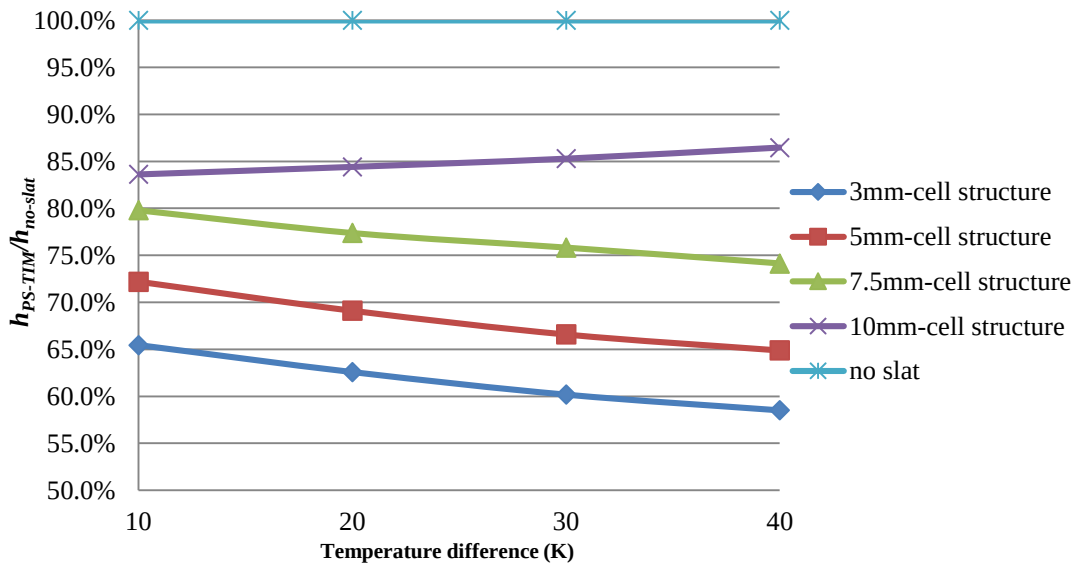


Figure 4-11: Ratio of thermal conductance of an air cavity with PS-TIMs with different cell dimension to an air cavity without PS-TIM at various glazing pane temperature differences

4.4.4 The effects of slat conductivity, thickness and emissivity on the thermal performance of PS-TIM

In this section, the effects of slat conductivity, thickness and emissivity on the overall thermal conductance of a double glazed window containing PS-TIM are

discussed. Again, the ratio of the thermal conductance of the window with PS-TIM to the thermal conductance of a standard double glazed unit, the window without TIM, ($h_{PS\text{-}TIM} / h_{no\text{-}slat}$) is used to quantify these effects. Data for the PS-TIM with 3 mm, 5 mm and 7.5 mm-cells, where convection is effectively suppressed, showed similar trends, therefore only the 3 mm data are presented. These are compared with data for the PS-TIM with 10 mm-cells where convection is present.

The effect of the material conductivity of the PS-TIM structure on the thermal conductance is illustrated in Figure 4-12. When the slat thermal conductivity increases from 0.1 to 0.5 W/mK (while maintaining D_s = 0.1 mm and ε = 0.65), the thermal conductance of the glazing system increases for both the 3 mm-cell and 10 mm-cell PS-TIMs. The slat conductivity has a more significant influence on the 3mm-cell PS-TIM because it has higher numbers of slats and hence a greater total area of structural bridging as compared with the 10 mm-cell PS-TIM. For example, when the temperature difference between the two panes of glass is 10 K, changing the conductivity of the slats from 0.1 W/mK to 0.5 W/mK increases the thermal conductance of the 3 mm-cell PS-TIM from approximately 63.5% to 78% (relative to a standard double glazed unit). For the 10 mm-cell PS-TIM at the same temperature difference, the thermal conductance only increases from 83% to 87.5%.

This pattern is consistent for all the temperature differences assumed in the simulation, i.e. thermal conductance ratio increases with increasing thermal conductivity, however, the combined influence of conduction, convection and radiation that is illustrated in Figure 4-11 is maintained. The overall benefits offered by the 3 mm-cell PS-TIM through reduced radiative and convective conductance more than outweigh these increases in conduction, so that at any given value of conductivity, the conductance ratio decreases with increasing temperature difference. By contrast, the 10 mm-cell PS-

TIM, where increasing temperature difference drives stronger convection, and exhibits an increasing conductance ratio, i.e. at any given value of conductivity, the conductance ratio increases with increasing temperature difference.

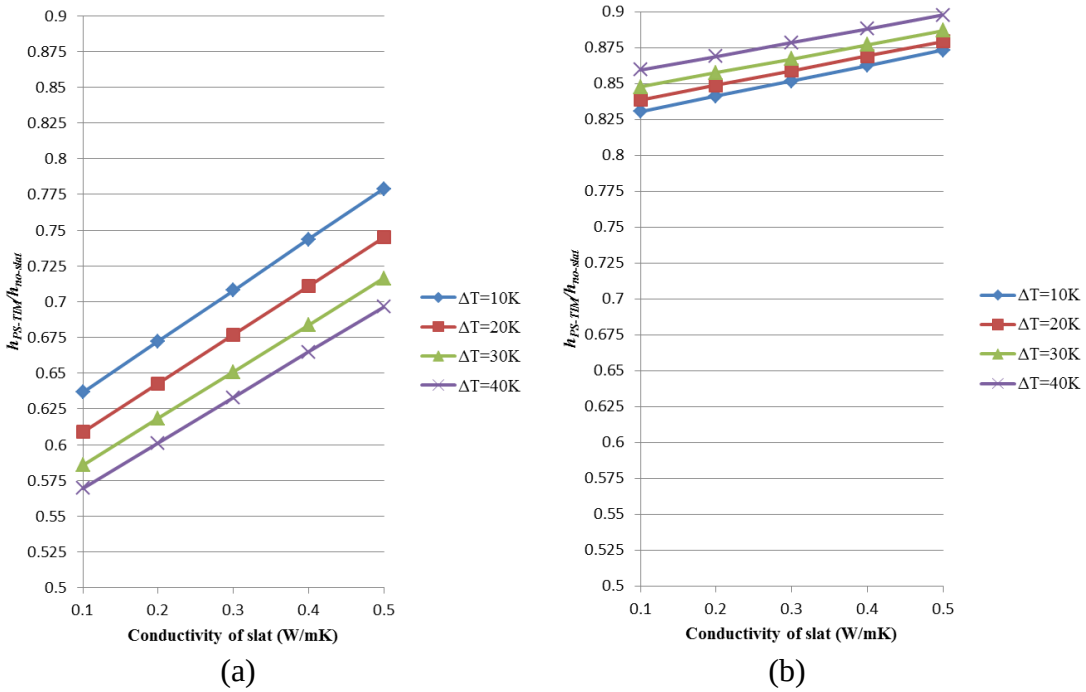


Figure 4-12: Thermal conductance ratio ($h_{PS\text{-}TIM}/h_{no\text{-}slat}$) for different slat conductivities (W/mK) at various glazing pane temperature differences of (a) 3 mm PS-TIM and (b) 10 mm PS-TIM

Figure 4-13 shows the influence of slat thickness, D_s, on of thermal conductance (while maintaining λ_s = 0.15W/mK and ε = 0.65, again measured relative to a standard double glazed unit. As might be expected, given the relationship between conductance, conductivity and the cross sectional area of any element through which conduction is occurring, the general pattern of behaviour illustrated in Figure 4-13 echoes that in Figure 4-12. The effect of increasing the slat thickness is, however, less pronounced than that of increasing its conductivity because in addition to increasing heat flux conducted across the cavity, it simultaneously reduces the height of the air cells in the PS-TIM. This in turn reduces heat transfer between the two glazing surfaces taking place by radiation and convection, reducing the slope of the curves in Figure 4-12.

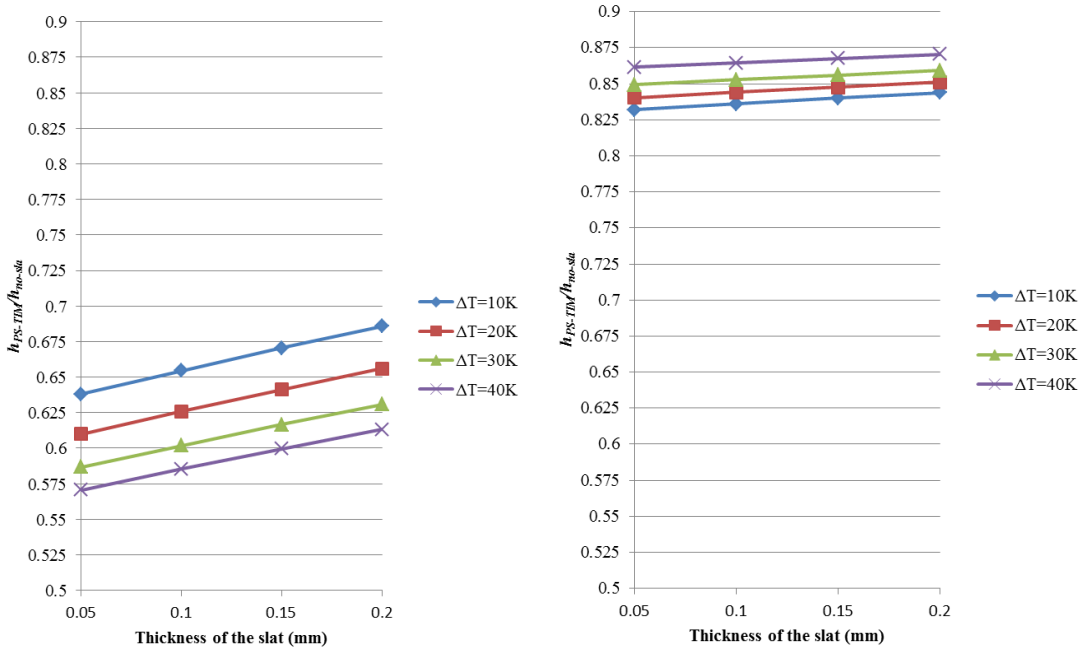
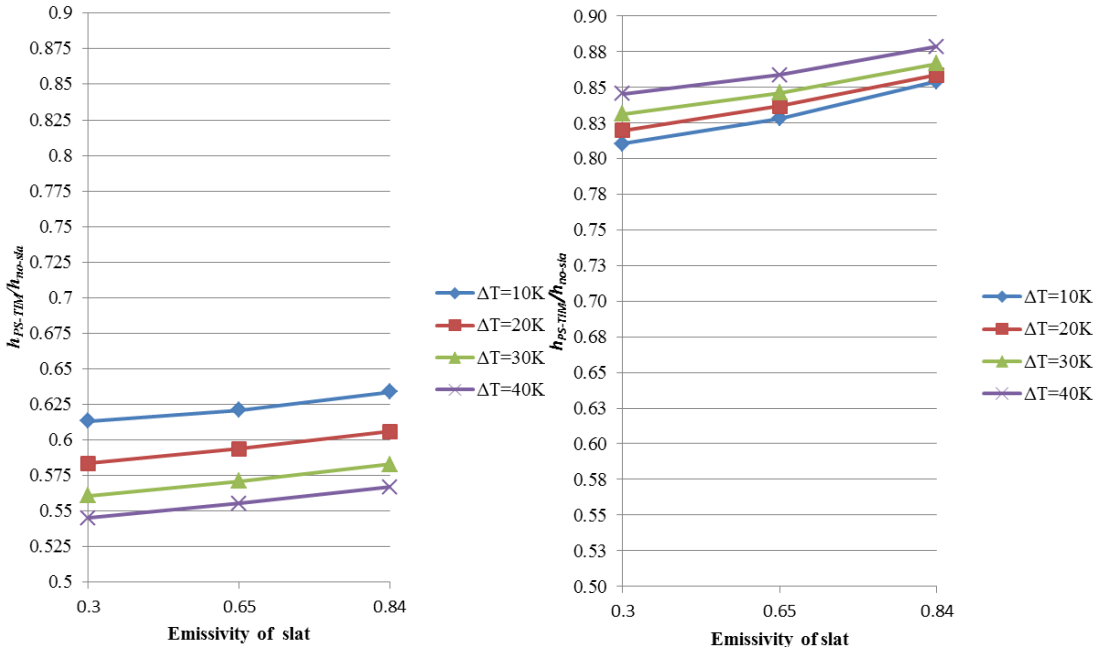


Figure 4-13: Thermal conductance ratio ($h_{PS\text{-}TIM}/h_{no\text{-}slat}$) for different slat thickness (mm) at various glazing pane temperature differences of (a) 3 mm PS-TIM and (b) 10 mm PS-TIM

The predicted variation of total thermal conductance ratio for three values of slat emissivity (ε = 0.3, 0.65 and 0.84) while maintaining D_s = 0.1 mm and λ_s = 0.15 W/mK, is shown in Figure 4-14 It can be seen that with increasing emissivity, the thermal conductance ratio for both the 3 mm and 10 mm-cell PS-TIMs increases. The effect is relatively weak however. For example, when the emissivity of the slat is increased from 0.3 to 0.84 under a temperature difference of 40 K, the thermal conductance ratio increases by only 2% for a 3 mm-cell structure and 3.5% for a 10 mm-cell structure. Given the strength of the radiative path indicated in Figure 4-10, this suggests that heat radiated and re-radiated from the slats is secondary to heat directly radiated across the cavity from one glazing pane to the other.



(a) (b)

Figure 4-14: Thermal conductance ratio ($h_{PS\text{-}TIM}/h_{no\text{-}slat}$) at different slat emissivity at various glazing pane temperature differences of (a) 3 mm PS-TIM and (b) 10 mm PS-TIM

In conclusion, decreasing slat conductivity and slat thickness result in the reduction of thermal conductance of double glazed windows containing PS-TIM held at a constant temperature difference: this effect is more significant on PS-TIMs with 'small' cells. Decreasing slat emissivity has a weak but beneficial effect, reducing the thermal conductance of double glazed windows containing a PS-TIM structure.

4.4.5 Total thermal resistance and U-value

The overall heat transfer of the glazing system under standard boundary conditions EN 673 [110] (temperature difference of 15 °C between two glazing panes, average glazing pane temperature of 10 °C) was simulated and is discussed in this section. Figure 4-15 illustrates the total thermal resistance ($R_t = \frac{1}{U}$), which is the sum of the thermal resistance between two glass panes ($\frac{1}{h}$), the glass panes thermal resistance ($\frac{2d}{k_g}$) and the external and internal surface thermal resistance ($\frac{1}{h_e}$ and $\frac{1}{h_i}$). The *U-values* of double glazing with and without Venetian blind configurations are shown in Table 4-3.

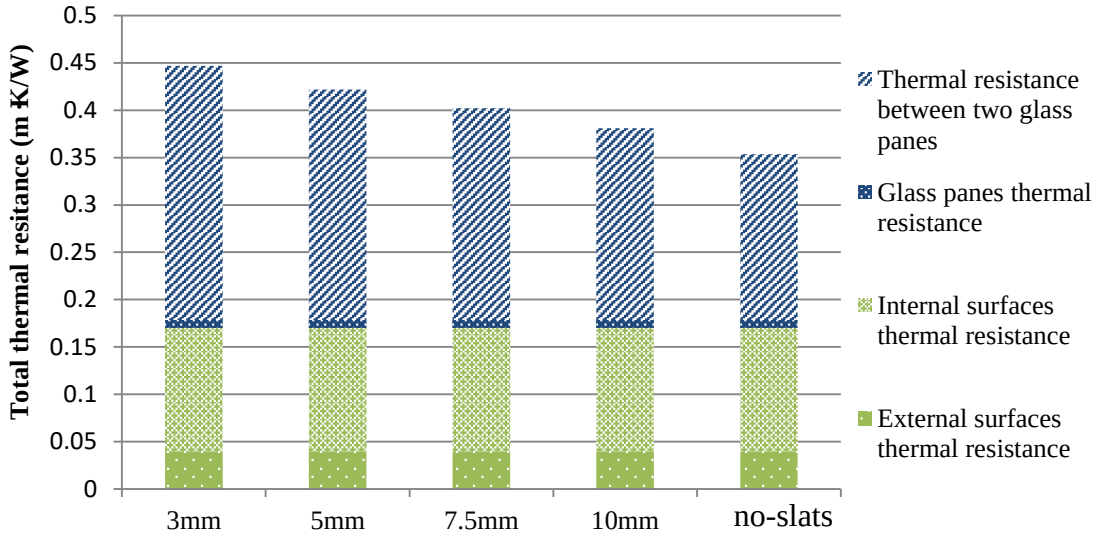


Figure 4-15: The thermal resistance ($\frac{1}{U}$) of a double glazed window containing PS-TIM structure

Table 4-3: The *U-values* of a double glazed window containing PS-TIM structure

	3 mm-cell structure	5 mm-cell structure	7.5 mm-cell structure	10 mm-cell structure	no-slats
U-value (W/m^2K)	2.238	2.371	2.487	2.626	2.829

From Figure 4-15 and Table 4-3, it can be seen that, as the surface thermal resistances and glass panes thermal resistance are assumed constant in all these structures, the change in predicted performance is due solely to the effect of the PS-TIM. Adding PS-TIM and reducing the slat interval distance from 10 mm to 3 mm leads to a gradual increase of thermal resistance between two glazing panes and hence a reduction of the *U-value*. The thermal resistance between two glazing panes only contributes to 49.5% of the total thermal resistance in the standard double glazed unit, and the contribution has been increased to 60% by adding 3 mm-cell structure in the air cavity. This is reflected in a 21% reduction of the *U-value*.

4.5 Conclusion

A detailed simulation based investigation of the thermal behaviour of Parallel Slat TIM (PS-TIM) structures sandwiched between the panes of a double glazed window unit has been conducted. Experimental results of thermal performance of a glazing system with a Venetian blind were used to validate the CFD simulation methodology. Venetian blind was selected because that this structure as an interstitial structure between two glazing panes shares many of the same characteristics as PS-TIMs. Experimental results and simulation results agree well with each other, and this provides a degree of confidence over the use of this numerical model to explore the thermal characteristics of glazing system with various interstitial PS-TIM structures under different temperature conditions. In addition, the following conclusions can be drawn:

1) For windows, when the *aspect ratio* of a cell (whose geometry is defined by the ratio of the PS-TIM slat spacing to the separation between glazing panes) is less than 0.35, free convection is fully suppressed and is independent of the temperature difference between the two surface panes;

2) In practice, selecting a suitable interval distance for the parallel slats in the air cavity such that the *Nusselt number* is less than 1.2 can provide good reduction of the convective heat transfer coefficient;

3) The results of a convection, conduction and radiation model show that a double glazed unit containing PS-TIM with a 3 mm-cell structure can offer a 35 ~ 42% reduction in thermal conductance as compared with an identical double glazed unit in the absence of PS-TIM. The equivalent performance for PS-TIM with a 10 mm-cell structure is a 16 ~ 18% reduction in conductance. The slat conductivity and

thickness have a significant influence on overall thermal conductance when the temperature difference between the glazing panes is small;

4) In general, the presence of interstitial PS-TIMs with different slat pitches can achieve 7% to 21% improvements in *U-value* when compared with a normal double glazed unit.

It should be noted that the double glazed unit used to benchmark the performance of the PS-TIM in this study does not reflect the current state of the art in relation to low emissivity coatings and gases used to fill the cavity. As a consequence, the *U-values* predicted in this study are higher than current industry best practice and it is likely that structured conduction would assure a greater role if benchmark against a best practice double glazing unit.

Chapter 5. Daylight performance prediction of applying glazing systems with Parallel Slat Transparent Insulation Material (PS-TIM)

5.1 Introduction

Chapter 4 discussed the potential of using Transparent Insulation Materials (TIM) sandwiched between the panes of a double-glazed window unit to increase the thermal resistance of a double glazed window. The results show that a double glazed unit containing PS-TIM with various slat pitches can offer a 7 ~ 21% reduction in U-value as compared with an identical double glazed unit in the absence of PS-TIM. The employment of PS-TIM does, however, reduce the amount of daylight transmitted through the window system as well as modify the daylight distribution within the space it serves. Defining and obtaining the optical behaviour of PS-TIM as well as assessing the daylight performance of applying PS-TIM in an office serve as the focus of this chapter.

In seeking to evaluate the quantity, quality and distribution of daylight accurately, traditional approaches, which are mainly based on the use of rule of thumb or simplified calculation methods (e.g. *daylight factor* (*DF*)) are increasingly deemed inadequate [159]. In a move to improve the objectivity and accuracy when evaluating daylight strategies, as detailed indicate in Chapter 3, a number of new and refined metrics, such as *useful daylight illuminance* (*UDI*), *daylight glare probability* (*DGP*) etc., have been proposed [160-162] and are becoming increasingly common in the literature [165, 167, 170, 171, 192]. These sophisticated metrics are evaluated using dynamic simulation tools (e.g. RADIANCE [43, 147, 163, 164]) in conjunction with a *Bidirectional Scattering Distribution Function* (*BSDF*) to represent the optical performance of complex window systems [36, 41, 43, 214].

This chapter provides a comprehensive picture of daylight performance when applying PS-TIMs to window system through using dynamic metrics. The *BSDF* method has been used to express optical behaviours (i.e. transmission and reflection of visible

light and solar) of glazing systems with PS-TIMs. RADIANCE has been used to determine the dynamic daylighting performance of a notional double glazed window system with and without PS-TIM installed in a typical office located in London, using a "Three-phase method", commonly employed in the daylight simulation of complex fenestration systems. In the simulation, a cellular office room with various window systems was modelled, and the illuminance distribution calculated for 1 hour time-step over the course of a year. The predicted illuminances during working hours were analysed using advanced metrics (e.g. *UDI, DGP* and *UR*). The influence of slat pitch (the distance between neighbouring slats), slat tilt angle, as well as the optical performance of the slat material itself for the PS-TIMs were also investigated to understand their effects on the overall daylight performance.

5.2 Ray-tracing method to obtain the BSDF of glazing systems with PS-TIMs

The optical behaviour for a glazing system with PS-TIM is expressed by *Bidirectional Scattering Distribution Function* (*BSDF*) files, which define coefficients to allocate light from each exterior direction to each interior direction. In so doing, the angularly resolved transmissions and reflections for a complex window system are included in the annual calculation process. The *BSDF* on the Klems angle basis is a primary format for RADIANCE. As shown in Figure 5-1, it comprises 145 × 145 matrices for fenestration systems, which can account for the transformations that occur to both solar and optical spectra. Each matrix describes reflectance or transmittance distribution in the outgoing hemisphere for each incident angle of the incoming hemisphere.

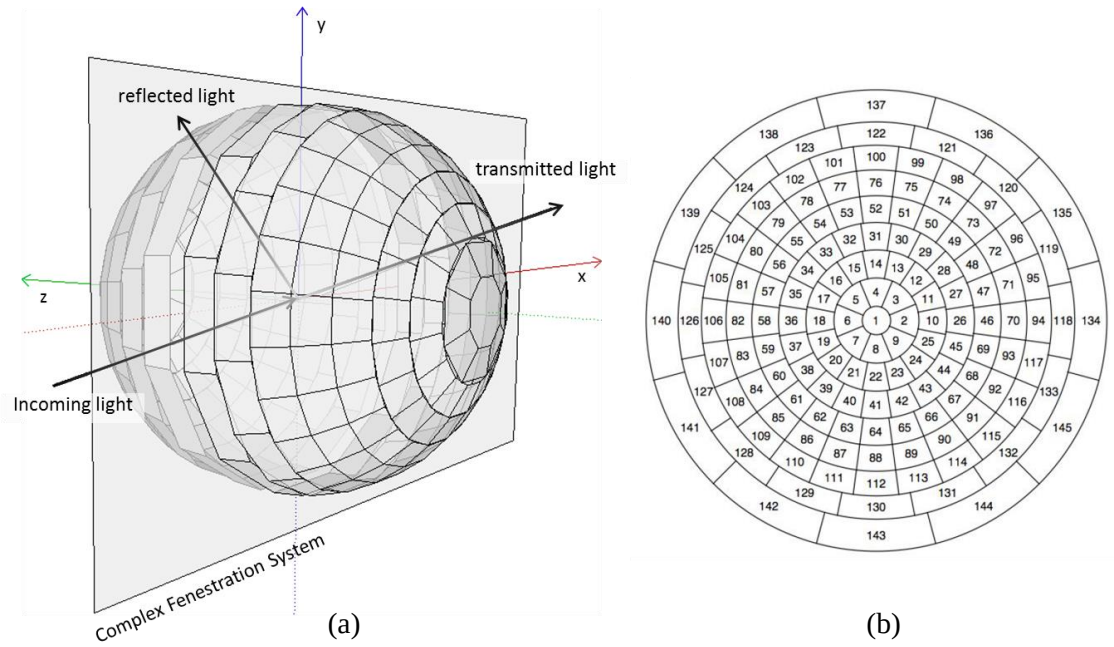


Figure 5-1: (a) schematic diagram of *BSDF* and (b) Klems 145-patch hemispherical basis with numbered subdivisions

The *BSDF* can be obtained by two methods: measurement using goniophotometric equipment [32, 33, 44] or calculation using validated ray-tracing methods [32, 33, 45]. A ray-tracing program "genBSDF" in RADIANCE [157], which has been validated by McNeil et al. [45], was used in this research to calculate the *BSDF* of different interstitial PS-TIM structures based on their geometry and material properties.

The *BSDF* data were calculated by RADIANCE for PS-TIM systems with 4 slat pitches (15mm 10mm 7.5mm and 5mm), at 7 different slat orientation angles (0 °, 30 °, 45 °, 60 °, -30 °, -45 °and -60 °) and 2 different slat materials (transparent and Lambertian diffuse translucent with 50% transmission). Examples of the investigated PS-TIM with different slat pitches are shown in Figure 5-2 (a), PS-TIM with different tilt angles are shown in Figure 5-2 (b) and PS-TIM with different slat materials are shown in Figure 5-2 (c).

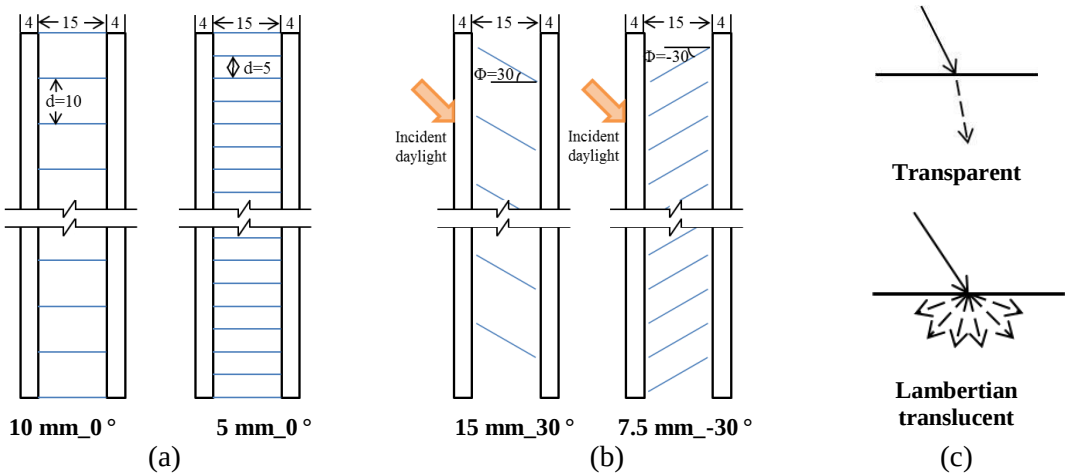


Figure 5-2: Schematic diagram of variables: (a) slat pitch (d mm); (b) tilt angle (Φ °) and (c) slat material

Taking 10 mm_0 °PS-TIM with diffuse translucent slats as an example, Figures 5-3 ~ 5-5 show the process of using RAIDANCE to obtain the BSDF matrix of glazing system with PS-TIM.

For example, as shown in Figure 5-3, the optical properties of slat material can be defined in the first four lines. The geometry of the PS-TIM itself can be generated using commode "genblinds", through which the depth, width, slat pitches and tilted angle can be defined. The material and geometry of the PS-TIM itself was then saved in a *.rad file. The rad file that contains PS-TIM's material and geometry were then combined with rad files of inner layer of glazing panes, outer layer of glazing panes and frame to form a rad file of the whole glazing system with PS-TIM (as demonstrated in Figure 5-4). Finally, genBSDF was used to generate the BSDF based on Klems angle basis of glazing system with PS-TIM and BSDF data was stored in an xml file (as demonstrated in Figure 5-5).

```
void trans tim_df
0
0
7     0.5     0.5     0.5     0     0    1     0


! genblinds  tim_df  tim_df_10_0  15  750  1320  132  0  | xform –rz 90 –rx  -90 \
–t  750  0  -4  >>  df_10_0.rad
```

Figure 5-3: Example of defining the material and geometry of the PS-TIM itself in RADIANCE

```
$ xform  –rz  180  –rx  -90  –t  2900  0  0  gp_in.rad   gp_out.rad   fram.rad \
df_15_0.rad > fwin_df_10_0.rad
```

Figure 5-4: Example of generating the geometry of the glazing system with PS-TIM in RADIANCE

```
$ genBSDF  +f  +b  –geom  millimetre  –dim  0  750  0  1320  -23  0  \
rad/ fwin_df_10_0.rad > xml/ fwin_df_10_0.xml
```

Figure 5-5: Example of using genBSDF to obtain the BSDF data of the glazing system with PS-TIM in RADIANCE

The results obtained from genBSDF, which is calculated from the descriptions of geometry and surface characteristics of the materials of complex fenestration system, can be used directly in RADIANCE to determine the daylighting performance or input into EnergyPlus to predict the energy performance of applying this system in a building.

5.3 Simulation methodology

The generation of daylight performance metrics can be performed using annual hourly simulation results obtained from RADIANCE [157]. RAIDANCE is a software tool based on a backward ray-tracing algorithm, which means that the rays are emitted from the point of interest and traced backwards until they either hit a light source or another object [198]. The accuracy of this research-grade simulation tool has been validated by several studies [43, 147, 163, 164].

5.3.1 Dynamic daylight simulation method

For a dynamic daylight simulation of a space, hourly based annual climate data, which includes direct sunlight and diffuse skylight, are required for the daylight performance prediction. For a space illuminated via a complex fenestration system, such as PS-TIM, the multiple inter-reflections that occur within the system become a further challenge for dynamic annual simulation. Swapping these complex interactions with a pre-calculated transmission matrix, (*T*), which characterizes flux output as a function of input for a particular configuration of light source and receiver, provides a simple but effective description of complex fenestration system in RADIANCE [43]. In addition, a daylight matrix, (*D*), and a view matrix, (*V*), that describe the external and internal conditions respectively, may also be calculated using a modified daylight coefficient method in advance of annual simulation [41]. Flux transfer represented by these three matrices forms a "Three-phase method", where the matrices are used in a multiple inner time-step loop with an assigned value for the sky condition (sky vector (*s*) or sky matrix (*S*)). This is proposed as a means of effectively and accurately performing annual daylight simulations of systems where complex fenestration systems are applied [41, 43, 215]. A schematic showing the three-phase method is illustrated in Figure 5-6, flux transfer through these three phases can be explained as:

1) from the point of interest in the simulated space to interior of fenestration (illustrated in red in Figure 5-6);
2) transmission through the fenestration system (illustrated in yellow);
3) from the exterior of the fenestration system to the sky (illustrated in orange).

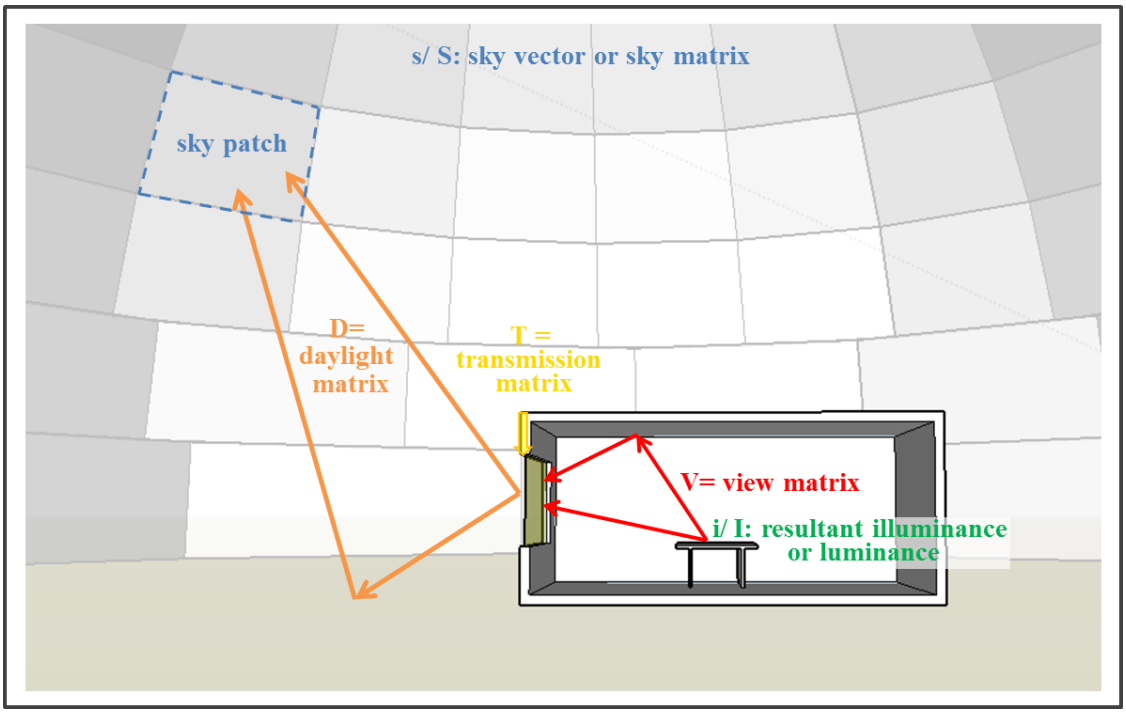


Figure 5-6: The illustration of the three-phase method

The results, which can be illuminance or luminance at any point of interest for a single time step (*i*) or for a time series (*I*), are computed using the following equations:

$$i=VTDs \tag{5-1}$$

$$I=VTDS \tag{5-2}$$

where *s* is the input data represented as a sky vector and *S* is the input data represented as a sky matrix. The sky vector (*s*) is generated by dividing the whole sky into discrete patches, with each patch being assigned an average radiance value for a given time and sky condition, while the sky matrix (*S*) is a time series of sky vectors. An annual sky matrix is generated from hourly input weather data for the 8760 hours in a year.

In this research, the 'Three-phase method' was used to conduct the dynamic annual daylight simulation of PS-TIM window systems in an office. The simulations were run at 1-hour time-steps for an entire year and the sky matrices were obtained from IWEC (International Weather for Energy Calculation) weather data for London. The diurnal direct and diffuse solar radiation can be found in Figure 5-7. The transmission

matrix for the window systems with PS-TIM was expressed using the *Bidirectional Scattering Distribution Functions* (*BSDFs*) (details can be found in section 5.2). The daylight matrix and view matrix were obtained based on the model's orientation, surrounding environment, geometry and surface properties of the indoor space (details can be found in section 5.3.1) using an embedded command in RADIANCE.

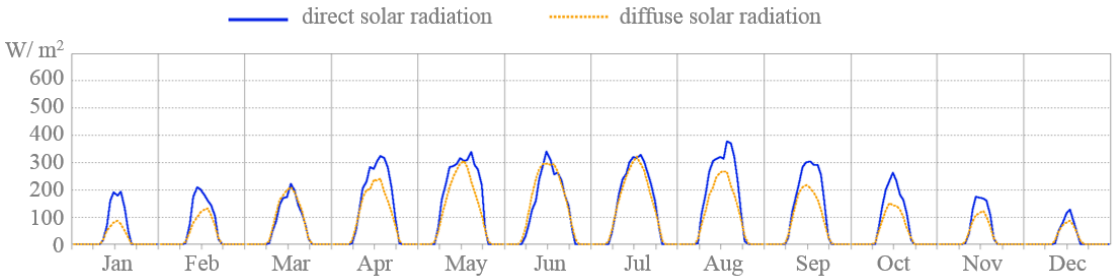


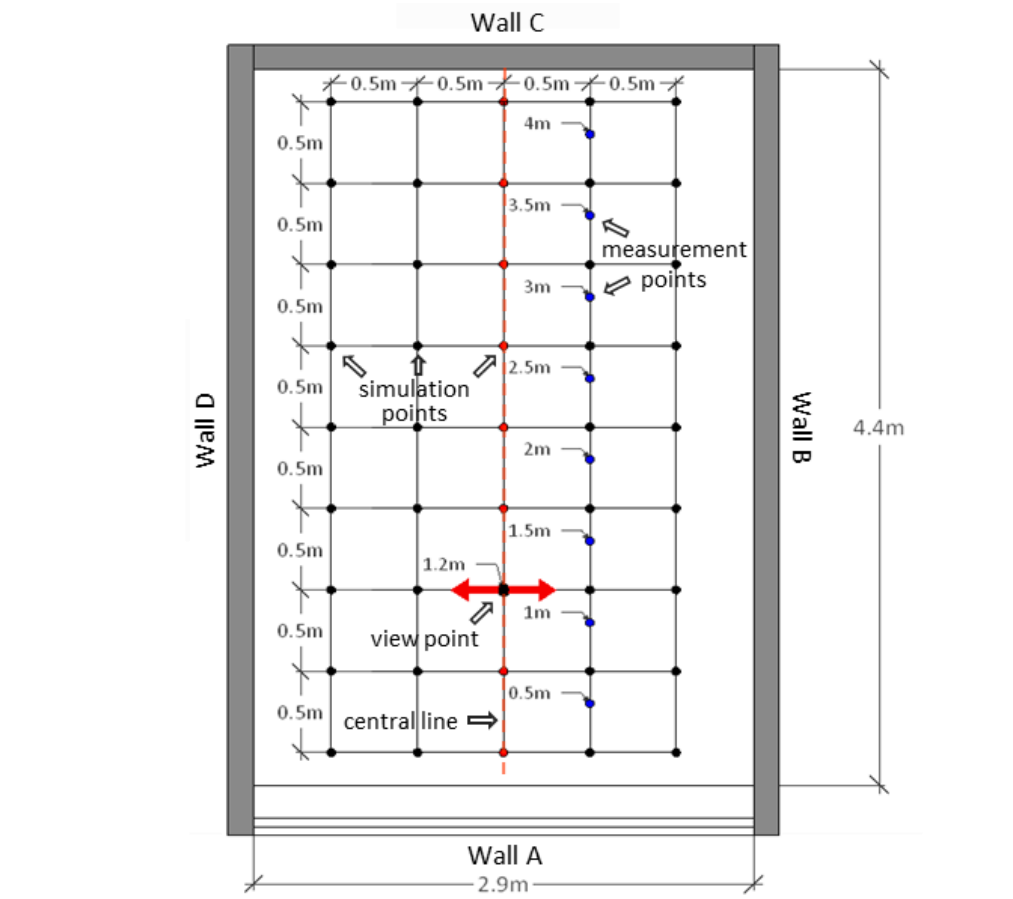
Figure 5-7: The diurnal average direct and diffuse solar radiation of London

5.3.2 RADIANCE simulation modelling

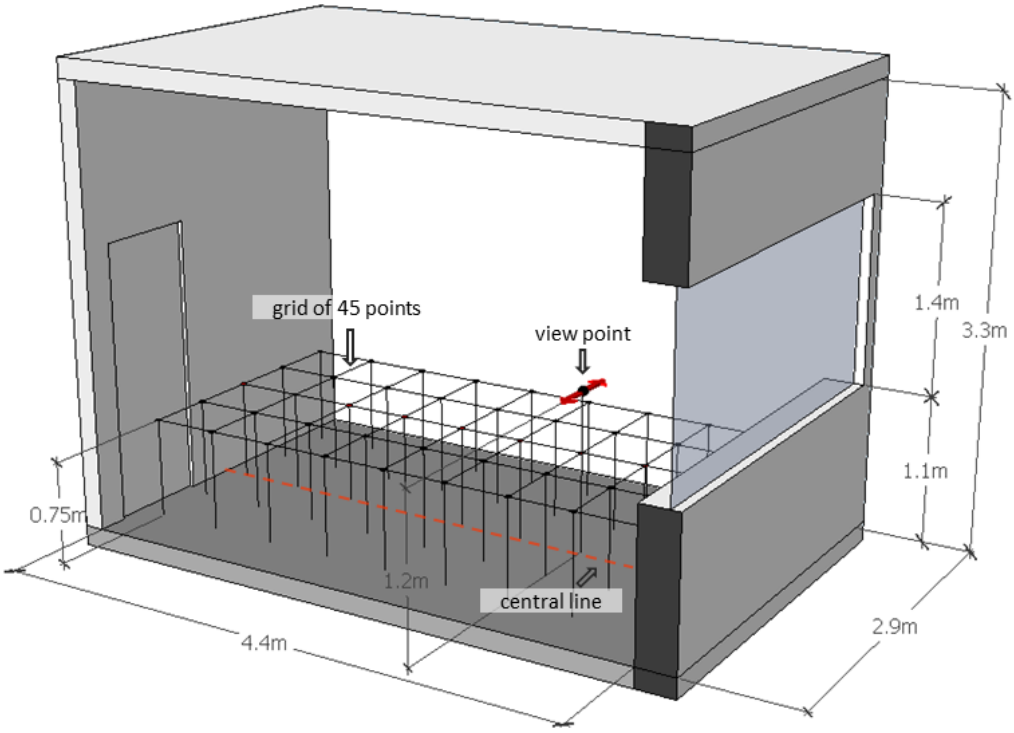
A side lit cellular office with dimensions 2.9 m (width) × 4.4 m (depth) × 3.3 m (height), which is based on a real room in the Energy Technologies Building in the University of Nottingham, UK, was chosen for the simulation. The office surfaces were treated as perfectly diffuse with typical visible reflectances of 30% (floor), 80% (walls) and 80% (ceiling). In order to clearly describe the geometry of the room, the four walls are represented by A, B, C and D as illustrated in Figure 5-8. A window with dimensions 1.4 m (height) × 2.9 m (width) is located in wall A with a sill height of 1.1 m above the floor. Four window orientations: South, East, West and North are considered in the studies. The original double glazed window has a visible light transmission of 78%. The room was used as a private office for two people, with one positioned near the window and the second at the back of the room. The furniture inside the room was modelled according to the layout of the prototype office. Both of the occupants work facing the walls, which means the view directions are facing toward wall B and D. It was assumed there were no surrounding buildings, vegetation or other obstructions outside the office.

An exterior ground with RGB reflectance of (0.4, 0.4 and 0.1) [157] was used to represent a grass green colour in the external environment. The enclosing surfaces of the room, all the furniture and exterior ground were constructed directly in RADIANCE.

A 9 × 5 grid comprising 45 points at 0.5m centres was used to estimate the illuminance distribution on a work plane positioned at a height of 0.75 m above floor level as illustrated in Figure 5-8. The grid was located centrally on plan, 0.2m away from wall A and C and 0.45 m away from wall B and D. As glare caused by daylight is less likely to be an issue at the back of the room, the glare evaluation was based on a view point representing the occupant near the window. This was located at a distance of 1.2 m from the window and at a height of 1.2 m above the floor on the centre axis of the room; facing wall B or D.



(a)



(b)

Figure 5-8: Selected points for evaluating illuminance distribution in the office space (a) Plan view and (b) sectional view

The room is taken to be a private office for two people with the occupancy schedule from 8:00 ~ 17:00. Within this study, the following rendering parameters for RADIANCE were used:

Table 5-1: RADIANCE simulation parameters

Ambient bounces (-ab)	Ambient divisions (-ad)	Ambient supersamples (-as)	Ambient resolution (-ar)	Ambient accuracy (-aa)	Direct sampling (-ds)
12	50000	512	256	0.13	0.2

According to investigations undertaken by Wienold and McNeil [160, 215],these settings seem to deliver reliable values for the given scenes.

5.3.3 Model validation

The accuracy of the RADIANCE algorithm, daylight coefficient method and Perez sky model have been discreetly validated under over 10,000 sky conditions including overcast skies, clear skies and partly cloudy skies by Reinhart [164, 216] and Mardaljevic [201, 217]. They used the data from a sky scanner to describe the luminance distribution of the celestial hemisphere including the sun in their simulation model, and then compared the simulated results of indoor illuminance level under each sky condition with the measured results under the same condition. The results indicated a high level of reliability in the use of RADIANCE to predict the annual indoor illuminance distribution in a space based on the building geometry, optical properties of the material surfaces and direct and diffuse irradiances. In this research, to provide confidence of accurately using RADIANCE for PS-TIM prediction, the illuminances for the prototype room were measured and compared with illuminances from simulation under the same conditions. The illuminance measurement method was a simplified version of the validated method for illuminance measurement developed by Reinhart [164, 216] and Mardaljevic [201, 217]. The measurements were conducted on two

overcast days in October 2015. As the sky conditions were totally overcast and there was no direct irradiance, the luminance distribution of the celestial hemisphere was assumed to be uniform in the simulation. The external non-obscured horizontal illuminance and indoor illuminances at the selected 8 measurement points (along the centre line of the room between the window and the end wall) were measured using calibrated chromameters, CL-200A (with an accuracy of ± 2% or ±1 the smallest digit of the displayed value). Comparison was made between the simulated indoor illuminance and the measured illuminance on the working plane (shown in Figure 5-8). The simulation assumed a typical double glazing (window without TIM) under two external illuminance levels: one with 10,000 lux and the other with 2,500 lux. In order to avoid the influence of a neighbouring building and vegetation on the measured illuminance, the study was based on an office on the top floor of the building.

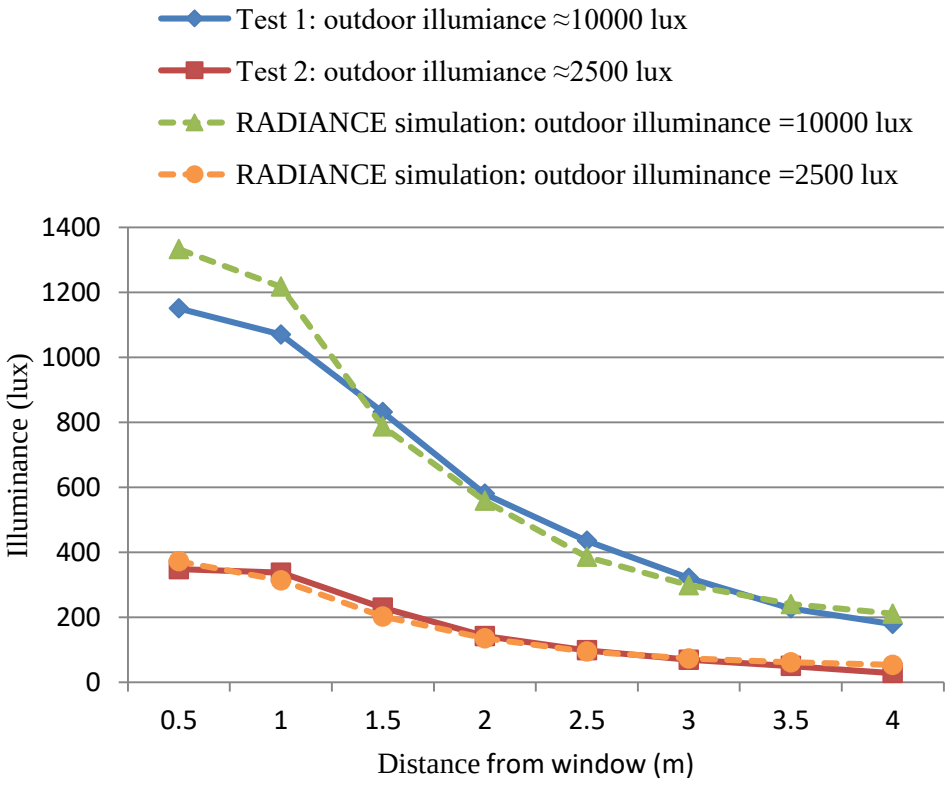


Figure 5-9: **Comparison between measured illuminance and illuminance calculated using Radiance at the 8 selected points in the room**

Figure 5-9 shows a comparison between measured and simulated values. The results agree reasonably well with the greatest deviation (13.5%) occurring 0.5m away from the window when the external horizontal illuminance was 10000 lux. This is due to the presence of a small window sill, which lead to more obstruction of light near the window neither of which was considered in the simulation. A photo of the prototype office room, which is taken during an overcast day, and a simulated render of the model are shown in Figure 5-10.



(a)



(b)

Figure 5-10: Comparison between (a) photo of test room and (b) rendered image using RADIANCE

5.4 Results and discussion of the effect of different PS-TIM on indoor daylight performance

The criterion for choosing the optimised PS-TIM configuration was to obtain a balance between the daylight availability and daylight comfort level.

5.4.1 The analysis of the effect of slat pitch

Simulations were undertaken for the PS-TIM with Lambertian diffuse translucent slats placed horizontally between two glazing panes, at various slat pitch of 15 mm, 10 mm, 7.5 mm and 5 mm, (labelled as '15 mm PS-TIM', '10 mm PS-TIM', '7.5 mm PS-TIM' and '5 mm PS-TIM' respectively in preceding discussions). For the results presented in this section, the office is assumed to be located in London with the window facing south.

The *useful daylight illuminance* (*UDI*) (see section 3.4.1 for more information) was determined by sorting the simulated hourly illuminance at the points of interest into 3 bins:

1) an *undersupplied* bin (illuminance value < 100 lux);
2) a *useful* bin (100 lux < illuminance value < 2000 lux);
3) an *oversupplied* bin (illuminance value > 2000 lux).

In this study, a more detailed picture of the middle 100 ~ 2000 lux bin is generated by splitting it into two ranges:

1) A *desired* range (500 ~ 2000 lux) where a typical office design illuminance is met and is not exceeded to the point where glare is highly likely [20];
2) A *sub-desired* range (100 ~ 500 lux) where there is an increasing likelihood that occupants will resort to supplementary lighting to meet their illumination needs.

In addition, the oversupplied bin is also divided into two ranges:

1) illuminance in the range of 2000 ~ 3000 lux, in which range occupants may tolerate strong daylight;
2) illuminance greater than 3000 lux, in which blinds or shades might be lowered [190].

Figure 5-11 shows the *UDI* predicted at points along the centre line of the room between the window and the end wall. As illustrated in Figure 5-11 (a), for the double glazing system, the period when there is an oversupply of daylight ($UDI_{>3000\ lux}$) accounts for a high proportion (i.e approximately 45% of working hours) at locations within 2.2 m of the window and it gradually reduces to less than 10%, for points further than 3.2 m from the window. This oversupply of daylight can be reduced to less than 20%, 10% 5% and 0% of working hours by integrating PS-TIM structure with slat pitches of 15 mm, 10 mm. 7.5 mm and 5 mm, respectively, as shown in Figure 5-11 (b), (c), (d) and (e). While the 5 mm PS-TIM can completely eliminate oversupply of daylight, the percentage of undersupplied daylight hours ($UDI_{< 100\ lux}$) increases from less than 10% for conventional double glazing to more than 20%. The remaining 3 configurations of PS-TIM give rise to undersupplied daylight hours in the range of 10% to 20% of working hours.

The average percentage of hours where the *UDI* is in the most desired range ($UDI_{500\text{-}2000\ lux}$) increase from 36% for conventional double glazing to 46 % and 50 % when applying PS-TIM with 15 mm slat pitch and 10 mm slat pitch respectively. The integration of PS-TIM improves the daylighting quality of the room, especially within the region that is close to the window where over illumination is frequently a problem with conventional glazing. Instead, more hours are predicted within the most desired range of *UDI* ($UDI_{500\text{-}2000\ lux}$), these being relatively evenly distributed throughout the room depth for PS-TIM with slat pitches of 10mm or less for around 50% of working hours.

Significant improvement over conventional double glazing is achieved by applying PS-TIM with 10 mm slat pitch and 7.5 mm slat pitch, which raises the average percentage of useful *UDI* ($UDI_{100\text{-}500\ lux}$ and $UDI_{500\text{-}2000\ lux}$) from 47% to approximately 76% and 79%, respectively.

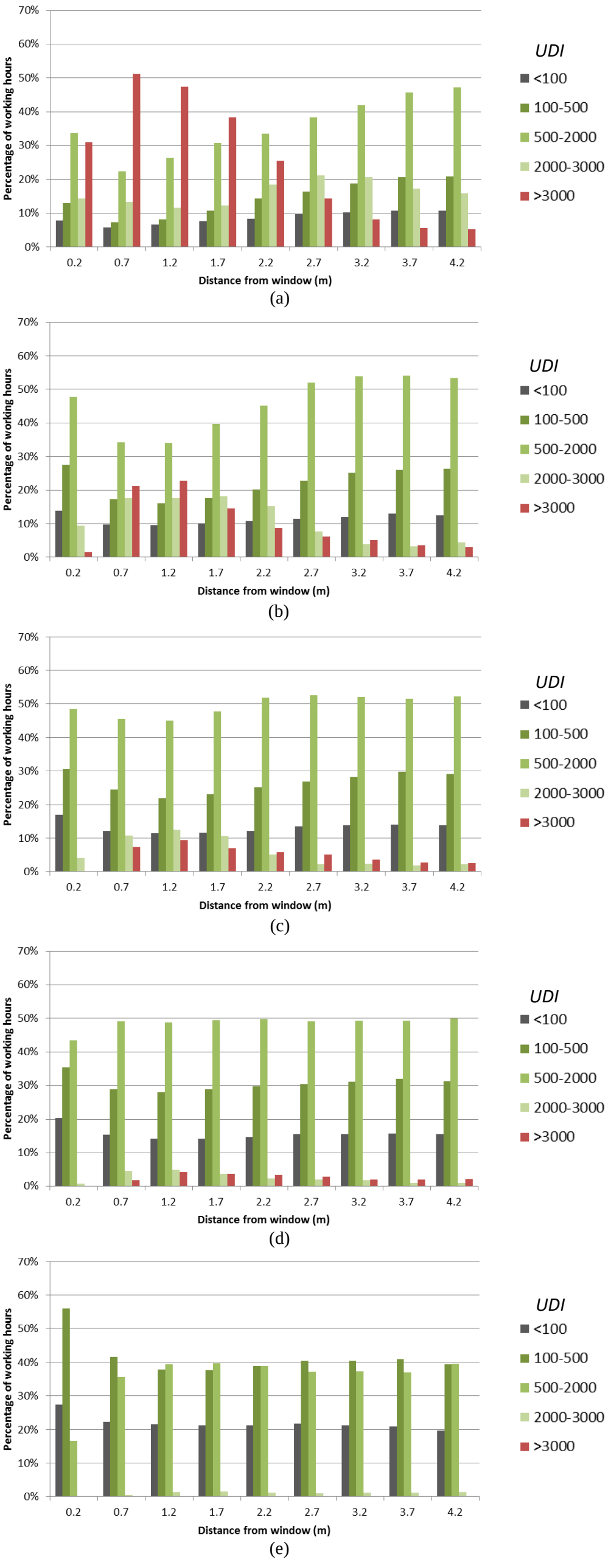


Figure 5-11: *UDI* bins for points located along the central line of an office from window to the end wall for the window system with and without PS-TIM: (a) DG; (b) 15 mm PS-TIM; (c) 10 mm PS-TIM; (d) 7.5 mm PS-TIM and (e) 5mm PS-TIM. Simulations are based on a London IWEC weather file.

The results for additional two metrics, *uniformity ratio (UR)* (see section 3.4.1 for more information) and *daylight glare probability (DGP)* (see section 3.4.1 for more information), which were used to assess the daylight comfort level are presented in Figure 5-12.

As with the previous analysis, the data are derived from the London climate data file. At this latitude, 3% of the working hours occur before sunrise or after sunset and so have no daylight at all: for 3% of the time therefore, the *UR* equals 0. For conventional double glazing, the daylight transmitted into the room produces extreme contrasts of illumination on the working plane: 42% of the annual working hours have a *UR* larger than 1:4.5 (labelled as > 4.5 in Figure 5-12 (a)) and of working hours 47% fall into the range between 1:3.5 and 1:4.5 (labelled as 3.5 - 4.5). The application of PS-TIM integrated double glazing improves the predicted illuminance uniformity. The percentage of annual working hours when *the UR* is over 1:2.5 (the sum of the data labelled as 2.5-3.5, 3.5-4.5 and > 4.5) reduces from 97% when applying double glazing to 34%, 15%, 10% and 4% when applying PS-TIM with slat pitches of 15mm, 10mm, 7.5mm and 5mm, respectively.

The *daylight glare probability* (*DGP*) is calculated based on a simplified annual simulation method for the assumed occupant position near the window (1.2 m away from window at 1.2 m height) [160, 161]. As shown in Figure 5-12 (b), for the normal double glazed window, the intolerable glare ($DGP \geq 0.45$), disturbing glare ($0.4 < DGP < 0.45$), and *perceptible* glare ($0.35 < DGP < 0.4$) account for 13.9%, 6.4% and 16.6% of working hours, respectively. When diffuse translucent PS-TIM structures are applied, significant improvement of the percentage of *imperceptible* glare ($DGP \leq 0.35$) is achieved. This increases from 63.1% of working hours for DG to 87.8%, 93.4%, 96.5% and 99.2% with the application of PS-TIM with slat pitches of 15 mm, 10 mm, 7.5 mm

and 5 mm, respectively. According to the Wienold's criteria [160] for categorising glare conditions in a room, when 7.5 mm PS-TIM and 5 mm PS-TIM are applied, the room has a '*Best*' classification for over 95% of office working hours and the glare sensation would be deemed *imperceptible*. The 10 mm PS-TIM offers a '*Good*' classification as over 95% of office working hours the glare is *perceptible* and the 15 mm PS-TIM has a '*Reasonable*' classification as fewer than 5% of office working hours have *intolerable* glare.

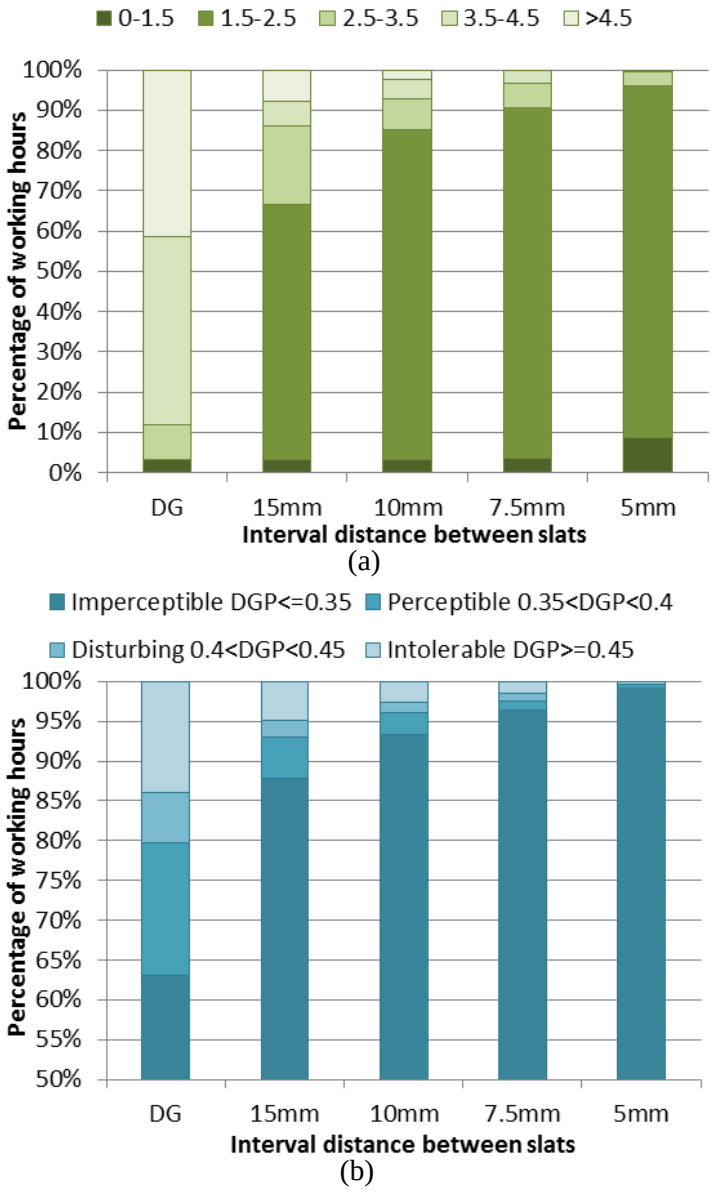


Figure 5-12: (a) Illuminance *uniformity ratios* (b) *daylight glare probability* (*DGP*) of window without and with diffuse translucent PS-TIM with 4 different slat pitches. Simulations are based on a London IWEC weather file.

In order to provide a more intuitive impression of the daylight distribution and glare in the office to accompany these metrics, false colour and true colour visualisations were generated and rendered images at noon on 21st March are shown in Appendix A as examples. The presence of PS-TIM results in a more homogenous distribution of daylight and the level of homogeneity increases as the slat pitch gets smaller.

5.4.2 Analysis of slat tilt angle

In this section, simulation was undertaken for the PS-TIM with Lambertian diffuse translucent slats placed with fixed slat pitch and the slat tilt angles, (ϕ), was varied between -60° and 60°, (labelled as '-60°', '-45°', '-30°', '0°', '30°', '45°' and '60°' respectively in preceding discussions). Figure 5-13 shows the variation of illuminance *UR* and *DGP* for a 15 mm PS-TIM at different tilt angles. This PS-TIM slat pitch was selected because it is the least effective of the non-tilted configurations studied in section 4.1 (see Figure 5-12), therefore, further investigations have been carried out to explore whether varying tilt angle has the potential to improve its performance.

It can be seen in Figure 5-13 (a) and (b), that with the slats tilted at positive angles relative to the sky vault (i.e. ϕ= 30°, 45° and 60°), the performance was worse than that of the PS-TIM with non-tilted slats in terms of both daylight *UR* and *DGP*. Improved performance can be observed in the data for slats with negative tilt angles if *UR* < 3.5 and *DGP* < 0.4 are used as metrics. The percentage of working hours with *UR* below 1:2.5 improves from 66% when slats are horizontally placed to 80% when slats are tilted at -30° and working hours with *DGP* below 0.35 improves from 87% when slats are horizontally placed to around 90% when slats are tilted at angles of -30°, -45°and -60°.

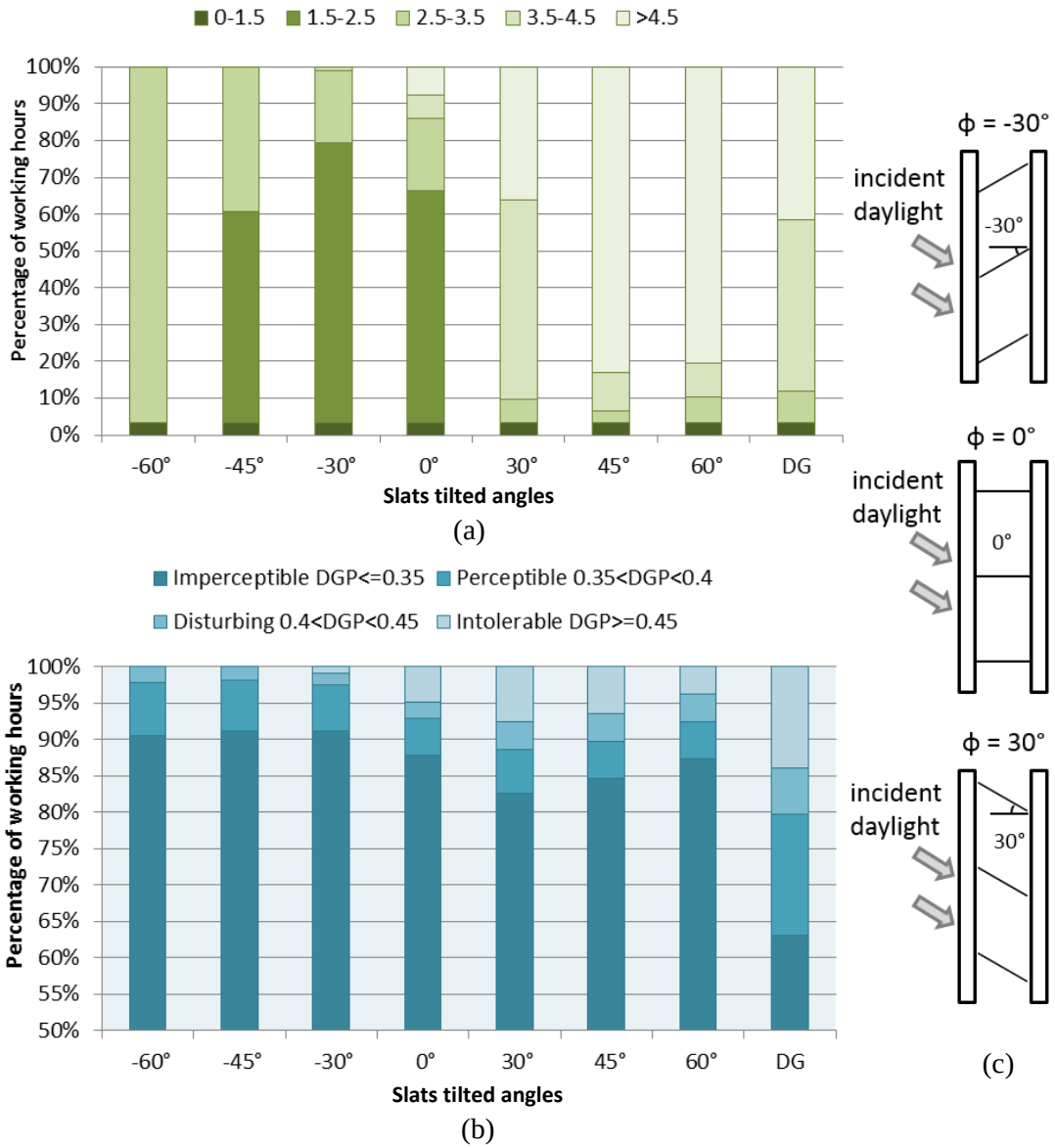


Figure 5-13: (a) Illuminance *uniformity ratios* (b) *daylight glare probability* (*DGP*) for a window with diffuse translucent PS-TIM with slat pitch of 15mm at 7 different tilt angles, and (c) definition of tilt angles, ϕ. Simulations are based on a London IWEC weather file.

In terms of improving daylight comfort levels, Figure 5-13 also suggests that only PS-TIM with a tilt angle of -30° offers improved comfort over horizontally placed slats. Section 5.4.1 indicated that the 7.5 mm PS-TIM was the optimised pitch configuration for improving both daylight availability and daylight comfort. On this basis, the performance of the 7.5 mm PS-TIM with -30° tilted slats and 7.5 mm PS-TIM with non-tilted slats (labelled as 0°) were compared in terms of daylight availability (i.e. $UDI_{100\text{-}2000\ lux}$ and $UDI_{500\text{-}2000\ lux}$) as shown in Figure 5-14. When evaluating the *UDI* in

the range from 100 to 2000 lux, there is no significant difference between the 7.5 mm PS-TIM system with slats tilted at angles of 0 ° and -30 °. For the most desired daylight range of 500 to 2000 lux, the *UDI* values of these two tilt angles are almost the same in the region close to the window (i.e. up to 1.7 m into the room). However, at locations deeper within the room, the *UDI* values for PS-TIM with non-tilted slats remain constant at around 50% of working hours, while those for the -30° tilted slats show a steady decrease with only 30% of working hours indicating a favoured *UDI*. It can be concluded that for the PS-TIM with slat pitch of 7.5 mm, 30° tilted slats do not provide significant improvement of daylight availability when compared with non-tilted slats.

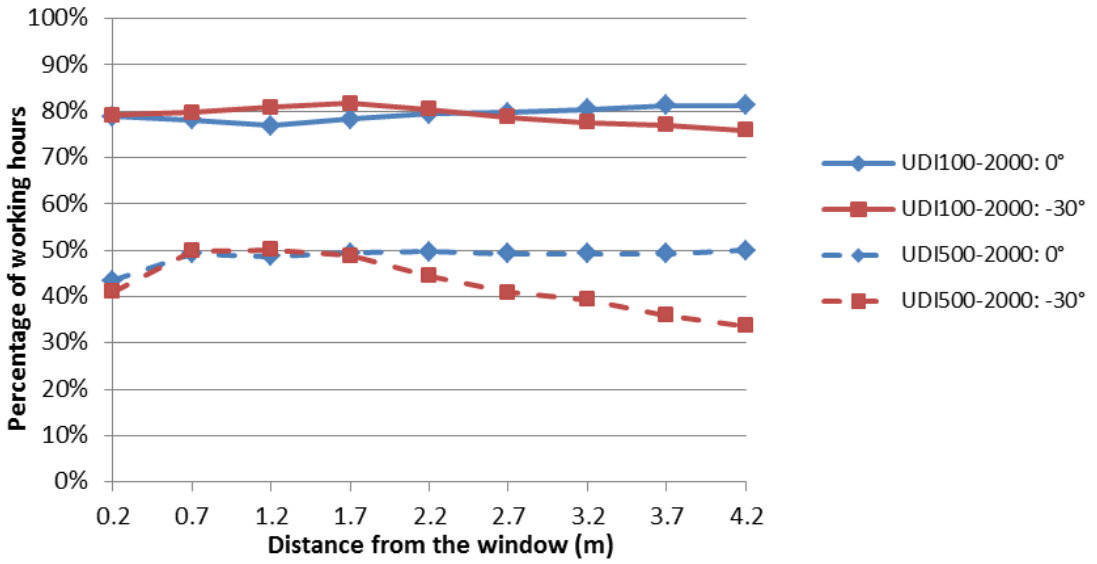


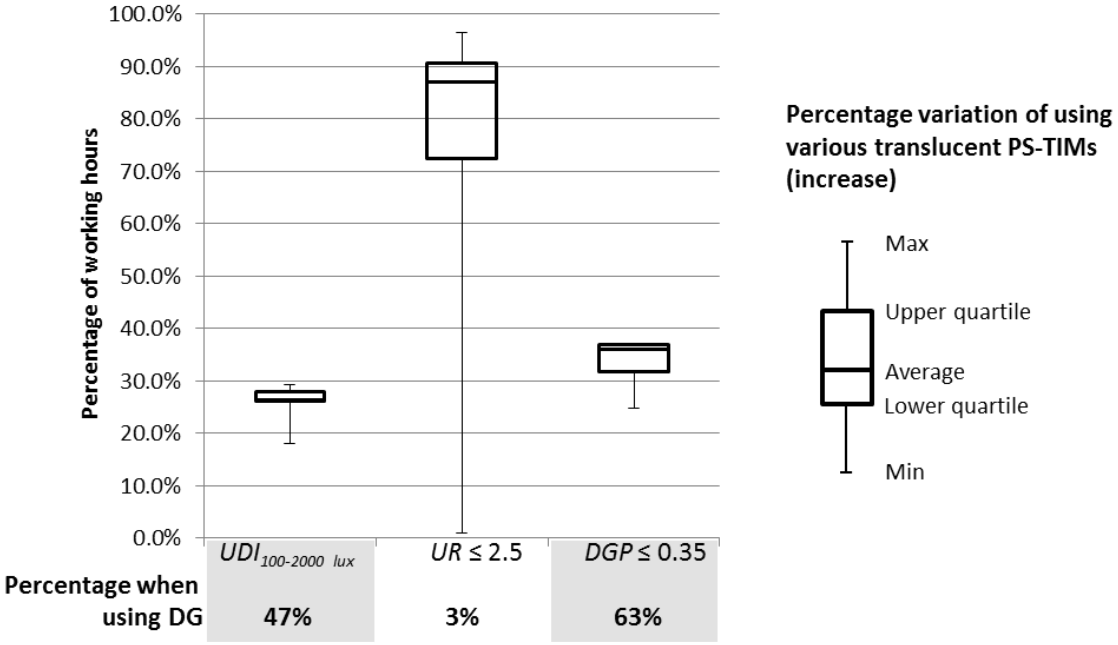
Figure 5-14: $UDI_{100\text{-}2000\ lux}$ and $UDI_{500\text{-}2000\ lux}$ for diffuse translucent PS-TIM with 7.5 mm slat pitch at 0 ° and -30 ° tilt angles. Simulations are based on a London IWEC weather file.

5.4.3 Analysis of slat material properties

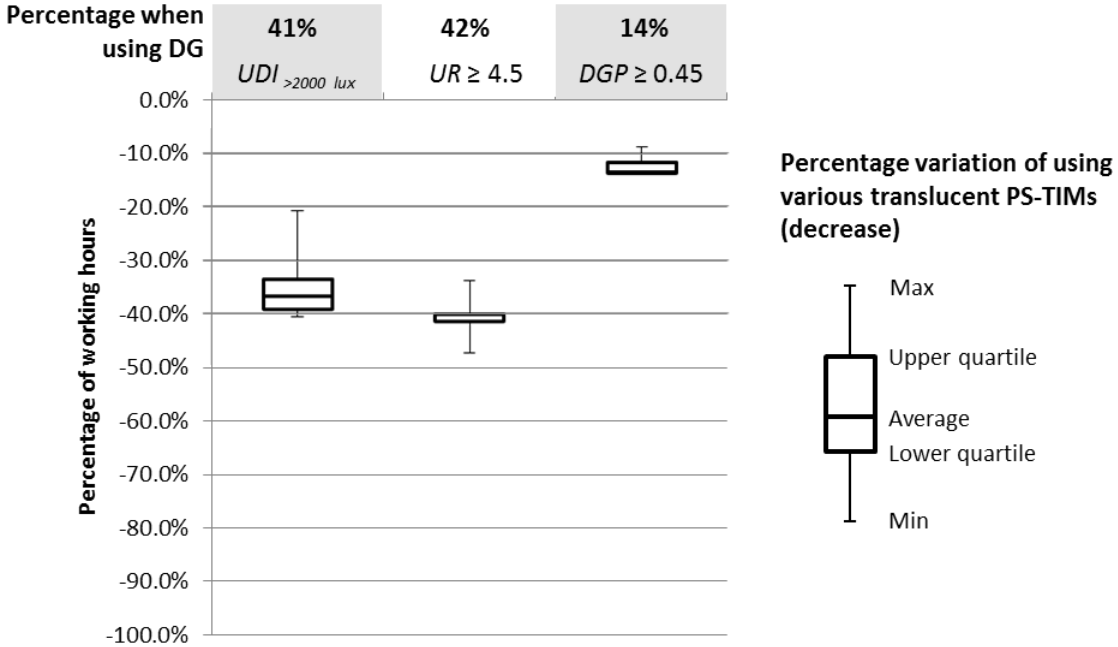
Section 5.4.1 and section 5.4.2 discussed the performance of PS-TIM with Lambertian diffuse translucent slats located in the air cavity between the two panes of a double glazing unit. The analysis was performed for various slat pitches (i.e. 15 mm, 10 mm, 7.5 mm and 5 mm) and various tilt angles (i.e. -60 °, -45 °, -30 °, 0 °, 30 °, 45 ° and 60 °) in a south facing office using the climate data for London. This section repeats part

of this analysis (i.e. *UDI*, *UR* and *DGP*) but replaces the PS-TIM diffusing slats with a transparent material.

The results of using *UDI*, *UR* and *DGP* to evaluate the performance of various configurations of PS-TIMs with Lambertian translucent slats are summarised in Figure 5-15. Figure 5-15 (a) indicates that applying translucent PS-TIMs could increase the percentage of working hours when the metrics lie in their desirable ranges (i.e. *UDI* in *useful* bin, uniformity below 2.5 and *DGP* below 0.35) when compared with a standard double glazed window. Figure 5-15 (b) shows the reduced percentage of working hours when the metrics lie in their undesirable ranges (i.e. *UDI* in *oversupplied* bin, *UR* over 4.5 and *DGP* over 0.45) as compared with the data for a standard double glazed window. As can be seen in Figure 5-15 (a), the percentage of working hours during which the average *UDI* lies in the range of 100-2000 lux, $DGP \leq 3.5$ and $UR \leq 1$: 2.5 were 47%, 3% and 63% for standard double glazing unit. These metrics can be increased by between 18 ~ 29% (*UDI*), up to 97% (*UR*) and 25 ~ 37% (*DGP*), respectively, when PS-TIMs are applied. In addition, for the undesired ranges of these metrics, as shown in Figure 5-15 (b), the percentage of working hours when the average *UDI* is over 2000 lux is 41% for the double glazing unit, and it can be reduced by between 21% and 40%, depending on the type of PS-TIM used. There are 42% of working hours where the *UR* is higher than 1: 4.5 and 14% of working hours where the *DGP* is higher than 0.45 when using a standard double glazing unit: these two undesired situations can be completely eliminated by integrating translucent PS-TIMs.



(a)



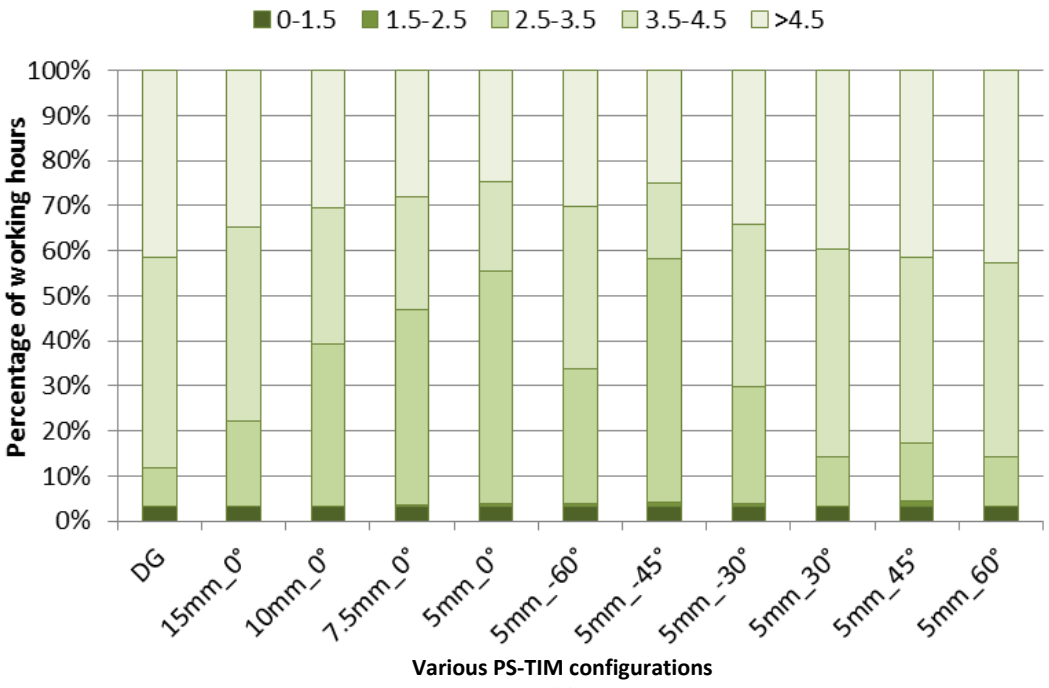
(b)

Figure 5-15: **Summary of metrics evaluating the performance of applying various PS-TIMs with translucent slats in (a) desirable ranges and (b) undesired ranges. Simulations are based on a London IWEC weather file.**

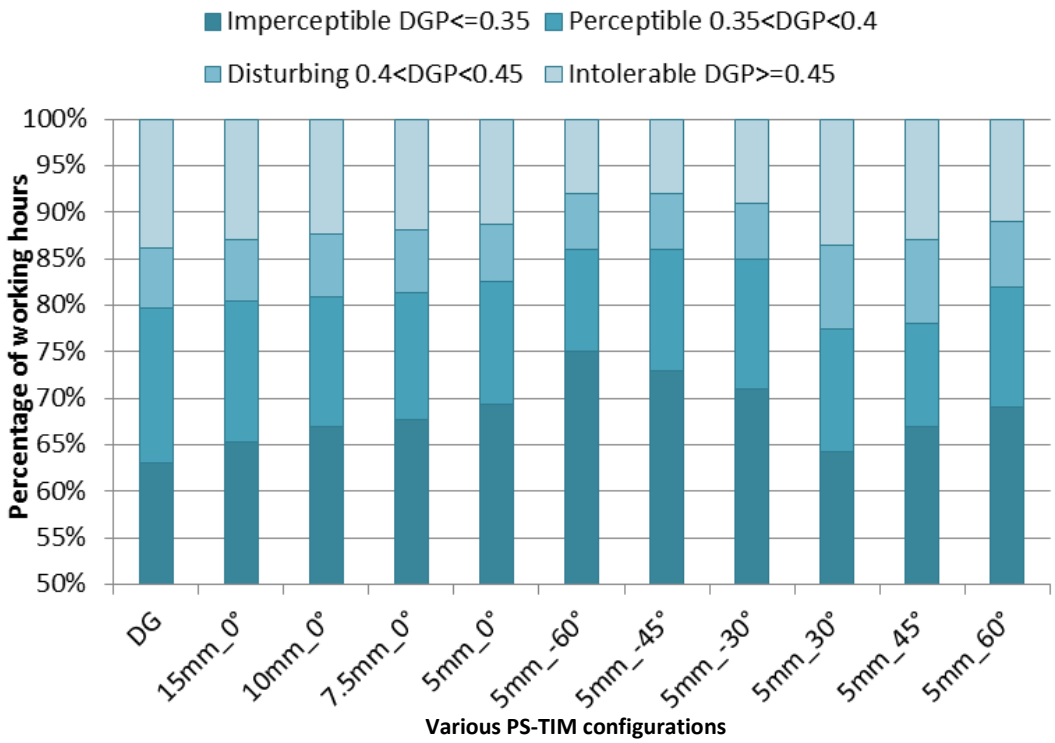
Figure 5-16 shows the *UR* and *DGP* after applying various configurations of PS-TIMs with transparent slats, and Table 5-2 shows the percentage of working hours where the *UDI* is in the range of 100-2000 lux. As can be seen from Table 5-2 and Figure 5-16, when comparing PS-TIMs with non-tilted transparent slats to standard double glazing,

the 5 mm PS-TIM provides the best performance in terms of reducing the percentage of working hours where the *UR* is over 1: 4.5 (i.e. dropping from 42% to 24%). It also increases the percentage of working hours with *DGP* below 3.5 from 63% to 69%, and slightly improves the percentage of working hours from 50% to 51% where the desirable $UDI_{100\text{-}2000\ lux}$ occurs.

On the basis of these results, the slats with 5 mm pitch were then investigated at various tilt angles (-60°, -45°, -30°, 30°, 45°, and 60°) to identify an optimised configuration. However, the results indicated that there was no obvious improvement in *UR* or *DGP* as compared with the results for the non-tilted slats. Tilt angle has a slight impact on the illuminance distribution. The -60 °tilted slats, which have the best overall performance, can improve the $UDI_{100\text{-}2000lux}$ by between 5% - 9% of working hours and improve the *imperceptible DGP* ≤ 3.5 by 11.5% of working hours as compared with the PS-TIM with horizontal slats. However, the window with transparent PS-TIMs does not yield significant improvement in either *UDI* distribution, *UR* or *DGP* as compared with the standard double glazed unit, the results for each being very similar.



(a)



(b)

Figure 5-16: (a) Illuminance *uniformity ratios* (b) *daylight glare probability* (*DGP*) of window without and with transparent PS-TIM for 4 different slat pitches at 7 different tilt angles. Simulations are based on a London IWEC weather file.

Table 5-2: $UDI_{100\text{-}2000lux}$ of window without and with transparent PS-TIM of 4 different interval distances at 7 different tilted angles.

	0.2	0.7	1.2	1.7	2.2	2.7	3.2	3.7	4.2
DG	47%	30%	34%	42%	48%	55%	61%	66%	68%
15 mm_0 °	48%	31%	36%	42%	48%	55%	60%	65%	67%
10 mm_0 °	49%	32%	37%	43%	48%	55%	60%	65%	67%
7.5 mm_0 °	50%	33%	38%	43%	48%	55%	60%	65%	67%
5 mm_0 °	51%	34%	38%	43%	49%	55%	61%	65%	67%
5 mm_30 °	50%	32%	36%	42%	49%	53%	59%	63%	64%
5 mm_45 °	46%	32%	37%	42%	50%	56%	63%	67%	69%
5 mm_60 °	48%	33%	40%	43%	50%	58%	66%	70%	71%
5 mm_-30 °	54%	35%	39%	43%	50%	57%	65%	69%	71%
5 mm_-45 °	55%	37%	41%	44%	52%	59%	66%	72%	74%
5 mm_-60 °	55%	38%	42%	46%	53%	61%	68%	75%	76%

5.5 Conclusion

An investigation of the daylight performance of a double glazed window with integrated parallel slat transparent insulation materials PS-TIMs was conducted using RADIANCE in combination with *Bidirectional Scattering Distribution Functions*

(*BSDFs*) to represent the PS-TIMs' optical performance. The following conclusions can be drawn:

1) PS-TIMs with translucent slats offer better performance than PS-TIMs with transparent slats in terms of *Useful Daylight Illuminance* (*UDI*), *uniformity ratio (UR)* and *Daylight Glare Probability* (*DGP*);
2) compared with slat tilt angle, the slat pitch (the distance between neighbouring slats) has a more significant influence on the overall daylight performance when the PS-TIM comprises translucent slats;
3) when compared with standard double glazing, glazing with integrated PS-TIM can increase the percentage of working hours when the *UDI* lies in the range of 100-2000 lux by between 47% and 79% depending on the type of the PS-TIM used, achieve a homogenous distribution of daylight, and effectively reduce the risk of glare under London's climate.

This chapter has restricted itself to exploring the effect of PS-TIM on indoor daylight level of an office under London's climate. The influence of applying PS-TIM on the overall energy performance of this prototype office will be presented in Chapter 7. The chosen PS-TIMs have also been investigated under different climate conditions and different building orientations to provide an indication of how site-specific variables influence their daylight and energy performance.

Chapter 6. Thermal and energy performance prediction of applying glazing systems with Parallel Slats Transparent Insulation Material (PS-TIM)

6.1 Introduction

The improved thermal insulation offered by integrating PS-TIM into windows, as detailed discussed in Chapter 4, and its effect on indoor illuminance level, as detailed discussed in Chapter 6, can ultimately affect the overall energy efficiency of the building. This chapter aims to comprehensively and accurately predict the thermal and energy performance in the context of applying PS-TIMs on a window of an office.

Current building energy simulation programs are not accurate enough for modelling these complex fenestration systems, often because of the simplified thermal and optical models used to solve heat transfer and light transmittance. i.e. one dimensional methods are used for both thermal transfer and light transmittance through fenestration systems [134]. In practice, with the integration of an interstitial structure within the air cavity of a double glazing unit, there will be a significant effect on the free convection, long-wave radiative heat transfer and solar energy (light and heat) transmitted through the system. Although, efforts have been made to combine *Bidirectional Scattering Distribution Function* (*BSDF*) with building performance simulation [209, 210] to achieve a more accurate solar and daylight distribution analysis through complex fenestration systems, the effect on free convection and long-wave radiation heat transfer by integrating interstitial structures have not been considered. In practice, these greatly affect predictions of thermal and energy performance.

The development of a comprehensive model, which can be used to investigate the thermal and optical performance of complex fenestration systems as well as their impact on building energy performance is presented in this chapter. Through this approach, the thermal characterisations of a complex fenestration system are obtained from Computational Fluid Dynamics simulation, meanwhile, a ray-tracing technique is used to predict the optical characterisations that were formatted into *BSDF* data. All of

these are input into building simulation software EnergyPlus to obtain building heating, cooling and lighting energy estimates, when PS-TIMs are applied within the window of a typical office.

6.2 Research methodology

6.2.1 Overview of the research framework

To comprehensively investigate the optical and thermal characteristics of a fenestration system with PS-TIM and predict building energy performance when this glazing system is applied, a comprehensive model has been developed. In brief, the developed holistic model consists of four major blocks as shown in Figure 6-1:

1) a fenestration thermal model where a two-dimensional Computational Fluid Dynamics (CFD) model has been used to investigate the dynamic thermal conductance across the glazing system caused by variation of environmental conditions (different glazing average temperature and different temperature across the glazing panes);

2) a fenestration optical model where a ray-tracing technique has been used to obtain a *Bidirectional Scattering Distribution Function* (*BSDF*) based on the geometry and optical properties of the glazing system;

3) a complementary building daylight model where the *BSDF*s for the glazing system are used in an annual simulation that takes the hourly solar irradiances used in the RADIANCE block to provide a detailed picture of daylight performance;

4) a building energy model where the optical and thermal characterisations of the glazing system obtained from the previous thermal and optical models are applied

in EnergyPlus to obtain building energy performance under the desired climatic conditions.

Ultimately, building energy performance prediction (i.e. heating, cooling and lighting energy consumption) and detailed daylight performance (i.e. useful daylight illuminance, daylight glare probability and etc.) can be generated. The theories and outcomes of each stage are described in the following sections.

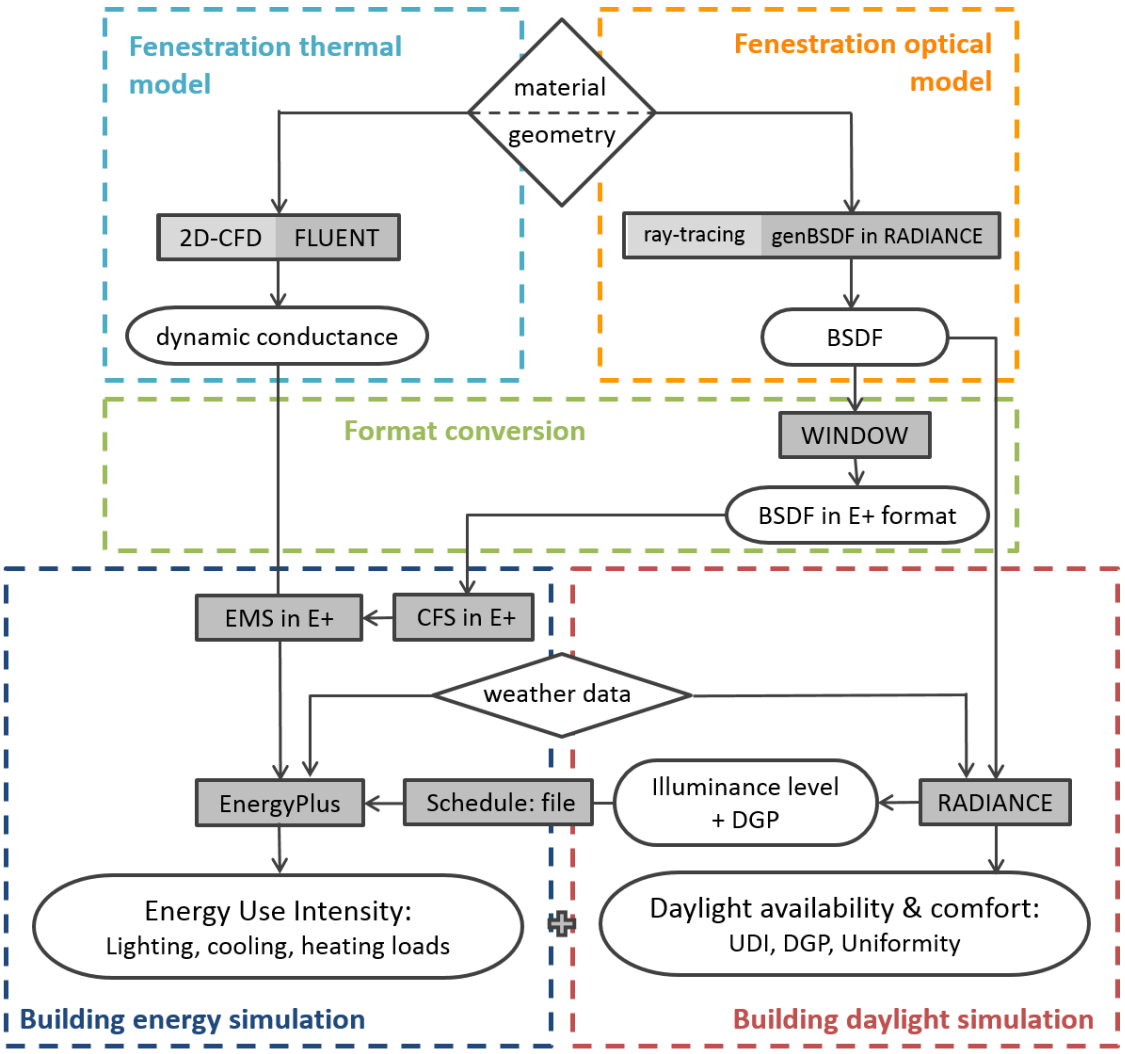


Figure 6-1: Flow chart of the comprehensive method for complex fenestration *

*: In this figure, grey rectangles illustrate the algorithm, software or sub-program used in the research, in which E+ is short for EnergyPlus, EMS is short for Energy Management System, CFS is short for Construction: Complex Fenestration State; rounded rectangles illustrate the expected result from the related algorithm, software or sub-program, in which *BSDF* is short for *Bidirectional Scattering Distribution Function*, *DGP* is short for Daylight Glare Probability, *UDI* is short for Useful Daylight Illuminance.

6.2.2 Theories of thermal model

This section introduces the fundamental theories of EnergyPlus that are used to predict the thermal and energy performance when applying complex glazing system into buildings, followed by the method of using Computational Fluid Dynamics package FLUENT to obtain the dynamic thermal characterisations of glazing system with PS-TIM integrated within the cavity of two glazing panes.

6.2.2.1 Heat transfer equations in building performance simulation (EnergyPlus)

EnergyPlus is a heat balance based simulation program to achieve space loads [207]. When solving for heat transfer through fenestration systems, the heat flow is assumed to be one dimensional and perpendicular to the glazing panes. A schematic diagram detailing the heat transfer in a double glazing system is presented in Figure 6-2 (a). The heat balance equation for each glazing unit's surfaces used in EnergyPlus can be written as:

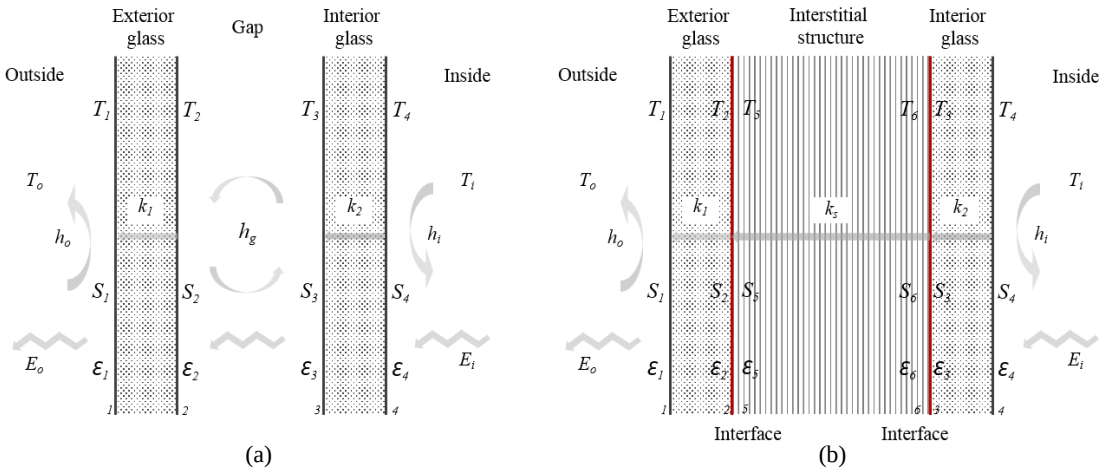


Figure 6-2: **Demonstration of heat transfer and the variables used in heat balance equations for (a) double-glazed window (b) window system with PS-TIM between two panes (adopted from [134])**

$$E_o\varepsilon_1 - \varepsilon_1\sigma T_1^4 + k_1(T_2 - T_1) + h_o(T_o - T_1) + S_1 = 0 \qquad (6-1)$$

$$k_1(T_1 - T_2) + h_g(T_3 - T_2) + \sigma\frac{\varepsilon_3\varepsilon_2}{1-(1-\varepsilon_2)(1-\varepsilon_3)}(T_3^4 - T_2^4) + S_2 = 0 \qquad (6-2)$$

$$k_1(T_4 - T_3) + h_g(T_2 - T_3) + \sigma\frac{\varepsilon_2\varepsilon_3}{1-(1-\varepsilon_3)(1-\varepsilon_2)}(T_2^4 - T_3^4) + S_3 = 0 \qquad (6-3)$$

$$E_i\varepsilon_4 - \varepsilon_4\sigma T_4^4 + k_2(T_3 - T_4) + h_i(T_i - T_4) + S_4 = 0 \qquad (6-4)$$

In the equations, the convective heat transfer coefficient (h_g) for a gas cavity between two glazing panes is determined by the non-dimensional parameter *Nusselt number* ($h_g = Nu\frac{k_g}{s}$), while the strength of radiative heat transfer between the two glazing surfaces that enclose the gas cavity is determined by the emissivity of the two surfaces and view factors between them. The *Nusselt number*, which is an empirical value calculated using correlations from experimental measurements, represents the dynamic natural convection under various boundary conditions associated with the *Grashof number*, the *Prandtl number* and the *aspect ratio* of the air cavity [109].

However, when a complex structure is presented within the air cavity, it provides resistance to convection within the cavity and interferes the radiative heat transfer between the two glazing panes. The strength of the heat transfer depends on the geometry and thermophysical properties of the structure layers. EnergyPlus simplifies the heat transfer process and converts the two-dimensional characteristics of the interstitial structure into a one-dimensional representation by assuming the interstitial structure to be a single solid layer similar to a glazing pane (illustrated in Figure 6-2 (b)). It applies an equivalent thermal conductivity (k_s) to replace the combined heat transfer through the complex structure and gas between the two glazing panes.

Normally, the equivalent thermal conductivity of the interstitial layer (k_s in in Figure 6-2 (b)) is obtained according to standard ISO 15099 [109], where radiative heat transfer is calculated through a radiosity method based on thermal radiation properties of the structure, but natural convection within the interstitial structure is not considered in detail. However, previous researchers [4, 25, 26, 29, 30, 47, 218] proved that the natural convection airflow within the geometry of a complex shading device significantly varies under dynamic boundary conditions (internal and external glazing

panes' temperature, average temperature of the interstitial structure, etc.), and these significantly affect the overall thermal conductance of the interstitial and gas cavity layer.

Thus, neither the standard method, which does not consider the effect of gas movement within the interstitial structure on heat transfer, nor using a single equivalent conductivity to replace its dynamic behaviour would result in an accurate prediction of the heat transfer. CFD calculation, as detailed and presented in Chapter 4, is a recognised method that has been widely used to predict the thermal characterisation of complex fenestration systems. Equivalent thermal conductivities under different thermal conditions (i.e. t_m and Δt) can be obtained by varying the boundary conditions in the CFD calculation. Thus, a series of individual values can be employed to represent the dynamic nature of equivalent thermal conductivity in building simulation. The detailed process of importing the dynamic thermal behaviour of glazing systems integrated with PS-TIMs into EnergyPlus is presented in section 6.3.5, when using the developed model to study the performance of a complex fenestration system.

6.2.2.2 Dynamic thermal properties acquiring method (CFD)

The equivalent thermal conductivities under different thermal conditions were obtained using CFD calculation. Details of simulation methods and relative results can been found in Chapter 4. In this chapter, PS-TIMs with slat pitches of 10mm, 7.5mm and 5mm were under investigation, a schematic diagram illustrating the geometry with PS-TIM is shown in Figure 4-6. The results of the thermal characterisations obtained under various boundary conditions from the CFD simulation are transferred into polynomial regression equations to determine the equivalent dynamic thermal conductivities of the PS-TIM layer, these input into EnergyPlus for building simulation. The conductivities are dynamic values and are function of mean temperature of the PS-TIM layer and the temperature difference between the two isothermal surfaces. Equation

(6-5) was used to correlate data and the regression coefficients for the fit for PS-TIMs with 10 mm 7.5 mm and 5 mm pitches (labelled as '10 mm PS-TIM', '7.5 mm PS-TIM' and '5 mm PS-TIM' respectively in preceding discussions) are given in Table 6-1.

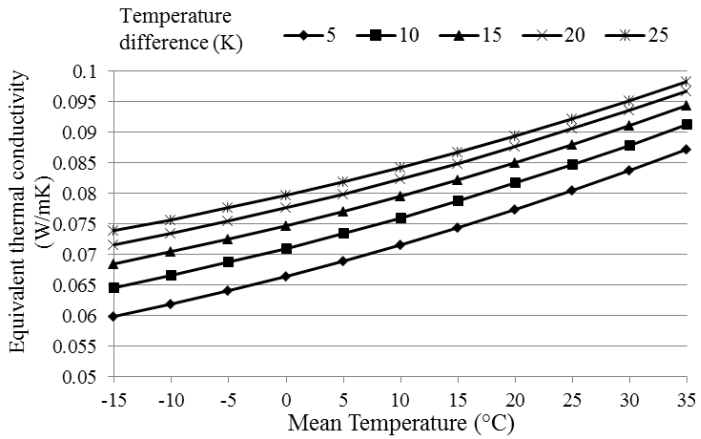
$$k_{PS-TIM} = a + bt_m + c\Delta + dt_m\Delta t + e\Delta t^2 + ft_m^2 \qquad (6-5)$$

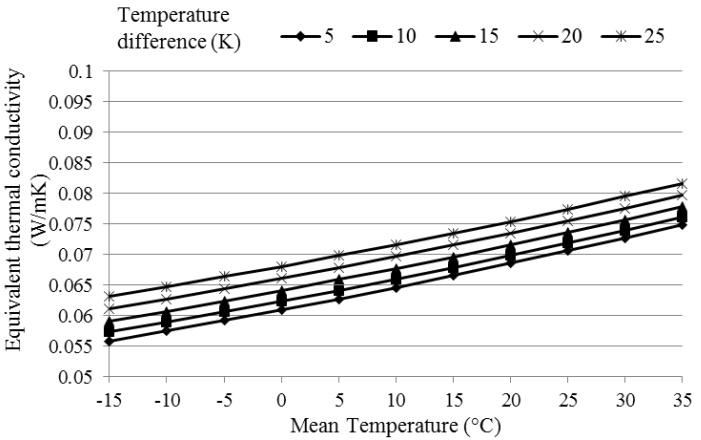
Here t_m (℃) is the mean temperature of two isothermal interfaces and Δt (℃) is the temperature difference between these two interfaces.

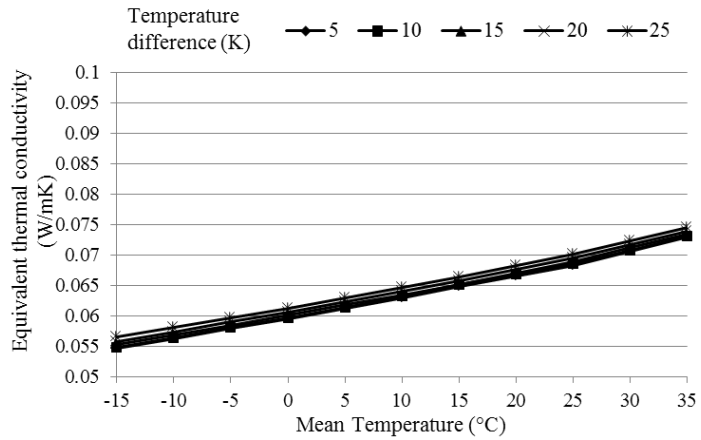
Table 6-1: Coefficients for the polynomial regression predicting equivalent thermal conductivities of different PS-TIM configurations for Equation (6-5)

	a	b	c	d	e	f
10 mm PS-TIM	0.0598	$4x10^{-4}$	$2\ x10^{-4}$	$-1x10^{-6}$	$5\ x10^{-6}$	$2\ x10^{-7}$
7.5 mm PS-TIM	0.0595	$3x10^{-4}$	$2\ x10^{-6}$	$2\ x10^{-6}$	$3\ x10^{-6}$	$2\ x10^{-6}$
5 mm PS-TIM	0.0568	$3x10^{-4}$	0	0	0	$1\ x10^{-6}$

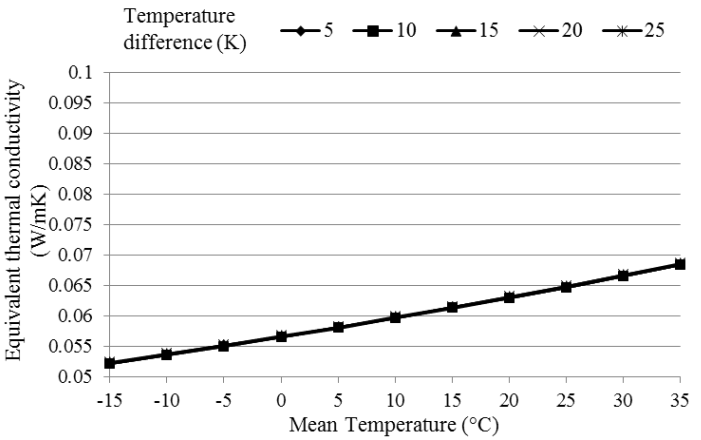
The dynamic thermal properties of the PS-TIM, which were calculated under various temperature conditions using CFD, are in the form of a series of equivalent thermal conductivities. The dynamic equivalent thermal conductivities of the glazing system integrated with PS-TIMs at different slat pitches (i.e. 10 mm, 7.5 mm and 5 mm) are illustrated in Figure 6-3.







(c) 7.5 mm PS-TIM structure



(d) 5 mm PS-TIM structure

Figure 6-3: The equivalent thermal conductivity of the air cavity between two panes with and without PS-TIM, pre-calculated by Computation Fluid Dynamics

6.2.3 Theories of optical model

This section introduces the fundamental theories of EnergyPlus and RADIANCE that are used to predict the daylight performance when applying complex glazing system into buildings, followed by the method of using ray-tracing to obtain the BSDF data of glazing system with PS-TIM integrated within the cavity of two glazing panes.

6.2.3.1 Daylight modelling in building performance simulation (EnergyPlus and RADIANCE)

The Radiosity method (DElight), and Split-flux method (Detailed), have been adopted in EnergyPlus to predict solar and daylight distribution in a space. According to [134], the radiosity technique, in which the reflecting surface in question is subdivided into nodal patches, and makes use of view factors applied to pairs of nodal patches provides greater accuracy than split-flux techniques in determining the overall contributing factor of reflected light within a space. On the other hand, as discussed previously, RADIANCE uses a backward ray-tracing method, which means that the rays are emitted from the point of interest and traced backwards until they either hit a light source or another object, to model daylight distribution in a space. Both programs are well recognised and are reliable for general building daylighting prediction and analysis of simple or classical fenestration systems [219, 220].

However, when complex fenestration systems (such as double glazing with an interstitial structure) are involved, the basic methods that work successfully for simple glazing become inefficient and inaccurate. One solution is to pre-calculate the optical characteristics of these complex fenestration systems before undertaking the performance prediction of their application to buildings. As introduced in section 3.3, the radiosity method, which is a commonly used method to solve the total amount of transmittance or reflectance of these complex fenestration systems, has been explained in international standard ISO 15099 [109]

and used by EnergyPlus to model window systems with shading devices. However, only knowing the quantity of transmitted light is also inadequate if you wish to obtain a precise interior illuminance distribution [45]. As discussed in section 3.3, the radiosity method also leads to errors when modelling highly specular surfaces as it assumes all surfaces exhibit Lambertian diffusion [142]. In order to include the angularly resolved transmissions and reflections in the calculation process, the generation of a *Bidirectional Scattering Distribution Function* (*BSDF*) for a complex window system is proposed and already detailed introduced in section 5.2. The *BSDF* based on Klems angle basis [143, 144] is a uniform format for both RADIANCE and EnergyPlus.

6.2.3.2 Bidirectional optical properties acquiring method (ray-tracing)

Bidirectional Scattering Distribution Function (*BSDF*) is currently regarded as the most important method for characterising a complex glazing systems allowing them to be represented with precision in daylight analysis simulations. The *BSDFs* of glazing systems integrated with PS-TIMs were calculated before undertaking the performance prediction of their application to buildings. As expressed in Chapter 5, to obtain the Klems-*BSDF*, genBSDF, a validated ray-tracing program in RADIANCE was used to generate a *BSDF* data from the selected geometry and material optical properties of the PS-TIMs. The generated *BSDF* can be used directly in RADIANCE to determine the daylighting performance or input into Window 6 and then further used in EnergyPlus to predict the energy performance of applying this system in a building.

6.3 Building performance simulations

A single room, based on an office in Energy Technologies Building, University of Nottingham in the UK, was selected for the simulation. The purpose of using a single office in

building simulation and performance analysis is to use a simple scenario to demonstrate how the PS-TIM integrated into a glazing system influences the indoor environment and energy efficiency of an office.

6.3.1 Weather data

The study was performed over one-hour time steps for an entire average year using IWEC weather file for London. The latitude is 51.5 °N and the longitude is 0 °W. The diurnal average temperature and direct and diffuse solar radiation of London can be found in Figure 6-4.

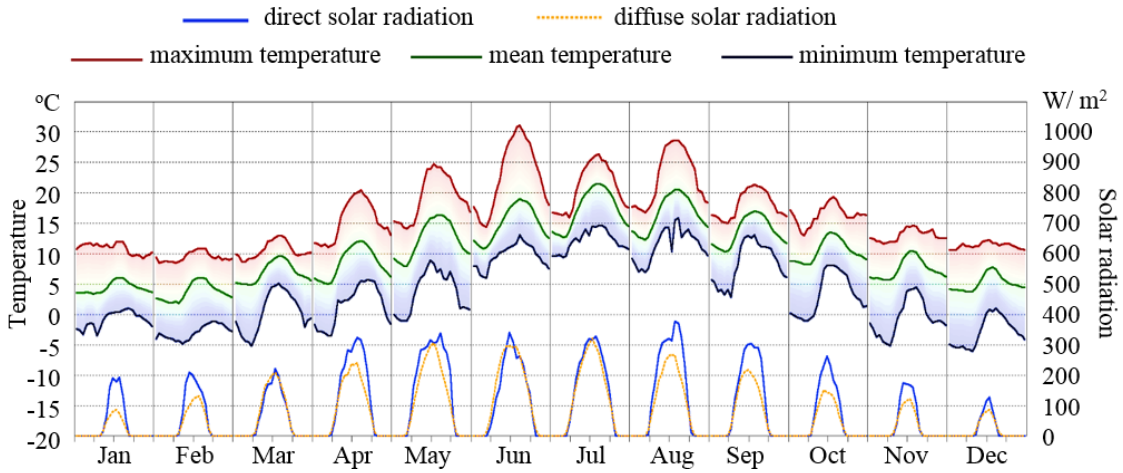
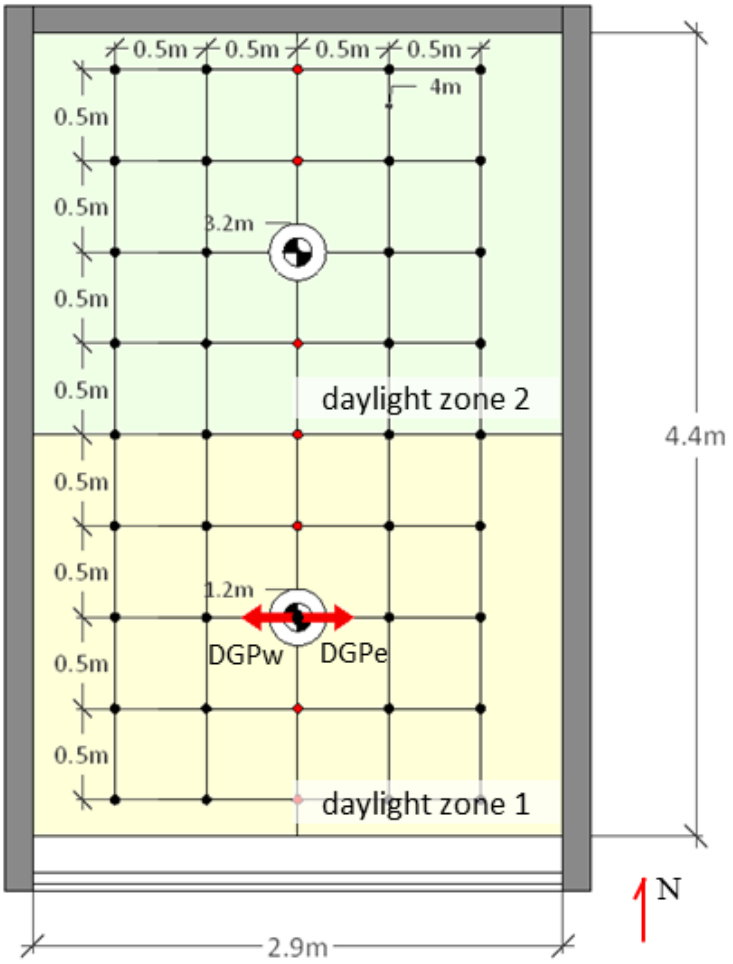


Figure 6-4: The diurnal average temperature and direct and diffuse solar radiation of London

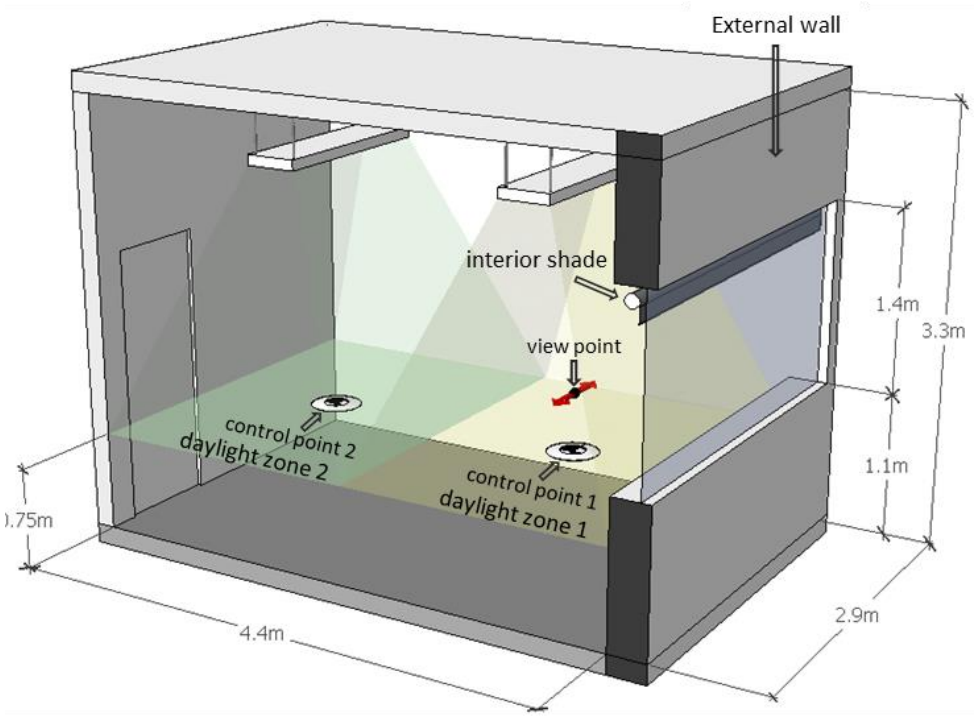
6.3.2 Prototype office geometry and modelling

The geometry of the prototype office is shown in Figure 6-5. The office is south facing and considered as part of a large building. It means that only the south wall of the room is exposed to external conditions while the other surfaces of the room are assumed to be buffered by mechanically conditioned spaces and therefore experience no net heat transfer across the boundaries. The office has dimensions of 2.9 m (width) × 4.4 m (depth) × 3.3 m (height). All the surrounding buildings, vegetation or other obstructions are not considered in this model. A window with dimension of 1.4 m (height) × 2.9 m (width) is located in the south exterior wall with a sill level of 1.1 m above the ground. The window-to-wall ratio is 0.42. As shown in

Figure 6-5, the room is divided into two daylighting zones with two control sensors located at the centre of each daylighting zone at a height of 0.75 m (representing the height of the working place). The daylight illuminance level at these two sensors determines the switching on/off of two lights for these two halves of the room.



(a)



(b)

Figure 6-5: (a) Plan view and (b) section view of the simulated office room

6.3.3 Modelling of building daylight simulation

A Three-Phase-Method in RADIANCE, which is based on hourly daylight weather data, was used for annual dynamic daylight simulation. The detailed daylight modelling method can be found in Chapter 6.

6.3.4 Modelling assumptions for building energy simulation

In the Energy Performance Simulation model, the *U-value* of the exterior south wall is assumed to be 0.43 W/m^{2}K in this research. The occupancy hours are assumed to be from 8:00 and 17:00 on weekdays. Equipment and lighting loads are assumed to be 13 W/m^2 and 16 W/m^2, respectively [221, 222]. Two daylight control sensors, with each sensor controlling the lighting for half of the room, are set within the room. If the detected illuminance falls below 500 lux during working hours, the artificial light above it will be turned on. The HVAC is assumed to be a unitary system with direct expansion cooling and gas heating. To simplify the assumptions, a single comfort set point temperature of 21 ℃ is used all year round. Two scenarios of HVAC operation were applied, one assumes that the HVAC only operates during working hours from 8:00 to 17:00 on weekdays and the other assumes that the HVAC is on through the year.

In practice, if occupants in an office are disrupted by bright daylight, they are likely to lower the interior shade or blind to block the sunlight. To represent this, a threshold for the horizontal daylight illuminance level on working plane, *(E)*, and a threshold for the *daylight glare probability (DGP)* have been introduced. When the *DGP* of facing east or west wall at the view point (*DGPe/ DGPw*) or illuminance level on point 1, *(E_1)*, exceed the limits illustrated in Table 5-2 [160, 223], the interior shade is considered to be lowered, then artificial light is applied. *DGPe/ DGPw* and *E_1* at each time-step are calculated using RADIANCE. Details of these two daylight metrics and the corresponding threshold can be found in Chapter 3. The annual daylight simulation results were used to generate a schedule to control shades that is used in annual energy performance simulation (i.e. EnergyPlus). When stressing the

investigation of PS-TIM's performance, the effects of shading device's optical properties (e.g. transmittance and reflectance) were not taken into consideration through making an assumption of using the interior shade with reflectance of 0.5 and transmittance of 0.1 to represent a typical medium reflective and low transparency shading device.

Table 6-2: Thresholds used to control lowing of interior shades

DGP_e *or* DGP_w **at view point**	**Illuminance value at point 1 (**E_1**)**
> 0.35	> 2000 lux

6.3.5 Importing of thermal and optical characteristics of PS-TIM into EnergyPlus

The optical properties, which were obtained using genBSDF within RADIANCE, are in the format of a Klems-*BSDF*. The *BSDF* data were then run through WINDOW to generate a unified file of the complete system that contains the PS-TIM and glazing layers in EnergyPlus format [45].These data were subsequently input into EnergyPlus to replace a traditional radiosity optical model.

The dynamic thermal properties of the PS-TIM, which were calculated under various temperature conditions using CFD, are in the form of a series of equivalent thermal conductivities. The dynamic equivalent thermal conductivities of the glazing system integrated with PS-TIMs at different slat pitches (i.e. 10 mm, 7.5 mm and 5 mm) are illustrated in Table 6-3. These data were input into EnergyPlus using its built-in 'Energy Management System (EMS)' function. This assumes two temperature sensors were arranged on the surfaces of the two glazing panes facing into the cavity. Based on the detected window surface temperatures, a corresponding thermal conductivity was selected from the dataset in EMS at the beginning of each time-step in the building simulation [224].

6.3.6 Model verification

In order to provide confidence using the developed "EMS" method (labelled as "EMS" in Figure 6-6 and Table 6-3) for thermal analysis, an annual simulation using EMS to setup dynamic thermal conductivity for a double glazing system without an interstitial structure was conducted. The hourly window heat gain and heat loss have been compared with simulation data obtained using the default method in EnergyPlus, (labelled as "Nu" in Figure 6-6 and Table 6-3). In this, the thermal conductivity of the air gap is determined in terms of the dimensionless *Nusselt number* [109, 134]. Figure 6-6 shows the heat losses obtained using these two methods for a notional 3 day period in heating period and the heat gains through window for a notional 3 days in cooling period. The annually total heating load under London's climate by EMS and Nu methods are 51.95 kWh/m^2 pa and 52.71 kWh/m^2 pa, respectively. And the cooling load by using these two methods are 56.05 kWh/m^2 pa and 55.50 kWh/m^2 pa, respectively. The deviation is less than 2% in each case. The comparison between these two methods provides a degree of confidence in the EMS model, and therefore confidence in further models developed using this method and their use to extend the building energy analysis of glazing with a PS-TIM.

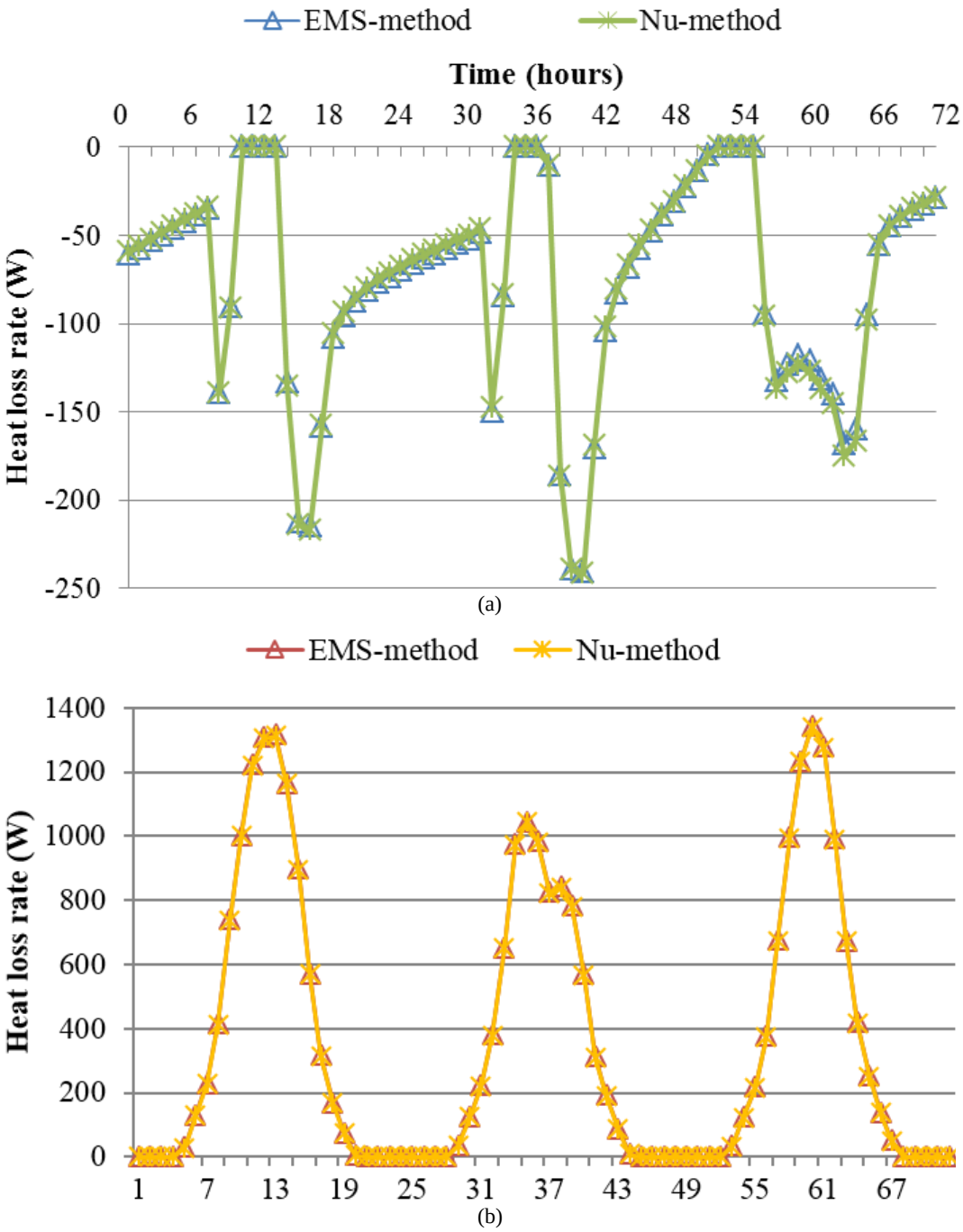


Figure 6-6: **(a) window heat loss under cold weather conditions—3 coldest days under London climate; (b) window heat gain under hot weather conditions—3 hottest days under London climate**

Table 6-3: Comparison of the annual prediction (kWh/m^2 a) of heating and cooling load obtained using two methods under different climate

Model	Stockholm		London		Beijing		Hong Kong		Singapore	
	Heating	Cooling	Heating	Cooling	Heating	Cooling	Heating	Cooling	Heating	Cooling
EMS	93.14	58.79	51.93	56.05	42.31	103.90	2.60	153.78	0	186.48
Nu	93.86	58.27	52.71	55.50	42.67	103.40	2.65	153.65	0	186.76

6.4 Building performance simulation results and discussion

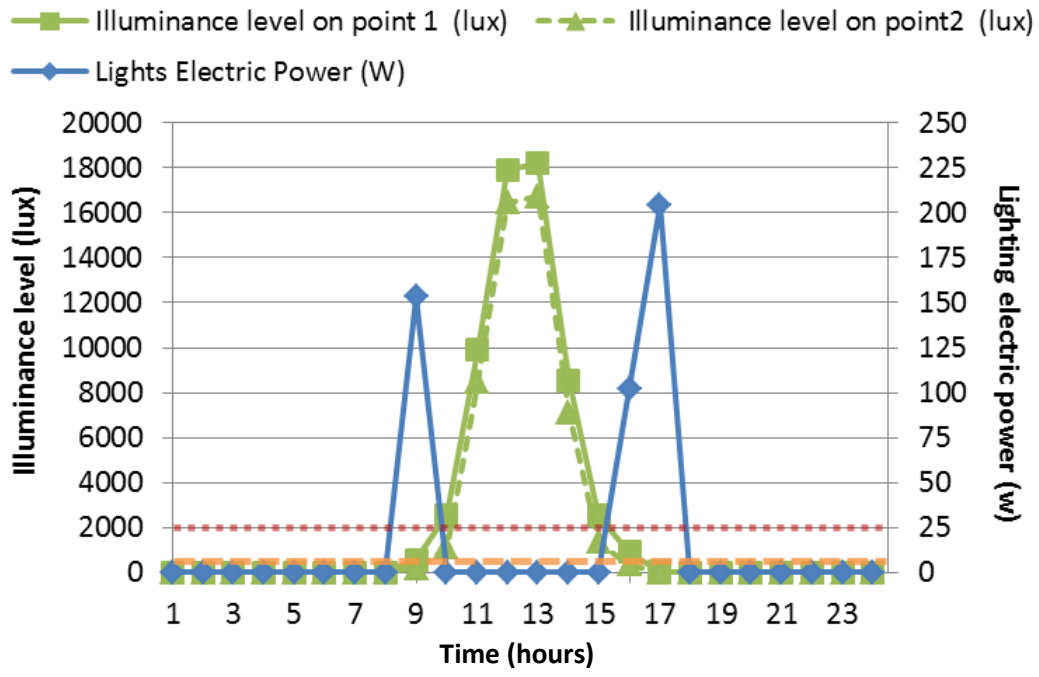
Based on the daylighting performance analysis, presented in Chapter 7, the building energy performance is investigated with three slat pitches (10mm, 7.5mm and 5mm) to reveal the influence of PS-TIM on the overall energy and daylight prediction of the office. The material used to form the parallel slats is assumed to be a Lambertian diffuser with 50% transmittance, as it can provide homogeneous daylight distribution within an office space.

Results of detailed daylight performances for glazing systems without PS-TIM and with translucent PS-TIMs at different slat pitches obtained using RADIANCE can be found in Chapter 7 and are not repeated in this section. However, the *DGP* and illuminance level on the working plane for each time-step, which were considered as a control strategy for the use of interior shading device, ultimately affected the overall energy demands. Thus, the effect of daylighting comfort level on the required hours of using interior shading is discussed in this section.

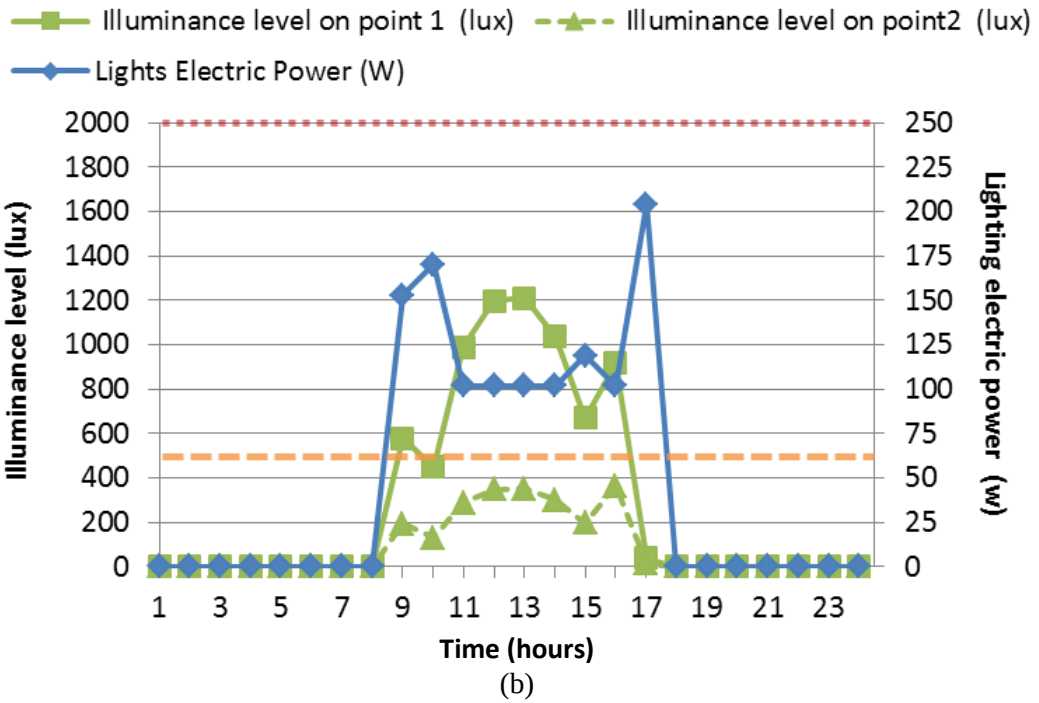
6.4.1 Requirement for interior shading to prevent strong daylight

In practice, if occupants in a working space are disrupted by high illuminance levels or glare from the windows, they are likely to lower the interior shade. This would significantly reduce the availability of daylight, and hence results in the illuminance level deeper within the space becoming insufficient for work. Consequently, artificial lighting is required. Figure 6-7 illustrates an example of hourly daylight illuminance level at the two sensors in each of the daylight zones with and without using an interior shade and the related lighting energy consumption on a typical sunny day. A typical interior shade with medium reflectance of 0.5 and low transmittance of 0.1 is used in simulation. From Figure 6-7, it can be seen that with the use of interior shade to block the strong daylight that occurs from 10:00 to 15:00, the illuminance level at the point 1

at 10 am and the illuminance level at point 2 for the whole period from 10:00 to 15:00 drops below 500 lux. Artificial light is required to illuminate the dark space around point 2, however, this would increase the use of electricity and therefore increase the building energy consumption. Therefore, reducing the probability of using interior shade to achieve a comfortable visual environment is very important for lighting energy saving.



(a)



(b)

Figure 6-7: (a) Lighting power and illuminance level at points 1 and 2 without interior shade; (b) Lighting power and illuminance level on point 1 and 2 with interior shade on a typical sunny day

PS-TIMs have been integrated into double glazing to reduce the probability of using interior blinds. Figure 6-8 shows the average hours per week where shade are lowered based on two thresholds (i.e. illuminance level >2000 lux and *DGP>0.35*). In the assumptions of this research, there are in total 63 working hours per week. The average hours per week of using shading device reduce from 34.3 hours when applying DG to 6.5 hours when applying 10 mm PS-TIM. Applying 5 mm PS-TIM can nearly eradicate the requirement for interior shade.

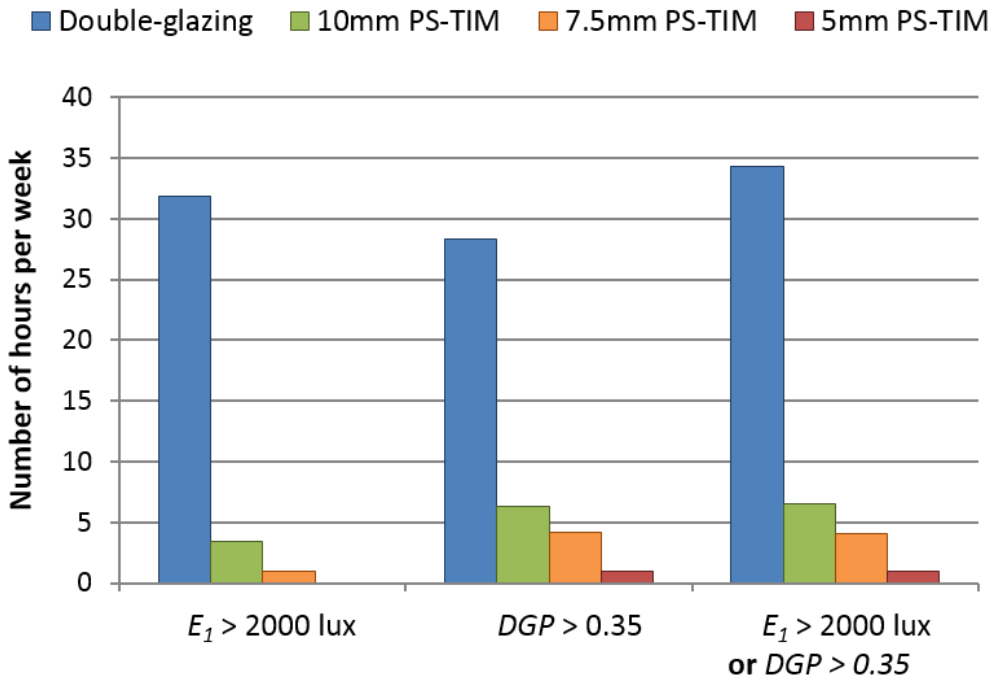


Figure 6-8: Average number of hours per week when discomfort daylight condition exist

6.4.2 Window heat loss and heat gain through windows with PS-TIM

In order to explore the key heat transfer paths for the office, a breakdown of annual heat loss and heat gain in the office with conventional double glazing is shown in Figure 6-9. The heat transfer between the room and its adjacent rooms is neglected, as they are assumed to be controlled at a similar thermal condition. As shown in Figure 6-9, under London's climate and these specific assumptions in this simulation, the heat gain through the window accounts for 56% of total heat gain, in which 29% of the total

heat gain comes from transmitted solar energy through the window, while 27% of total heat gain enters the space through convection and radiation. The heat loss through the window accounts for 55% of the total losses. It can be concluded that the heat gains and heat losses through the window represent more than half of the room total heat gain and heat loss in this model. This means strategies for improving the thermal and optical properties of the window have the potential to significantly reduce the system heating and cooling load.

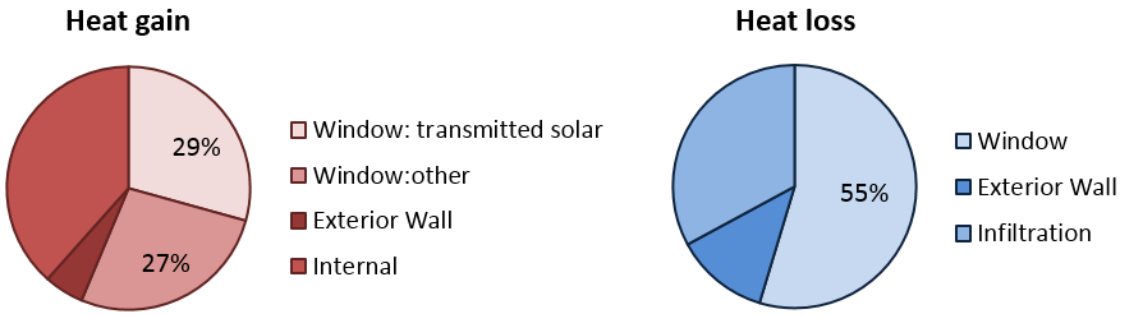


Figure 6-9: Breakdown of annual heat loss and heat gain for the office with a normal double glazing under five different climates

Figure 6-10 shows the change in window heat loss and heat gain after applying different PS-TIM structures to the cavity of a double glazing system. The window heat gains reduce to 38%, 42% and 46% for the 10 mm, 7.5 mm and 5 mm PS-TIM respectively. The reductions of heat loss are 23%, 25% and 30% respectively. The presence of PS-TIM has a more obvious influence on the window heat gain than the window heat loss. This is because the window heat gain is dominant by the direct transmitted solar radiation and the presence of translucent parallel slats dramatically reduces transmission through the window system. In contrast, although the presence of PS-TIM increases the thermal resistance of the air cavity between two glazing panes, the overall heat loss through window is dramatically affected by the convective heat transfer on the external surface of window (i.e. the exterior surface convective heat

transfer coefficient is determined by the wind speed as well as the temperature difference between window surface and ambient environment).

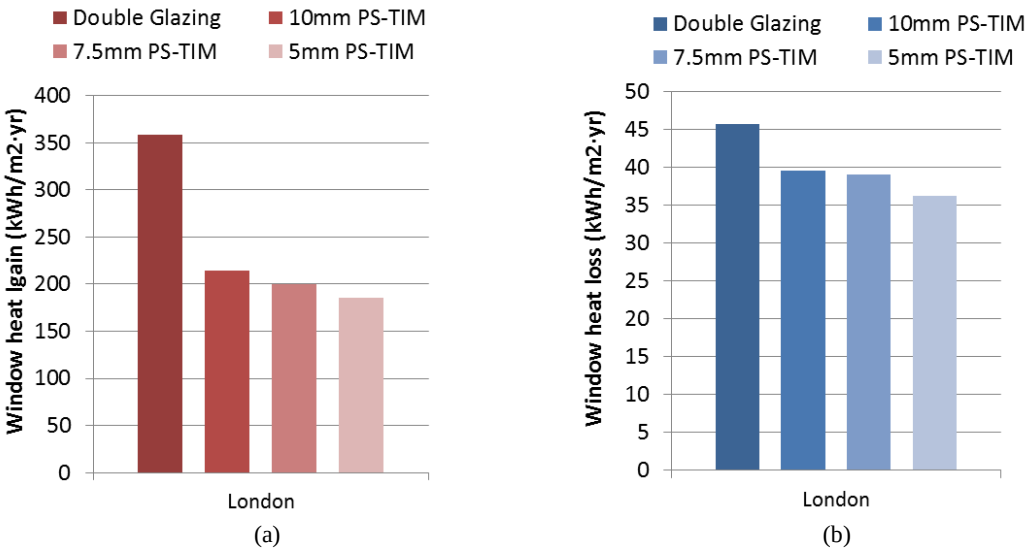


Figure 6-10: (a) heat gain and (b) heat loss through windows (kWh/m^2·yr) after applying different configurations of PS-TIM under five climates

6.4.3 Total energy consumption after applying PS-TIM

This section presents the annual energy consumption for the office after applying different PS-TIM configurations. The energy consumption is expressed in terms of kWh/m^2 per year and they are further divided into heating, cooling and lighting energy consumption. For the purpose of predicting the potential energy saving by applying PS-TIMs, the energy consumption using a conventional double gazed window with and without an interior shade are also calculated for comparison. Two HVAC scenarios of scheme were applied, Figure 6-11 shows data where the HVAC is only operating during working hours from 8:00 to 17:00 on weekdays and Figure 6-13 shows data for the scenario where the HVAC is always on through the whole year.

As shown in Figure 6-11, under London's climate, the 10 mm PS-TIM provides the best energy efficiency when the HVAC system only works during working hours on weekdays. Compared with the conventional double glazed window with interior shade,

an overall energy reduction of 15.5% can be achieved. Most of the energy reduction occurs in the lighting and cooling demand. 10 mm PS-TIM leaded to 25.7% lighting energy savings, 24.6% cooling energy saving and only 2.4% heating energy saving. Although, the presence of PS-TIM increases the thermal resistance of the window system and reduces the heat loss through window, it simultaneously reduces the solar heat that transferred from the window to warm up the room during daytime. The balance between these two is not sufficient to yield a reduction in heating demand. This is illustrated by the hourly window heat gain, heat loss and space heating loads for a window with and without a 10 mm PS-TIM on typical winter days (48 hours) as shown in Figure 6-12 (a) and (b). Therefore, when the HVAC system only operates during working hours, window system with a better thermal resistance provided by PS-TIM does not result in a significant reduction of total heating energy demand.

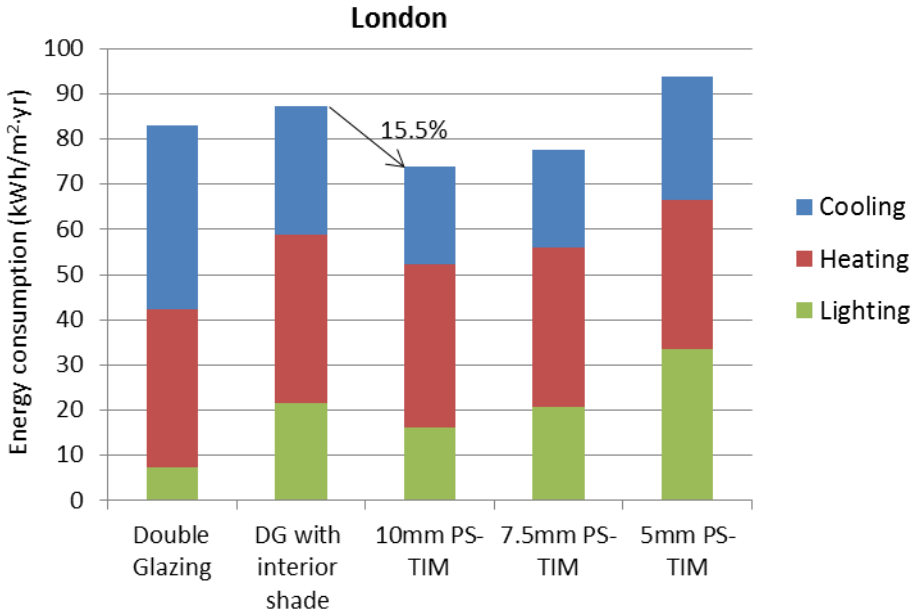
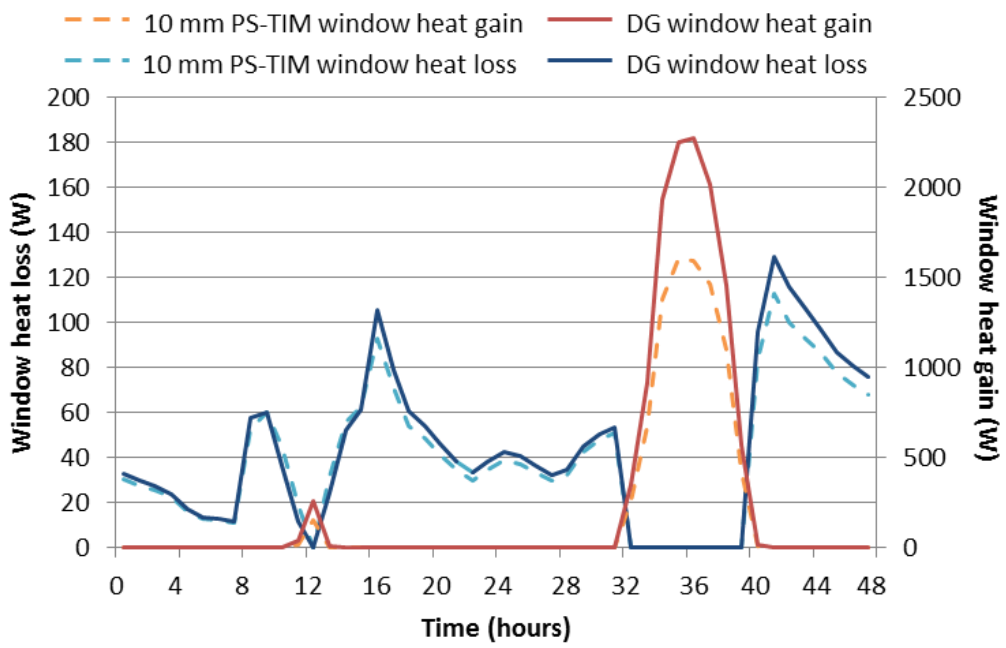
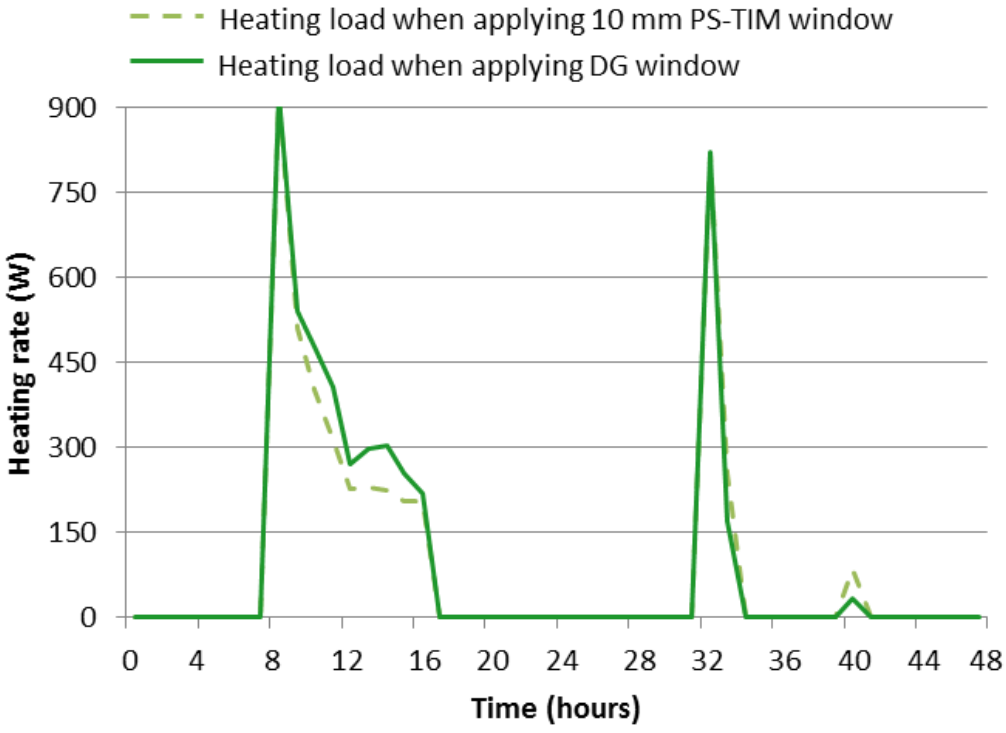


Figure 6-11: Annual heating, cooling and lighting energy consumption when HVAC works between 9:00-17:00 on workdays



(a)



(b)

Figure 6-12: Hourly window (a) heat gain, heat loss and (b) space heating loads of applying window system with and without PS-TIM when HVAC works on working hours

However, the energy efficiencies of using various PS-TIMs changes when the HVAC system works continuously during the year (see Figure 6-13). The 7.5 mm PS-TIM provides the best energy saving potential. It can be seen that, the heating demands dramatically reduced by 30.9% when applying 7.5 mm PS-TIM. Also, the 7.5 mm PS-

TIM can achieve a lighting energy savings of 31.2% and a cooling energy saving of 42.8%. The reason for a better performance of PS-TIM with smaller interval distance (i.e. 7.5mm and 5 mm) is that the improved thermal resistance of the PS-TIM results in a dramatic reduction of heating energy demand during night time when HVAC system is always on as illustrated in Figure 6-14.

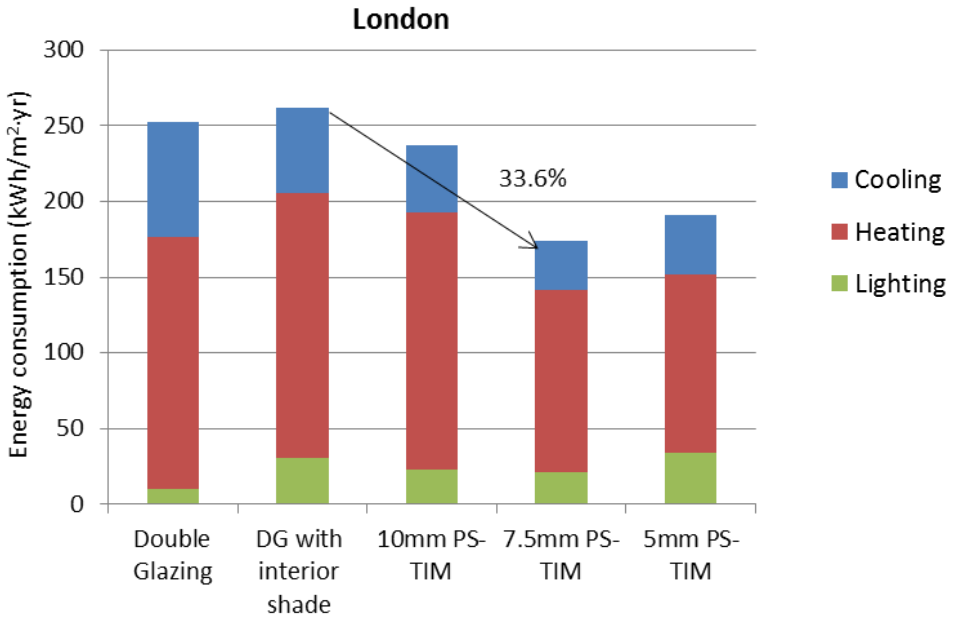
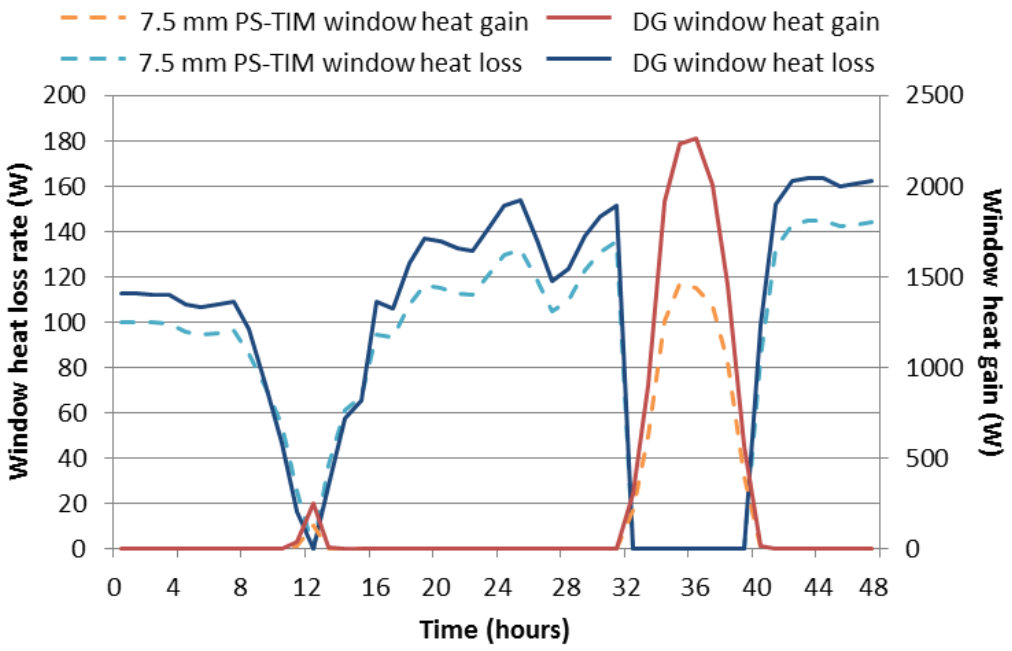
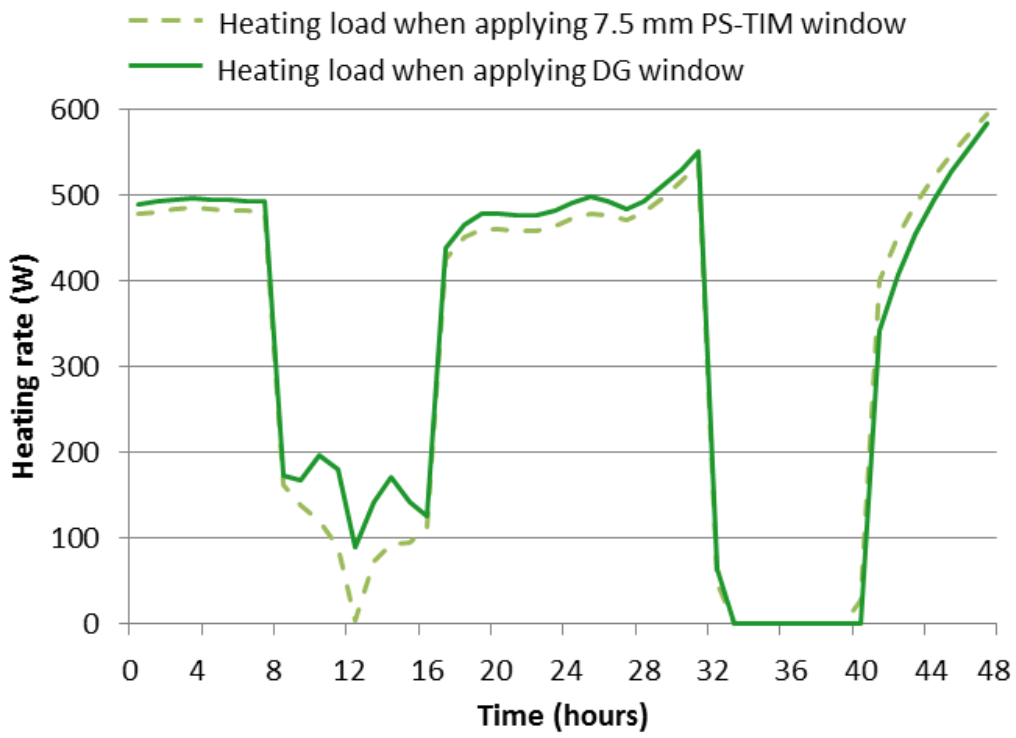


Figure 6-13: Annual heating, cooling and lighting energy consumption when HVAC is always on.



(a)



(b)

Figure 6-14: Hourly window (a) heat gain, heat loss and (b) space heating loads of applying window system with and without PS-TIM when HVAC when HVAC always on

The analysis of energy consumptions in these two ideal scenarios of HVAC operation schemes provides a quantitative assessment of the effect of varying thermal and optical properties of PS-TIMs with different configurations on the overall heating, cooling and lighting energy consumption.

6.5 Conclusion

A good fenestration system needs to simultaneously solve the problem of both visual discomfort and energy inefficiency that are evident when conventional double glazed window systems are used. This research uses a comprehensive model to investigate the thermal and optical performance of a window system with Parallel Slats Transparent Insulation Material (PS-TIM) and also its impact on building performance. EnergyPlus has been combined with thermal model developed using Computational Fluid Dynamics and an optical model developed using a ray-tracing technique to predict its impact on window heat gain and heat loss plus the overall heating, lighting and

cooling energy consumption. RADIANCE has also been used to predict detailed daylight performance of applying PS-TIM. Based on the specific assumptions in the building performance predictions, the following conclusion can be drawn:

1) The presence of PS-TIM can result in a 23% ~ 30% reduction in window heat loss and 38% ~ 46% reduction in window heat gain.

2) PS-TIM can provide a more homogenous distribution of daylight, and effectively eliminate glare.

3) When compared with conventional double glazed window with interior shade, applying PS-TIM can achieve up to 15.5% energy reduction when HVAC operates during working hours and up to 33.6% energy reduction when HVAC is always on.

Chapter 7. Applying PS-TIM under different climates

7.1 Introduction

In Chapter 6, the daylight performance (i.e. useful daylight illuminance, daylight glare probability and etc.) of a glazing unit with integrated parallel slat transparent insulation materials PS-TIMs was investigated using RADIANCE in combination with *Bidirectional Scattering Distribution Functions* (*BSDFs*) to represent the PS-TIMs' optical performance. In Chapter 7, the building energy performance prediction (i.e. heating, cooling and lighting energy consumption) of this glazing system was generated using EnergyPlus in combination with the dynamic thermal characterisations of the glazing system obtained from Computational Fluid Dynamics calculation. However, both of the daylight and energy building performance prediction were solely conducted under London's climate. This chapter extends the building performance investigation to four additional climates in order to demonstrate how PS-TIM performs under different environmental conditions.

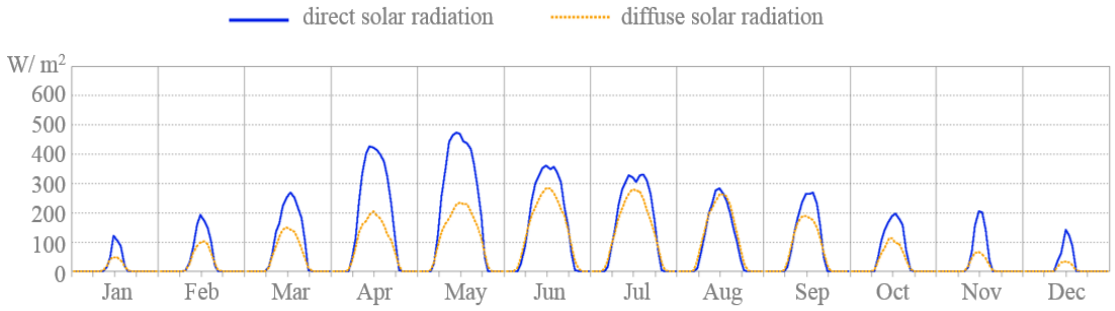
7.2 Applying PS-TIM under different climates: weather data

In this chapter, the methods used for building daylight, thermal and energy performance prediction are exactly the same as those in Chapter 6 and 7. Four other cities: Stockholm, Beijing, Hong Kong and Singapore, which represent different geographical and weather conditions (i.e. temperature, solar radiation intensity etc.), were selected to show the different ways PS-TIM influences building performance. The selection of these cities was based on their latitudes (i.e. approximate 20 ° intervals between each other span a latitude range between 1.3 °N to 59.3 °N) and also confined by highly available and reliable weather files. The study was performed over one-hour time steps for an entire average year using IWEC (International Weather for Energy Calculation) weather data for these cities. The latitude, longitude, summer and winter

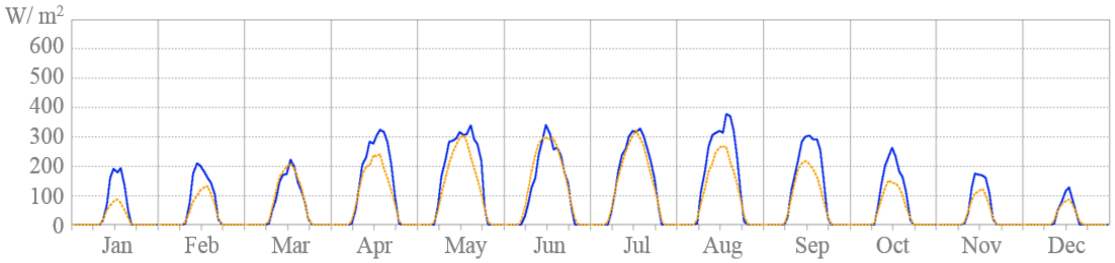
average temperatures and solar radiation conditions of London and these four cities are shown in Table 7-1. The diurnal direct and diffuse solar radiation of these five cities can be found in Figure 7-1.

Table 7-1: Latitude, longitude, summer and winter average temperatures and solar irradiance of 5 cities

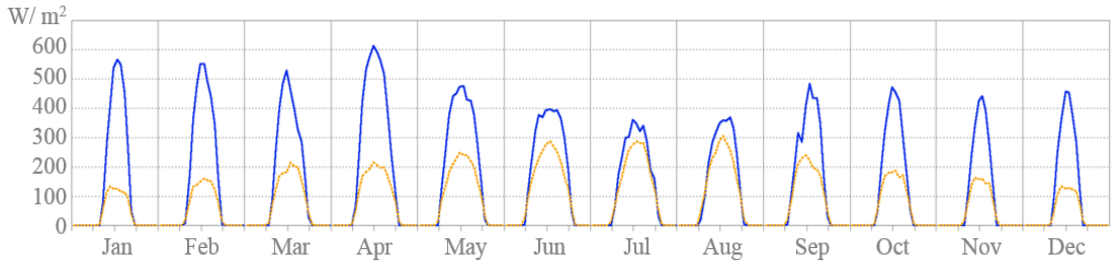
	Latitude	**Longitude**	**Summer avg. temp. (°C)**	**Winter avg. temp. (°C)**	**Annual average solar irradiance (kWh/m^2)**
Stockholm	59.3 °N	18 °E	15.8	-2.0	900-1000
London	51.5 °N	0 °W	16.3	4.5	1000-1100
Beijing	39.9 °N	116 °E	25.4	-1.1	1400-1500
Hong Kong	22.3 °N	114.2 °E	28.4	16.5	1500-1600
Singapore	1.3 °N	103.8 °E	Annual avg. 27.4		1600-1700



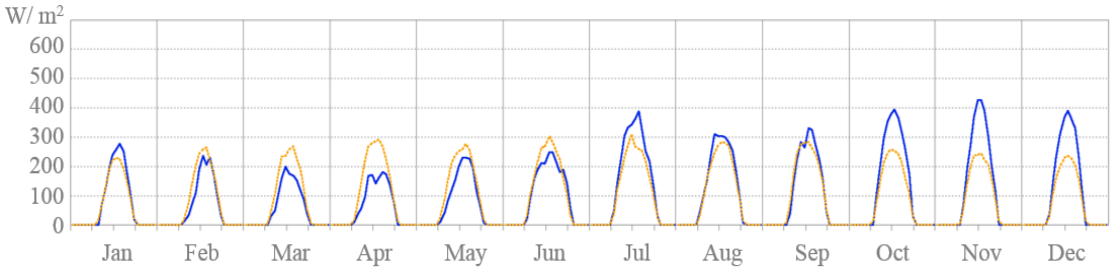
(a) More direct solar radiation than diffuse solar radiation in Stockholm's climate



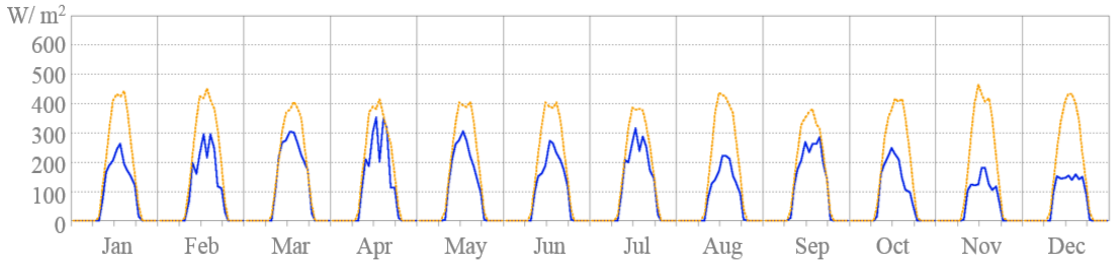
(b) Approximately equal direct and diffuse solar radiation in London's climate



(c) Very strong direct solar radiation in winter, skies diffuse in summer in Beijing's climate



(d) Approximately equal direct and diffuse solar radiation in Hong Kong's climate



(e) Diffuse solar radiation greater than direct throughout the year in Singapore's climate

Figure 7-1: The diurnal average direct and diffuse solar radiation of (a) Stockholm, (b) London, (c) Beijing, (d) Hong Kong and (e) Singapore

7.3 Results and discussion

7.3.1 Daylight performance

The daylight performance of the PS-TIM window systems will be influenced by the latitude of the site which they are used on and the orientation of the glazing relative to the sun path. In addition, climatic influences that dictate the balance between clear skies with direct sunlight and overcast skies with diffuse light also influence performance.

In addition to exploring the daylight performance under different geographical locations and weather/solar conditions, this section also investigate the daylight performance for the prototype office facing four different orientations (East, West, South and North) located in London (a relatively high latitude site outside the Tropics) and Singapore (located within the Tropics, close to the equator).

In these studies, the PS-TIM comprises diffused translucent non-tilted slats contained within a double glazing unit. Slat pitch is the sole PS-TIM variable explored in this section. As in the Chapter 6, the *useful daylight illuminance* (*UDI*) was predicted at regular points located along the centre line of the room between the window to the end wall. The other two metrics, *UR* and *DGP*, were not considered because PS-TIMs with all proposed slat pitches showed significant improvement of daylight performance in these two metrics.

7.3.1.1 PS-TIMs' performance under different climates

Figure 7-2 (a) ~ (e) shows the distribution of standard *UDI* bins used to quantify performance for the five different climates considered. The blue, green and red lines represent *undersupplied UDI* bin, *useful UDI* bin and *oversupplied UDI* bin, respectively. Figure 7-2 (f) ~ (j) shows data for the modified bin size ($UDI_{500\text{-}2000\ lux}$), which captures

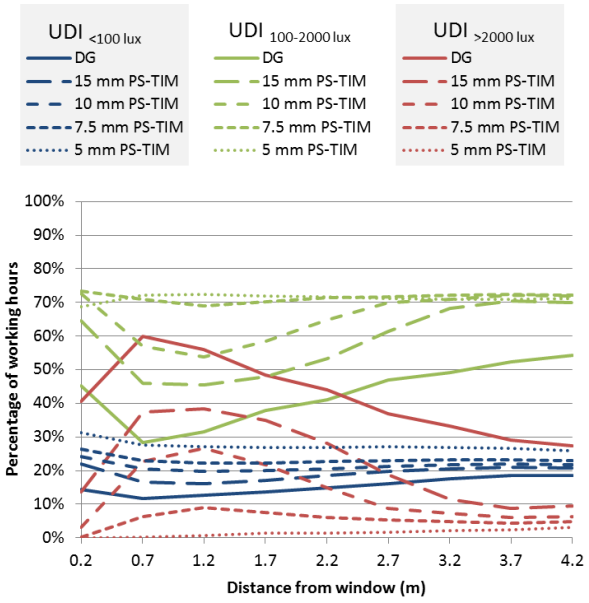
only data that meet the design illuminance of at least 500 lux. This provides greater detail than using the $UDI_{100\text{-}2000\ lux}$ bin alone.

The standard double glazed system shows similar daylight performance for each of the cities considered. In the region close to the window, a significant proportion of the working hours shows *over* illumination (i.e. appearing in the $UDI_{>2000}$ bin). As a consequence, only a small number of hours fall into the *desirable* levels of illumination (i.e. appearing in the $UDI_{500\text{-}2000\ lux}$ bin). The inclusion of PS-TIM improves the luminous environment in the region close to the window by reducing the hours of over illumination and in so doing provides a more uniform illumination of the working plane. As can be seen in Figure 7-2 (a) and (b), the application of PS-TIMs with 7.5 mm and 5 mm slat pitch can provide relatively even distribution of $UDI_{100\text{-}2000\ lux}$ and improve its proportion to approximately 70% and 80% of working hours in Stockholm and London, respectively. When using the additional criteria $UDI_{500\text{-}2000\ lux}$ (as shown in Figure 7-2 (f) and (g)), it can be seen that with a decrease the slat pitch from 7.5 mm to 5 mm, the percentage of working hours with illuminance in the most desired range reduced. Thus, PS-TIM with a 7.5 mm slat pitch provides the best all round performance in Stockholm and London. For Beijing, as shown in Figure 7-2 (c) and (h), the PS-TIM with a 5 mm slat pitch can improve the $UDI_{100\text{-}2000\ lux}$ to around 90% of working hours and achieve a homogenous light distribution. However, when compared with PS-TIM with a 10 mm or 7.5 mm slat pitch, it performs worse in the illuminance range of 500-2000 lux, with a greater proportion of working hours falling in the range of 100-500 lux. The application of PS-TIMs with 7.5 mm and 5 mm slat pitch provide a relatively even distribution of $UDI_{100\text{-}2000\ lux}$ and improve the metric to around 90% of working hours. PS-TIM with a 10 mm slat pitch offer the best performance of $UDI_{500\text{-}2000\ lux}$ in Hong Kong (as shown in Figure 7-2 (d) and (i)). All but PS-TIM with 15mm slat pitch can improve the

illuminance in the range of 100-2000 lux to 90% of working hours in Singapore and PS-TIM with a 10 mm slat pitch performed best in the additional $UDI_{500\text{-}2000\ lux}$ criteria.

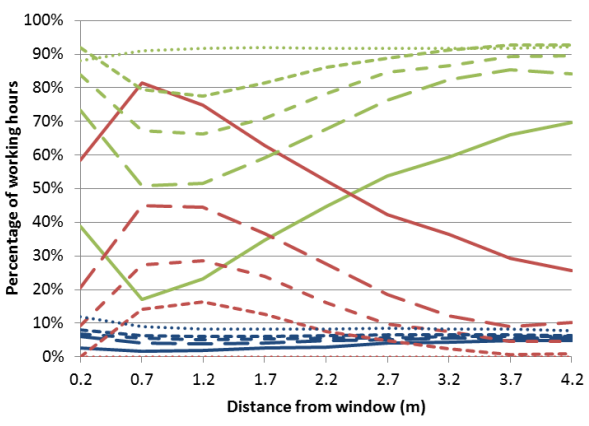
Generally, as latitude increases a smaller slat pitch is required to achieve optimised performance and evenly distribute the daylight. For example, the 7.5mm slat pitch PS-TIM can provide relatively even distribution of $UDI_{500\text{-}2000\ lux}$ and $UDI_{100\text{-}2000\ lux}$ when applied in London, and PS-TIM with a 10mm slat pitch can achieve similar effect when used in Singapore. This is a consequence of the relationship between solar altitude and the pass angle for the PS-TIM (i.e. $\tan^{-1}$ (slat pitch / cavity width)). This dictates whether direct solar radiation can reach the working plane in the region close to the window or whether this light is incident on the slat and diffused. It is worth noting that for Beijing, only the PS-TIM with a 5 mm slat pitch can achieve a homogenous distribution of $UDI_{100\text{-}2000\ lux}$. This is because the direct solar irradiation is strong in the year of IWEC weather data (as shown in Figure 7-1) and leads to significant numbers of hours of over supply (i.e. $UDI_{> 2000lux}$) despite undergoing attenuation in the diffusing PS-TIM.

To conclude, both the solar irradiation intensity and the solar altitude angle affect the process of selecting an optimal slat pitch for a window integrating with PS-TIM.

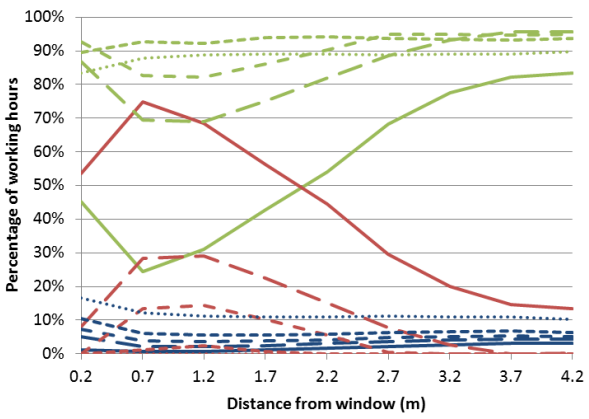


(a) Stockholm *UDI* bins

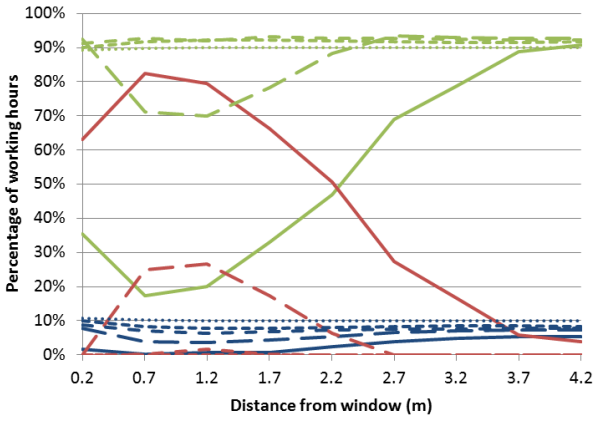
(b) London *UDI* bins



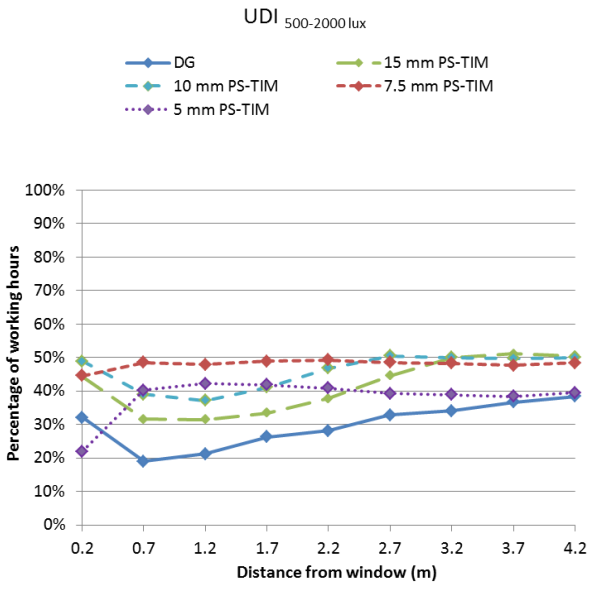
(c) Beijing *UDI* bins



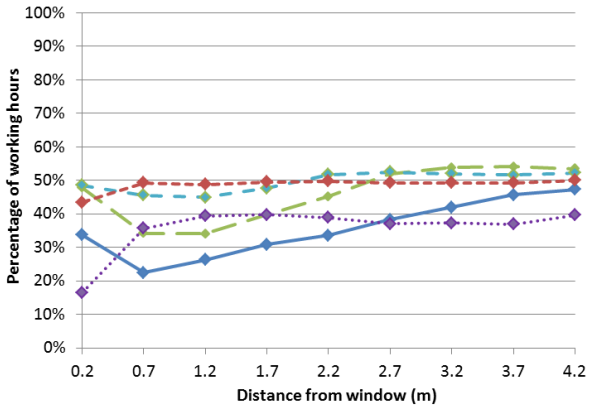
(d) Hong Kong *UDI* bins



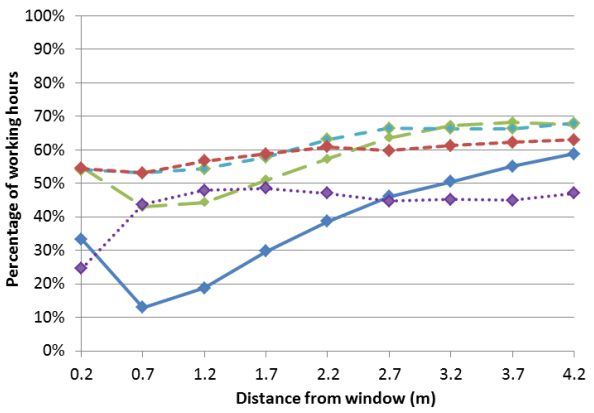
(e) Singapore *UDI* bins



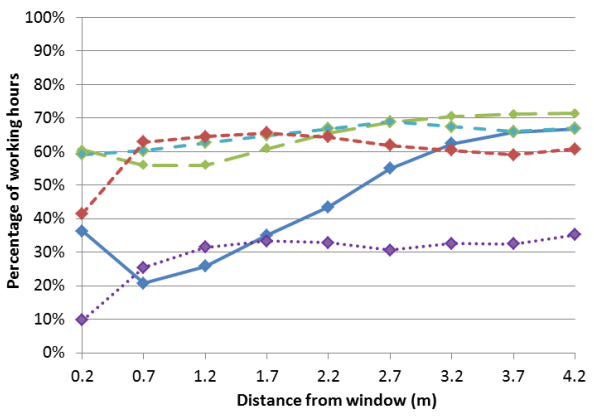
(f) Stockholm $UDI_{500\text{-}2000lux}$



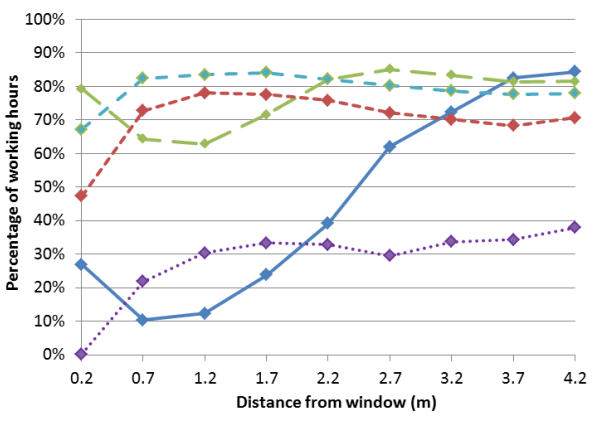
(g) London $UDI_{500\text{-}2000lux}$



(h) Beijing $UDI_{500\text{-}2000lux}$



(i) Hong Kong $UDI_{500\text{-}2000lux}$



(j) Singapore $UDI_{500\text{-}2000lux}$

Figure 7-2: (a-e) *UDI* bins and (f-j) $UDI_{500\text{-}2000\ lux}$ at points along central line from south-facing window to end wall with and without PS-TIM with 4 different interval distances under 5 different climates: (a) and (f) Stockholm, (b) and (g) London, (c) and (h) Beijing, (d) and (i) Hong Kong and (e) and (j) Singapore

7.3.1.2 PS-TIMs' performance under different orientation

The studies thus far in this paper have focused on equator facing facades. These are subject to highest altitude direct solar irradiation in the sun path. This section explores glazing positioned in east and west facades, where lower altitude morning and evening sun predominates, as well as north facing facades, where for the sites chosen in this study, diffuse light tends to dominate.

In this section, only the useful bin (100 ~ 2000 lux) of the common three bins *UDI* metric is explored to provide an approximate picture of daylight performance. For a south facing window in London, as shown in Figure 7-3 (a), the 7.5 mm PS-TIM provides an even distribution and the highest percentage of operating hours (80%) with a useful $UDI_{100\text{-}2000\ lux}$. The north-facing façade mainly receives diffuse skylight rather than direct sunlight, thus, as shown in Figure 7-3 (b), PS-TIM with any slat pitch can provide a homogenous distribution of $UDI_{100\text{-}2000\ lux}$ with the 15 mm slat pitch providing the highest percentage of $UDI_{100\text{-}2000\ lux}$ being met. For the east and west orientation, the direct solar radiation is incident on the façade at low altitude angles for a short period after sunrise or before sunset and the radiation is not generally as strong as radiation incident on the south façade at noon. Under these conditions, 10 mm PS-TIM is sufficient to achieve a homogenous distribution of light and the highest level of $UDI_{100\text{-}2000\ lux}$ (Figure 7-3 (c) and (d)). Summarising, for cities with relatively high latitude (e.g. London), the south facing façade requires the smallest PS-TIM slat pitch to maximise useful daylight levels and distribution. Larger slat pitches can be used on the east and west facing façades, while the north facing façade can achieve comfortable daylight using the PS-TIM with largest slat pitch (in this case the 15 mm slat pitch).

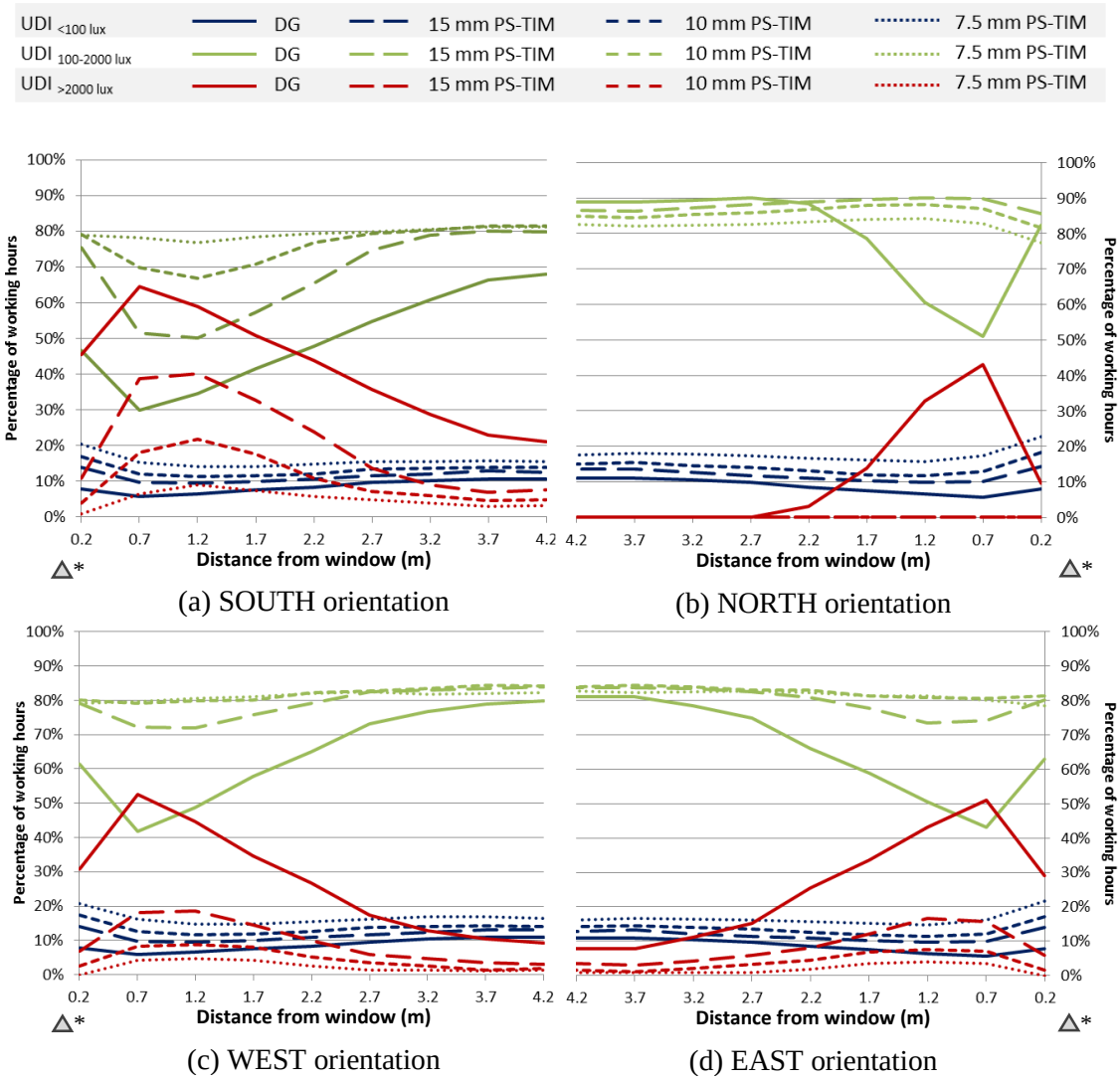


Figure 7-3: *UDI* bins for points along central line from window to end wall for (a) south, (b) north, (c) west and (d) east orientations with and without PS-TIM with 3 different slat pitches under London climate

Singapore (see Figure 7-4), lies in the Tropics near the equator. As a consequence, the noon solar altitude is high (i.e. over 65 °) all over the year and the sunlight is incident on the north and south facades depending on the season. Similar to the conditions in London, the sunlight with relatively low solar altitude is incident on east and west facades in the early morning and late afternoon respectively and has the potential to penetrate deeper into rooms, often with high irradiation levels. However, it is incident for a shorter period of time at the tropics as it quickly rises in altitude as compared to higher latitudes. Thus, compared with south and north facing facades, where PS-TIM with a 10mm slat pitch is sufficient to deliver a homogenous distribution of $UDI_{100\text{-}2000}$

* : Window position

lux, the east and west facing façades require PS-TIM with 7.5 mm slat pitch to achieve similar effect. It can be concluded that, for cities with relatively low latitude (e.g. Singapore), PS-TIM applied to east and west facing façades, requires smaller slat pitches than PS-TIMs applied to south and north facing façades.

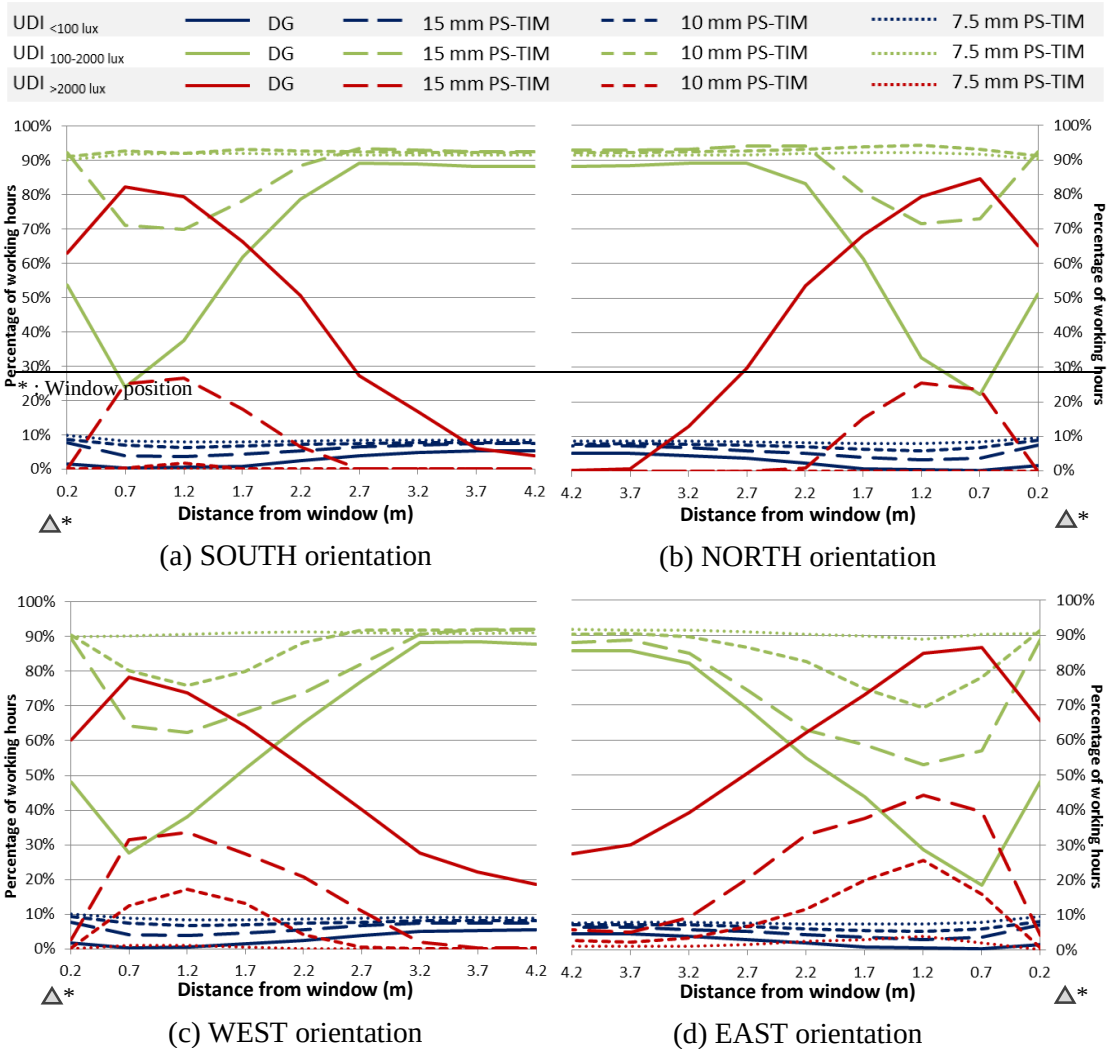


Figure 7-4: *UDI* bins at points along central line from window to end wall at (a) south, (b) north, (c) west and (d) east orientations with and without PS-TIM with 3 different interval distances under Singapore climate

Based on the daylighting performance analysis presented in this section, the building performance investigations presented in the following sections were conducted for PS-TIMs with three slat pitches (10mm, 7.5mm and 5mm) as the PS-TIM with 15 mm slat pitch provided very limited improvement.

* : Window position

7.3.2 Requirement for interior shading to prevent strong daylight

As discussed in section 6.4.1, if occupants in a working space are disrupted by high illuminance levels or glare from the windows, they are likely to lower the interior shade. This would significantly reduce the availability of daylight, and hence results in the illuminance level deeper within the space becoming insufficient for work. Consequently, artificial lighting is required. PS-TIMs have been integrated into double glazing to reduce the probability of using interior blinds.

Figure 7-5 shows the average hours per week where shade are lowered based on two metrics (i.e. *UDI* and *DGP*) under 5 climates. Applying 10 mm PS-TIM can result in reduction of the requirement of interior shade to under 15 hours per week in Stockholm, to under 10 hours per week in London, Beijing and Hong Kong, and almost eliminate the requirement for interior shade in Singapore. Applying 7.5 mm PS-TIM reduced the requirement for interior shade to under 5 hours per week for Stockholm, London and Beijing while it can totally eliminate the requirement for interior shade in Hong Kong and Singapore. Applying 5 mm PS-TIM can nearly eradicate the requirement for interior shade under all these 5 climates. The results suggested that, the presence of PS-TIMs can effectively reduce the requirement for interior shade under all these climates. With increasing latitude, a smaller slat pitch is required to minimise the probability of using interior shade to achieve a comfortable daylight environment.

It should be mentioned that, in this research, only a typical shade with medium reflectance of 0.5 and low transmittance of 0.1 is used. Although, the transmittance of the shade significantly affects the daylight illuminance on the working plane, but this has been explored in depth in this research.

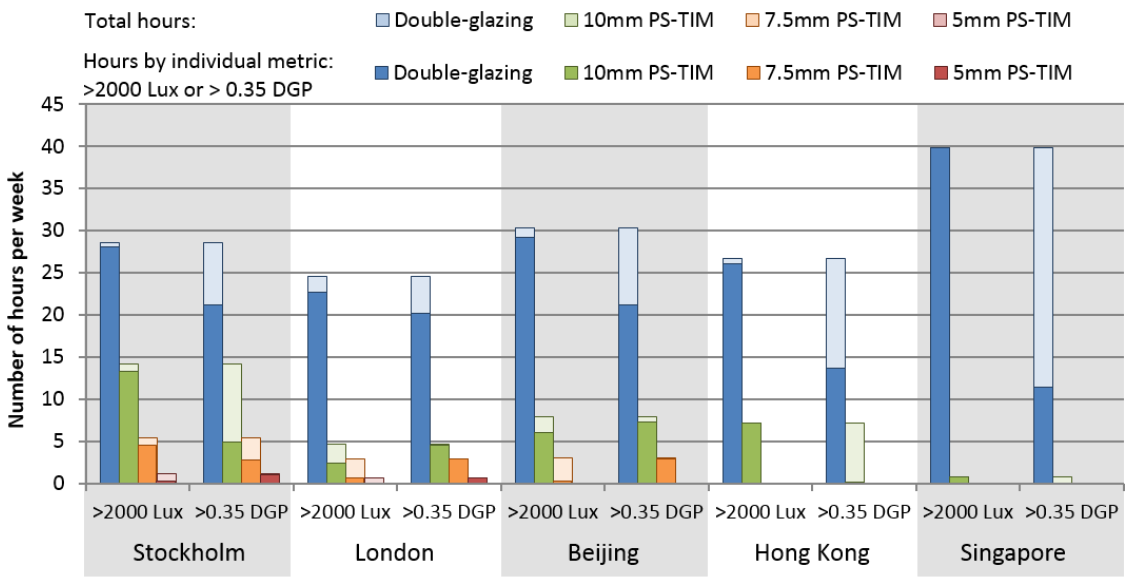


Figure 7-5: Average number of hours per week when discomfort daylight condition exist

7.3.3 Window heat loss and heat gain through windows with PS-TIM

As in section 6.4.2, breakdowns of annual heat losses and heat gains under five climates for the office with conventional double glazing are shown in Figure 7-6 to explore the key heat transfer paths for the office under different climates. The conclusions drawn from section 6.4.2 are also appropriate for other four climates: the heat gains and heat losses through the window represent more than half of the room total heat gain and heat loss, which means strategies for improving the thermal and optical properties of the window have the potential to significantly reduce the system heating and cooling load. Under the specific assumptions in this simulation, the heat gain through the window accounts for 56% to 69% of total heat gain in all the five climatic conditions. As the direct solar irradiation in the IWEC weather data of Beijing accounts for higher percentage than that under each other climate, the corresponding percentage of the transmitted solar heat gain through window is the highest. The heat loss through the window accounts over 50% of the total losses under Stockholm, London, Beijing and Hong Kong climates but there is almost no heat loss for Singapore. This is because of a constant high annual outdoor ambient temperature.

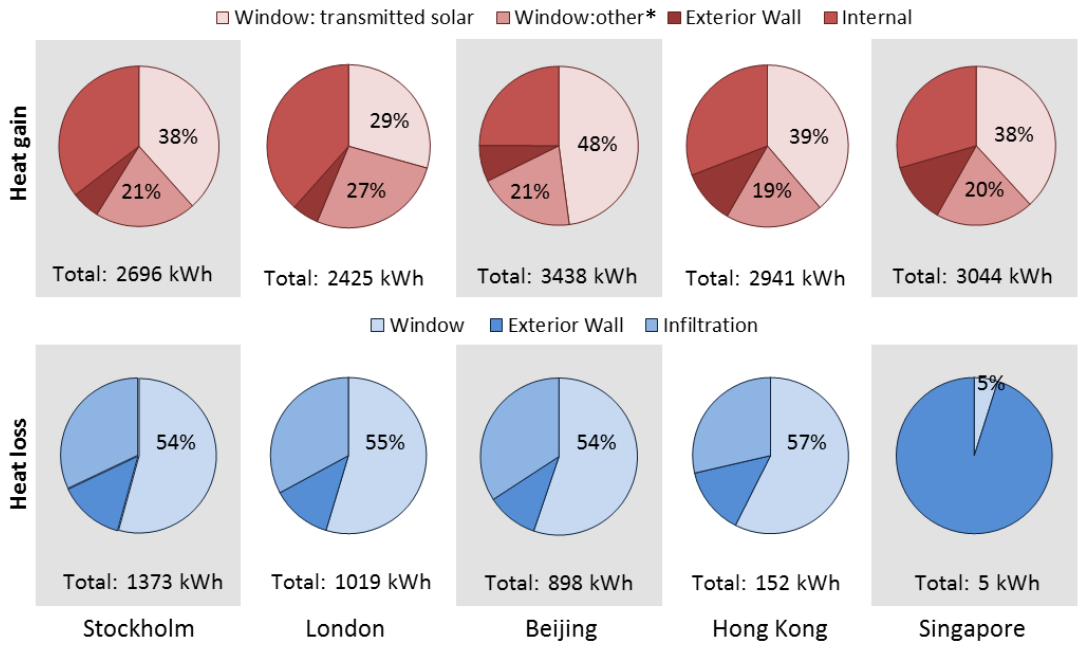


Figure 7-6: Breakdown of annual heat loss and heat gain for the office with a normal double glazing under five different climates

Figure 7-7 shows the change in window heat loss and heat gain after applying different PS-TIM structures to the cavity of a double glazing system under five climates. The window heat gains affected by applying PS-TIMs are all in a similar manner as London. Although Beijing gains the largest heat gain reduction amount, the percentage of reduction is similar as that of Stockholm and London. The average reduction percentages under these three climates are 40%, 44% and 48% for the 10 mm, 7.5 mm and 5 mm PS-TIM respectively. The presences of PS-TIMs have less significant effect on reducing window heat gains for sites located inside of the Tropics, as average reduction percentages under Hong Kong and Singapore's climates are 35%, 38% and 42% for the 10 mm, 7.5 mm and 5 mm PS-TIM respectively. The reduced percentag of heat loss for applying 5 mm PS-TIM under the climates of Stockholm, London, Beijing, Hong Kong and Singapore are 18%, 21%, 26%, 40% and 48%, respectively. Similar tendencies can be found for the 7.5 mm PS-TIM and the 10 mm PS-TIM. Overall, the presence of PS-TIM has a more obvious influence on the window heat gain than the window heat loss in all climates.

*: this comprises indirect window heat gain, including conductive, convective and radiative window heat gain

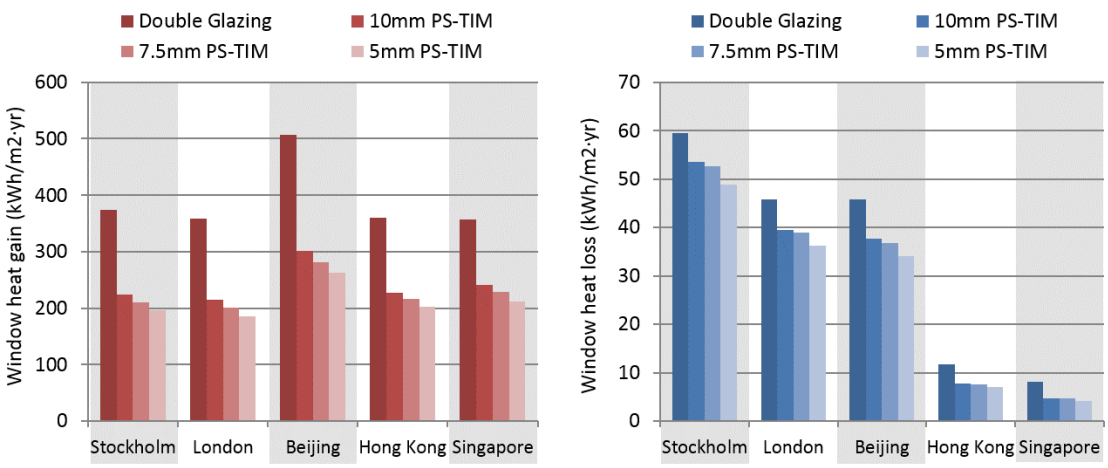


Figure 7-7: (a) heat gain and (b) heat loss through windows (kWh/m^2·yr) after applying different configurations of PS-TIM under five climates

7.3.4 Total energy consumption after applying PS-TIM

This section presents the annual energy consumption for the office after applying different PS-TIM configurations under the five sites' climates. Similar to section 6.4.3, there were also two HVAC scenarios of scheme applied, Figure 7-8 shows data where the HVAC is only operating during working hours from 8:00 to 17:00 on weekdays and Figure 7-9 shows data for the scenario where the HVAC is always on through the whole year.

As shown in Figure 7-8, under all five climates, the 10 mm PS-TIM provides the best energy efficiency when the HVAC system only works during working hours on weekdays. Compared with the conventional double gazed window with interior shade, an overall energy reduction of 13.7% to 18.6% can be achieved. Most of the energy reduction occurs in the lighting and cooling demand. As discussed in section 6.4.3, reductions in heating demand are not able to be achieved, as the presence of PS-TIM reduces the solar heat that transferred through the window. For Singapore, the application of 10mm PS-TIM can lead to light energy savings of 54.9% and a cooling energy saving of 9.7%. For Stockholm, the reduction in lighting energy is 33.2% and

the reduction in cooling energy is 24.5%, while only a 2.9% heat energy saving is achieved.

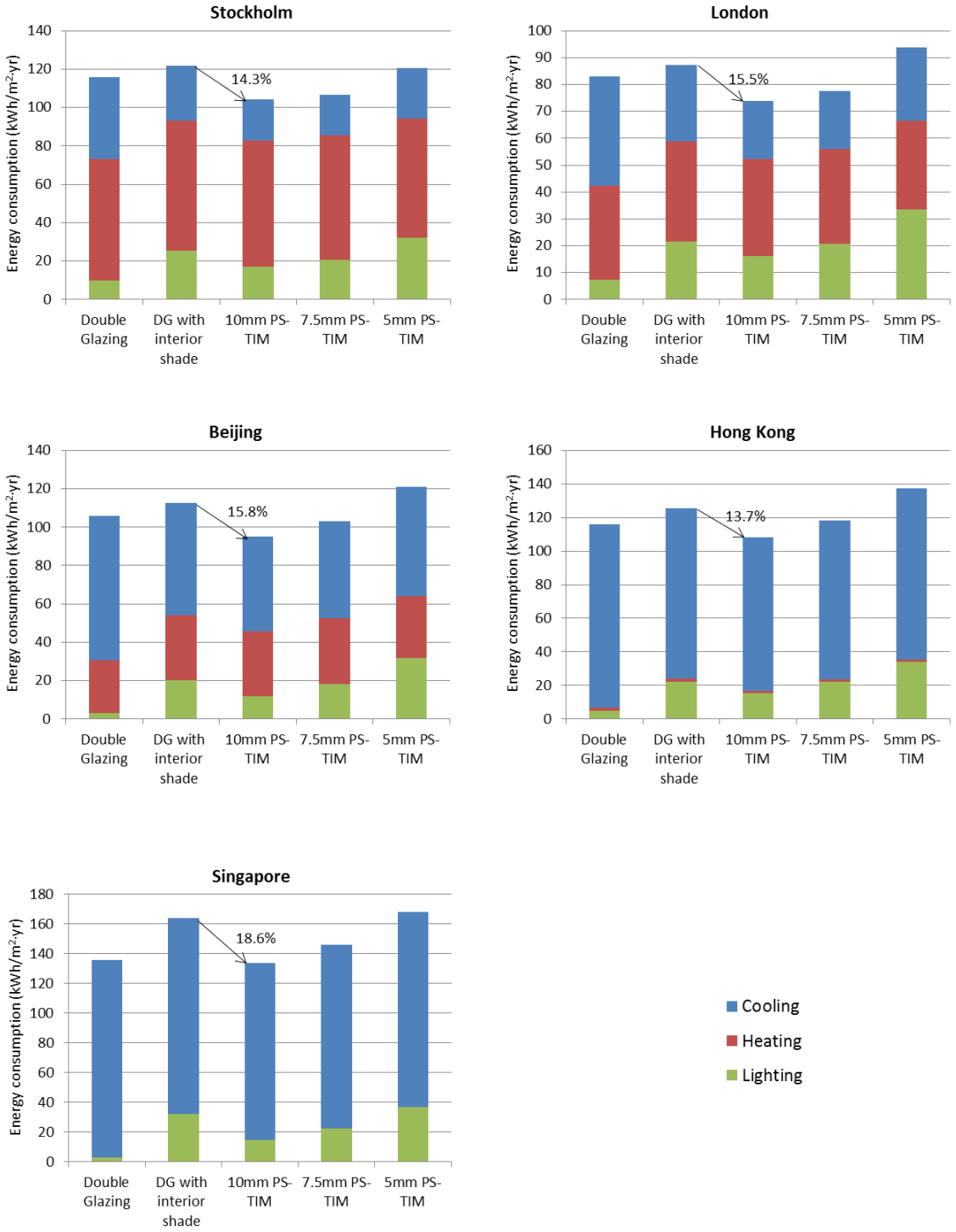


Figure 7-8: Annual heating, cooling and lighting energy consumption when HVAC works between 9:00-17:00 on workdays.

Figure 7-9 shows the energy efficiencies when using various PS-TIMs in another scenario, i.e. the HVAC system works continuously during the year. The 7.5 mm PS-TIM provides the best energy saving potential under all climates except in Beijing, where the energy consumption of the 5 mm PS-TIM is slightly lower than the 7.5 mm configuration. It can clearly be seen that, the heating demands under Stockholm, London, Beijing and Hong Kong climates dramatically reduced when applying 7.5 mm PS-TIM and 5 mm PS-TIM, spanning from 27.4% to 32.2%. Also, the 7.5 mm PS-TIM can achieve an average cooling consumption reduction of 38.3 % while 5 mm structure reduce cooling load by 31.1%. The reason for a better performance of PS-TIM with smaller interval distance (i.e. 7.5mm and 5 mm) is that the improved thermal resistance of the PS-TIM results in a dramatic reduction of heating energy demand during night time when HVAC system is always on as detailed discussed in section 6.4.3.

The analysis of energy consumptions in these two ideal scenarios of HVAC operation schemes provides a quantitative assessment of the effect of varying thermal and optical properties of PS-TIMs with different configurations on the overall heating, cooling and lighting energy consumption

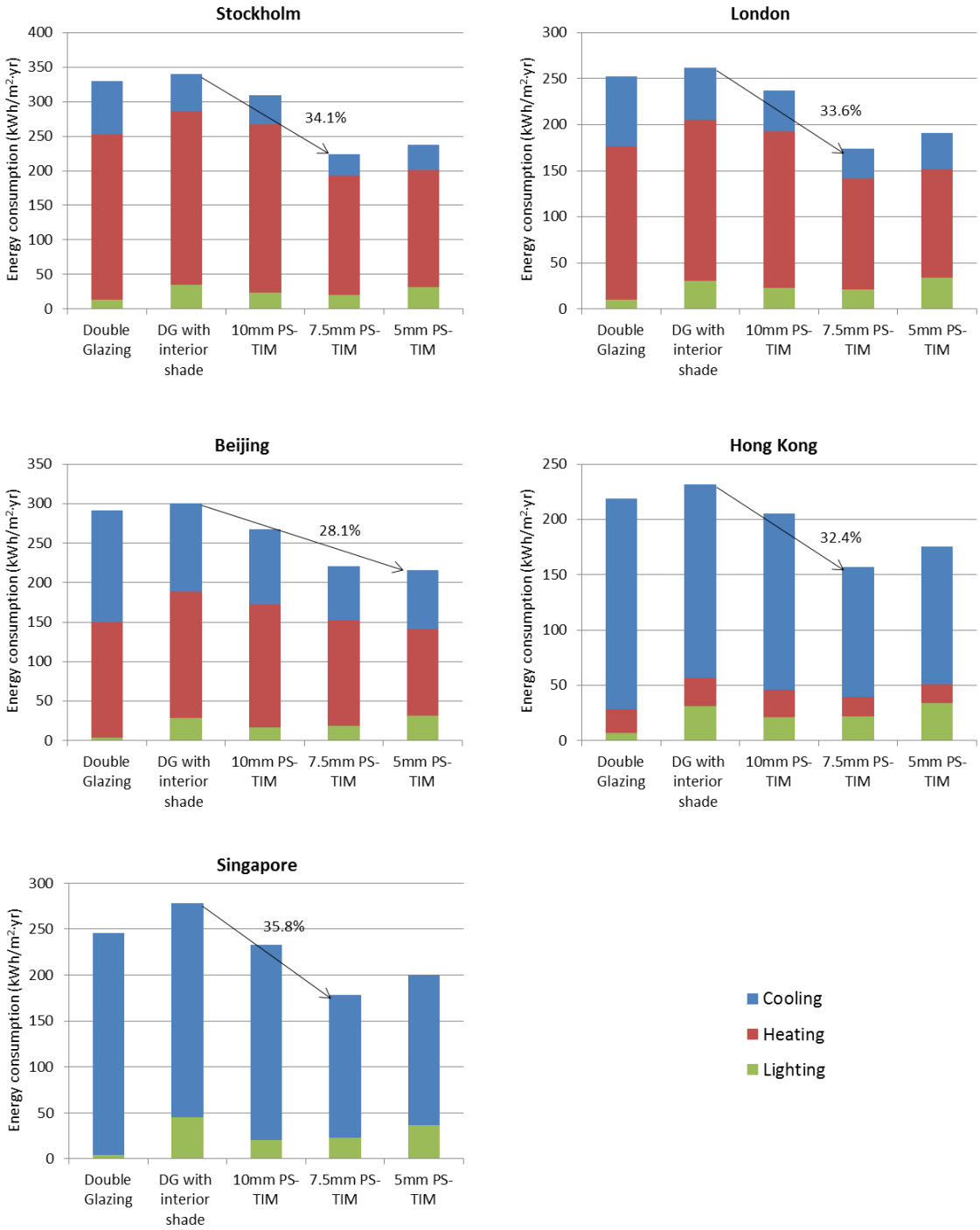


Figure 7-9: Annual heating, cooling and lighting energy consumption when HVAC is always on.

7.4 Conclusion

This chapter investigated the daylight and energy performance of applying PS-TIMs under different climate conditions and different building orientations to provide an indication of how site-specific variables influence their building performance. The following conclusion can be drawn:

1) The use of PS-TIMs at different latitudes suggested that with increasing latitude, a smaller slat pitch is required to maximise useful daylight ($UDI_{100\text{-}2000lux}$) and evenly distribute the daylight. The intensity of solar radiation and the balance of time where clear or overcast skies prevail affect the process of identifying an optimal PS-TIM configuration. While some observations are made, the relationships are not quantified in this study;
2) When applying PS-TIMs to windows with different orientations a general observation for sites located outside of the Tropics is that the smallest slat pitch is required on the equator facing façade, east/west facades provide daylight with a slightly larger pitches and facades facing away from the equator can operate effectively with the largest slat pitch. For sites within the Tropics, north and south facades receive direct irradiation and the slat pitch required is likely to reflect the relative exposure of the two facades ranging from equal on the equator to relatively smaller pitches on the equator facing façade as you move away from the equator.
3) The results suggested that, the presence of PS-TIMs can effectively reduce the requirement for interior shade under all these climates. With increasing latitude, a smaller slat pitch is required to minimise the probability of using interior shade to achieve a comfortable daylight environment.
4) The presence of PS-TIM has a more obvious influence on the window heat gain than the window heat loss in all climates.
5) Applying PS-TIM when the HVAC system is always on can reduce greater degree of total energy consumption than that when the HVAC system only works on working hours in all climates.

Chapter 8. Conclusion and recommendation for further works

8.1 Conclusion

A good window system needs to simultaneously solve the problem of both visual discomfort and energy inefficiency that are evident when conventional double glazed window systems are used. Various strategies have been used to overcome these drawbacks corresponding to energy efficient. These include thermal resistance improvements (e.g. low emission coating, multiple glazing, inert gases filling and vacuum glazing etc.), daylight penetration control (e.g. shading devices, tinted coating and reflective coatings etc.) and novel smart window techniques (e.g. electrochromic thermochromics, photochromic etc.). In this thesis, a further strategy that could potentially provide a balanced improvement in terms of both increased thermal resistance and controlled solar and daylight admittance, this requiring a relative low investment whilst providing long-time stability was proposed. This is a glazing system integrated with Parallel Slat Transparent Insulation Material (PS-TIM) sandwiched between two glass panes.

As discussed in Chapter 2, various Transparent Insulation Materials (TIMs) have been investigated over the past two decades, much of this work focused on their application to solar collectors. Although, applying TIMs has been proven to effectively reduce heat losses and improve the efficiency of solar collectors, relatively few studies exist regarding the thermal and optical performance of TIMs contained within the cavities of double glazed windows or glazing façade. This research originally evaluated the thermal and optical performance of a glazing system with PS-TIM, as well as the building performance after applying PS-TIM to buildings. In so doing, this research provides a clearer picture of the benefits in terms of energy saving and daylight perfection when applying TIM in building windows.

However, the heat transfer and light transmittance through the window system become complicated when integrating TIM structures with glazing units. It requires effective methods to obtain precise and accurate definitions of their thermal and optical behaviours. This has been reviewed in Chapter 3. Investigations of thermal and optical characteristics of glazing system with interstitial structures, such as horizontal Venetian blinds, pleated blinds and different configurations of fins, within the air cavity of a double glazed unit had been widely seen in literature. These structures share many of the same characteristics as TIMs and hence these research provides methods used for reference to resolve similar problems in the window system with TIMs. Computational Fluid Dynamics has been proven as a reliable method to analysis the convection and radiation occurs at the air cavity between two glazing panes. On the other hand, the *Bidirectional Scatter Distribution Function* (*BSDF*) data obtained from ray-tracing technique provides opportunities for precisely defining the optical behaviours of glazing systems with PS-TIM.

In Chapter 4 of this research, detailed investigations of the PS-TIM on the reduction of heat transfer in terms of both convection, which is driven predominately by temperature difference across the two glass panes, and radiation, which is driven predominately by glazing system mean temperature, under different environmental conditions that are commonly encountered in buildings were studied using a two-dimensional Computational Fluid Dynamics (CFD) model. This model had been validated by an experimental investigation of a glazing system with interstitial Venetian blind that conducted in a large climate chamber. The results showed that selecting a proper slat pitch for the PS-TIM in the air cavity can provide effective reduction of the convective heat transfer coefficient. The slat conductivity and thickness have a significant influence on overall thermal conductance when the temperature difference

between the glazing panes is small. This section of the research also distinguish itself from using the results obtained under various boundary conditions in the CFD simulation to transfer into polynomial regression equations and furtherly used to represent the dynamic thermal conductivities of the PS-TIM layer.

Furthermore, in Chapter 5 the *Bidirectional Scattering Distribution Functions* (*BSDFs*) of PS-TIM with various configurations were obtained from three-dimensional ray-tracing simulation. Other than only generating a result of a total transmittance or reflectance, this method considers the directional distribution of each flux, which is essential for accurately predicting of illuminous environment in a space when applying PS-TIM in the building windows.

In seeking to evaluate the quantity, quality and distribution of daylight accurately when applying PS-TIM to buildings, traditional calculation methods and assessment metrics (e.g. daylight factor (DF)) are increasingly deemed inadequate. Advanced daylight assessment metrics (e.g. *useful daylight illuminance* (*UDI), daylight glare probability* (*DGP*) etc) along with a dynamic simulation tool (i.e. RADIANCE) used to realise dynamic annual analysis, in conjunction with *BSDF* data obtained previously, were used to evaluate the daylight performance of applying PS-TIM with various configurations to a prototype office. The results showed that applying an optimised PS-TIM can increase the percentage of working hours when the *UDI* lies in the range of 100-2000 lux by up to 32%, achieving a homogenous distribution of daylight and effectively reduce the possibility of glare. PS-TIMs with translucent slats offered better performance than PS-TIMs with transparent slats in terms of improving daylight availability and daylight comfort level. Compared with slat tilt angle, the slat pitch (the distance between neighbouring slats) had a more significant influence on the overall daylight performance when the PS-TIM comprises translucent slats.

In seeking to effectively and accurately predict the energy performance of applying PS-TIM to buildings, current building energy simulation programs are not accurate enough, often because of the simplified thermal and optical models used to solve heat transfer and light transmittance. In practice, there will be a significant effect on the free convection, long-wave radiative heat transfer and solar energy (light and heat) transmitted through the system with the presence of PS-TIM between two glazing panes. Chapter 6 in this research developed a comprehensive model, in which the thermal characterisations obtained from original Computational Fluid Dynamics simulation and *BSDF* data obtained from a ray-tracing calculation are input into building performance simulation tool (i.e. EnergyPlus) to obtain relatively accurate building energy and daylight performance estimates. RADIANCE simulation result for daylight performance was also used as a supplementary analysis for this holistic prediction. The work flow that combines the outputs from CFD and optical modelling tools and integrates them into EnergyPlus to provide a holistic energy simulation is new. Based on the specific assumptions in the building performance predictions, the simulation shows that applying PS-TIM with optimized slat pitches can achieve 18.6% to 35.8% energy reduction when compared with conventional double glazed window with interior shade depending on the operating hours of HVAC system.

Finally, in Chapter 7, the chosen PS-TIMs have also been investigated under different climate conditions and different building orientations to provide an indication of how site-specific variables influence their daylight and energy performance. The intensity of solar radiation and the balance of time where clear or overcast skies supply daylight does have an effect, however, this is more complex and while effects were observed they were not quantified in this research.

In general, integrating PS-TIM in glazing unit could effectively reduce the convective and radiative heat transfer through two glazing panes. The presence of PS-TIM provides the potential to effectively increase the daylight availability and reduce the possibility of glare. It can also result in a reduction of energy consumption in terms of heating, cooling and lighting. The workflow that combines the thermal and optical behaviours from CFD simulation and ray-tracing calculation and integrates them into EnergyPlus to provide a holistic energy simulation is new.

8.2 Recommendations for further work

The innovative façade system where parallel transparent plastic slats are sandwiched between glass panes to form a Parallel Slat Transparent Insulation Material (PS-TIM) has been proven to have superior performance compared to conventional double-glazed window system in terms of energy saving and daylight comfort improvement.

However, to optimise the present system and accelerate its application in window system or glazed façade, further research is required as follows:

- Although PS-TIM can potentially provide a more comfortable daylight environment, it also brings risk of interrupting view when applying it to windows of buildings. This research did not consider the effect that PS-TIM has on the view into and out of a building. Further research to analysis the obstruction of vision caused by PS-TIM as well as its effect on occupant satisfaction, productivity, health and wellbeing needs to be conducted by subjective evaluations.
- The presence of translucent PS-TIM reduces the desired solar heat gains through window due to a low solar transmittance of the slats.However, transparent PS-TIM

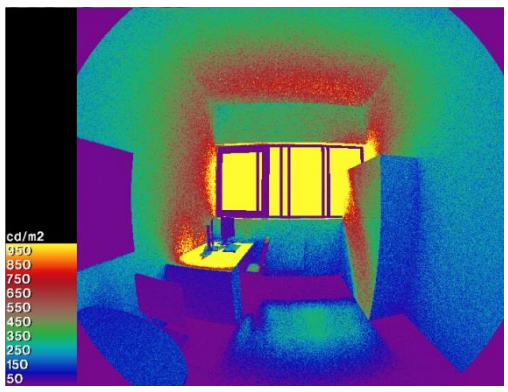
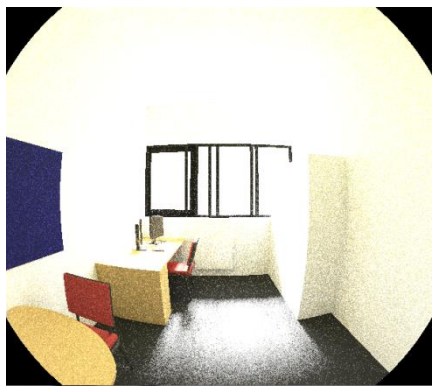
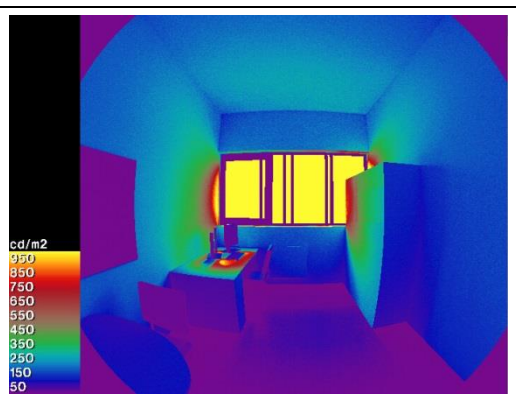
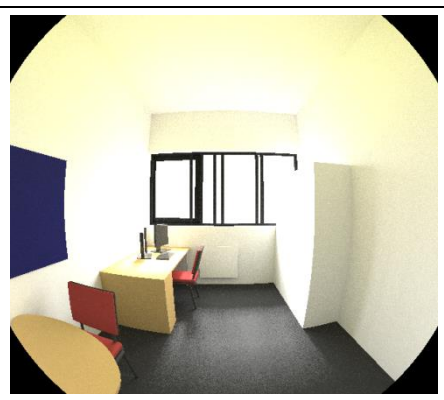
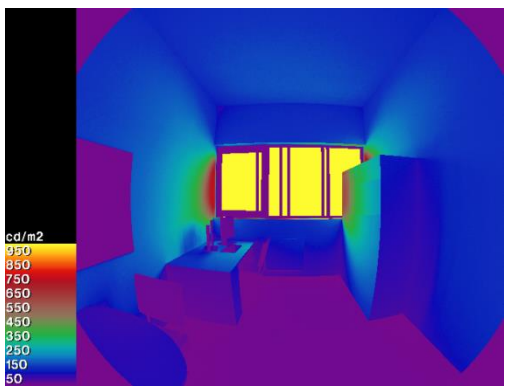
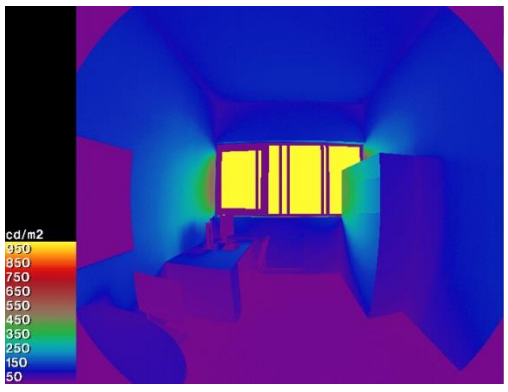
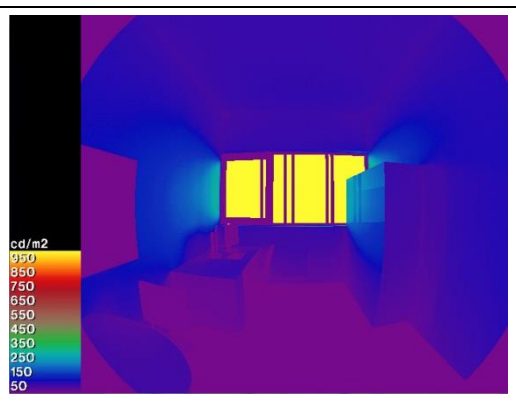
cannot provide significant improvements in terms of daylight availability and daylight comfort level. Thermotropic materials, which switch from a transparent to a translucent state once it reaches a designed temperature, can overcome the shortcomings of the presented PS-TIM. Applying thermotropic materials on the parallel slats of PS-TIM might have a potential to maximise the energy efficiency of the system.

- The effects on PS-TIM's daylight performance from solar radiation intensity and the balance of time where clear or overcast skies supply daylight were observed but not quantified in this study. A detailed analysis of the effect of solar radiation and weather conditions on the overall performance of PS-TIM systems needs further exploration
- By using this holistic method presented in this thesis, the investigation of window system or glazing façade integrated with TIM can be extended to other structures, such as honeycomb TIM, capillary TIM, etc.

The above recommended research would provide a better understanding or a more optimised design of window system with Transparent Insulation Material, and hence offer suggestions as to how architects and engineers could potentially apply TIMs in buildings, contribute to their spread into the building construction market.

Appendix A:

RADIANCE false colour and visualizations and associated *DGP*s for window with and without PS-TIM with different slats interval distance on 21st March at 12pm under a CIE clear sky.

	Equinox (March) 12pm	
DG		
15mm		
10mm		
7.5mm		
5mm		

Reference:

1. Gratia, E. and A. De Herde, *Natural cooling strategies efficiency in an office building with a double-skin fa çade.* Energy and Buildings, 2004. **36**(11): p. 1139-1152.
2. Ding, W., Y. Hasemi, and T. Yamada, *Natural ventilation performance of a double-skin fa çade with a solar chimney.* Energy and Buildings, 2005. **37**(4): p. 411-418.
3. Shameri, M.A., et al., *Perspectives of double skin fa çade systems in buildings and energy saving.* Renewable and Sustainable Energy Reviews, 2011. **15**(3): p. 1468-1475.
4. Giorgi, L.D., V. Bertola, and E. Cafaro, *Thermal convection in double glazed windows with structured gap.* Energy and Buildings, 2011. **43**(8): p. 2034-2038.
5. Xam án, J., et al., *Computational fluid dynamics for thermal evaluation of a room with a double glazing window with a solar control film.* Renewable Energy, 2016. **94**: p. 237-250.
6. Oleskowicz-Popiel, C. and M. Sobczak, *Effect of the roller blinds on heat losses through a double-glazing window during heating season in Central Europe.* Energy and Buildings, 2014. **73**: p. 48-58.
7. Zhang, C., et al., *Modeling and thermal performance evaluation of a switchable triple glazing exhaust air window.* Applied Thermal Engineering, 2016. **92**: p. 8-17.
8. Amaral, A.R., et al., *A thermal performance parametric study of window type, orientation, size and shadowing effect.* Sustainable Cities and Society, 2016.
9. Konroyd-Bolden, E. and Z. Liao, *Thermal window insulation.* Energy and Buildings, 2015. **109**: p. 245-254.
10. Konstantzos, I., A. Tzempelikos, and Y.-C. Chan, *Experimental and simulation analysis of daylight glare probability in offices with dynamic window shades.* Building and Environment, 2015. **87**: p. 244-254.
11. Piccolo, A. and F. Simone, *Effect of switchable glazing on discomfort glare from windows.* Building and Environment, 2009. **44**(6): p. 1171-1180.
12. Karlsen, L., et al., *Verification of simple illuminance based measures for indication of discomfort glare from windows.* Building and Environment, 2015. **92**: p. 615-626.
13. Shih, N.-J. and Y.-S. Huang, *An analysis and simulation of curtain wall reflection glare.* Building and Environment, 2001. **36**(5): p. 619-626.
14. Bernier, M. and S. Hall é, *A critical look at the air infiltration term in the canadian energy rating procedure for windows.* Energy and Buildings, 2005. **37**(10): p. 997-1006.
15. Bakonyi, D. and G. Dobszay, *Simulation aided optimization of a historic window's refurbishment.* Energy and Buildings, 2016. **126**: p. 51-69.
16. Russell M. Sanders and C.A. Hargrove, *Preventing and Treating Failure in Glazed Curtain Wall Systems.* Journal of architectural technology, 2012. **29**(2): p. 1-8.
17. Nielson, K.J., *Interior textiles: fabrics, applications and historical styles*. 2007: Hoboken, N.J. : Hohn Wiley & Sons.
18. Arulanantham, M., T.P. Singh, and N.D. Kaushika, *Convective heat transfer across transparent honeycomb insulation materials.* Energy Convers. Mgmt 1994. **35**(2): p. 111-116.

19. Kaushika, N.D., et al., *Transparent insulation characteristics of honeycomb and slat arrays* Energy and Buildings, 1994. **19**(10): p. 1037-1041.
20. Kaushika, N.D. and P. Kumar, *Convective effects in air layers bound by cellular honeycomb arrays.* Journal of Scientific & Industrial Research, 2005. **64**: p. 602-612.
21. Arulanantham, M. and N.D. Kaushika, *Coupled radiative and conductive thermal transfers across transparent honeycomb insulation materials.* Applied Thermal Engineering, 1996. **16**(3): p. 209-212.
22. Suehrcke, H., et al., *Heat transfer across corrugated sheets and honeycomb transparent insulation.* Solar Energy, 2004. **76**(1-3): p. 351-358.
23. Wright, J.L., et al., *Flow visualization of natural convection in a tall, air-filled vertical cavity.* International Journal of Heat and Mass Transfer, 2006. **49**(5-6): p. 889-904.
24. Huang, N.Y.T., J.L. Wright, and M.R. Collins, *Thermal resistance of a window with an enclosed Venetian blind: guarded heater plate measurements.* ASHRAE Transactions, 2006. **112**(2): p. 13-21.
25. Dalal, R., D. Naylor, and D. Roeleveld, *A CFD study of convection in a double glazed window with an enclosed pleated blind.* Energy and Buildings, 2009. **41**(11): p. 1256-1262.
26. Naylor, D. and M. Collins, *Evaluation of an Approximate Method for Predicting The U-value of a Window with a between-Panes Blind.* Numerical Heat Transfer, Part A: Applications, 2005. **47**(3): p. 233-250.
27. Almeida, F. and D. Naylor, *Experimental study of free convection in a window with a heated between-panes blind.* Energy and Buildings, 2011. **43**(10): p. 2647-2655.
28. Naylor, D. and B.Y. Lai, *Experimental Study of Natural Convection in a Window with a Between-Panes Venetian Blind.* Experimental Heat Transfer, 2007. **20**(1): p. 1-17.
29. Avedissian, T. and D. Naylor, *Free convective heat transfer in an enclosure with an internal louvered blind* International Journal of Heat and Mass Transfer, 2008. **51**(1-2): p. 283-293.
30. Collins, M., S. Tasnim, and J. Wright, *Numerical analysis of convective heat transfer in fenestration with between-the-glass louvered shades.* Building and Environment, 2009. **44**(10): p. 2185-2192.
31. Gomes, M.G., A.J. Santos, and A.M. Rodrigues, *Solar and visible optical properties of glazing systems with venetian blinds: Numerical, experimental and blind control study.* Building and Environment, 2014. **71**: p. 47-59.
32. Andersen, M., et al., *Bi-directional transmission properties of Venetian blinds: experimental assessment compared to ray-tracing calculations.* Solar Energy, 2005. **78**(2): p. 187-198.
33. Andersen, M., M. Rubin, and J.-L. Scartezzini, *Comparison between ray-tracing simulations and bi-directional transmission measurements on prismatic glazing.* Solar Energy, 2003. **74**(2): p. 157-173.
34. Wang, Y., et al., *Development of a Solar Control Method of the Venetian Blinds.* Procedia Engineering, 2015. **121**: p. 1186-1192.
35. Wang, Y. and Y. Chen, *Modeling and calculation of solar gains through multi-glazing facades with specular reflection of venetian blind.* Solar Energy, 2016. **130**: p. 33-45.

36. Konstantoglou, M., J. Jonsson, and E. Lee, *Simulating Complex Window Systems using BSDF Data,* in *26th Conference on Passive and Low Energy Architecture*. 2009: Quebec City, Canada.
37. Tzempelikos, A., *The impact of venetian blind geometry and tilt angle on view, direct light transmission and interior illuminance.* Solar Energy, 2008. **82**(12): p. 1172-1191.
38. Konstantzos, I., et al., *View clarity index: A new metric to evaluate clarity of view through window shades.* Building and Environment, 2015. **90**: p. 206-214.
39. Sun, Y., et al., *Thermal evaluation of a double glazing façade system with integrated Parallel Slat Transparent Insulation Material (PS-TIM).* Energy and Buildings, 2016. **In Press**.
40. *ISO 15099.*
41. Ward, G., et al., *Simulating the daylight performance of Complex Fenestration Systems using Bidirectional Scattering Distribution Functions within Radiance.* Journal of the Illuminating Engineering Society of North America 2011. **7**(4).
42. Kämpf, J.H. and J.-L. Scartezzini, *Ray-tracing simulation of complex fenestration systems based on digitally processed BTDF data*, in *CISBAT*. 2011: Lausanne, Switzerland.
43. M. Saxena, et al., *Dynamic RADIANCE – Predicting annual daylight with variable fenestratio optics using BSDFs*, in *Fourth National Conference of IBPSA-USA*. 2010: New York City, USA.
44. Andersen, M. and J. de Boer, *Goniophotometry and assessment of bidirectional photometric properties of complex fenestration systems.* Energy and Buildings, 2006. **38**(7): p. 836-848.
45. McNeil, A., et al., *A validation of a ray-tracing tool used to generate bi-directional scattering distribution functions for complex fenestration systems.* Solar Energy, 2013. **98**: p. 404-414.
46. Wong, I.L., P.C. Eames, and R.S. Perera, *A review of transparent insulation systems and the evaluation of payback period for building applications.* Solar Energy, 2007. **81**(9): p. 1058-1071.
47. Sun, Y., et al., *Experimental measurement and numerical simulation of the thermal performance of a double glazing system with an interstitial Venetian blind.* Building and Environment, 2016 **103**: p. 111-122.
48. Berardi, U., *The development of a monolithic aerogel glazed window for an energy retrofitting project.* Applied Energy, 2015. **154**: p. 603-615.
49. Jensen, K.I., J.M. Schultz, and F.H. Kristiansen, *Development of windows based on highly insulating aerogel glazings.* Journal of Non-Crystalline Solids, 2004. **350**: p. 351-357.
50. Gao, T., et al., *Insulating glazing units with silica aerogel granules: The impact of particle size.* Applied Energy, 2014. **128**: p. 27-34.
51. Buratti, C. and E. Moretti, *Experimental performance evaluation of aerogel glazing systems.* Applied Energy, 2012. **97**: p. 430-437.
52. EASE, *Section 3.1 Advanced glazing and transparent insulation*, in *Advanced Glazing*. Education of Architecture in Solar Energy and Environment. p. 16-25.
53. Buratti, C. and E. Moretti, *Transparent insulating materials for buildings energy saving: experimental results and performance evaluation*, in *Third International Conference on Applied Energy*. 2011. p. 1421-1432.
54. Felland, J.R. and D.K. Edwards, *Solar and Infrared Radiation Properties of Parallel-Plate Honeycomb.* Journal of Energy, 1978. **2**(5): p. 309-317.

55. Hollands, K.G.T., K.N. Marshall, and R.K. Wedel, *An approximate equation for predicting the solar transmittance of transparent honeycombs.* Solar Energy, 1978. **21**(3): p. 231-236.
56. Symons, J.G., *The solar transmittance of some convection suppression devices for solar energy applications: An experimental study.* Journal of Solar Energy Engineering, 1982. **104**: p. 251-256.
57. Platzer, W.J., *Solar transmittance of transparent insulation materials.* Solar Energy Materials, 1987. **16**.
58. Kaushika, N.D. and R. Padmapriya, *Solar transmittance of honeycomb and parallel slat arrays.* Energy Conversion and Management, 1991. **32**.
59. Platzer, W.J., *Calculation procedure for collectors with a honeycomb cover of rectangular cross section.* Solar Energy, 1992. **48**.
60. Platzer, W.J., *Directional-hemispherical solar transmittance data for plastic type honeycomb structures.* Solar Energy, 1992. **49**.
61. Arulanantham, M. and N.D. Kaushika, *Global radiation transmittance of transparent insulation materials.* Solar Energy, 1994. **53**.
62. Kaushika, N.D. and K. Sumathy, *Solar transparent insulation materials: a review.* Renewable and Sustainable Energy Reviews, 2003. **7**(4): p. 317-351.
63. Buratti, C. and E. Moretti, *Glazing systems with silica aerogel for energy savings in buildings.* Applied Energy, 2012. **98**: p. 396-403.
64. Platzer, W.J., *Total heat transport data for plastic honeycomb-type structures.* Solar Energy 1992. **49**(5): p. 351-358.
65. Goetzberger, A., *Transparent Insulation Technology for Solar Energy Conversion (second ed.).* 1991, Fraunhofer Institute for Solar Energy Systems: Freiburg.
66. Francia, G., *A new collector of solar radiant energy: theory and experimental verification*, in *In: Proceedings of the United Nations Conference on New Sources of Energy, 4*. 1961: Rome.
67. Hollands, K.G.T., *Honeycomb devices in flat plate solar collectors.* Solar Energy 1965. **21**.
68. Tabor, H., *Cellular insulation (honeycombs).* Solar Energy, 1969. **12**(4): p. 549-552.
69. Rommel, M. and A. Wagner, *Application of transparent insulation materials in improved flat-plate collectors and integrated collector storages.* Solar Energy, 1992. **49**(5): p. 371-380.
70. Goetzberger, A., et al., *A new transparently insulated, bifacially irradiated solar flat-plate collector.* Solar Energy, 1992. **49**(5): p. 403-411.
71. Nordgaard, A. and W.A. Beckman, *Modelling of flat plate collectors based on monolithic silica aerogel.* Solar Energy, 1992. **49**(5): p. 387-402.
72. Ghoneim, A.A., *Performance optimization of solar collector equipped with different arrangements of square-celled honeycomb.* International Journal of Thermal Sciences, 2005. **44**(1): p. 95-105.
73. Symons, J.G., *Calculation of the transmittance-absorptance product for flat-plate collectors with convection suppression devices.* Solar Energy 1984. **33**(6): p. 637-640.
74. Kaushika, N.D., M.S. Sharma, and K. Sanjay, *Honeycomb roof cover system for passive solar space heating.* Energy Conversion and Management, 1987. **27**(1): p. 99-102.

75. Kaushika, N.D., M.S. Sharma, and R. Padmapriya, *Solar thermal analysis of honeycomb roof cover system for energy conservation in an air conditioned building.* Energy and Buildings, 1992. **18**(1): p. 45-49.
76. IEA, *Solar Heating and Cooling Programme Task 20: Solar Energy in Building Renovation*. 1997, James and James Ltd.: London.
77. Voss, K., *Solar energy in building renovation– results and experience of international demonstration buildings.* Energy and Buildings, 2000. **32**(3): p. 291-302.
78. Braun, P.O., et al., *Transparent insulation of building facades - steps from research to commercial applications.* Solar Energy, 1992. **49**(5): p. 413-427.
79. Athienitis, A.K. and H. Ramadan, *Numerical model of a building with transparent insulation.* Solar Energy, 1999. **67**(1-3): p. 101-109.
80. Wallner, G.M., et al., *Development and application demonstration of a novel polymer film based transparent insulation wall heating system.* Solar Energy materials and Solar Cells, 2004. **84**(1-4): p. 441-457.
81. Manz, H., et al., *TIM-PCM external wall system for solar space heating and daylighting.* Solar Energy, 1997. **61**(6): p. 369-379.
82. Heim, D., *Whole year analysis of TIM-PCM solar thermal storage wall*, in *In: Proceeding of SimBuild 2004, IBPSA*. 2004: USA National Conference Boulder, CO.
83. Twidell, J.W., et al., *Strathclyde University's passive solar, low-energy, residences with transparent insulation.* Solar Energy, 1994. **52**(1): p. 85-109.
84. Lien, A.G., A.G. Hestnes, and O. Aschehoug, *The use of transparent insulation in low energy dwellings in cold climates.* Solar Energy, 1997. **59**(1-3): p. 27-35.
85. Bahaj, A.S., P.A.B. James, and M.F. Jentsch, *Potential of emerging glazing technologies for highly glazed buildings in hot arid climates.* Energy and Buildings, 2008. **40**(5): p. 720-731.
86. Wong, I.L., P.C. Eames, and R.S. Perera, *Energy simulations of a transparent - insulated office façade retrofit in London, UK.* Smart and Sustainable Built Environment, 2012. **1**(3): p. 253-276.
87. Platzer, W.J., *Advances in Transparent Insulation Technology.*
88. He, W., et al., *Experimental and theoretic study of heat transfer and transmittivity of shutter-type transparent honeycomb structure.* Taiyangneng Xuebao/Acta Energiae Solaris Sinica,, 2003. **24**(3): p. 290-294.
89. ISO, *12567-1: Thermal performance of windows and doors -- Determination of thermal transmittance by the hot-box method -- Part 1: Complete windows and doors*. 2012.
90. ISO, *9869-1: Thermal insulation -- Building elements -- In-situ measurement of thermal resistance and thermal transmittance Part 1: Heat flow meter method*. 2014.
91. ISO, *8990: Thermal insulation – determination of steady-state thermal transmission properties – calibrated and guarded hot box.* . 1996.
92. ISO, *8301: Thermal insulation -- Determination of steady-state thermal resistance and related properties -- Heat flow meter apparatus*. 1991
93. ISO, *8302:Thermal insulation -- Determination of steady-state thermal resistance and related properties -- Guarded hot plate apparatus*. 1991.
94. ASTM, *C1363: Standard Test Method for Thermal Performance of Building Materials and Envelope Assemblies by Means of a Hot Box Apparatus*. 2011.
95. ASTM, *C1199: Standard test method for measuring the steady-state thermal transmittance of fenestration systems using hot box methods.* . 2009.

96. ASTM, *C1046: Standard Practice for In-Situ Measurement of Heat Flux and Temperature on Building Envelope Components*. 2013.
97. EN, *674: Glass in building-- Determination of thermal transmittance (U value) –Guarded hot plate method*. 2011
98. EN, *675: Glass in building. Determination of thermal transmittance (U value). Heat flow meter method*. 2011
99. EN, *1946-2: Thermal performance of building products and components. Specific criteria for the assessment of laboratories measuring heat transfer properties. Measurements by guarded hot plate method*. 1999.
100. EN, *1946-3: Thermal performance of building products and components. Specific criteria for the assessment of laboratories measuring heat transfer properties. Measurements by heat flow meter method*. 1999.
101. GOST, *26602.1: Windows and doors. Methods of determination of resistance of thermal transmission*. 1999.
102. Yesilata, B. and P. Turgut, *A simple dynamic measurement technique for comparing thermal insulation performances of anisotropic building materials.* Energy and Buildings, 2007. **39**(9): p. 1027-1034.
103. Baldinelli, G. and F. Bianchi, *Windows thermal resistance: Infrared thermography aided comparative analysis among finite volumes simulations and experimental methods.* Applied Energy, 2014. **136**: p. 250-258.
104. Fang, X., *A Study of the U-Factor of the Window with a High-Reflectivity Venetian Blind.* Solar Energy, 2000. **68**(2): p. 207-214.
105. Fang, Y., et al., *Experimental validation of a numerical model for heat transfer in vacuum glazing.* Solar Energy, 2006. **80**(5): p. 564-577.
106. Chen, F. and S.K. Wittkopf, *Summer condition thermal transmittance measurement of fenestration systems using calorimetric hot box.* Energy and Buildings, 2012. **53**: p. 47-56.
107. Asdrubali, F. and G. Baldinelli, *Thermal transmittance measurements with the hot box method: Calibration, experimental procedures, and uncertainty analyses of three different approaches.* Energy and Buildings, 2011. **43**(7): p. 1618-1626.
108. ISO, *10292: Glass in building -- Calculation of steady-state U values (thermal transmittance) of multiple glazing*. 1994.
109. ISO, *15099: Thermal performance of windows, doors and shading devices -- Detailed calculations*. 2003.
110. EN, *673: Glass in building-- Determination of thermal transmittance (U value) – Calculation method*. 2011
111. ISO, *10077-1:Thermal performance of windows, doors and shutters -- Calculation of thermal transmittance -- Part 1: General*. 2006.
112. ISO, *10077-2: Thermal performance of windows, doors and shutters – calculation of thermal transmittance – numerical method for frames*. 2003.
113. NFRC, *100-2010: Procedure for Determining Fenestration Product U-factors.* 2010.
114. ASHRAE, *Standard Method for Determining and Expressing the Heat Transfer and Total Optical Properties of Fenestration Products*, in *Public Review Draft of Standard* 1998: Atlanta, .
115. Blanusa, P., et al., *Comparison between ASHRAE and ISO thermal transmittance calculation methods.* Energy and Buildings, 2007. **39**(3): p. 374-384.

116. Zhao, Y., D. Curcija, and W.P. Gross, *Prediction of multicellular flow regime of natural convection in fenestration glazing cavities.* ASHRAE Transactions, 1997. **103**(1): p. 1-12.
117. Gan, G., *Thermal transmittance of multiple glazing: computational fluid dynamics prediction.* Applied Thermal Engineering, 2001. **21**(15): p. 1583-1592.
118. Wright, J.L. and F.F. Sullivan, *A two-dimensional numerical model for natural convection in a vertical rectangular window cavity.* ASHRAE Transactions, 1993. **99**(2): p. 1193-1206.
119. Ganguli, A.A., A.B. Pandit, and J.B. Joshi, *CFD simulation of heat transfer in a two-dimensional vertical enclosure.* Chemical Engineering Research and Design, 2009. **87**(5): p. 711-727.
120. Ganguli, A.A., A.B. Pandit, and J.B. Joshi, *Numerical predictions of flow patterns due to natural convection in a vertical slot.* Chemical Engineering Science, 2007. **62**(16): p. 4479-4495.
121. ISO, *9050: Glass in building. Determination of light transmittance, solar direct transmittance, total solar energy transmittance, ultraviolet transmittance and related glazing factors*. 2003.
122. EN, *410: Glass in building. Determination of luminous and solar characteristics of glazing.* 2011.
123. CIE, *No. 130. Practical methods for the measurement of reflectance and transmittance.* 1998.
124. Jonsson, J.C. *Optical measurement techniques for complex fenestration systems (CFS).* in *Radiance workshop*. 2011.
125. Jonsson, A., A. Roos, and E.K. Jonson, *The effect on transparency and light scattering of dip coated antireflection coatings on window glass and electrochromic foil.* Solar Energy Materials and Solar Cells, 2010. **94**(6): p. 992-997.
126. Long, L., et al., *Performance demonstration and simulation of thermochromic double glazing in building applications.* Solar Energy, 2015. **120**: p. 55-64.
127. Ye, H., et al., *The demonstration and simulation of the application performance of the vanadium dioxide single glazing.* Solar Energy Materials and Solar Cells, 2013. **117**: p. 168-173.
128. Goia, F., et al., *Spectral and angular solar properties of a PCM-filled double glazing unit.* Energy and Buildings, 2015. **87**: p. 302-312.
129. Gowreesunker, B.L., et al., *Experimental and numerical investigations of the optical and thermal aspects of a PCM-glazed unit.* Energy and Buildings, 2013. **61**: p. 239-249.
130. Liu X, et al., *Thermal and optical analysis of a passive heat recovery and storage system for greenhouse fa ҫade/roof.* 2016.
131. Gao, T., et al., *Perspective of aerogel glazings in energy efficient buildings.* Building and Environment, 2016. **95**: p. 405-413.
132. Berardi, U., *Development of Glazing Systems with Silica Aerogel.* Energy Procedia, 2015. **78**: p. 394-399.
133. Tsangrassoulis, A. and V. Bourdakis, *Comparison of radiosity and ray-tracing techniques with a practical design procedure for the prediction of daylight levels in atria.* Renewable Energy, 2003. **28**(13): p. 2157-2162.
134. EnergyPlus, *Engineering Reference*. 2013.
135. Xu, X.-l. and Z. Yang, *Natural ventilation in the double skin facade with venetian blind.* Energy and Buildings, 2008. **40**(8): p. 1498-1504.

136. Kotey, N.A., et al., *A Simplified Method for Calculating the Effective Solar Optical Properties of a Venetian Blind Layer for Building Energy Simulation.* Journal of Solar Energy Engineering, 2009. **131**(2): p. 021002.
137. Gomes, M.G., A.M. Rodrigues, and J.A. Bogas, *Numerical and experimental study of the optical properties of venetian blinds.* Journal of Building Physics, 2012. **36**(1): p. 7-34.
138. Chaiyapinunt, S. and N. Khamporn, *Shortwave thermal performance for a glass window with a curved venetian blind.* Solar Energy, 2013. **91**: p. 174-185.
139. Chaiyapinunt, S. and S. Worasinchai, *Development of a mathematical model for a curved slat venetian blind with thickness.* Solar Energy, 2009. **83**(7): p. 1093-1113.
140. Somsak Chaiyapinunt and Nopparat Khamporn, *Heat transmission through a glass window with a curved venetian blind installed.* Solar Energy, 2014. **110**: p. 71-82.
141. Somsak Chaiyapinunt and S. Worasinchai, *Development of a model for calculating the longwave optical properties and surface temperature of a curved venetian blind.* Solar-Energy, 2009. **83**: p. 817-831.
142. Chan, Y.-C. and A. Tzempelikos, *A hybrid ray-tracing and radiosity method for calculating radiation transport and illuminance distribution in spaces with venetian blinds.* Solar Energy, 2012. **86**(11): p. 3109-3124.
143. Klems, J.H., *A new method for predicting the solar heat gain of complex fenestration systems II. detailed description of the matrix layer calculation.* ASHRAE Transactions, 1994. **100**(1).
144. Klems, J.H., *A new method for predicting the solar heat gain of complex fenestration systems—1, overview and derivation of the matrix layer calculation.* ASHRAE Transactions, 1994. **100**(1).
145. Andersen, M. and J. de Boer, *Goniophototmetry and assessment of bidirectional photometric properties of complex fenestration systems*, in *IEA SHC TASK 31, Daylighting buildings in the 21st century*. 2005: Stuttgart, Germany.
146. G. Ward, *Measuring and modeling anisotropic reflection.* ACM SIGGRAPH Computer Graphics, 1992. **26**(2): p. 265-272.
147. Reinhart, C. and M. Andersen, *Development and validation of a Radiance model for a translucent panel.* Energy and Buildings, 2006. **38**(7): p. 890-904.
148. Papamichael, K.M., J. Klems, and S. Selkowitz, *Determination and application of bidirectional solar-optical properties of fenesration materials*, in *Technical report LBL-25124*. 1988, Lawrence Berkeley National Laboratory: Berkeley.
149. Klems, J.H., *A new method for predicting the solar heat gain of xomplex fenestration systems. I. Overview and derivation of the matrix layer calculation, ,* in *ASHRAE Winter Meeting* 1994: New Orleans, LA.
150. Klems, J.H. and J.L. Warner, *Measurement of bidirectional optical properties of complex shading devices.* ASHRAE Transactions, 1995. **101**(1): p. 791-801.
151. Klems, J.H., J.L. Warner, and G.O. Kelley, *A comparison between calculated and measured SHGC for complex glazing systems.* ASHRAE Transactions, 1997. **102**(1): p. 931-939.
152. Apian-Bennewitz, P. and J.v.d. Hardt, *Enhancing and calibrating a goniophotometer.* Solar Energy Materials and Solar Cells, 1998. **54**(1-4): p. 309-322.
153. J. Breitenbach, et al., *Optical and thermal performance of glazing with integral venetian blinds.* Energy and Buildings, 2001. **33**: p. 433-442.

154. Apian-Bennewitz, P. *pab gonio-photometer ii.* 07/09/2016]; Available from: http://www.pab-opto.de.
155. Kostal, H., D. Kreysar, and R. Rykowski, *WHITE PAPER: Application of Imaging Sphere for BSDF Measurements of Arbitrary Materials*. 2013.
156. Boer, J.d., *Numerical Goniophotometer, User Manual*. 2004: Fraunhofer Institute of Building Physics, Stuttgart.
157. G. Ward and R. Shakespeare, *Rendering with Radiance: The Art and Science of Lighting Visualization, Revised Edition*. 2004: BookSurge, LLC.
158. SHC, *Daylight in Buidling*, in *ECBCS Annex 29/ SHC Task 21 Project Summary Report*, Kjeld John and R. Watkins, Editors. 2010: Hertfordshire, United Kingdom.
159. Pellegrino, A., *Traditional and new metrics for effective daylighting design*, in *Advanced Builidng Skins, Energy Forum*. 2013: Bressanone, Italy.
160. Wienold, J., *Dynamic daylight glare evaluation.* , in *Builing simulation 2009 the 11th international IBOSA conference*. 2009: Glasgow, UK. p. 44-51.
161. Wienold, J., *Dynamic simulation of blind control strategies for visual comfort and energy balance analysis.* , in *Building simulation 2007, the 10th international IBOSA conference*. 2007: Beijing, China. p. 1197-204.
162. Nabil, A. and J. Mardaljevic, *Useful daylight illuminances: A replacement for daylight factors.* Energy and Buildings, 2006. **38**(7): p. 905-913.
163. Reinhart, C. and S. Herkel, *The simulation of annual daylight illuminance distributions — a state-of-the-art comparison of six RADIANCE-based methods.* Energy and Buildings, 2000. **32**(2): p. 167-187.
164. Reinhart, C. and O. Walkenhorst, *Validation of dynamic RADIANCE-based daylight simulations for a test office with external blinds.* Energy and Buildings, 2001. **33**(7): p. 683-697.
165. Bellia, L., A. Pedace, and F. Fragliasso, *The role of weather data files in Climate-based Daylight Modeling.* Solar Energy, 2015. **112**: p. 169-182.
166. Hiyama, K. and L. Wen, *Rapid response surface creation method to optimize window geometry using dynamic daylighting simulation and energy simulation.* Energy and Buildings, 2015. **107**: p. 417-423.
167. Li, L., M. Qu, and S. Peng, *Performance evaluation of building integrated solar thermal shading system: Building energy consumption and daylight provision.* Energy and Buildings, 2016. **113**: p. 189-201.
168. Bellia, L., A. Pedace, and F. Fragliasso, *The impact of the software's choice on dynamic daylight simulations' results: A comparison between Daysim and 3ds Max Design®.* Solar Energy, 2015. **122**: p. 249-263.
169. Bellia, L., A. Pedace, and F. Fragliasso, *Dynamic daylight simulations: Impact of weather file's choice.* Solar Energy, 2015. **117**: p. 224-235.
170. Mangkuto, R.A., M. Rohmah, and A.D. Asri, *Design optimisation for window size, orientation, and wall reflectance with regard to various daylight metrics and lighting energy demand: A case study of buildings in the tropics.* Applied Energy, 2016. **164**: p. 211-219.
171. Kapsis, K., V. Dermardiros, and A.K. Athienitis, *Daylight Performance of Perimeter Office Fa ̧ades utilizing Semi-transparent Photovoltaic Windows: A Simulation Study.* Energy Procedia, 2015. **78**: p. 334-339.
172. Moon, P. and D. Spencer, *Illumination from a Nonuniform Sky.* Illuminating Engineering, 1942. **37**(10): p. 707-726.
173. Institution, B.S., *Lighting for Buildings--Part 2: Code of Pratice for Daylight*, in *British Standard BS8206*. 1992, BSI: London.

174. IESNA, *IESNA Lighting Handbook, 9th ed.* 2000, Illuminating Engineering Society of North America: New York.
175. Construction, P.s.R.o.C.M.o., *Chinese Standard for daylight design of building*, in *GB/T 50033- 2001*. 2001, China Building Industry Press: Beijing.
176. Li, D.H.W. and E.K.W. Tsang, *An analysis of daylighting performance for office buildings in Hong Kong.* Building and Environment, 2008. **43**(9): p. 1446-1458.
177. CF. Reinhart, *Daylight performance predictions*, in *Building performance simulation for design and operation* Jan L.M. Hensen and R. Lamberts, Editors. 2011, Spon Press: London.
178. Du, J. and S. Sharples, *Assessing and predicting average daylight factors of adjoining spaces in atrium buildings under overcast sky.* Building and Environment, 2011. **46**(11): p. 2142-2152.
179. Lim, Y.-W., et al., *Building fa ̧ade design for daylighting quality in typical government office building.* Building and Environment, 2012. **57**: p. 194-204.
180. USGBC. *LEED-NC (leadership in energy and environmental design) version 3.0*. 2006 [cited 2006; www.usgbc.org/LEED/].
181. Acosta, I., et al., *Analysis of daylight factors and energy saving allowed by windows under overcast sky conditions.* Renewable Energy, 2015. **77**: p. 194-207.
182. Fasi, M.A. and I.M. Budaiwi, *Energy performance of windows in office buildings considering daylight integration and visual comfort in hot climates.* Energy and Buildings, 2015. **108**: p. 307-316.
183. C.F. Reinhart, O.W., *Dynamic radiance-based daylight simulations for a full-scale test office with outer venetian blinds.* Energy & Buildings, 2001. **33**(7): p. 683-697.
184. Reinhart, C. and D. Weissman, *The daylit area – Correlating architectural student assessments with current and emerging daylight availability metrics.* Building and Environment, 2012. **50**: p. 155-164.
185. Saxena, M., et al., *61 Flavors of daylight*, in *the ACEEE Summer study on energy efficiency in buildings*. 2010, American council for an energy-efficient economy: Asilomar, CA, USA.
186. Reinhart, C., T. Rakha, and D. Weismann, *Predicting the daylit area: a comparison of students assessments and simulations at eleven schools of architecture.* Leukos, 2014. **10**: p. 193-206.
187. IESNA, *LM-83-12 IES Spatial Daylight Autonomy (sDA) and Annual Sunlight Exposure (ASE)*. 2012, NY: New Yourk.
188. Reinhart, C., J. Mardaljevic, and Z. Rogers, *Dynamic daylight performance metrics for sustainable buidling design.* Leukos, 2006. **3**: p. 1-25.
189. Rogers, Z., *Daylighting Metric Development Using Daylight Autonomy Calculations in the Sensor Placement Optimization Tool*. 2006, Architectural Energy Corporation.: Boulder, Colorado, USA.
190. Mardaljevic, J., *Daylight design, simulation and compliance for solar building envelopes*, in *Energy Forum*. 2013: Bressanone, Italy.
191. Mardaljevic, J., L. Heschong, and E. Lee, *Daylight metrics and energy saving.* Lighting Research + Technology, 2009. **41**: p. 261-283.
192. Berardi, U. and H.K. Anaraki, *Analysis of the Impacts of Light Shelves on the Useful Daylight Illuminance in Office Buildings in Toronto.* Energy Procedia, 2015. **78**: p. 1793-1798.
193. Franks, M., *Daylight in Museums*, in *International Radiance Workshops*. 2005.

194. Wienold, J. and J. Christoffersen, *Evaluation methods and development of a new glare prediction model for daylight environments with the use of CCD cameras.* Energy and Buildings, 2006. **38**(7): p. 743-757.
195. Ochoa, C.E., et al., *Considerations on design optimization criteria for windows providing low energy consumption and high visual comfort.* Applied Energy, 2012. **95**: p. 238-245.
196. CIBSE, *Guide A - Environmental Design*. 2006, CIBSE Publications: London.
197. BRE, *BREEAM Hea 1:Visual comfort*. 2014: London.
198. Jacobs, A. *Radiance Tutorial*. 2012 [cited 2016.
199. Reinhart, C. and A. Fitz, *Findings from a survey on the current use of daylight simulations in building design.* Energy and Buildings, 2006. **38**(7): p. 824-835.
200. Jacobs, A., *UNIX for RADIANCE Tutorail.*
201. Mardaljevic, J., *Validation of a lighting simulation program: a study using measured sky brightness distributions, Lux, ,* in *The Eighth European Lighting Conference,*. 1997: Amsterdam. p. 555-569.
202. Mohsenin, M. and J. Hu, *Assessing daylight performance in atrium buildings by using Climate Based Daylight Modeling.* Solar Energy, 2015. **119**: p. 553-560.
203. Bueno, B., et al., *Fener: A Radiance-based modelling approach to assess the thermal and daylighting performance of complex fenestration systems in office spaces.* Energy and Buildings, 2015. **94**: p. 10-20.
204. Alzoubi, H.H. and S.M. Al-Rqaibat, *The effect of hospital design on indoor daylight quality in children section in King Abdullah University Hospital, Jordan.* Sustainable Cities and Society, 2015. **14**: p. 449-455.
205. Yun, G., K.C. Yoon, and K.S. Kim, *The influence of shading control strategies on the visual comfort and energy demand of office buildings.* Energy and Buildings, 2014. **84**: p. 70-85.
206. Chen, Y., et al., *Experimental and simulation study on the performance of daylighting in an industrial building and its energy saving potential.* Energy and Buildings, 2014. **73**: p. 184-191.
207. Yoon, Y.B., D.S. Kim, and K.H. Lee, *Detailed heat balance analysis of the thermal load variations depending on the blind location and glazing type.* Energy and Buildings, 2014. **75**: p. 84-95.
208. Fernandes, L.L., et al., *Angular selective window systems: Assessment of technical potential for energy savings.* Energy and Buildings, 2015. **90**: p. 188-206.
209. Hoffmann, S., et al., *Balancing daylight, glare, and energy-efficiency goals: An evaluation of exterior coplanar shading systems using complex fenestration modeling tools.* Energy and Buildings, 2016. **112**: p. 279-298.
210. Firląg, S., et al., *Control algorithms for dynamic windows for residential buildings.* Energy and Buildings, 2015. **109**: p. 157-173.
211. Loonen, R.C.G.M., et al., *Review of current status, requirements and opportunities for building performance simulation of adaptive facades.* Journal of Building Performance Simulation, 2016: p. 1-19.
212. Duffie, J.A. and W.A. Beckman, *Solar engineering of thermal processes*. 3rd ed. 2006, Hoboken, N.J. : Wiley.
213. Lee, Y. and S.A. Korpela, *Multicellular natural convection in a vertical slot.* J. Fluid mech, 1983. **126** p. 91-121.
214. de Boer, J., *Modelling indoor illumination by complex fenestration systems based on bidirectional photometric data.* Energy and Buildings, 2006. **38**(7): p. 849-868.

215. McNeil, A., *The Three-Phase Method for simulation Complex Fenestration with Radiance*. 2014.
216. Reinhart, C.F. and M. Andersen, *Development and validation of a Radiance model for a translucent panel.* Energy and Buildings, 2006. **38**(7): p. 890-904.
217. J, M., *Validation of a lighting simulation program under real sky condtions.* Lighting Research + Technology, 1995. **27**(4): p. 181-188.
218. Sun, Y., et al., *Thermal evaluation of a double glazing fa ̧ade system with integrated Parallel Slat Transparent Insulation Material (PS-TIM).* Building and Environment, 2016. **105**: p. 69-81.
219. Yoon, Y., W. Jeong, and K. Lee, *Window Material Daylighting Performance Assessment Algorithm: Comparing Radiosity and Split-Flux Methods.* Energies, 2014. **7**(4): p. 2362-2376.
220. McNeil, A. and E.S. Lee, *A validation of the Radiance three-phase simulation method for modelling annual daylight performance of optically complex fenestration systems.* Journal of Building Performance Simulation, 2013. **6**(1): p. 24-37.
221. IEA and ECBCS, *Annex 45 Energy Efficient Electric :ighting for Buildings: Lighting energy in buildings* in *Guidebook on Energy Efficient Electric Lighting for Buildings*, Liisa Halonen, Eino Tetri, and P. Bhusal, Editors. 2006: France.
222. Sheppy, M., L. Gentile-Polese, and S. Gould, *Plug and Process Loads Capacity and Power Requirements Analysis*. 2014, U.S. Department of Energy.
223. Singh, R., I.J. Lazarus, and V.V.N. Kishore, *Uncertainty and sensitivity analyses of energy and visual performances of office building with external venetian blind shading in hot-dry climate.* Applied Energy, 2016. **184**: p. 155-170.
224. EnergyPlus, *EnergyPlus EMS Application Guide.* 2015.